SYNTHESIS, CRYSTAL GROWTH AND CHARACTERIZATION OF PHOSPHIDES, SELENIDES, SULFIDES AND OXIDES

by

CHUN-MIN FENG

A dissertation submitted to the Graduate Faculty in Chemistry in partial fulfillment of the requirements for the degree of Doctor of Philosophy, The City University of New York

2010

This manuscript has been read and accepted for the
Graduate Faculty in Chemistry in satisfaction of the
dissertation requirement for the degree of Doctor of Philosophy.

Dr. Glen R. Kowach

Date | Chair of Examining Committee

Dr. Mahesh K. Lakshman

Date | Executive Officer

Dr. Harry D. Gafney

Dr. Zhonghua Yu

Dr. Maria C. Tamargo

Supervisory Committee

THE CITY UNIVERSITY OF NEW YORK

Abstract

Synthesis, Crystal Growth, and Characterization of Oxides, Phosphides, Selenides, and Sulfides.

By

Chun-Min Feng

Advisor: Professor Glen Kowach

The desire to build smaller, faster, inexpensive electronics has prompted researchers to exploit electron "spin" in transistors. Spin in semiconductors offers a pathway towards integration of storage and processing in a single material. These "spintronic" transistors could be highly energy-efficient and perform more computations than traditional transistors in a smaller space. In addition, in optoelectronic applications, lasers and light-emitting diodes that take advantage of electron spin could increase the data-carrying capacity of light. But one of the key hurdles in this emerging field is that the magnetic and semiconducting materials needed to make a spintronic device are notoriously incompatible. We have focused on different oxides, phosphides and sulfides to study crystal growth and properties of spintronics.

We have reported the synthesis of pure ZnO and Mn substituted ZnO crystals from sodium hydroxide and potassium hydroxide flux for the first time. Various oxides, including boron oxide (B_2O_3), vanadium oxide (V_2O_5), tungsten oxide (WO_3) and

molybdenum oxide (MoO_3), were also used for crystal growth. A non-uniform distribution of Mn substitution was found in ZnO single crystals, and 3 at.% Mn concentration was identified. In addition, polycrystalline Mn-substituted ZnO powder samples exhibited solubility of Mn in the ZnO lattice. SQUID magnetic properties investigation of Mn-substituted polycrystalline samples indicated paramagnetism down to 5 K.

We have also investigated phosphides, selenides, and sulfides for spintronic applications, based on the well-studied spintronic material, gallium arsenide (GaAs), with a Curie temperature of 110K. GaAs has the zincblende structure with Ga in tetrahedral coordination. $ZnSiP_2$, $CdSiP_2$, $KGaS_2$ and $KGaSe_2$ have metal atoms in tetrahedral coordination with no localized spin. Localized spin will be present if transition metals are substituted in. The synthesis of single phase $ZnSiP_2$ and $CdSiP_2$ were grown from two different heat treatments. Also, potassium gallium selenide ($KGaSe_2$) and potassium gallium sulfide ($KGaS_2$) were reported. Temperature dependence susceptibility data revealed a ferromagnetic transition near 300 K followed by an antiferromagnetic transition near 50 K. Hysteresis loops at room temperature were present in all Mn substituted samples. Magnetic properties of Mn substituted samples are comparable with the crystalline MnP sample; they remain unidentified in X-ray diffraction data.

ACKNOWLEDGEMENTS

I wish to express my deep appreciation to Professor Glen R. Kowach, President of American Association for Crystal Growth-Mid-Atlantic Section, for giving me an opportunity to work under his supervision for Ph. D. degree as his student. I would also like to express my regards to him for teaching and moulding me to understand and to pursue the research in the field of solid state chemistry. I am really indebted for his keen interest, invaluable guidance and constant encouragement at each and every step of scientific and personal activities.

I place on record my sincere gratitude to Professor Simon Simms, Chair, Chemistry Department, CCNY-CUNY, for kindly giving me the permission to enroll for Ph. D program.

I sincerely convey my regard to Dr. Deok-Yang Kim and Dr. S. N. Achary, Postdoctoral Associates in the Kowach research group for their help with my experimental work and valuable suggestions.

I am extremely thankful to Dr. Jorge Morales, Manager, Electron Microscopy Center, CCNY, for his support and encouragement to my research.

I thank my committee members: Professor Harry D. Gafney, Professor Maria Tamargo and Professor Zhonghua Yu for their valuable suggestions of the dissertation and research.

In addition, a thank you to Professor Yuh-Kang Pan, Professor Michel Green, and Professor John Lombardi who introduced me to the City University of New York. Also, I would like to thank Professor Yuh-Kang Pan, my professor for the special topic on crystal field theory, for taking care me in many ways since I come to New York.

I would like to thank my group members, Daniel Margul and Aisha Farooq (ZnO project), Anelisa Jones, Daniel Margul, and Bas Van Eck ($ZnSiP_2$ and $CdSiP_2$ project) and Malick Samateh, Shreya Amin, and Quddus Nizami ($KGaS_2$ and $KGaSe_2$ project) for their experimental support.

I sincerely thank to all my friends, Dr. Dionne Miller, Julieth Ballesteros, Sherene Ishithar, and Yadi Li for their moral support, proof reading, and their company.

I would like to thank Jie Gao for the most substantial mental support in the last two years of my Ph. D.

I am greatly indebted to my parents and families for their moral support, constant advice and care in the every step of my life. I thank all my teachers from whom I learnt many valuable things. It is my deep sense of love and gratitude that I dedicate this dissertation to my parents, families and teachers.

Chun-Min Feng

TABLE OF CONTENTS

LIST OF FIGURES

LIST OF TABLES

Chapter 1 Introduction of Crystal Growth

1.1. History of Crystal Growth

Crystal growth is one of the foundations of material science. The word "crystal" originates from the Greek κριος (coldness) or κριμος (ice). "Crystal" creates a mental picture of a transparent or clear solid with well defined shape. Crystals are ordered arrangements of atoms (or molecules). In a natural process the shape of the crystal is governed by these ordered arrangements of atoms (molecules). Materials in crystalline form have special optical and electrical properties, and in many cases improved properties over randomly arranged materials (also said to be amorphous or glassy).[1-4] Several crystal growth methods occurring in nature have been adopted in laboratory research and in industry applications. The oldest type of crystal growth is the crystallization of salt from sea water by evaporation. The formation of sea salt crystals has been occurring everywhere since prehistoric time. Crystallization procedures are recorded in documents written before the Christian era. Plinius mentioned the crystallization of number of salt like vitriols and the alchemist Geber described the preparation and purification of various materials. The father of crystal fabrication technology is A. Verneuil, who with his flame-fusion growth method described growth of ruby crystal in 1902 and this was later extended by Nassau.[5, 6] A historical development of crystal growth has been reviewed in several references.[7-10] The major theoretical account of crystal growth concepts and technologies was developed by the rapid advancement of science and technology in the 20th century.[11-15]

1.2.1 Mechanism of Crystal Growth

The developments in the physics and chemistry of crystal growth started from the Newton era at the beginning of the18th century. However crystal growth was just an educational science in the early 20th century. Its rapid development began mid century with the applications of semiconductors and functional materials. Also, micro and macroscopic understanding of the growth process of a crystal attracts thermodynamics and kinetic aspects of the crystal growth.[11, 16-21] Early studies of mechanisms of the crystal growth process from solution indicate the adherence of a thin but dense layer of atoms at the surface of crystals during growing process. Thus, it has been postulated that the atoms or clusters move further close to the crystal and permanently fix on the surface of crystal, while the loss of atoms from the layer is compensated from the solution. Thus, essentially the growth is controlled by the diffusion of the atoms though the dense preformed (adsorbed) layer.[11, 21]

The thermodynamic understanding of the crystal growth indicates that the excess energy at the surface of a crystal due to the unsaturated bonds of atoms at the surface is lowered by formation of bonds with added atoms and thus the crystal structure expands. The difference in growth rates of different faces dominates the crystal morphology. The origin of the difference in growth rate of different faces is related to the amount of energy released on the attachment of atoms to them.[11, 21-25] In general, the growth velocity of the plane is inversely related to the atomic density of the plane. The driving force for crystallization comes from the lowering of the potential energy of the atoms or molecules when they form bonds with each other[22-26]. The crystal growth process starts with the nucleation stage. Several atoms or molecules in a supersaturated vapor or liquid start

forming clusters; the bulk free energy of the cluster is less than that of the vapor or liquid. The total free energy of the cluster is increased by the surface energy (surface tension); however, this is significant only when the cluster is small.[17-20, 26] A cluster with a radius smaller than a critical radius, r^*, will evaporate (or dissolve in the solution) while a cluster of radius greater than r^* will become stable (Figure 1.1), will increase its size by the addition of other atoms and is thus "growing". The critical radius, r^*, also defines a critical energy barrier, ΔG, that we need to overcome in order to obtain a stable nucleus that will keep growing, eventually becoming a large single crystal. Thermodynamics can help us describe the process. Assuming a spherical shape for the nucleus the free energy of its formation is:

$$\Delta G = 4 \pi r^2 s + [(4/3) \pi r^3] G_v \qquad (1.1)$$

Where ΔG is the total free energy; ΔG_v is the free energy change per unit volume forming the stable solidification from vapor or liquid. r is the radius of cluster; s is the surface tension; The total free energy ΔG goes through a maximum ΔG^* at a critical radius r^* which can be obtained by derivation of total free energy as given above with respect to radius and equating to 0, (i.e., $(d\Delta G^o/dr) = 0$) Thus, surface tension becomes an important factor for the growth of crystals. However, this effect dominates only below certain crystal dimensions. Therefore, it is very common to observe a crystal as an entity of intimately linked small crystallites. The growth of the large crystals is thus driven by thermodynamic stability of the crystalline state over the molten or super saturated solution states.

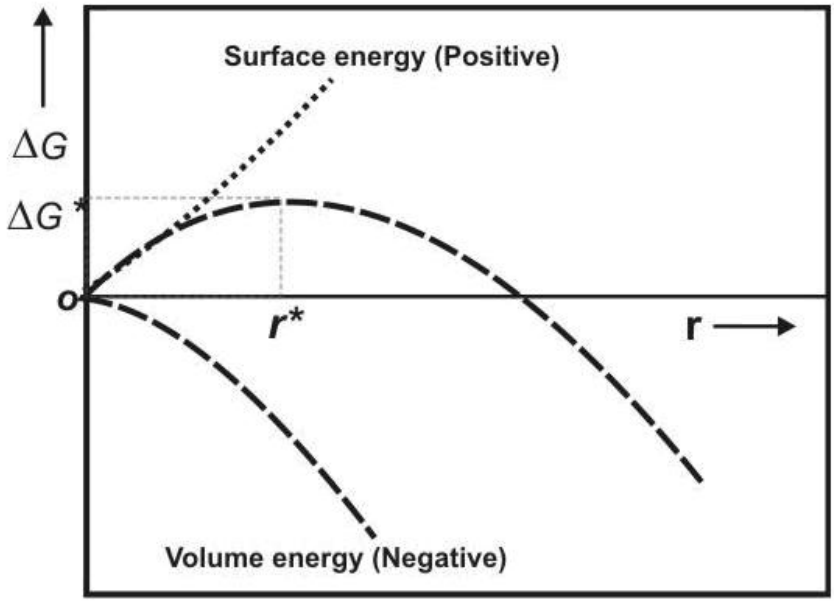

Figure 1. 1 Overall free energy for nucleation as a function of the nucleus size. The critical value G* for creating a nucleus of critical radius r* must be reached.

1.2. Development of Crystal Growth Methods

French chemist, Auguste Verneuil, is regarded as the pioneer of crystal growth. In 1902, he developed the first commercial crystal growth process for manufacturing synthetic gemstones. His crystal principle nucleation control and crystal-diameter control have been adapted in later growth methods from the melt, such as Stober Bridgman, Czochralski, Stöckbarger etc. The principles of the Verneuil method with nucleation, growth rate and diameter control have been applied and described in many crystal growth process such as Stöckbarger 1925, Bridgman 1926, and in the Czochralski process 1918. The crystal growth methods can be categorized into three broad categories, namely, solid growth, solution growth and vapor growth[12].

Solid growth: This growth process involves Solid-to-Solid phase transition. The formation of crystallite in a common solid state reaction and the development of crystallite dimension in sintering process are the causes of this growth. Furthermore, they are also diffusion controlled and the precursor is usually heated at high temperatures (below melting temperature) to achieve sizable crystals. However, the sizes of the crystals are too small to be considered as single crystals for any practical applications.

Solution growth: This growth process involves Liquid-to-Solid phase transition. This category is a widely used procedure for the growth of single crystals. The large single crystals can be produced by this method. A liquid (solution) of a material is cooled in an optimized rate to pass though solid-liquid phase transition reversibly. This procedure also produces high quality and impurity-free crystals and thus is extensively used for purification of crystals. Zone refining is an example of Solid-Liquid-Solid phase transition. Crystallization from solution and hydrothermal methods in a broader sense can

be considered as subclasses of this, where the solute in solution state transforms to the solid depending on the precipitation rate.

Vapor growth: The vapor to solid equilibrium drives the formation of crystal in the vapor growth process. The condensation of vapor in a controlled manner forms the single crystals. The sublimation and vapor transport are general procedures followed the vapor-solid transformation. The source of the feed is heated at higher temperature to evaporate atoms (molecules or clusters) and they are transported though diffusion or by a carrier gas to a temperature where the vapors condense to crystal. In such a process, a large number of nuclei is produced at a time and thus often ends with an agglomeration of a large number of crystals. This method has been extensively used in semiconductor industry for predation of films or coating[27, 28]. But, it is not a popular method for growing large single crystals. Modern methods like molecular beam evaporation (sometimes epitaxy) and flash evaporation takes the advantage of this solid-vapor equilibrium. In the presence of carrier gas the growth is faster and vapors of the solute can be attained at relatively lower temperature by the formation of volatile complexes with solute.

In general, melt growth involving the Solid-Liquid equilibrium is a widely used commercial crystal growth procedure. As mentioned earlier, this procedure has a long history and successive modification and development of experimental procedures, like flame fusion, Bridgman, Czochralski, zone melting methods have evolved as industrial methods. Further attention was made in solution growth, like isothermal precipitation or hydrothermal, solvent evaporation, and flux methods are also commercially used procedures for growing sizable single crystals. Salient details of these methods are explained briefly in the subsequent section.

1.2.1 Flame Fusion

In this method the feed is heated with a flame and the molten drops are collected over a seed crystal or allowed to crystallize on a support at lower temperature. Feed r materials are continuously brought to the flame to supply a steady liquid drop at the crystallization point. This method is the first commercially successful method to produce gem crystals, in particular ruby and sapphire[5, 6]. A schematic of flame fusion method is depicted below.

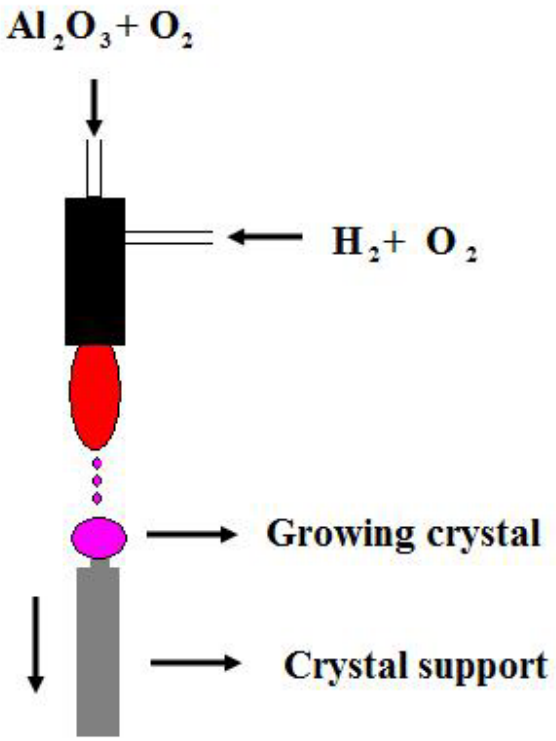

Figure 1. 2 Schematic of Verneuil's flame fusion method for ruby crystal growth

1.2.2 Czochralski method[11-15]

The Czochralski process is named after a Polish scientist Jan Czochralski, the most important method of fabrication of semiconductor and oxide crystals, which are crystals from melts contained in crucibles (Figure 1.3). Jan Czochralski developed this crystal growth technique in 1926 while investigating the crystal growth rates of different metals[29, 30]. This is a method of single crystal growth from a melt of the same composition and therefore this technique can only be applied to congruently melting materials. Unfortunately, high internal strain in the crystal is a significant drawback. Another consideration for this crystal growth method is the convection of the melt. The compositional inhomogeneity and morphological instability caused by the melt convection influences the quality of the crystals. In order to reduce the convection, double crucible for GaAs and stoichiometric $LiNbO_3$ is utilized, and magnetic field are used to approach crystals with low displacement and large size[12]. Similar to the Verneuil process, the Czochralski process begins with a movable seed crystal. The sample is heated just above the melting point in a crucible. A seed crystal adhered to a pulling rod is kept at the melt surface. Sometimes during the growth process both crucible and pulling rod are rotated constantly, usually in opposite directions to maintain constant temperature and uniform melt. The pulling rod is then moved upward at an optimized rate. The melt crystallizes at the surface of seed and large cylindrical crystals with orientation of the seed crystal can be obtained by this process. Crystals are grown in well controlled temperature gradients, pulling rate and rotating speed in Czochralski technique. There are many theoretical models that have assisted these developments to increase crystal size and quality: For

instance, the optimization of the crystal and crucible rotation rates and of the temperature distribution and the design of heaters. A schematic of Czochralski technique is shown in Figure 1.3. Large single crystals for semiconductors, like Si, Ge etc. have been obtained by this method. The size of the crystal depends on the amount of charge and size of the crucible. Often a protective environment is used to maintain purity.

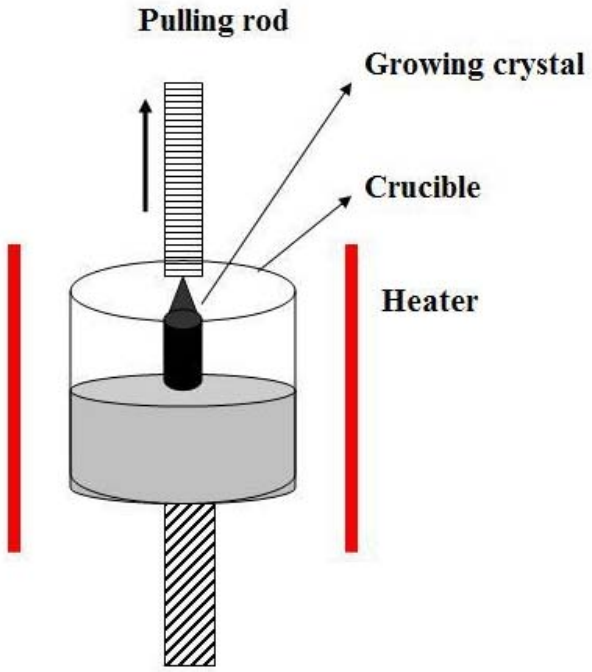

Figure 1. 3 Schematic of Czochralski method.

1.2.3 Bridgman-Stöckbarger Method[11-15]

The Bridgman method is also a widely used technique for growing single crystals. In this method a sample (melt) is passed though a temperature gradient, where the melt-solid equilibrium is attained at the growth point of the crystal.

The Stöckbarger method is a type of zone melting method but only a small part of the feed is melted. Crystal synthesis occurs when the crucible moves toward the low temperature zone of the furnace. In this method the polycrystalline material in a container is heated above its melting point and slowly cooled from one end where a seed crystal is placed. The temperature gradient is attained by either directional movement of the furnace (as in Bridgman method) or directional movement of melt (as in Stöckbarger method). Single crystal material is progressively formed along the length of the container. The process can be carried out in a horizontal or vertical geometry. The seed crystal may or may not be required in this method as the seed can be formed by instantaneous nucleation of the melt as it faces the temperature gradient. Also, a protective atmosphere may be used. This has been a unique method producing certain semiconductor crystals, like, GaAs, where the Czochralski process is more difficult[31].

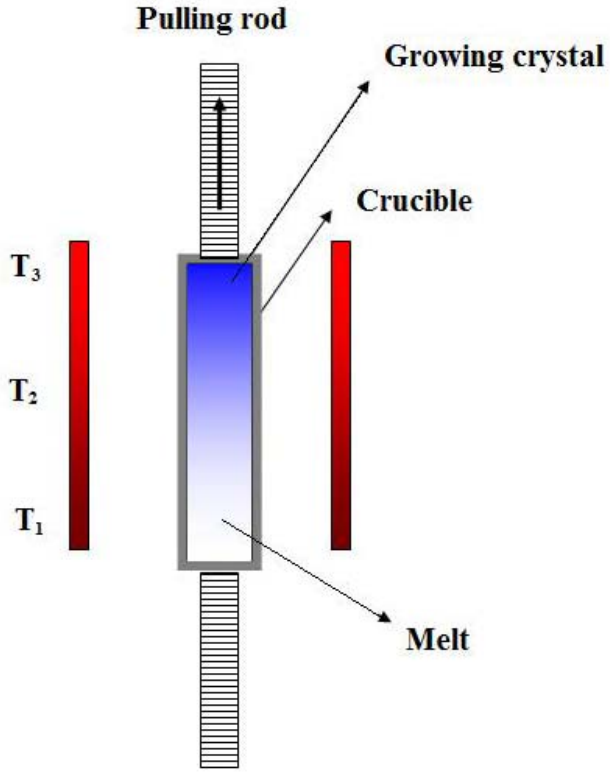

Figure 1. 4 Schematic of Bridgman-Stockbarger method (T3 < T2< T1)

1.2.4 Solvothermal Crystal Growth Method[32-34]

The solvothermal method utilizes the isothermal and isobaric conditions to grow crystals from an accelerated chemical reaction of materials. In this process a chosen solvent helps the pressure transiting medium in liquid and vapor phase as well as partially or fully dissolving the reacting solids. So the reaction proceeds in homogeneous reaction medium. However, the cases of heterogeneous reaction are also known. Due to the presence of the solvent as well as pressure the reaction usually occurs at much lower temperatures compared to the same reaction in solid state. The reaction can lead to single crystals under appropriate thermal or pressure gradient.

Solvothermal reactions are carried out in a closed enclosure called autoclave. The system is heated below its critical temperature for crystal synthesis. Such process often leads to metastable compounds which are unstable at high temperature. Typical solvents used in solvothermal reaction vary from the reaction desired; however, the most commonly used solvent is water. If water is used, the process is called hydrothermal method[34].

Hydrothermal crystal growth is another important solution crystal growth method occurring in nature to grow large number of minerals. In laboratory, the German chemist Robert Bunsen synthesized barium carbonate and strontium carbonate above 200 ˚C and the pressure above 100 bar. The preparation of crystals of large numbers of phosphates, silicates, vanadates as well as various oxides by hydrothermal reaction are known[34-36]. It can also be mentioned that the use of seed crystal in hydrothermal reaction usually favors the growth of larger crystals. Crystallization of quartz in laboratory by the hydrothermal method has been used for the fabrication of commercial products. The hydrothermal

method of growth of microscopic size quartz crystals was reported by Schafhäult in 1845 and by de Sénarmont in 1851. G. Spezia, (1898-1908) published reports on the growth of macroscopic (15mm) quartz crystals from solutions of sodium silicate, natural crystals as seeds and supply in a silver-lined vessel in temperature gradient between to 320-350 °C to 165-180 °C in a period of 200 day[33, 37]

The major limitation of this procedure is due to the critical temperature of solvent. The high temperature solvolthermal reactions are carried out with high boiling point liquids. Also, corrosion of the reaction vessel due to solvent at high pressure and temperature is accelerated. Hence, these methods are mainly used for selective materials, like silicates and phosphates only. Solvothermal reaction using aq. or pure HF has been used to produce crystals of various metastable and unusual structured fluorides. Preparations of zeolites, mesoporous siliceous or silicophosphates are mainly prepared by hydrothermal reaction.

1.2.5 Flux Crystal Growth

Growth of crystal from a flux is a closely similar technique adopted for the growth of crystal from solution[38-41]. The basic difference is that in the case of solution growth a liquid medium is used while in the flux growth a solid which melts at a relatively lower temperature is involved to dissolve the solute. Thus both the methods can be considered as solution growth procedures. In such cases the crystal growth occurs well below the melting point of the solid. Thus the risk of thermal decomposition and strained crystals can be avoided. The crystals grow usually in their natural habit, thus aiding optical identification of the crystallographic axes. Trapping/incorporation of the solvent into the crystal is a disadvantage, which may sometimes be minimized by a careful choice of

solvent.

In this method desired solids are mixed with low melting solids in appropriate ratio (usually eutectic composition) and heated to a temperature where maximum solubility is achieved. This molten mass is slowly cooled. Due to the decrease in solubility product nucleation occurs instantaneously and then grows by further precipitation. The typical solubility of materials shows an increase with a raise in temperature. For instance the solubility of NaCl in water is 34.6 g/100ml at 0 °C. When the temperature heated to 350 °C, the solubility is 74 g/100g. (Figure 1.5) The higher solubility of precursor in the flux the more crystal growth there is. A simple NaCl-H_2O binary phase equilibrium diagram reveals the NaCl phase available area above 25 wt% NaCl. (Figure 1.6)

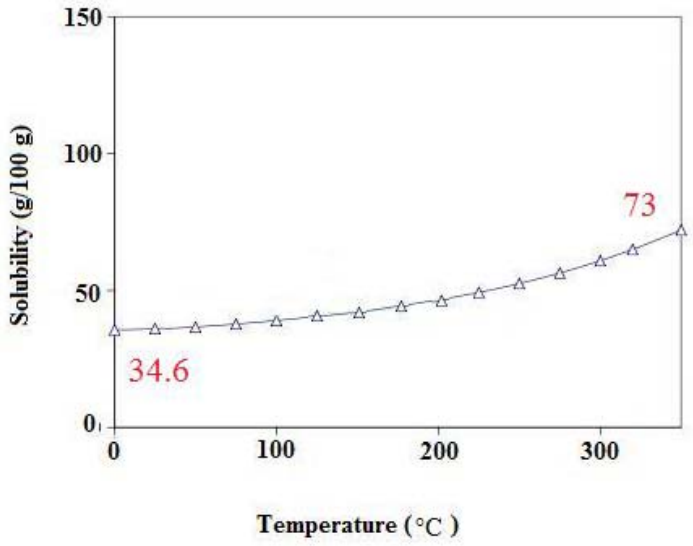

Figure 1. 5 Temperature dependence solubility of NaCl in water

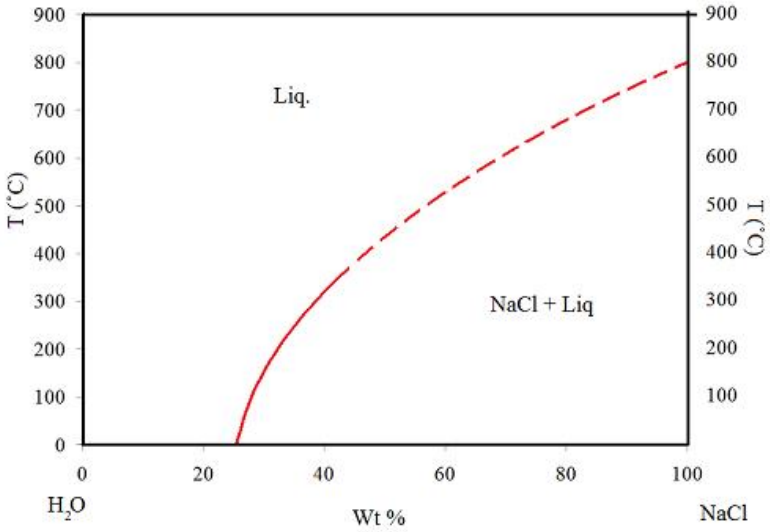

Figure 1. 6 NaCl-H_2O phase equilibrium diagram

The supersaturated region (labile region or metastable) is obtained when the solubility reaches the limits. As the temperature is lowered the solution prefers the unsaturated state and the excess solute precipitates out as crystal feed. In this kind of growth the solution chemistry is important due to its role in breaking the bond of the solute. A general guide line is obtained by studying the solubility curve of the material in a flux. A typical solubility curve is shown in Figure 1.7.

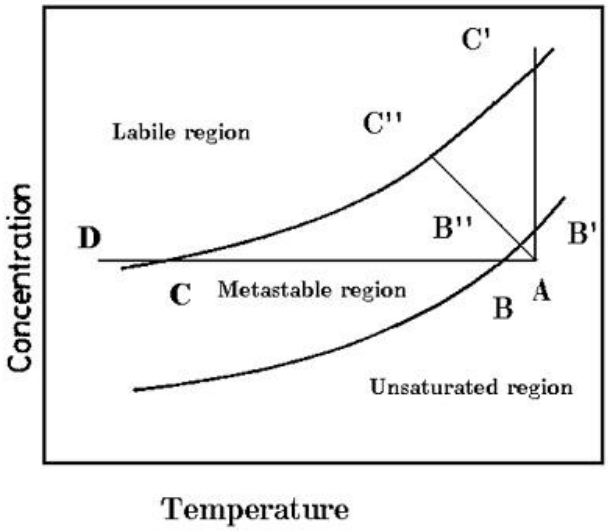

Figure 1. 7 Typical Solubility curve.

As observed from the figure the growth of crystals is possible from both the labile and metastable regions, while accelerated growth is possible in labile or supersaturated region due to spontaneous nucleation. No crystal can be grown from the unsaturated region. Flux evaporation often follows in the flux growth method so as to bring the unsaturated state to super saturated or metastable state.

For optimum crystal growth, the compound should be moderately soluble under the crystallization conditions. If the solubility is too high, the solvent incorporation becomes more intense. If it is not soluble enough, then there is not enough solute around to supply the growing crystal surface and one tends to get small crystals. To get the best solubility one should carefully match the solute and solvent. Parameters like solvent polarity and dielectric constant may be important in choosing the solvent. Knowledge of the density of the solution is often needed for mass balance, flow rate, and product yield calculations.

Since the growth of crystals from solution is mainly a diffusion-controlled process, the medium must be less viscous to enable faster transference of the growth units from the bulk solution by diffusion. Hence a solvent with less viscosity is preferable. Fundamentally, the solvent can influence crystal structure, crystal size, morphology, and purity by modifying solution properties (i.e., density, viscosity and component diffusivities), solute solubility, as well as the structure of the crystal-liquid interface. A large number of materials like, alkali halide, alkali carbonates, PbO, PbF_2, B_2O_3, Bi_2O_3. tungstates and molybdates are practically used as flux[11, 12, 14, 39]. Low melting metals, like, Sn. Pb, Bi, Na, Li etc have been used to grow crystal of various intermetalics and nitrides, phosphides etc[42].

Crucible selection is again an important limitation for the flux growth. Usually, the material for crucible has low reactivity (i.e. platinum, tantalum, and niobium) and low porosity ceramics (i.e. alumina, zirconia, boron nitride, and quartz) are preferred. Crucibles are normally sealed in evacuated quartz ampoules or reactions take place in controlled atmosphere furnaces.

Growing materials at lower temperature is most important benefit of this method. Especially for the material have high melting temperature, metastability, and incongruent melting. Crystals with natural morphology can be obtained. However, the availability of suitable flux, suitable container and inclusion of the solution, are major limitation for growth of large single crystals.

1.3. Chapter 1 References

1. Heck, C., *Magnetic Materials and Their Applications*. Butterworths: 1974.

2. Grant, P., High-Temperature Superconductivity: Four Years Science Bednorz end Mueller. *Advanced Materials* 1990, 2, 232.

3. Lines, E. M.; Glass, M. A., *Principles and Applications of Ferroelectrics and Related Materials*. Clarendon Press 1977.

4. Nye, F. J., *Physical Properties of Crystals: their Representation by Tensors and Matrices*. Oxford University Press: 1985.

5. Nassau, K., ``Reconstructed"or``Geneva"ruby. *Journal of Crystal Growth* 1969,*5*, 338.

6. Verneuil, A., Production Artificielle du Rubis par Fusion. *Paris Acad. ScL, Comptes Rendus* 1902, 135,791.

7. Bohm, J., The Historical Development of Crystal Growing - a bibliography. *Crystal Research and Technology* 1981, 16, 275.

8. Hulliger, J., Chemistry and Crystal Growth. *Angewandte Chemie International Edition in English* 1994, 33, 143.

9. Scheel, H., Historical Aspects of Crystal Growth Technology. *Journal of Crystal Growth* 2000, 211, 1.

10. Scheel, J. H., Historical Introduction in *Handbook of Crystal Growth*. Hurle, T. J. D., Ed. North-Holland: 1993; Vol. Volume 1, Part 1.

11. Buckley, E. H., *Crystal Growth*. John Wiley and Sons Inc.: 1951.

12. Laudise, R. A., *Growth of Single Crystal*. Prentice Hall Inc. Englewood Cliffs, New Jersey 1970.

13. Lawson, W. D.; Nielsen, S., *Preparation of Single Crystal*. 1st edition ed.; Academic

Press: 1958.

14. Pamplin, B. R., *Crystal Growth*. The Science of Solid State. Pergamon Press: 1975; Vol. 6.

15. Rosenberger, F., *Fundamental of Crystal Growth*. Spinger Verlag, Gemany: 1979.

16. Dirksen, J.; Ring, T., Fundamentals of Crystallization: Kinetic Effects on Particle Size Distributions and Morphology. *Chemical Engineering Science* 1991, 46, 2389.

17. Larson, M.; Garside, J., Solute clustering and interfacial tension. *Journal of Crystal Growth* 1986, 76, 88.

18. Söhnel, J., Solute clustering and nucleation. *Journal of Crystal Growth* 1988, 89, 202.

19. Larson, M.; Garside, J., Solute Clusering in Supersaturated Solutions. *Chemical Engineering Science* 1986, 41, 1285.

20. Na, H.; Arnold, S.; Myerson, A., Cluster Formation in Highly Supersaturated Solution Droplets. *Journal of Crystal Growth* 1994, 139, 104.

21. Azároff, V. L., *Introduction to Solids*. McGraw-Hill: 1960.

22. Hartman, P.; Perdok, W., On the Relations Between Structure and Morphology of Crystals. III. *Acta Crystallographica* 1955, 8, 525.

23. Boek, E.; Feil, D.; Briels, P., From Wave Function to Crystal Morphology: Application to Urea and Alpha-glycine. *Journal of Crystal Growth* 1991, 114, 389.

24. Hartmai, P.; Perdok, W., On the Relations Between Structure and Morphology of Crystals. II. *Acta Cryst* 1955, 8, 521.

25. Hartman, P.; Perdok, G. W., On the Relations Between Structure and Morphology of Crystals. I. *Acta Crystallographica* 1955, 8, 49.

26. Burda, C.; Chen, X.; Narayanan, R.; El-Sayed, M., Chemistry and Properties of

Nanocrystals of Different Shapes. *Chemical Reviews* 2005, *105* (4), 1025.

27. Cullen, W. G.; Wang, C.-C.; Ban, S. V., *Heteroepitaxial Semiconductors for Electronic Devices*. Springer-Verlag 1978.

28. Arthur, J., Molecular Beam Epitaxy. *Frontiers in Surface and Interface Science* 2002, 500, 189.

29. Czochralski, J., Measuring the Velocity of Crystallization of Metals. *Zeitschrift fur Physikalische Chemie* 1918, 92, 219.

30. Czochralski, J.; Garlicka, W., Crystallization Rate of Sodium and the Relations Between Atomic Heat of Solidification and Crystallization Rate. *Wiadomoœci Instytut Metalurgii i Metaloznawstwo* 1936, 3, 39.

31. Sonnenberg, K.; Kuessel, E., Developments in Vertical Bridgman Growth of Large Diameter GaAs. *III-Vs Review* 1997, 10, 30.

32. Laudise, A. R., Hydrothermal Synthesis of Crystals. *Chemical And Engineering News* 1987, 65, 30.

33. Johnson, G.; Foise, J., Quartz. *Encyclopedia of Applied Physics* 1996, *15*, 365.

34. Byrappa, K.; Haber, M., *Handbook of Hydrothermal Technology* William Andrew Publishing: 2001.

35. Caporaso, J. A.; Kolb, D. E.; Laudise, A. R. *Hydrothermal Crystal Growth Processes.* United States Patent 4579622, 1986.

36. Bardsley, W., *Hydrothermal Growth in Crystal Growth: An Introduction*. North Holland Publishing Co. Amsterdam: 1973.

37. Bordui, P., Growth of Large Single Crystals from Aqueous Solution: A Review. *Journal of Crystal Growth* 1987, 85, 199.

38. Elwell, D.; Scheel, J. H., *Crystal Growth from High Temperature Solutions*. Academic Press, London: 1975.

39. Laudise, A. R.; Carruthers, R. J.; Jackson, A. K., Crystal Growth. *Annual Review of Materials Science* 1971, 1, 253.

40. Scheel, J. H.; Fukuda, T., *Crystal Growth Technology*. John Wiley, Chichester: 2004.

41. Wanklyn, B., The Present Status of Flux Growth. *Journal of Crystal Growth* 1983, 65, 533.

42. Kanatzidis, M.; Pottgen, R.; Jeitschko, W., The Metal Flux: A Preparative Tool Tor the Exploration of Intermetallic Compounds. *Angewandte Chemie International Edition in English* 2005, 44, 6996.

Chapter 2 Introduction of Characterization Method

2.1 Introduction

X-rays are electromagnetic radiation which have the same properties as light， but shorter in wavelength. Since 1912, Max von Laue discovered that crystalline substances act as three-dimensional diffraction gratings for X-ray wavelengths similar to the spacing of planes in a crystal lattice. Crystallography developed as a discipline of mineralogy, which involved the crystal identification, description, and classification. Dorothy Hodgkin, a Nobel Laureate in 1965, wrote “a great advantage of a X-ray analysis as a method of chemical structure analysis is its power to show totally unexpected and surprising structure with, at the same time, complete certainty.” [1] X-ray diffraction is now a common technique for the study of crystal structures and atomic spacing.

X-ray microanalysis is a powerful technique for demonstrating information from a small area of a sample. The technique comprises of detecting the characteristic X-rays generated from the interaction of accelerated electrons and specimen. An energy dispersive spectrometer can apply for the detection of X-rays, called Energy Dispersive Spectroscopy (EDS). Now an energy dispersive spectroscope is often attached to a scanning electron microscope to reveal the surface three-dimensional topography and chemical analysis.

2.2 X-ray Diffractometer

2.2.1 The Development of X-ray

X-radiation is also called Röntgen radiation, which is a form of electromagnetic radiation. It has wavelengths that range from 0.5 to 2.5 Å which is shorter than UV radiation, but longer than γ-rays. The major use of X-rays is for diagnostic radiography and crystallography. X-rays were first discovered in Crookes tubes. Cathodes rays were created from electrons through the ionization of residual air in the tube by a high DC voltage. This voltage accelerated the electrons coming from the cathode to a sufficient velocity that created x-rays when the electrons struck the anode or tube wall. Many early scientists did not realize the radiation from Crookes tubes until Wilhelm Röntgen gave the first systematical investigation in 1895.[2]

Diffraction is the phenomenon of bending light passing an obstacle through a small slit. The diffracted waves can interfere with each other giving bright and dark fringes, depending on the phase differences of the wave. To explain the behavior of radiation, a Dutch physicist Christiaan Huygens wrote a treatise on the theory of light wave called Huygen's principle. Max Von Laue first demonstrated diffraction with X-rays in 1912.[3] Since the crystal with the arrangement consists of parallel rows of atoms equivalent to the parallel lines of the diffraction grating, the d-spacing could be successfully determined from the separations of bright fringes of the diffraction pattern. The classical Bragg law of diffraction relates the possibility of constructive interference to the inter-planar separations.

English physicists, Sir W.H. Bragg and his son Sir W.L. Bragg in 1913, derived Bragg's Law[4]. Some X-rays reflect off the first plane, but the rest subsequently are reflected by succeeding planes (Figure 2.1).[5] In first order reflection, scattered X-rays will have the difference in a whole number wavelength. The secondary X-rays, scattered by atoms in all planes, are completely in phase and reinforce each other. This is described as Bragg's Law:

$$2d\sin\theta = n\lambda \qquad (2.1)$$

λ = wavelength of x-rays

θ = glancing angle (called as Bragg angle)

d = inter planar separations

n = order of diffraction

Later many theoretical and experimental investigations made the X-ray diffraction (XRD) a powerful tool for crystallography.

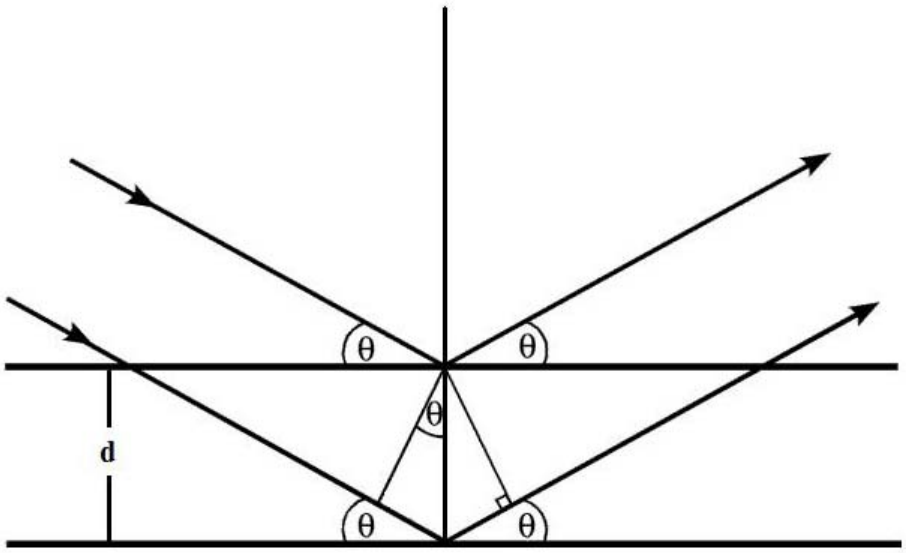

Figure 2. 1 Diffraction of X-rays by a crystal (Edit from West "Solid state Chemistry and its Application)

The peaks (also known as reflections) in the XRD pattern correspond to a set of parallel planes with inter-planar spacing, d. The d-values are calculated from the position of the peaks. Thus, for a particular sample, a set of d-values giving constructive interference is observed. The peak positions are related with the unit cell parameters of the lattice. Also, a particular sample gives a characteristic a set of d-values. Thus, they generally act as a fingerprint for the crystalline materials, and they can be used for identification of materials. The intensity distribution of the reflections is governed by the nature and kind of distribution atoms in the unit cell.

X-ray scattering is a phenomena caused by the interaction between the electron and X-ray radiation. Coherent scattering happens with no X-ray energy loss, and is also called elastic scattering. Another X-ray scattering is called inelastic scattering or Compton scattering. This inelastic scattering was proposed by Arthur Holly Compton in 1923.[6] The

change in momentum of the X-ray radiation is due to the change in its direction of the scattering electron. The energy in the scattered electron is thus less than the energy in the incident X-rays.

The scattering of X-rays from the electron of atoms is possible in all the directions. The intensity of radiation scattered by an electron is discussed by the classical Thomson equation and called scattering power of an electron (f_e). The amplitude of wave scattered by an atom is proportional to its atomic number (Z).[7, 8] The higher the atomic number, the higher is the scattering power (f_a). Also, atom scattering power, usually expressed as the ratio of scattering of an atom factor to the scattering by a single electron under the same conditions.[7-12] Thus, the scattering factors is expressed as $f_a/f_e = Zf_e/f_e$. The mean position of atoms in the unit cell is vibrating at any temperature. The scattering factor of an atom decreases with their amplitude of atomic vibration. Also, the scattering factor decreases with the increase of the diffraction angle due to the atomic size, showing the mutual destructive interference of the X-ray scattered from the atoms. The scattering factor of an atom is given as:

$$f = f_0 e^{\frac{-BSin^2\theta}{\lambda^2}} \tag{2.2}$$

f_0 : Scattering factor of an atom when it is rest and at 0°

λ : Wavelength of x-ray

θ : Angle of diffraction

B : A constant (called isotropic temperature factor, which is related to the amplitude of atomic vibration is given as $B = 8\pi^2 \overline{u^2}$, where $\overline{u^2}$ = mean of square displacement of the

atom from the mean position) (The exponential term is called Debye-Waller factor)

A crystal lattice consists of atoms which form three-dimensional arrays. The structure factor for a particular plane *hkl,* F(*hkl*) consistents angul part $g_{j,\vartheta}$ and scattering factor from the plan (hkl), F_{hkl}. The structure factor of a plane *hkl* is expressed as:

$$F(hkl) = \sum_{j=1}^{j=N} g(j,\theta) e^{2\pi i(h_{xj} + k_{yj} + l_{zj})} \tag{2.3}$$

F_{hkl}: Amplitude of scattered radiation from the plane *hkl*

g (j,θ): Scattering factor of the atom j at the diffraction angle θ

In an X-ray diffraction experiment, the intensity is promotional to the square of the amplitude of the wave.

$$I_o(hkl) \propto \left|F(hkl)\right|^2 \tag{2.4}$$

or

$$I_o(hkl) = I(hkl)\left|F(hkl)\right|^2 N^2 \tag{2.5}$$

I_o(hkl): experimental observed intensity

I(hkl): a function of the experimental conditions, Lorentz-polarization factor, polarization, and absorption correction

N: a scale factor associated with the amplitude of scattered radiation

2.2.2 Powder X-ray Diffractometer

A powder x-ray diffractometer consists of an X-ray source and the detector for the sensing of diffracted X-rays. The common diffractometer geometries are based on Bragg-Brentano geometry. Although there are several types of X-ray sources available. A sealed X-ray tube is the most common X-ray source used in a laboratory. A block sketch of powder diffractometer is shown in the Figure 2.2.[13]

There are several kinds of X-ray sources, but the most common laboratory diffractometer uses a sealed tube X-ray source. The basic construction of the tube is similar to the Coolidge tube. The X-rays are generally produced from electron collisions with a metal target. A small fraction of electron energy is used for generating x-rays, which are a combination of continuous radiation with wavelengths starting at the short-wavelength limit (λ_{swl}). There are several intense peaks from the target elements, called characteristic radiation. Only a small fraction of electron energy is used for the production of x-rays and the rest is lost in the form of heat.

X-rays are allowed to escape from a particular direction (usually from Be window) for data collecting, although they are able to scatter in all the directions. The beam of X-rays is passed through the antiscattering and divergence slits, and then allowed to fall on the sample.

The fine grains of the sample are generally spread uniformly over an X-ray exposed area of a slide. There are many different sample preparations for X-ray data collection. For non-air sensitive samples, such as ZnO, $KGaSe_2$, fine powder are mixed with internal standard Si and applied on the sample slide. Air sensitive samples are prepared on a microscopy slides or spinner sample holder sealed with grease and kapton.

A flat sample surface is preferred.

The depth of X-ray penetration is another issue taken into consideration. Most metallurgical specimens strongly absorb X-rays. The intensity of incident beam is reduced to zero in a very short distance, about 80 μm, below the sample surface.

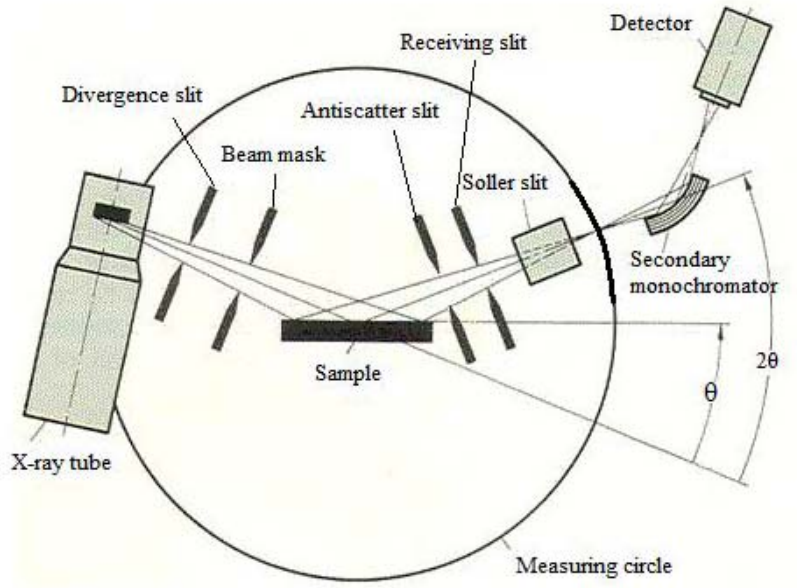

Figure 2. 2A typical X-ray diffractometer design with an X-ray tube, optics, and detector. (Edit form KSA system)

2.3 Scanning Electron Microscope

A microscope enables one to view images of objects that cannot be viewed by the human eye. The technique is used extensively in the field of biology, material science and agriculture, wherein a microscope can provide the surface information of the sample. There are three types of microscopes: optical, electron and ion microscopes. Although the classical optical microscope is still widely used for studying surface morphology and for similar other applications, its resolution is limited to around 1μm due to the wavelength of optical light. Scanning Electron Microscopy (SEM) is one of the techniques that uses electrons to measure these small size features even for nanoscale particle, since De Broglie wavelength of electrons can be manipulated to very small values (much smaller than the wavelength of optical light).

Scanning electron microscopy is an electron microscopic technique that provides surface information, texture, and three-dimensional topography. Knoll proposed the earliest concept of SEM in 1935.[14] Following, Von Ardenne built the first scanning transmission electron microscopy and also discussed the detail in both theoretical and practical aspects of his instrument.[15] Generally, a SEM contains electron source gun, high vacuum sample chamber and optics (Figure 2.3). In a SEM, an accelerated beam is focused on the surface of sample by a set of optical assembly and it scans over a small area where from secondary electrons, backscattered electrons, X-rays, and other photons that eventually fall on suitable detectors. For image investigation, secondary and backscattering electrons are primary for the surface topography. The X-rays are important for the chemical analysis (Figure 2.4).

The brightness and contrast of image depends on the amplitude of signal current which depends on the morphology and changes in the atomic number of element present in the sample probed. The first SEM examination of thick specimens was described by V. Zworykin *et. al.* in 1942.[16] In their report, the authors realized that the secondary electrons responsible for the topography. They also revealed the relationship of lens aberrations, gun brightness, and spot size as function of beam current. After a few years a SEM with resolution 50 nm was constructed by C.W. Oatley and D. McMullan.[17] The signal process of this modern SEM was improved by introducing the signal amplification (Smith 1956).[18] A first prototype commercial product was built by R. Pease in 1963.[19] Since the first commercial instrument, many improvements were made, such as the high-brightness electron source, LiB_6, and filed emission electron source. These high current electron sources made the improvement in the spot size, brightness and resolution. Until today, a recent development of new SEM system is variable-pressure scanning electron microscopy. G. D. Danilatos had reviewed the environment for this variable press microscope in his papers.[20, 21] This variable pressure system allows the measurement of almost any wet or dry specimen.

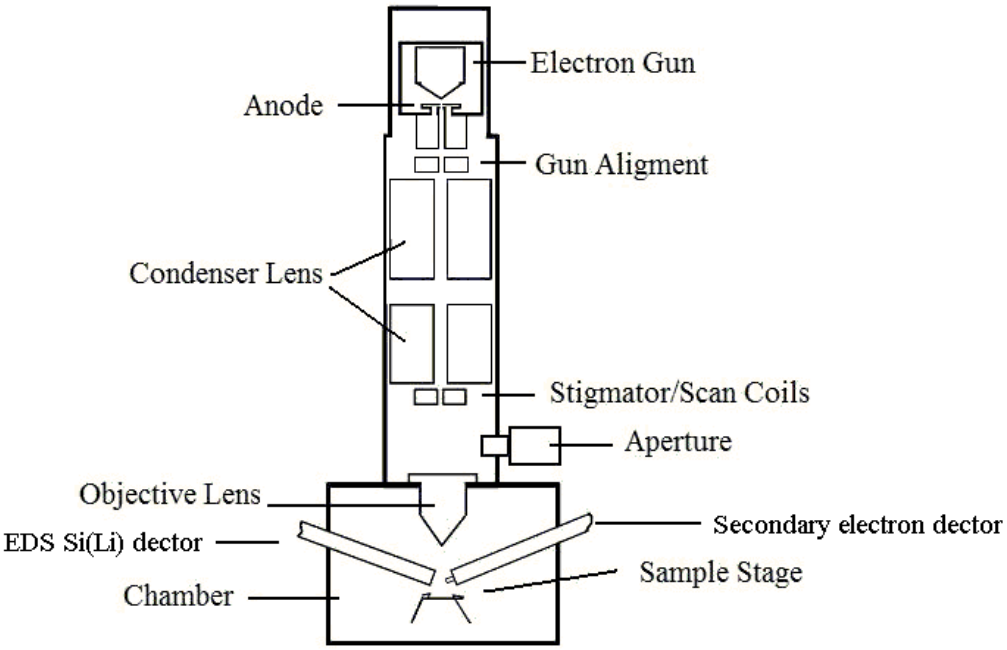

Figure 2. 3 Sketch of scanning electron microscope. Generally, a SEM contains electron source gun, high vacuum sample chamber, optics, and detectors.

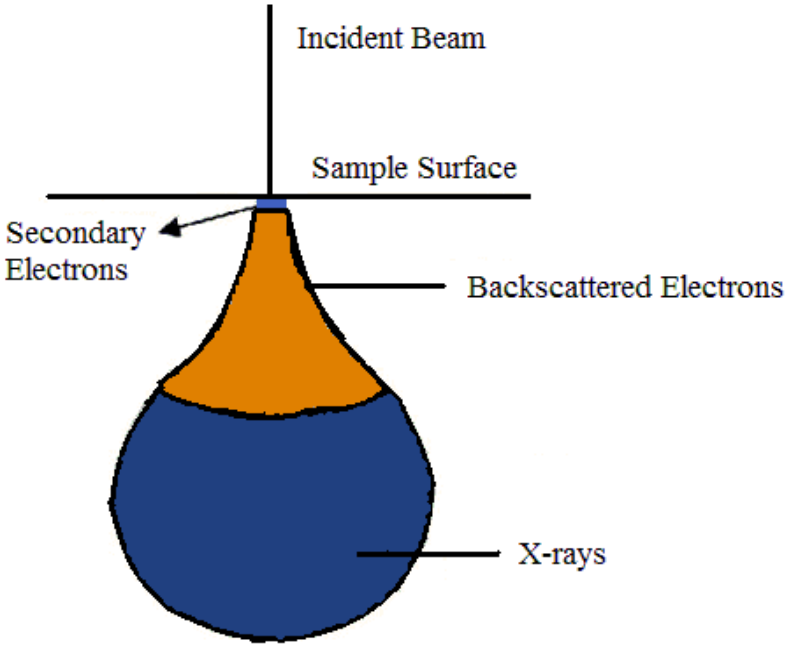

Figure 2. 4Interaction volumes for secondary electron, backscattered electrons and X-rays.

2.4 Energy Dispersive Spectroscopy

Energy dispersive X-ray spectroscopy (EDS) is a technique developed for the elemental analysis and chemical characterization of samples. It is a microanalysis technique in which the X-ray produced form the interaction of electromagnetic radiation and specimen is detected. The development of an EDS instrument for measuring the chemical analysis was simaltaneous with SEM. James Hillier proposed the concept of electron probe microanalyzer (EPMA).[22] Castaing described the first static electron beam microprobe in his Ph.D. thesis; but it was not until 1956, the first instrument, built by R. Castaing and A. Guinier, became a reality.[23] In general, SEM and EDS were maintained separately, SEM used for high quality imaging, EDS for X-ray analysis. After all, the combination of EDS and SEM for the analysis of X-ray signal and image has been applied today.

The development of microbeam instrument and solid-state X-ray detector was concurrent. A diode of lithium-drafted silicon, Si(Li), was used to detect X-ray photons of different energies simultaneously. The high efficiency of X-ray detector and their improving resolution made them attractive for application on a SEM. Princeton-Gamma-Tech first instilled a silicon detector on a SEM in 1968. At times, high purity germanium has been used for the high energy gamma-ray detection. Recently, there was a report of the significant development in EDS. In this report, Mott revealed the development of digital signal processing for producing higher quality spectra. In the future the digital processing technology will play an important role in spectrum system.

The characteristic X-rays in the EDS microanalysis is scanned and analyzed for their energy and intensity. Energy is the signature of the emitting for elements and the intensity indicates how much of it is present in a specimen. Thereby, not only to identify qualitatively the different elements present in the sample, but also using suitable correction provides their relative abundance in the sample. In the quantitative analysis, matrix corrections are used for the correction of uncorrected concentration to get reliable concentrations. There are some variations, related to sample composition that can affect the X-ray spectrum produced in an electron microprobe analysis which is needed to be corrected. These matrix corrections are named ZAF corrections, in reference to the three components of matrix effects; atomic number (Z), absorption (A) and fluorescence (F).

Atomic Number Correction: The atomic number factor (Z factor) corrects the amount of X-rays from specimen. The Z factor correction is directly related to the backscattering coefficient and stop energy. The interaction between the sample and accelerated electron beam generate the backscattering electrons. The reduced amount of X-ray signal is due to the loss of backscattering electrons. Also, the X-ray loss due to the inelastic scattering depends on the atomic number. P. Duncumb and S.J.B. Reed proposed the Z factor is the function of atomic number, atomic weight, and accelerating voltage.[24]

Absorption Correction: Absorption factor, A, is the most significant one. This factor corrects the X-ray generated in the sample but absorbed before falling into the detector. At the same depth within a sample, the number of X rays generated increases as the overvoltage increased. Also, the X-rays produced in the deep sample are more likely

absorbed than those generated near the surface. Besides the overvoltage, the absorption is also affected by the taking-off angle. The higher take-off angle makes the path length shorter. The formulation of absorption was proposed by J. Philibert (1963). [25] He revealed that absorption is function of acceleration voltage, critical excitation potential, atomic number, atomic weight, mass absorption coefficient, and take-off angle.

Fluorescence Correction: Usually the fluorescence factor (F factor) is less important. F factor corrects the X-ray signal which is not produced from the electron beam. F factor correction is a function of fluorescence yield which is proposed by S. Reed (1965).[26]

2.5 Chapter 2 References

1. Hodgkin, D., The X-ray Analysis of Complicated Molecules. *Science* 1965, 150, 979.

2. Filler, A., The History, Development and Impact of Computed Imaging in Neurological Diagnosis and Neurosurgery: CT, MRI, and DTI. 2009.

3. Laue, M., Die Interferenzerscheinungen an Rötgenstrahlen, Hervorgerufen Durch das Raumgitter der Kristalle. *Jahrb. Radioakt. Elektron* 1914, 11, 308.

4. Bragg, W., X-rays and Crystals. *Nature* 1912, 90, 219.

5. West, A., *Solid state Cemistry and its Applications*. Wiley-India: 2009.

6. Compton, A., A Quantum Theory of the Scattering of X-rays by Light Elements. *Physical Review* 1923**,** 21, 483.

7. Hartree, D., The Atomic Structure Factor in the Intensity of Reflexion of X-rays by Crystals. *Philosophical Magazine,* 1925**,** 50, 289.

8. James, R., The Optical Principles of the Diffraction of X-rays, p. 622. *London: Bell* 1954.

9. Cromer, D.; Waber, J., Scattering Factors Computed from Relativistic Dirac-Slater Wave Functions. *Acta Crystallographica* 1965, 18, 104.

10. James, R.; Brindley, G., Some Numerical Calculation of Atomic Scattering Facetors. *Philosophical Magazine* 1932, 12, 81.

11. Stewart, R.; Davidson, E.; Simpson, W., Coherent X-ray scattering for the Hydrogen Atom in the Hydrogen Molecule. *The Journal of Chemical Physics* 1965, 42, 3175.

12. Viervoll, H.; Ögrim, O., An Extended Table of Atomic Scattering Factors. *Acta Crystallographica* 1949, 2, 277.

13. KSAnalytical KS Analytical Systems.

14. Knoll, M., Charging Potential and Secondary Emission of Bodies Under Electron Irradiation. *Zeitschrift fur Technische Physik,* 1935, 16, 467.

15. Von Ardenne, M., Das Elektronen-Rastermikroskop. *Zeitschrift fur Physik A Hadrons and Nuclei* 1938, 109, 553.

16. Zworykin, V.; Hillier, J.; Snyder, R., A Scanning Electron Microscope, ASTM. *Bulletin No* 1942, 117, 15.

17. Oatley, C.; Everhart, T., The Examination of pn Junctions with the Scanning Electron Microscope. *Journal of Electronics* 1957, 2, 568.

18. Smith, K.; Oatley, C., The Scanning Electron Microscope and its Fields of Application. *British Journal of Applied Physics* 1955**,** 6, 391-399.

19. Pease, R.; Nixon, W., High Resolution Scanning Electron Microscopy. *Journal of Scientific Instruments* 1965**,** 42, 81.

20. Danilatos, G., Review and Outline of Environmental SEM at Present. *J. Microsc* 1991**,** 162, 391.

21. Danilatos, G., Introduction to the ESEM Instrument. *Microscopy Research and Technique* 1993**,** 25, 354.

22. Hiller, J. Electron Probe Analysis Employing chi-ray Spectrography 1947.

23. Castaing, R. Application of Electron Beams to a Method of Local Chemical and Crystallographic Analysis. Ph. D. thesis, University of Paris, 1951.

24. Duncumb, P.; Reed, S., In Quantitative Electron Probe Microanalysis (KFJ HEINRICH, ed.), NBS Spec. *Publ* 1968**,** 298, 133.

25. Philibert, J., Proceedings of the 3rd International Conference on X-ray Optics and Microanalysis. 1963.

26. Reed, S., Characteristic Fluorescence Corrections in Electron-probe Microanalysis. *British Journal of Applied Physics* 1965**,** 16, 913.

Chapter 3 Flux Growth of Pure and Mn-Substituted ZnO Crystals

3.1 Introduction

Dilute magnetic semiconductors (DMS) have attracted attention of scientists in recent years. There are some unique properties that enhance their potential for applications in electronic devices. DMS materials are semiconductors with a small fraction of their constituent ions replaced by transition metal ions. These materials have similar properties with their host semiconductors. Ferromagnetic Mn-substituted GaAs is one of the well known DMS materials. The discovery of Mn-substituted GaAs by H. Ohno et al[1] in 1995 promoted numerous studies on DMS. At an optimum low temperature, doped GaAs films with 3-5 at.% Mn have been grown by molecular beam epitaxy (MBE).

Dilute ferromagnetic oxides with Curie temperatures (T_c) exceeding room temperature are attractive compounds[2]. Transition metal substituted compounds, such as ZnO, GaN, and InN are promising materials for high Curie temperature ferromagnetism[3-5]. These frontier materials have novel applications in faster central processing unit chips and high storage density hard drives. The importance of spintronics materials has been explained in several review papers[6-8]. A schematic of possible applications is depicted in Figure 3.1. Such a wide expectation places spintronic materials at the leading edge of microelectronics[6]. New DMS devices exploit spin transistors in mobile phones, optical emitters and non-volatile, semiconductor memories, which have very broad applications.

Most of the initial work on DMS focused on II-VI semiconductors, in which a fraction of group II elements were randomly substituted by Mn atoms[9, 10]. ZnO is one of the proposed spintronic materials, which has a wurtzite structure and E_{gap} = 3.2 eV, exhibits both semiconducting and piezoelectric properties. Due to these unique properties, ZnO can be used in piezoelectric transducers, gas sensors and ultraviolet light emitting diodes. An eventful paradigm shift in this field came with the Dietl's Zener model theoretical prediction; 5 at.% manganese substituted ZnO and GaN, containing $3.5x10^{20}$ holes per cm^3, are promising to attain T_c above 300 K[11]. However, the synthesis of DMS materials with high Curie temperature and sufficient hole carriers is difficult. Sato and Katayama-Yoshida predicted ferromagnetism by *ab* initio calculation in n-type ZnO doped with various transition metals, including Co and Cr, but no ferromagnetism exists in Mn substituted ZnO, which is consistent with experimental results[12, 13].

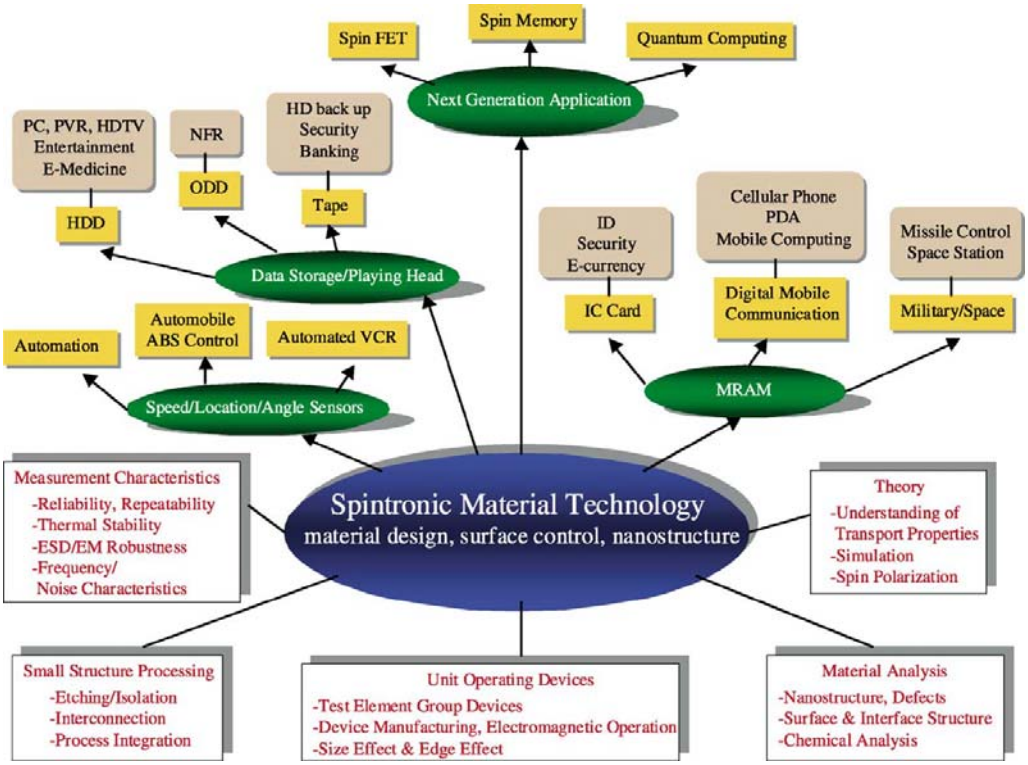

Figure 3.1 Technology tree for spin-based devices and their potential application.[6]

3.2 Structure and Properties of Zinc Oxide

Zinc oxide, ZnO with formula weight (F.W.) 81.369 g/mole, is a metal-oxide semiconductor. It is a multifunctional n-type material with a direct and wide band gap energy (3.37 eV) at room temperature and a high free-exciton binding energy (60 meV).[8, 14] These attractive properties make ZnO a versatile material with various applications for UV-light emitters, piezoelectric transistors, solar cells, and gas sensors. The tetrahedral coordination of ZnO is also a common indicator of sp^3 covalent bonding; however, the Zn-O bond also possesses very strong ionic character. Thus, ZnO lies on the borderline between being classed as a covalent and ionic compound, with an iconicity of f_i=0.616 on the Phillips iconicity scale.[15] The lattice parameters and atomic positions of the hexagonal unit cell are shown in Table 3.1.[16] The peak positions and the corresponding atomic plan are list in the Table 3.2. Figure 3.2 shows the hexagonal ZnO lattice. In this structure, oxygen and zinc atom are in a hexagonal close packed arrangement with space group $P6_3mc$ (No. 186). Its non-centrosymmetry gives rise to piezoelectric properties. The atomic coordination and XRD peaks are listed in

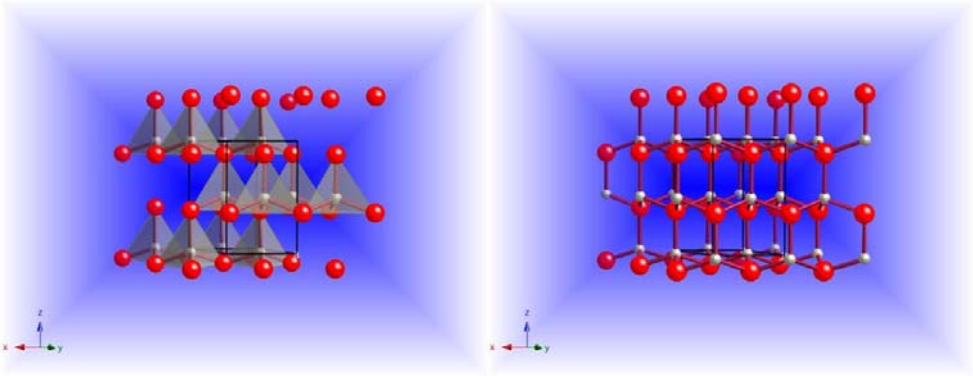

Figure 3.2 Wurtzite crystal structure of ZnO with space group $P6_3mc$ (a) polyhedral representation (b) ball-and-stick representation showing hexagonal structure of ZnO

Metal Zn (gray) is placed in the tetrahedral coordination and surround by four O atoms (red).

Table 3.1 The unit cell parameters and atom coordinates.

	x	y	z	*occ.*
Zn	1/3	2/3	0	1
O	1/3	2/3	0.3821	1
a = 3.2495 Å, c = 5.2069 Å, and γ = 120˚				

Table 3.2 A list of peaks position and corresponding atomic plans (*h, k, l*) from JCPDS 36-1451.

2θ (˚)	Intensity	h	k	l	2θ(˚)	Intensity	h	k	l
31.770	57	1	0	0	95.304	6	2	1	1
34.422	44	0	0	2	98.613	4	1	1	4
36.253	100	1	0	1	102.946	2	2	1	2
47.539	23	1	0	2	104.134	5	1	0	5
56.603	32	1	1	0	107.430	1	2	0	4
62.864	29	1	0	3	110.392	3	3	0	0
66.380	4	2	0	0	116.279	8	2	1	3
67.963	23	1	1	2	121.572	4	3	0	2
69.100	11	2	0	1	125.188	1	0	0	6
72.562	2	0	0	4	133.932	3	2	0	5
76.955	4	2	0	2	136.520	1	1	0	6
81.370	1	1	0	4	138.513	2	2	1	4
89.607	7	2	0	3	142.918	3	2	2	0
92.784	3	2	1	0					

3.3 Experimental Methods

The growing conditions of ZnO crystals from various fluxes, such as oxides (V_2O_5, MoO_3, WO_3, and B_2O_3) and hydroxides (KOH, NaOH or both) will be discussed. Like other oxide powders, ZnO powder is not air sensitive. For this reason, all experiments were prepared at ambient conditions. The several experimental conditions used for growing ZnO crystals are given in appendix I. A CM muffle furnace with $MoSi_2$ heating elements was used. The reaction conditions, phase diagrams and quantity of Mn substitution in the ZnO crystals were determined by X-ray diffraction (PANalytical PW and PANalytical PW 3830) and scanning electron microscopy (SEM) (Zeiss DSM 940 and Zeiss FESEM Supra 55 VP) with energy-dispersive spectroscopy (EDS) (PGW and EDAX).The magnetic property was studied by the Superconducting Quantum Interference Device (SQUID) magnetometer.

3.3.1 Pure ZnO Crystal Growth from ZnO-V_2O_5 System

Pure ZnO crystals were synthesized by heating the mixture of ZnO powder (99.0% Alfa-Aesar) and V_2O_5 powder (99.2%) in an alumina crucible or iron crucible at 1300 °C, and then slowly cooled to room temperature.

3.3.2 Pure ZnO Crystal Synthesis form ZnO-B_2O_3 System

Pure phase crystals were carried out from the ZnO-B_2O_3 system. The precursor mixture of ZnO and B_2O_3 (99.985% Alfa-Aesar) were mixed well using an agate mortar and pestle. The ZnO-B_2O_3 system, used for pure ZnO crystal growth, has been reported in previous literature[17]. The mixture, packed in a 110 ml platinum

crucible, was heated at 1300 °C for 40 hours and then slowly cooled. The solidification temperature was previously reported at 1160 °C. However, the reaction showed the solidification temperature to be 1045 ºC. After sintering, a powder X-ray diffractometer was used for phase identification.

3.3.3 Mn-substituted ZnO Polycrystalline

Mn-substituted ZnO polycrystalline samples were prepared by solid state reactions. Varying Mn concentrations from 1.7 at.% (reaction CMF 24 A) to 37. at.% (reaction CMF 24 D) were added to ZnO. Mn_2O_3 (powder 99% Alfa-Aesar), the Mn source, was mixed and ground well in a mortar. After grinding, the mixture was pelletized using a die plunger at 5000 psi. Four pellets, each with a different Mn concentration, were place on platinum foil and left at the center of a muffle furnace. The temperature reached the sintering temperature of 1300 °C at 220 °C/hr from room temperature. Once the system reached 1300 °C, it dwelled for 10 hours and ramped down to room temperature at 250 °C/hr.

3.3.4 Pure Hexagonal Prism ZnO Single Crystal from NaOH Flux

Our group had synthesized pure ZnO crystals from NaOH flux for the first time in CMF 26C. Starting materials consisted of ZnO 1.01 g (0.0122 mole) and NaOH 4.88 g (0.122 mole) (Spectrum) in a lidded alumina crucible. A muffle furnace was used for the reaction. The mixture heated up to 750 °C in 7.25 hours and dwelled at 750 °C for ten hours. The reaction temperature slowly cooled down to 600 °C

within 136.4 hours and then dropped to room temperature with the furnace power shut off.

3.3.5 Mn-substituted ZnO Single Crystal Synthesis from NaOH Flux

Mn-substituted ZnO single crystal synthesis (CMF 34_2), NaOH flux was used for the crystal growth in a Pt crucible and sealed Ag tubes. For the growth in a Pt crucible, host lattice material, ZnO 1.13 g (0.0137 mole), was mixed with Mn source $MnCO_3$ 1.27 g (0.01 mole) in an agate mortar pestle, and then packed in a platinum crucible with NaOH 5.48 g (0.137 mole). A pendulum type heating profile was applied in this reaction. The reaction took place in a muffle furnace at peak temperature of 500 ˚C and dwelled for 20 hours.

Nominal composition $Zn_{0.95}Mn_{0.05}O$ single crystal synthesis was carried out from NaOH flux technique in sealed silver tubes. The starting material, $Zn_{0.95}Mn_{0.05}O$, was previously sintered by solid state reaction at 1300 ˚C. It was heated to 1300 °C at 100 ˚C/hr, dwelled at this temperature for 60 hours and cooled down to room temperature. NaOH flux was dehydrated at 500 ˚C under vacuum. All reaction tubes were annealed at 750 ˚C under Ar gas for 6 hours. Precursors were placed in an annealed silver tube, welded closed and then placed in a stainless steel bag. All reaction tubes were placed in a furnace, heated to 500 ˚C and held at 500 ˚C for 60 hours, cooled down to room temperature at 8 ˚C/hr, and at room temperature, NaOH flux was removed by water.

3.3.6 SEM Sample Preparation

Due to non-uniform diffusion of manganese in the entire crystal, the crystal was polished to study manganese distribution. We had cut 1/2 in. rubber tubing with a 1/2 in. inner diameter. The tube was filled in with epoxies, A and B, in a 1:1 ratio. Crystals were spread in the center. A 20 μm MD-Plaw Pad was used for flattening the sample surface. Then it was roughly polished with 12 μm alumina polishing compound. After this rough polishing, fine polishing was carried out using by 5μm alumina and 1μm diamond polishing compounds. The SEM sample was fixed on the SEM sample pin. Silver paint was applied to the surface for good electrical contact around the sample.

3.4 Results and Discussions

3.4.1 Phase Diagram

The phase diagram is from an equilibrium pressure-temperature-composition system. A two component, temperature versus composition phase diagram provides information, such as composition, eutectic temperature and phase change to choose a favorable reactive environment. Although a phase diagram is valuable, the boundary conditions of phase diagrams are not reliable due to differences in the experimental conditions or poorly characterized phase boundaries and liquidus temperature.

3.4.2 Pure ZnO Crystal Growth form ZnO- V_2O_5 System

The ZnO – V_2O_5 phase diagram (Figure 3.3) reveals crystal growing conditions.[18] There is a ZnO phase area shown in the temperature versus composition phase diagram. In this binary phase diagram, the ZnO crystal growth working area, above eutectic temperature 910 ˚C and composition with greater 75 mol% ZnO, is identified. Moreover, there were some limitations of having high vapor pressure, low separability and reaction of V_2O_5 with the porous Al_2O_3 crucible (Figure 3.4).[19] These reasons make the composition shift to the more ZnO rich region. An iron crucible had also been tried, but vanadium oxide reacts severely with the iron crucible. Thus V_2O_5 is not a good flux for our ZnO crystal synthesis.

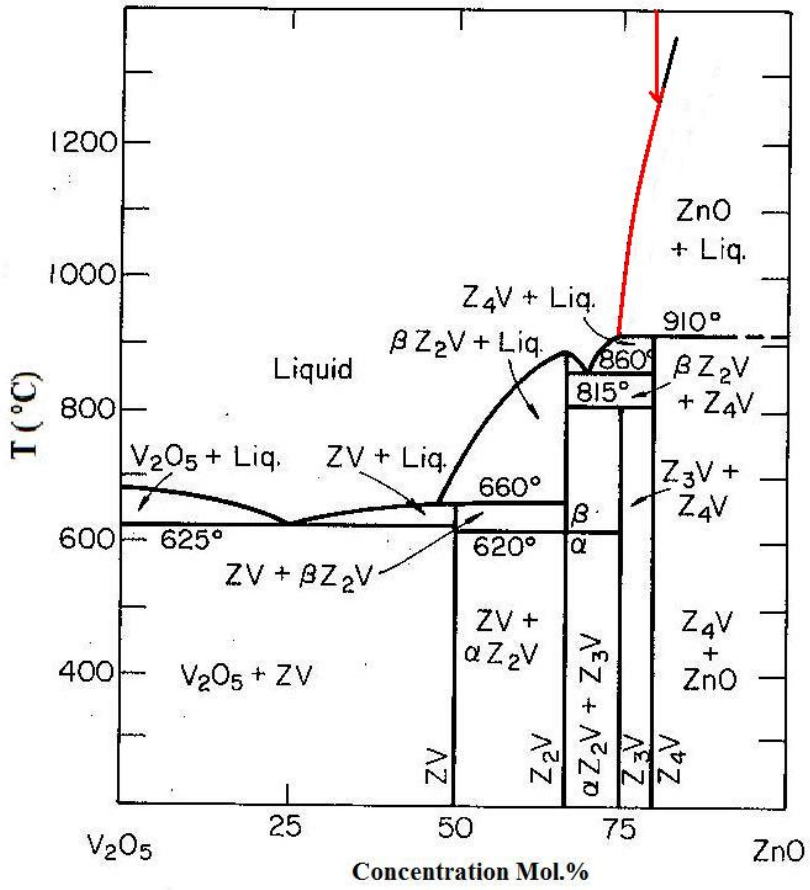

Figure 3.3 Temperature vs. composition ZnO – V_2O_5 binary phase diagram. The red arrow indicates the starting composition of ZnO crystal growth. In order to investigate the growth of ZnO crystals, 0.85 mol % ZnO and 0.15 mol% V_2O_5 were utilized. (Ref.18)

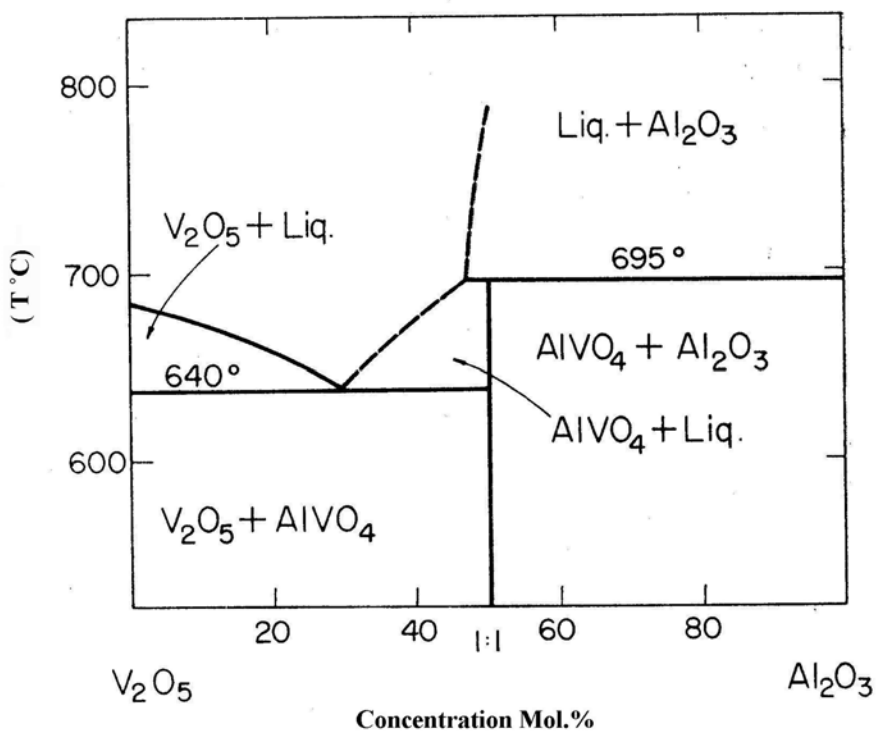

Figure 3.4 Temperature vs. composition phase diagram of V_2O_5 and Al_2O_3. It shows that $AlVO_4$ is the compound of V_2O_5 flux and Al_2O_3 crucible. (Ref.19)

In Wanklyn's letter,[20] crystal growth was carried out within the ratio 3·ZnO: V_2O_5 or 2.8·ZnO: V_2O_5 using a platinum crucible at growing temperature of 1300 ˚C. However, at the composition 3.2 ZnO:V_2O_5, the starting material ZnO was not dissolved completely at 1300 ˚C. This indicates that the melting point of the mixture is greater than 1300 ˚C. ZnO crystal growth didn't occur when the composition 2.5·ZnO:V_2O_5 was used. Comparing the previous report with currents observations, crystal growth was not located at the optimal composition, and a different container was used. A V_2O_5 and Al_2O_3 temperature-composition phase diagram in Figure 3.4 reveals the reaction of V_2O_5 with the crucible.

3.4.3 Pure ZnO Crystal Growth from ZnO- B_2O_3 System

Although B_2O_3 is a good flux to grow oxide crystals, there are several challenges and difficulties to work with this flux to grow ZnO. Similar to other oxide fluxes, it may form one or more oxide phases. Most of these oxide compounds have similar properties as the target ZnO crystal, so it is hard to separate ZnO crystals from other oxide fluxes. From the ZnO- B_2O_3 binary phase diagram (Figure 3.5), the phase space available for ZnO crystal growth is a region with a composition greater than 77 mol% ZnO and temperatures above the peritectic temperature of 1045 ˚C [17, 21, 22].

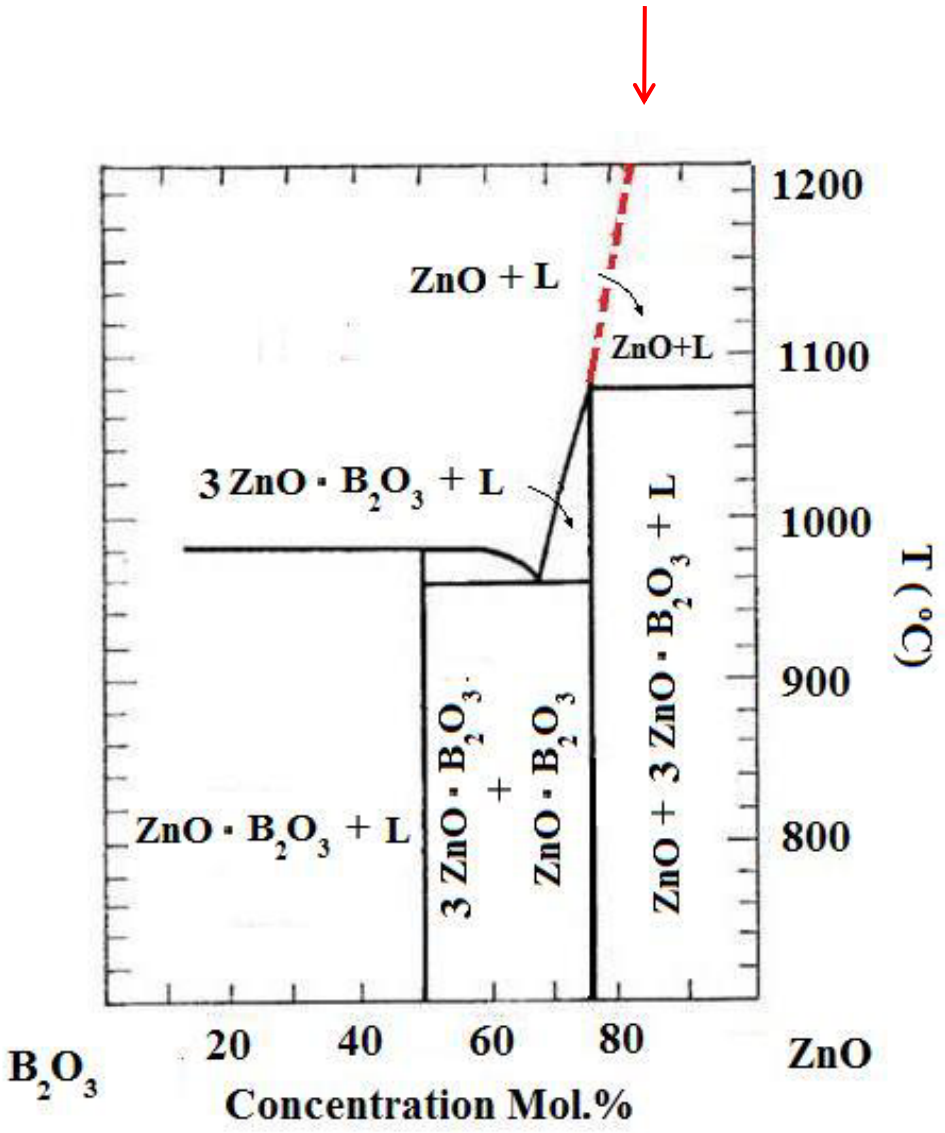

Figure 3.5 B_2O_3 is a frequently used flux for ZnO crystal. This ZnO-B_2O_3 binary phase diagram shows the ZnO phase available area. The red arrow indicates the starting composition for crystal growth. The mixture with 82 mol % ZnO heated up to 1300 ˚C and then slowly cooled down to 1045 ˚C. (modified from the Ref. 22)

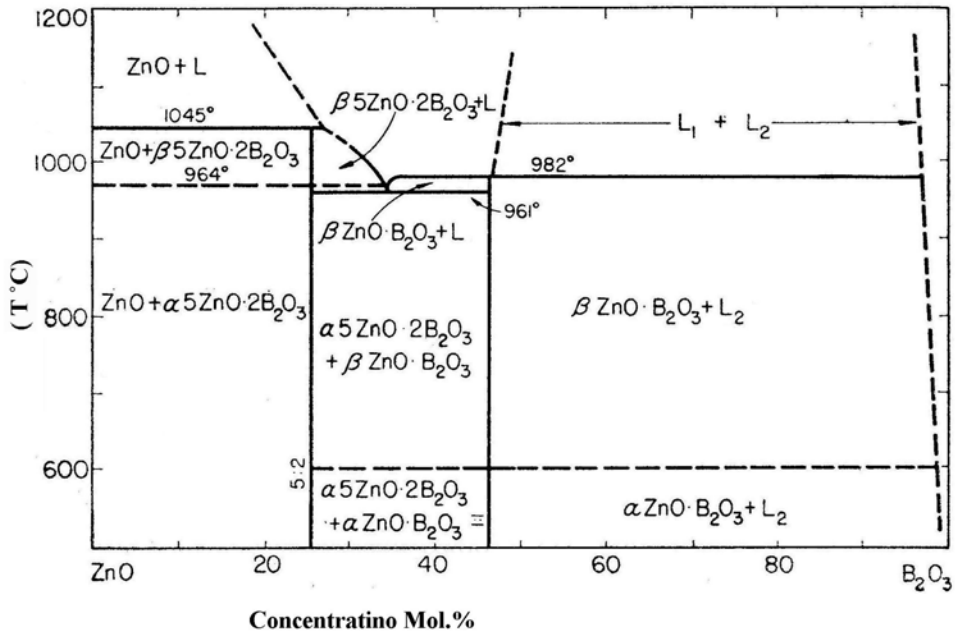

Figure 3.6 ZnO and B_2O_3 temperature vs. composition binary phase diagram reveals the minimum crystal growth temperature, 1045 ˚C. (Ref. 21)

While the temperature for ZnO crystal growth reported by Harrison[17] (Figure 3.6) doesn't match our observation, according to Leonov's phase diagram (Figure 3.5),[22] the phase transition temperature between ZnO+ liq. and ZnO+ 3ZnO. B_2O_3 is about 1080 ˚C. Kunihiko Oka *et. al.*[23] reveals the lowest growing temperature is 1045 ˚C. An initial mixture of ZnO: B_2O_3 in the ratio of 4.56:1 was heated to 1300 ˚C and cooled to 1165 ˚C. After pouring out most of the flux at 1165 ˚C, pale green, plate-like ZnO crystals were observed at the bottom of the platinum crucible (Figure 3.6). To remove the $Zn_3B_2O_6$ flux, the platinum crucible with ZnO and $Zn_3B_2O_6$ crystals were put in opposite position in the furnace at 1300 ˚C. After decanting, both plate-like ZnO and $Zn_3B_2O_6$ ($3ZnO:B_2O_6$) crystals were obtained.

Figure 3.7 ZnO crystal growth with 18 mol % B_2O_3 as a flux at 1300 ˚C. Two liquid systems are shown. Due to density differences, the ZnO rich side settles down at the bottom of the platinum crucible. The borate ($Zn_3B_2O_6$ JCPDS 37-1486) is found on the top. (CMF 26C)

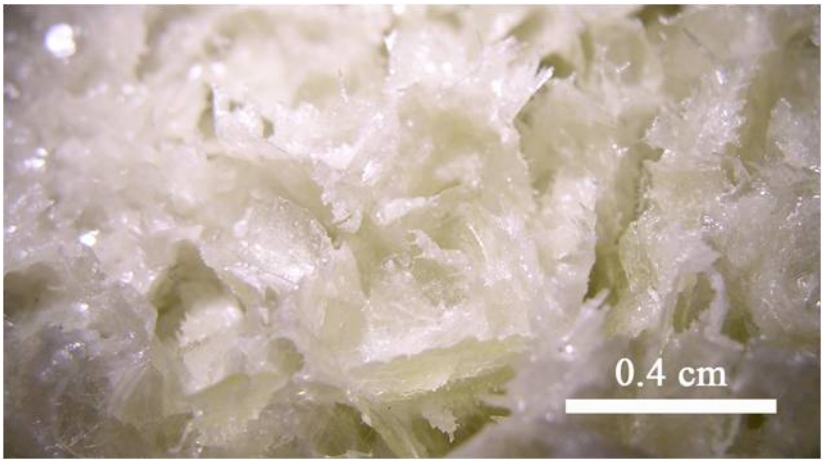

Figure 3.8 Magnified view of plate-like pure ZnO crystals grown from a ZnO-B_2O_3 system. (CMF 26C)

The product was examined by powder XRD, where ZnO was observed in addition to a small amount of crystallized flux (Figure 3.7). The X-ray powder pattern of the crystals (Figure 3.8) matched ZnO (JCPDS 36-1451) very well, while the crystallized flux was identified as zinc borate ($Zn_3B_2O_6$). With the chemical and physical properties of zinc borate and ZnO being similar, the different crystals are not easily separated from this flux by chemical means.

Flux growth of ZnO has been previously demonstrated by many research groups in V_2O_5, PbF_2, B_2O_3, and WO_3[17, 21, 24, 25]. Desirable fluxes, particularly in oxide crystal synthesis, are those which significantly decrease the growing temperature. These molten fluxes encourage crystal growth, but restrictions placed on vapor pressure, solubility, and etching must be taken into account. None of the aforementioned fluxes are ideal for such reasons: V_2O_5 and WO_3 have high vapor pressure, PbF_2 and B_2O_3 form low solubility fluxes and the ZnO crystal can not be separated from PbF_2.

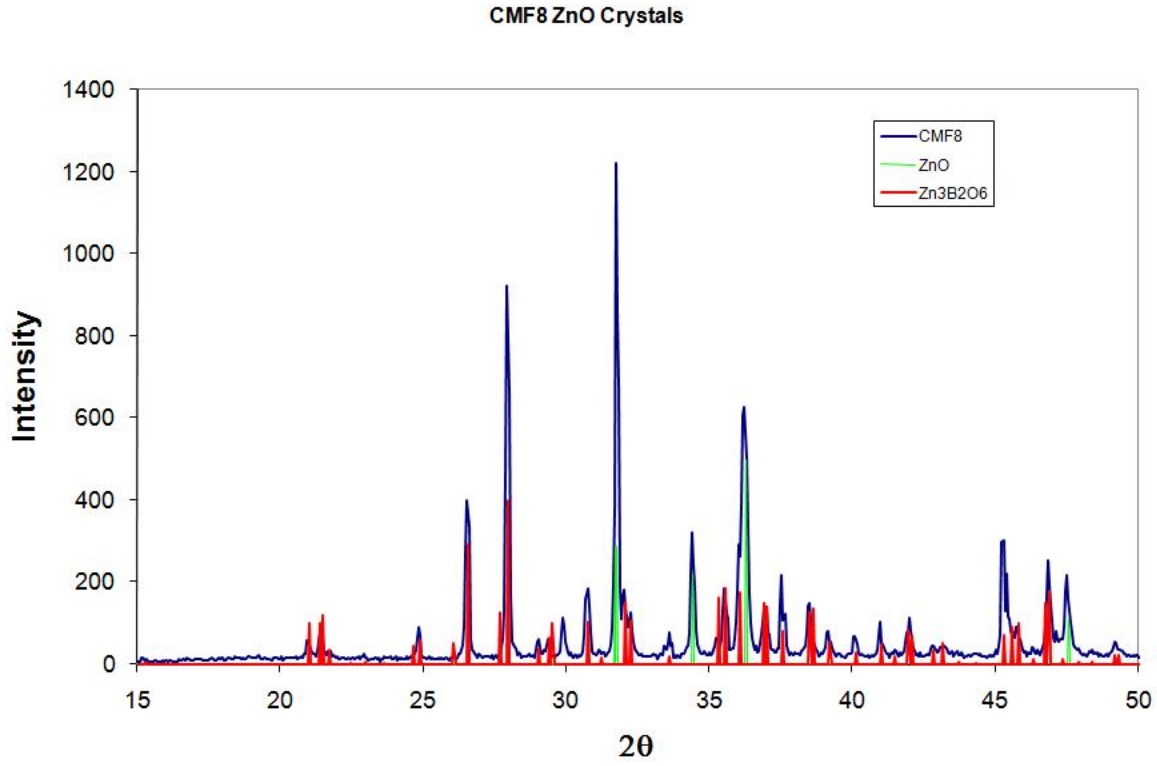

Figure 3.9 Powder XRD pattern of plate-like ZnO (JCPDF 36-1451) with $Zn_3B_2O_6$ (JCPDF 37-1486) flux. (CMF 8)

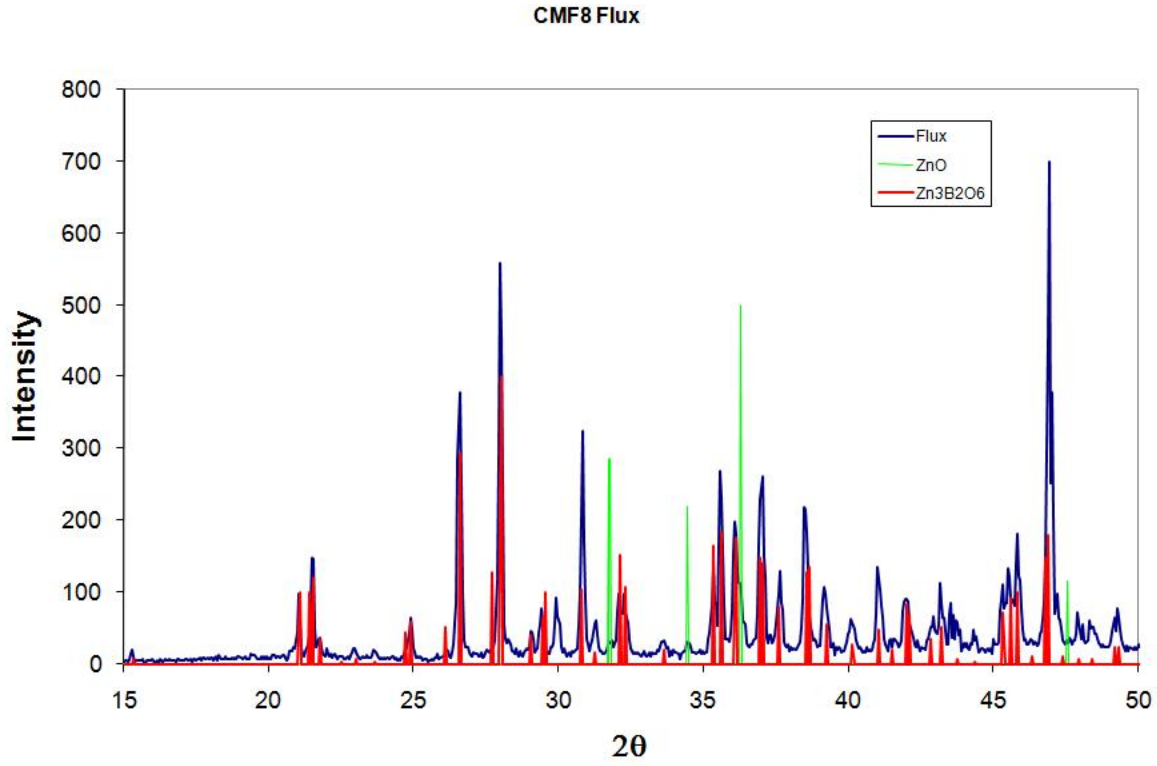

Figure 3.10 Powder pattern of flux $Zn_3B_2O_6$ ($3ZnO: B_2O_3$) (JCPDF 37-1486) with a small amount of ZnO (JCPDF 36-1451). (CMF 8)

3.4.4 Pure ZnO Single Crystals from NaOH and KOH Fluxes

This study describes the NaOH flux method to grow ZnO crystals. Both in terms of ease of separation of the flux from the crystals and the quality of the ZnO morphology; the NaOH and KOH fluxes are superior to previously explored fluxes. For this reason, Mn substituted ZnO crystals are also grown from the hydroxide flux.

Previously reported hydrous NaOH and hydrous KOH melts, in which the amount of H_2O was initially around 30 wt.%, were found to produce ZnO crystals with prismatic or needle-like morphology[26, 27]. However, plate-like morphology was observed for ZnO grown from ZnO:NaOH:LiOH:H_2O with molar ratios of 1:4.5:1.3:6[28]. For our synthesis conditions, in order to confirm negligible role of water, we chose a temperature above the dehydration temperature, but at a temperature with limited decomposition of NaOH. The NaOH has a few weight percent of water present in the pellets. Thermogravimetric analysis of NaOH with original mass 70.532 mg is shown in Figure 3.11. The physisorbed and chemisorbed water dehydration starts when the temperature reached 100 °C. After 400 °C, the NaOH starts to decompose. After 6 hours at 500 °C, nearly all adsorbed or dissolved water was lost forming anhydrous, molten NaOH[29]. The process can be described as following: most of the adsorbed water evaporates just above 100 ˚C; then the NaOH melts around 318 ˚C, which still contains some dissolved water in molten NaOH; then it dissolves in the NaOH and evaporates after a few hours at 500 ˚C.

The dehydration of NaOH involved two conjugated process:

$$NaOH \cdot H_2O \rightarrow H_2O + NaOH \text{ (dehydration)} \quad (1.1)$$

$$NaOH \rightarrow Na_2O \text{ (decomposition)} \quad (1.2)$$

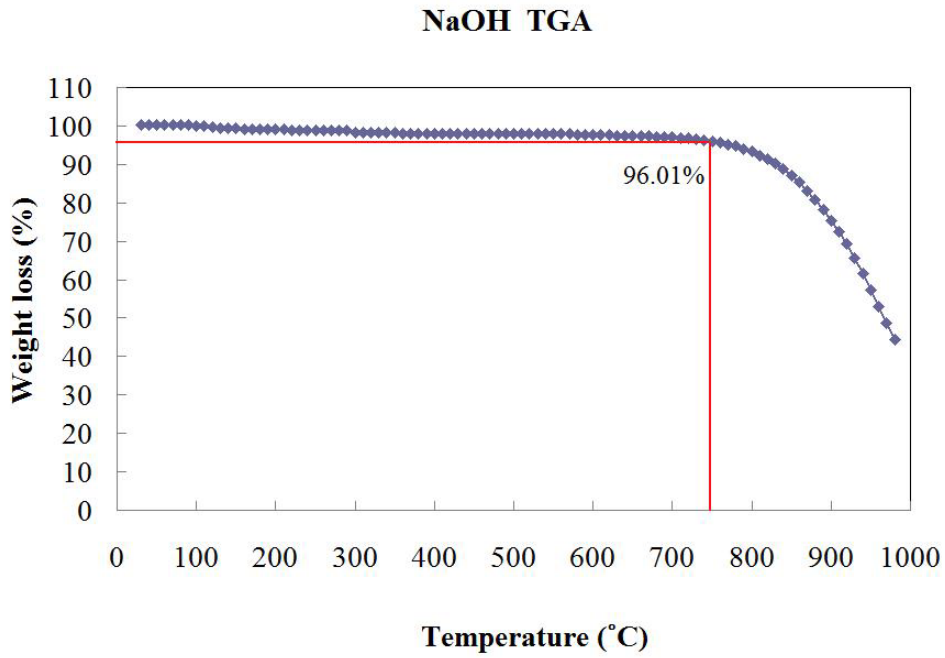

(A)

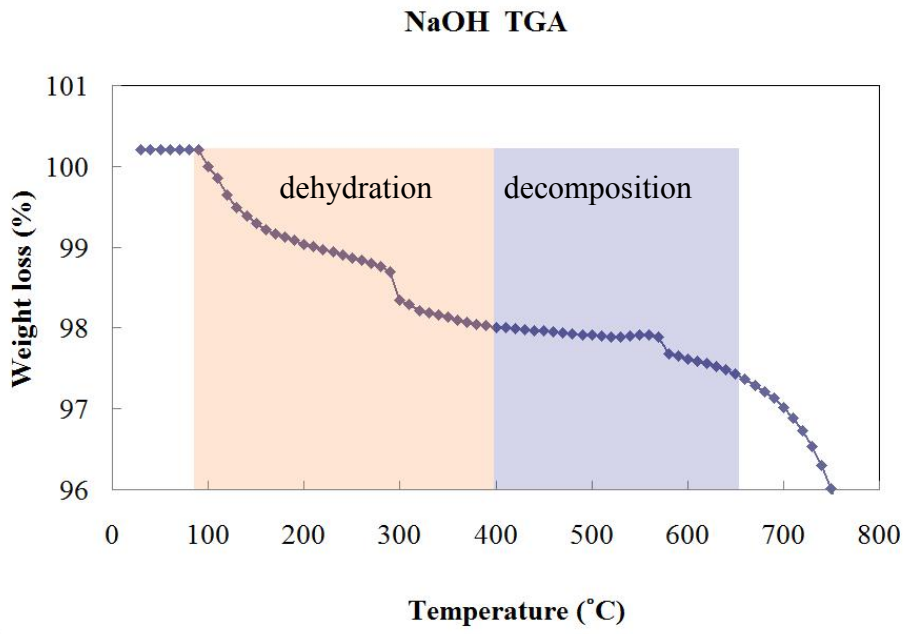

(B)

Figure 3.11 Thermogravimetric analysis of 70.532 mg NaOH by the heating rate 10 ˚C/min. (A) full spectrum (B) magnified view.

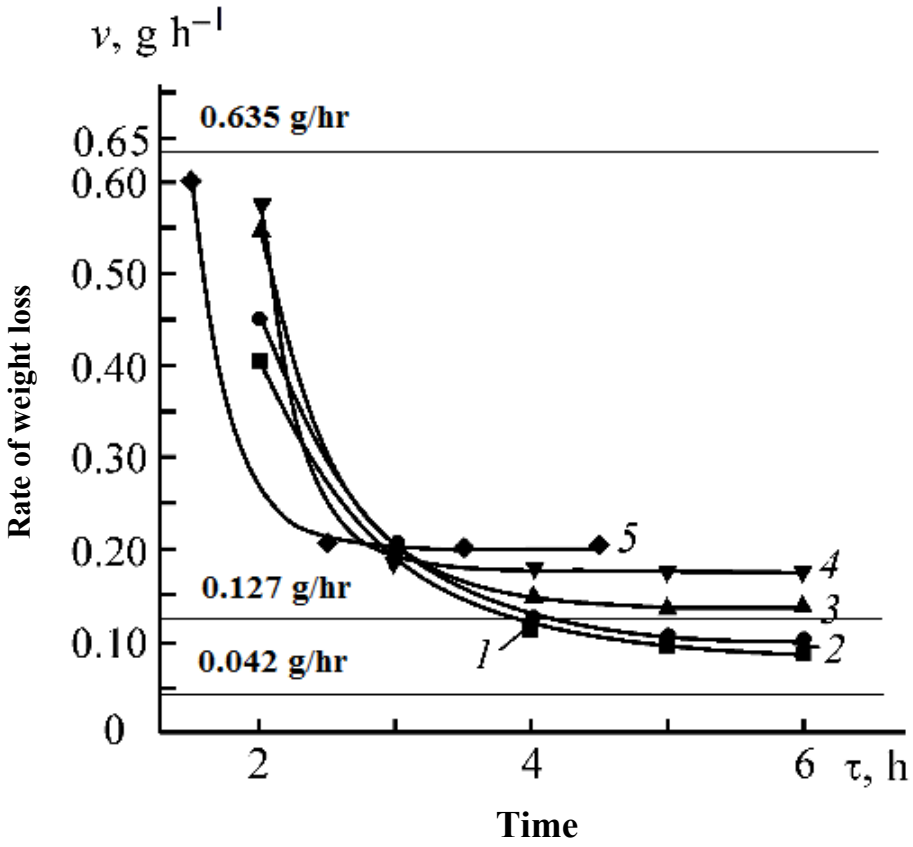

Figure 3.12 Time dependent NaOH dehydration rate at different temperatures (1) 750 K (2) 773 K (3) 823 K (4) 873 K (5) 906 K. Three lines indicate the incident dehydration rate from our NaOH TGA data. The initial rate was 0.635 g/hr. When heated to 500 ˚C and 750 ˚C, the rates became 0.127 g/hr and 0.0423 g/hr, respectively. (modified from ref. 28)

In various mole ratios of NaOH: ZnO (1:1, 5:1, 10:1, 50:1) and KOH: ZnO (3:1, 10:1, 20:1, 50:1), we found that the 10:1 composition gave the best crystal morphology and size. The ZnO single crystals exhibited symmetrical, hexagonal prismatic habit, which was observed by SEM imaging (Figure 3.12).[28] The dehydration rate at 200˚C is roughly 0.03 g/hr. A pendulum temperature profile for

reducing the number of seeds was used in some experiments. Based on 20 experiments with various dwelling times varying from 1 to 48 hr, and temperatures of 500 ˚C and 750 ˚C, we found that crystal size and morphology are not correlated to the variables in the pendulum heating profile. Although the crystal dimensions show no significant change, thin hexagonal prisms were aggregated into bundled needles in a pendulum heating profile.

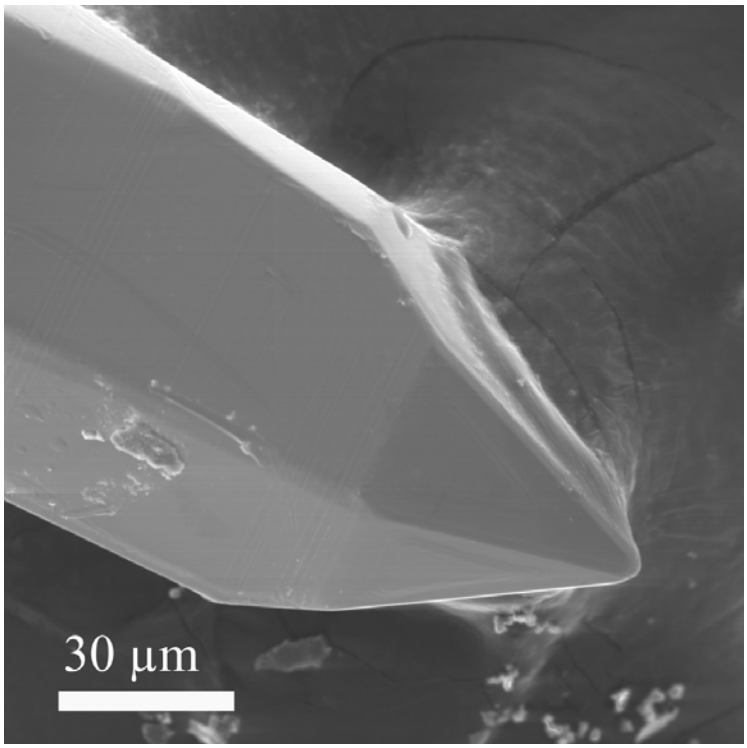

Figure 3.13 Needle like ZnO single crystal in the NaOH flux growth shows wurtzite ZnO structure. There is no adhered NaOH observed after water washing. (CMF 26C)

3.4.5 Mn-substituted ZnO single crystal from NaOH flux

In order to substitute Mn in the ZnO crystal, an initial mixture of ZnO and $MnCO_3$ was used as a Mn source. The starting material for the manganese substitution, $MnCO_3$, decomposes around 200 ˚C to form MnO[30]. The oxygenation of MnO at moderate temperature, 500 ºC-1050 ˚C, gave rise to a mixed valence Mn compound, Mn_2O_3, which has been discussed by Zaki et al.[31]. The Mn (II) and Mn (III) are the predominated species of the substituent. Short hexagonal prisms of ZnO, exhibiting yellowish orange color, were observed. Various colors, including green, orange and transparent Mn- substituted ZnO crystals, are demonstrated here (Figure 2.13). Because of manganese distribution, manganese does not separate uniformly.

From the EDS spot analysis on Mn-substituted ZnO, there is no preferential trend of Mn distribution crossing over the crystal. Mn concentration was detected in a light orange crystal from 0 at.% to 5 at.% (Figure 3.14, 3.15 and 3.16) for an initial Mn concentration of 35 at.%. The average Mn concentration in 130 EDS data points is 1.54 at.% (Figure 3.14 A). Figure 3.15 showing no preference Mn distribution, a small dark area has a higher Mn concentration above 5 at.%. It is due to the higher Mn inclusion.

Mn-substituted ZnO single crystals were also synthesized in a sealed sterling silver tube. The precursor, $Zn_{0.95}Mn_{0.05}O$ powder sample was synthesized at 1300 ˚C. NaOH was dehydrated at 200 ˚C overnight. The orange color single crystals were obtained when the NaOH flux was removed. The average of crystal size is 10 μm, which is shown by the FESEM image (Figure 3.17) and optical microscope photo (Figure 3.17). Investigation of Mn concentration in Mn-substituted ZnO crystals is

exhibited by EDS data. The mean Mn ratio among 4 EDS spot analysis is 4.11 at.% with original 5 at.% Mn. (Table 3.3)

Table 3.3 EDS spots analysis for CMF 91 (Figure 3.17).

Spot position	Mn (at.%)	Zn (at.%)
1	5.20	94.80
2	2.63	97.37
3	4.09	95,91
4	4.51	95.49
Average	4.11	95.89

Diffusion of impurities in the semiconductor melt extensively affects crystal growth process. The dopant distribution depends on the dopant concentration in the melt around the materials. According to previous publications about the impurity in the semiconductor melt.[32] The dopant concentration in the melt near the crystal surface decreases with reaction time. There are some other factors to affect the dopant diffusion such as crystal melting speed and the diffusion coefficient of impurity in the melt. These are significant features for the dopant diffucient in the crystals. After the dopants diffuse into the materials from the melt, the diffusion in the solid become a significant.

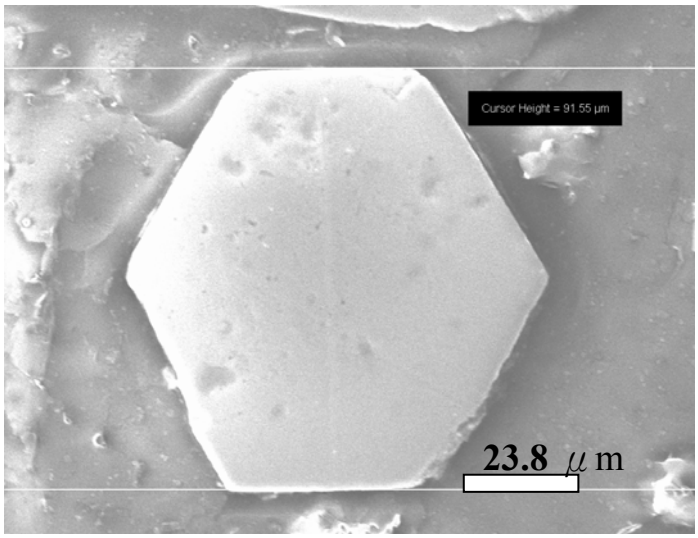

(A)

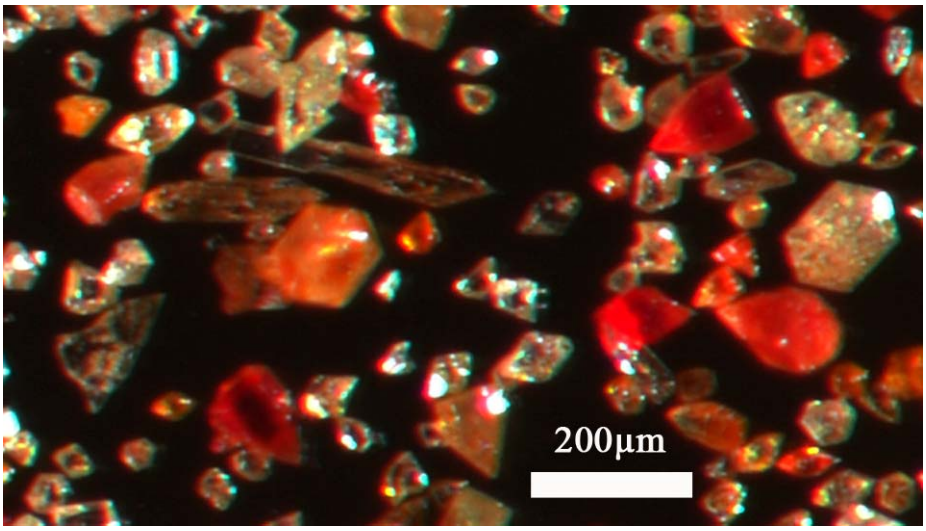

(B)

Figure 3.14 Mn-substituted ZnO single crystals (CMF 34_2) prepared by NaOH flux technique. (A) SEM and (B) optical image Orange ZnO are the desired crystals. There were many various color distributions.

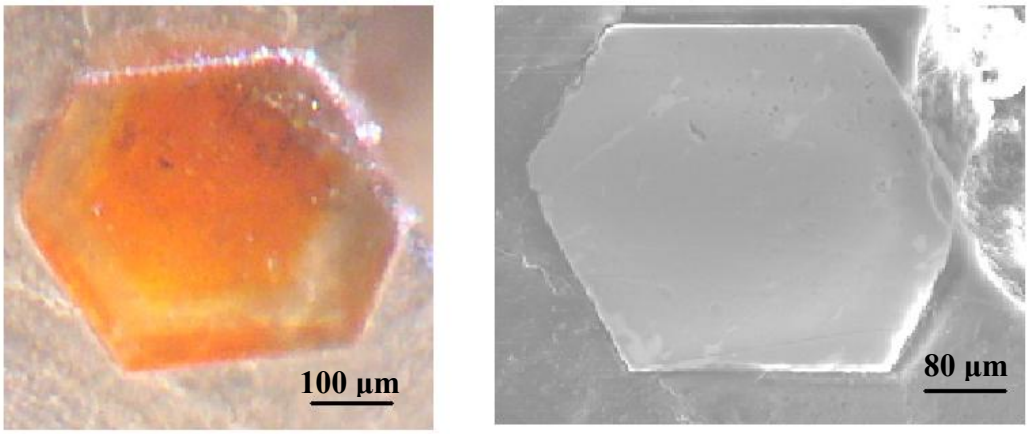

Figure 3.15 A Mn-substituted ZnO single crystal. The circle indicates the area with higher Mn concentration due to an inclusion, presumably of ZMn_2O_4. (CMF 34_2)

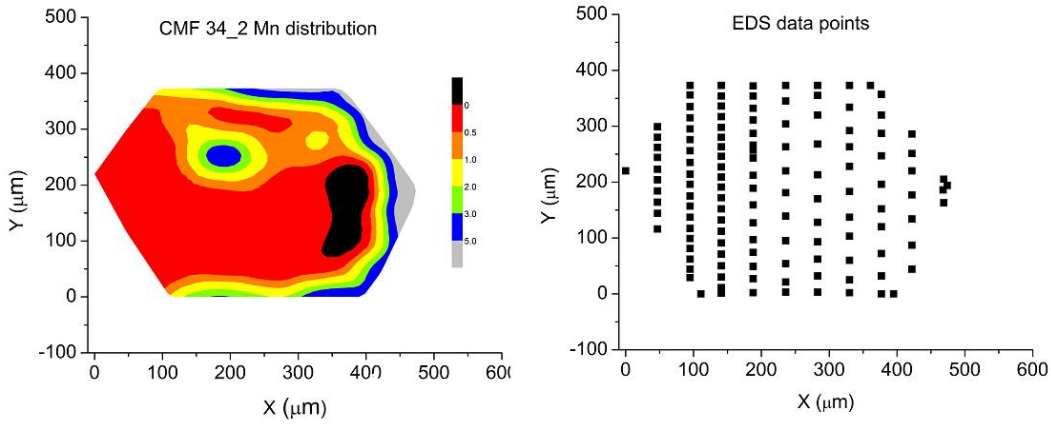

Figure 3.16 The EDS data of Mn-substituted ZnO orange single crystal reveals mostly uniform Mn distribution except for inclusion and edge effects. The average Mn concentration is about 0.5 at.%. (CMF 34_2)

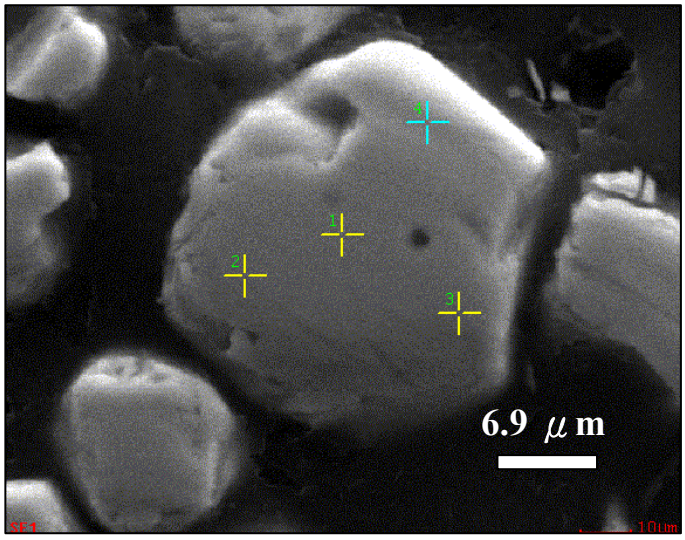

Figure 3.17 FESEM image of Mn-substituted ZnO single crystals. The EDS data reveals the average of Mn concentration is 4.11 at.%. (CMF 91)

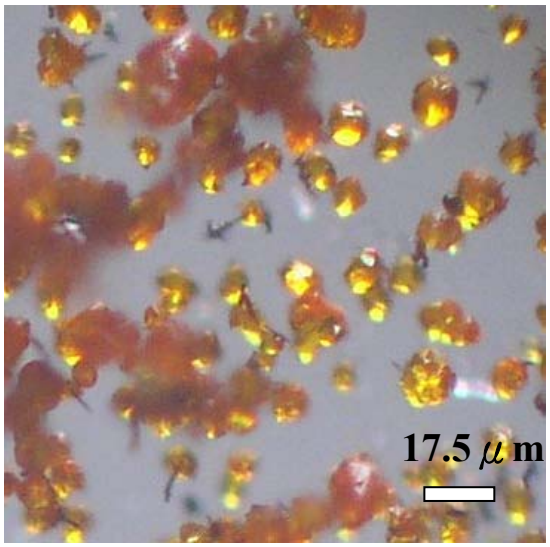

Figure 3.18 Optical microscope image of Mn-substituted ZnO single crystals (CMF 91) from NaOH flux synthesis. The average crystal size is 10 μm.

3.4.6 Manganese-substituted ZnO polycrystalline powder

Polycrystalline samples of ZnO containing different proportions of Mn were prepared by solid state reaction of Mn_2O_3 and ZnO at 1300 ˚C. The products were of reddish-brown color, and the color is enhanced from light to dark with the increase in Mn concentration. The powder XRD patterns of the prepared sample are shown in Figure 3.18. The powder XRD pattern, containing higher than 5.46 at.% Mn, shows an additional identified phase of $ZnMn_2O_4$ (JCPDS 18-1484). The peaks due to this phase are further enhanced in XRD patterns of increased Mn_2O_3 concentrations (Figure 3.18). This indicates that the saturation limit for Mn substitution is around 5.46 at.%. The spinel structures, $Zn_xMn_{3-x}O_4$ and $ZnMnO_3$, were also previously observed in Mn-substituted ZnO[33-35]. For Mn concentrations below 5 at.%, the unit cell parameters a and c of polycrystalline ZnO increase with an increasing manganese ratio from 3.2528 Å and 5.2113 Å (ZnO starting material) to 3.2614 Å and 5.2209 Å ($Zn_{94.54}Mn_{5.46}O$), respectively (Figure 3.19). The unit cell volume exhibits a similar increasing trend from 47.753 $Å^3$ (ZnO starting materials powder) to 48.093 $Å^3$ ($Zn_{94.54}Mn_{5.46}O$). Unit cell parameters for various Mn substituted compositions are shown in Table 3.4. Similar unit cell parameter variations in Mn substituted ZnO have been reported in earlier literature[36-38]. Common reported unit cell variations for Mn substituted ZnO, prepared by such high temperature reactions, are: (0 at.% Mn a = 3.2486 Å c = 5.2045 and 5 at.% Mn, a = 3.2552 Å c = 5.2115 Å), (0 at.% Mn a = 3.249 Å, c = 5.206 Å and 6 mol.% Mn, a = 3.250 Å, c = 5.224 Å) and (0 at.% Mn a = 3.2501 Å c = 5.2065 Å and 5 at.% Mn a = 3.2556 Å c = 5.2095 Å)[36-38]. The present observed unit cell parameters are in agreement with these previous investigations. In such substituted solid solutions, the unit cell volumes were increasing with further

increasing nominal Mn concentration. However, the maximum unit cell volume was 48.093 $Å^3$ (5.46 at.% Mn), which was higher than previous results of 47.82 $Å^3$ (8 at.% Mn), 47.82 $Å^3$ (5 at.% Mn) and 47.79 $Å^3$ (6 at.% Mn).

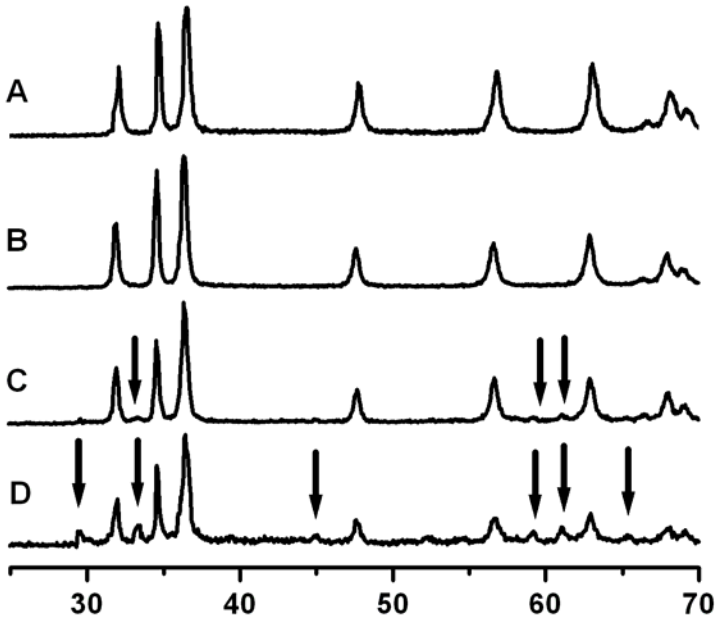

Figure 3.19 ZnO-$MnCO_3$ polycrystalline sample XRD powder pattern. (A) 1.72 (B) 5.46 (C) 18.36 (D) 37.13 at.% Mn. Peak shift is observed with increasing Mn concentration. When the Mn concentration is above 5 at.%, the secondary phases, spinel $ZnMn_2O_4$ (JCPDS-18-1484), separated beside ZnO. (CMF 24A, CMF 24B, CMF 24C, and CMF 24D)

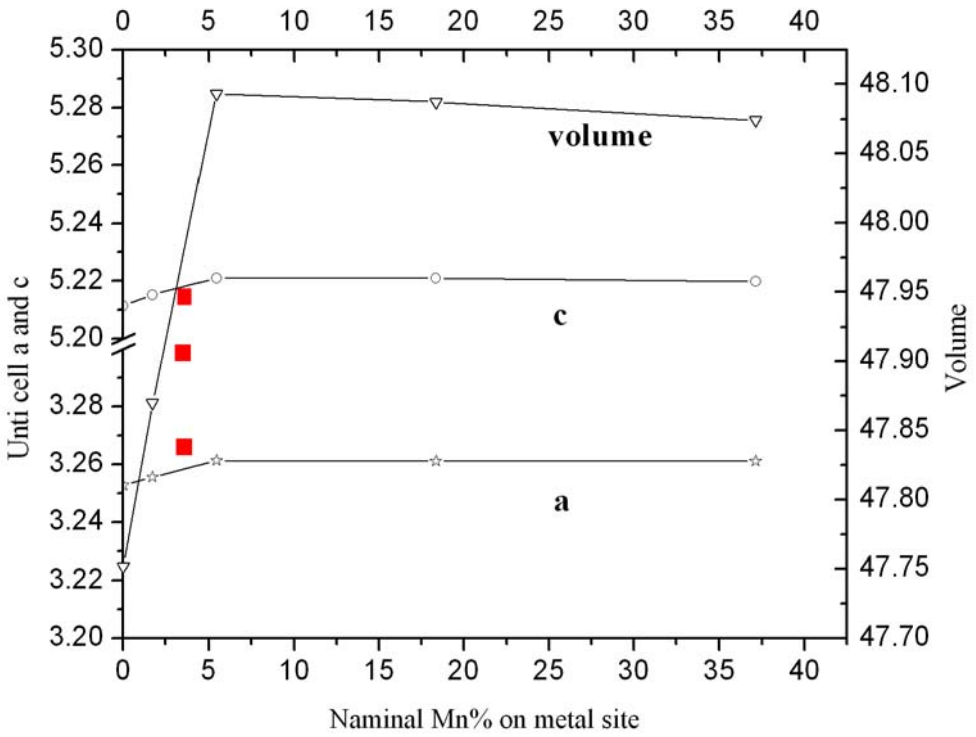

Figure 3.20 Unit cell parameters and volume (☆*a*, ○*c*, and ▽ V) of starting materials, ZnO and polycrystalline samples of Mn-substituted ZnO, versus nominal Mn at.% on metal site. The solid markers indicate natural zincite lattice parameters and volume. (CMF 24A, CMF 24B, CMF 24C, and CMF 24D)

Table 3.4 Unit cell parameters for various Mn substituted ZnO compositions.

Reaction	Hexagonal	*a* (Å)	*c* (Å)	Volume
Starting material	ZnO	3.2528	5.2113	47.753
CMF 24A	$Zn_{0.982}Mn_{0.017}O$	3.2556	5.2152	48.871
CMF 24B	$Zn_{0.94}Mn_{0.053}O$	3.2614	5.2209	48.093
CMF 24C	$Zn_{0.83}Mn_{0.17}O$	3.2612	5.2209	48.086
CMF 24D	$Zn_{0.63}Mn_{0.37}O$	3.2611	5.2198	48.075

3.4.7 Naturally occurring Mn-substituted ZnO crystal

Sedimentary deposits form in an aqueous medium (seawater, lake water, or a hot spring) with temperatures in the range of 70 to 350 ˚C, and sometimes higher[39]. Zinc ore, such as franklinite ($(Zn)(Fe,Mn)_2O_4$), willemite (Zn_2SiO_4), and zincite (ZnO), from Franklin and Furnace-Sterling Hill, New Jersey are notable examples of hydrothermally grown Mn substituted minerals[40]. Here, we investigated the natural zincite mineral from the Ogsdenburg district, near Franklin, New Jersey.

The natural Mn-substituted ZnO mineral exhibited 3.5 at.% Mn substitution by EDS, and no additional elements were substituted into the zincite, as observed by EDS. The XRD pattern of Mn-substituted zincite mineral is similar to that of the Mn-substituted ZnO polycrystalline samples. However, the unit cell parameters: a = 3.2568 Å, c = 5.2153 Å and volume = 47.907 $Å^3$ demonstrate a significant difference with c being smaller and a being larger for the natural zincite mineral. In our Mn-substituted ZnO samples, the Mn concentration reached the maximum around 5.46 at.%. The concentration of Mn, in natural zincite mineral from Franklin N.J. and Sterling N.J, has been presented by previous chemical analysis, giving Mn ratios of 7.28 at.%, 6.87 at.% (Franklin N.J.), 7.4 at.% and 6.3 at.% (Sterling N.J.) [41, 42]. The results indicate that the maximum Mn concentration in Mn-substituted ZnO powder samples is higher than the concentration in natural zincite mineral.

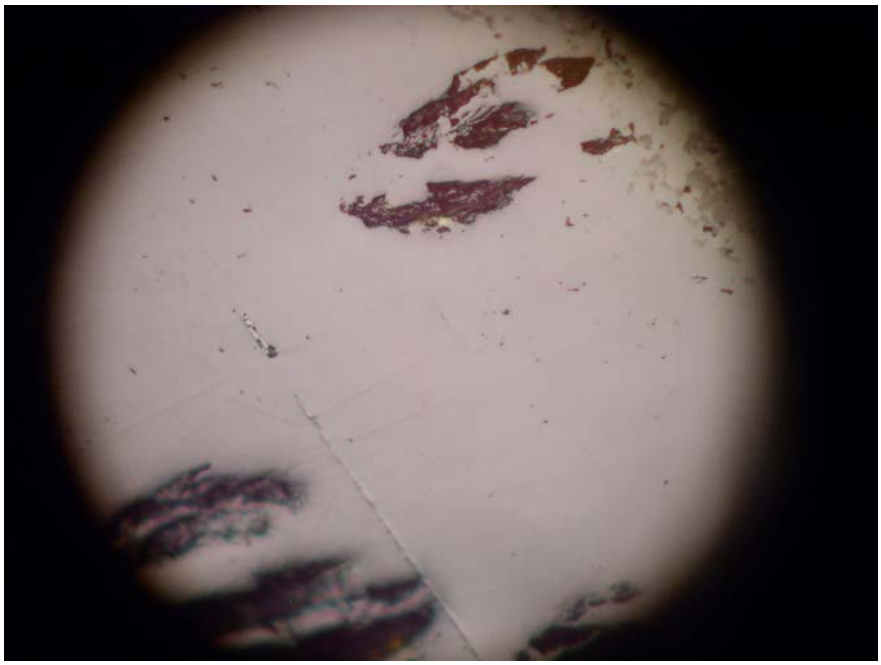

Figure 3.21 Optical microscopic image of polished natural zincite from NJ.

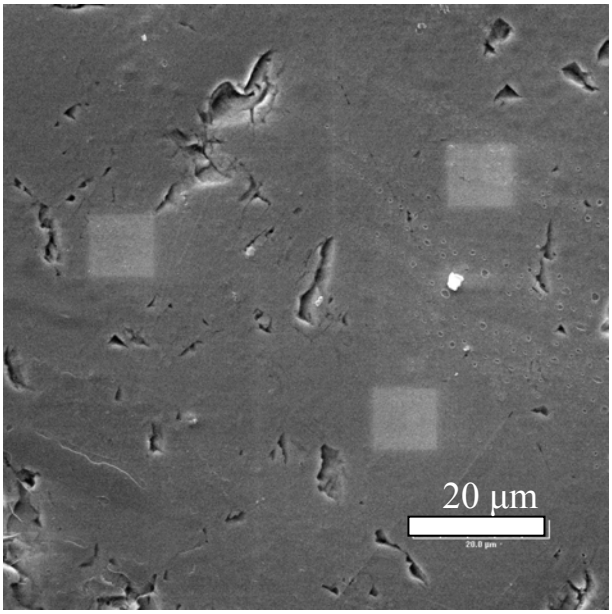

Figure 3.22 EDS data on the surface of polished nature zincite mineral. It has an average Mn concentration of 3.5 at.%.

3.4.8 Magnetic Susceptibility

Many reports suggested that the substitution of Zn^{2+} in ZnO by magnetic transition ions especially, Mn^{2+} can effect in samples with room temperature Curie temperature (shown in Table 3.4); however, there were several research papers which doubt on this long range order magnetic interaction. The recent experimental results have the favorite on the discovery of non intrinsic ferromagnetism in $Zn_{1-x}Mn_xO$. The possible secondary phases are responsible for the magnetic properties. (Table 3.4)

In order to clear this ambiguous situation, the polycrystalline samples prepared by the solid state reactions were used for the investigation. The magnetic properties of $Zn_{98.28}Mn_{1.72}O$ and $Zn_{94.54}Mn_{5.46}O$ samples had been determined using a SQUID magnetometer with various temperatures from 5 K to 370 K.

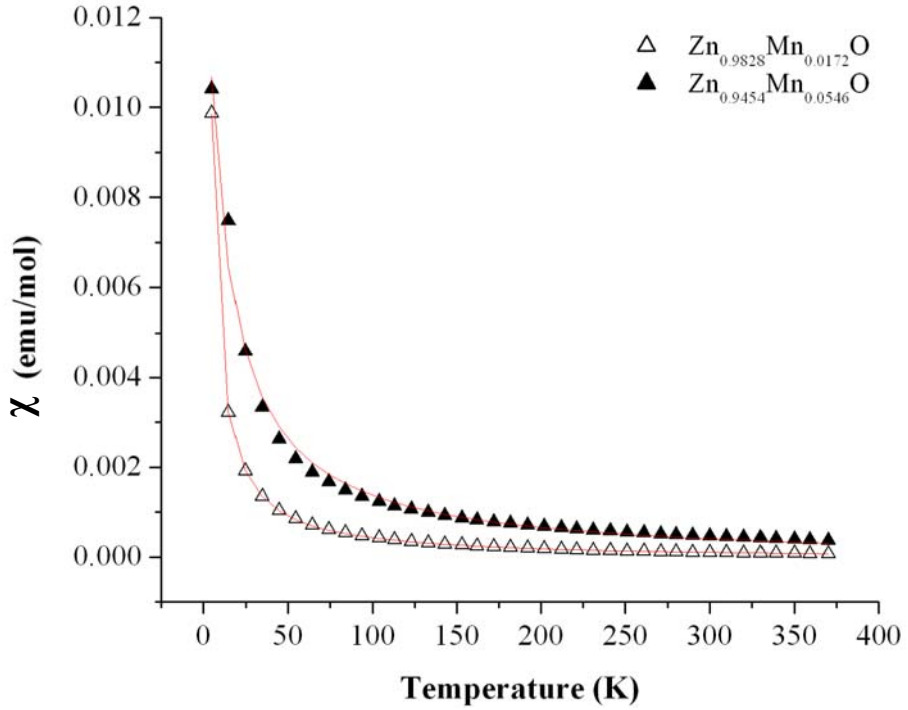

Figure 3.23 Susceptibility of polycrystalline $Zn_{0.0983}Mn_{0.0172}O$ (hollow triangle) (CMF 24A) and $Zn_{0.9454}Mn_{0.546}O$ (solid triangle) (CMF 24B) plotted from 5 K to 370 K. The red connecting line shows the fit to Curie-Weiss law.

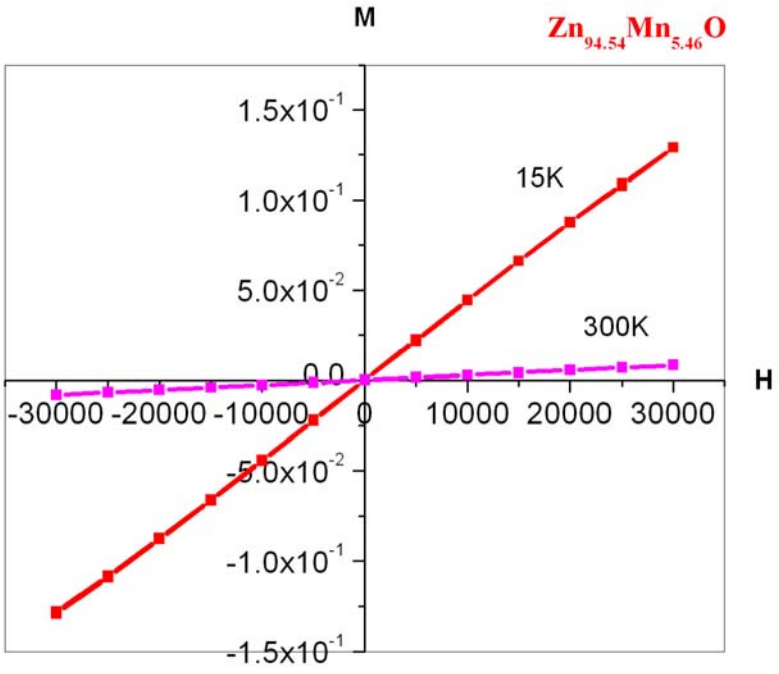

Figure 3.24 Field dependent magnetization of $Zn_{94.54}Mn_{5.46}O$ polycrystalline pellet under (A) 15 K and (B) 300 K with paramagnetic behavior. (CMF 24B)

The applied magnetic field was 0.1 Tesla (1 T = 1000 Oe). As in the χ-T curves, $Zn_{98.28}Mn_{1.72}O$ and $Zn_{94.54}Mn_{5.46}O$ (Figure 3.23) show the paramagnetic behavior as low as 15 K. The susceptibility is plotted from 5 to 370 K, and fitted by the non-linear Curie-Weiss law to obtain the values for χ_0, C, and θ. (Note: χ is

susceptibility, χ_0 is temperature independent term, C is Curie constant, and θ is Curie-Weiss constant)

$$\chi = \frac{C}{(T-\theta)} + \chi_0$$

The Curie constant is related to the magnetic moment (μ) of ions present in the substance. We derive the relationship between χ and μ from the Curie Law:

$$\chi = \frac{C}{T}$$

where

$$C = \frac{xN_0\mu^2}{3k}$$

The spin moment of each magnetic element with an unpaired electron is estimated by:

$$\mu_{eff} = g\sqrt{S(S+1)}$$

The Curie and Curie-Weiss constants were estimated from varying susceptibility with temperature.

For $Zn_{98.28}Mn_{1.72}O$:

$$C = 0.04878,\ \theta = 0.10321 \text{ and } \chi = -0.00006$$

and for $Zn_{94.54}Mn_{5.46}O$

$$C = 0.167,\ \Theta = -10.42446 \text{ and } \chi = -0.00013.$$

The Curie constant, C, is proportional to the square of the magnetic moment, μ^2. Due to the large initial particle size of starting materials, there may be small amount of impurities lead to high observed moments. The $Zn_{98.28}Mn_{1.72}O$ sample demonstrates a moment of 4.7608 μB/Mn atom, and $Zn_{94.54}Mn_{5.46}O$ has a moment of

4.944 μB/Mn. Divalent manganese ions, Mn^{2+}, have S=5/2 and g ~ 2.00, yielding a spin only moment of μ = 5.92 μB/Mn^{2+} and for trivalent manganese ions μ = 4.89 μB/Mn^{3+}. Base on the initial assumption, the oxidation state for the Mn impurity is +2. Base on the magnetic, Mn^{3+} is the predominated. Deoxygenation of MnO_2 between 630 ˚C and 1100 ˚C gives a reasonable explanation of the presence of manganese oxide species in the samples.[42] The mixed oxidation state compound Mn_2O_3 appears when the temperature heated to 1050 ˚C in air. Magnetic properties of Mn-substituted ZnO have been discussed in previous literature for both bulk and thin film samples (Table 3.4). Small magnetic moments on the order of 1.05 μB/Mn, for a $Zn_{0.96}Mn_{0.04}O$ thin film, and 0.36 μB/Mn, for a $Zn_{0.98}Mn_{0.02}O$ bulk sample, have been reported[43, 44]. The authors attribute these small moments to the competition of antiferromagnetic and ferromagnetic interaction. On the other hand, Lawes et al. found high magnetic moments for various Mn concentrations for the polycrystalline ZnO. (2 at.% Mn, μB = 4.6/Mn; 4 at.% Mn, μB = 4.5/Mn; 8 at.% Mn, μB = 3.9/Mn; and 15 at.% Mn, μB = 5.9/Mn. Phase separated out in the higher doped sample.)[37].

Table 3.5 List of several reported magnetic properties of ZnO-based DMS materials. Dopant concentrations, Curie temperatures (T_c), and corresponding magnetisms are listed.[3, 45-55]

Compound	TM (at.%)	Synthesis method	Growth Temperature (˚C)	Magnetism	T_c (K)
$Zn_{1-x}Mn_xO$	< 0.35	PLD	600		
$Zn_{1-x}Mn_xO$	0.36	PLD	600	Spin glass	
$Zn_{1-x}Mn_xO$	0.01~0.36	PLD	610	Paramagnetic	
$Zn_{1-x}Mn_xO$	0~0.3	PLD		0.15-0.17 μ_B/Mn	> 30-45
$Zn_{1-x}Mn_xO$	<0.04	solid state reaction	500-700	0.16 μ_B/Mn	>425
$Zn_{1-x}Mn_xO$	0.0221	PLD	400	0.05 emu/g	>425
$Zn_{1-x}Mn_xO$	0.04~0.09	Reactive sputtering	200-380	3 μ_B/Co	>400
$Zn_{1-x}Mn_xO$	0.07	Sputtering	400	Paramagnetic	
(ZnO:Mn, Sn)	0~0.3	Implantation		Ferromagnetic	250
(ZnO:Mn, Cu)	0.1 (Mn) <0.05 (Cu)	PLD	650	0.1 μ_B/Mn	400

Table 3.6 Possible secondary phases observed in TM-substituted ZnO and their magnetic properties.[38, 45, 55-59]

Phase	Magnetism	T_c or T_N (K)
MnO	Antiferromagnetic	116
MnO_2	Antiferromagnetic	92
Mn_2O_3	Antiferromagnetic	76
Mn_3O_4	Ferromagnetic	43
Mn_3O_4 (distorted spinel)	Ferromagnetic	46
Mn_3O_4 (Hausmannite)	Ferromagnetic	40
$(Zn,Mn)Mn_2O_4$	Ferromagnetic	40
$ZnMnO_3$ (cubic)	Spin glass	
Zn_3MnO_6 (hexagonal)		

3.5 Conclusions

Experiments in the various oxide systems, using B_2O_3, MoO_3, WO_3 and V_2O_5, produced green color ZnO crystals. However the secondary phases appeared on the product surface was a major challenge. According to the results of ZnO-V_2O_5 system, the high vapor pressure led to difficult ZnO crystal growth. Moreover, the insoluble phases on the ZnO crystal surface made the separation difficult. In the ZnO-KPF_6 and ZnO-Na_3AlF_6 reactions, hollow pellets were produced after heating process. The ZnO phase from B_2O_3 system was identified by powder X-ray pattern matching with the JCPDS database card number: 36-1451. The secondary phase $Zn_3B_2O_6$ was also found in the products.

Based on the study on the growth of ZnO single crystals using KOH and NaOH melts as fluxes, green color ZnO from NaOH flux and colorless crystals from KOH were synthesized successfully for the first time. Beautiful hexagonal morphology samples were obtained. The high solubility of hydroxides enables the flux to be easily separated out from the ZnO crystals. Also, comparing the crystal growth temperatures of oxide fluxes to hydroxide fluxes, hydroxides allow the growth proceed at lower temperatures.

The Mn-substituted ZnO samples were carried out by NaOH flux technique in a Pt crucible and sealed Ag tubes. In a Pt crucible, crystals with less than 1 at.% Mn incorporation with a original Mn concentration up to 80 at.% was identified. A even orange color distribution in Mn-substituted ZnO crystals were found in a sealed Ag tube. There were 4.11 at.% Mn concentration was observed by EDS data with the original 5 at.% Mn concentration.

ZnO based DMS polycrystalline samples with Mn substitution were also synthesized. According to the lattice parameter refinement for the powder samples, Mn was found to be dissolved in wurtzite host materials and lattice constants increased with increasing Mn concentration. The solubility of Mn in ZnO was found to be 5 at.%. Secondary phases, spinal $ZnMn_2O_4$ (JCPDS 18-1484) when the Mn concentration was above 5 at.%. Investigation on carefully characterized bulk samples of Mn substituted ZnO seems to suggest the absence of long range magnetic order. Paramagnetism is determined base on the M-H and χ-T curves. The previous reports of ferromagnetism were rather weak. They were much smaller than the expected Mn^{2+} spin-only moments, 5.92 μ_B/Mn.

3.6 Chapter 3 References:

1. Ohno, H.; Shen, A.; Matsukura, F.; Oiwa, A.; Endo, A.; Katsumoto, S.; Iye, Y., (Ga,Mn)As: A New Diluted Magnetic Semiconductor Based on GaAs. *Applied Physics Letters* 1996, 69, 363.

2. Prellier, W.; Fouchet, A.; Mercey, B., Oxide Diluted Magnetic Semiconductors: A Review of the Experimental Status. *Journal of Physics: Condensed Matter* 2003, 15, R1583.

3. Sharma, P.; Gupta, A.; Rao, K. V.; Owens, F. J.; Sharma, R.; Ahuja, R.; Guillen, J. M. O.; Johansson, B.; Gehring, G. A., Ferromagnetism Above Room Temperature in Bulk and Transparent Thin Films of Mn-doped ZnO. *Nature Materials* 2003, 2, 673.

4. Reed, M. L.; El-Masry, N. A.; Stadelmaier, H. H.; Ritums, M. K.; Reed, M. J.; Parker, C. A.; Roberts, J. C.; Bedair, S. M., Room Temperature Ferromagnetic Properties of (Ga,Mn)N. *Applied Physics Letters* 2001, 79, 3473.

5. Frazier, R. M.; Stapleton, J.; Thaler, G. T.; Abernathy, C. R.; Pearton, S. J.; Rairigh, R.; Kelly, J.; Hebard, A. F.; Nakarmi, M. L.; Nam, K. B.; Lin, J. Y.; Jiang, H. X.; Zavada, J. M.; Wilson, R. G., Properties of Co-, Cr-, or Mn-implanted AlN. *Journal of Applied Physics* 2003, 94, 1592.

6. Pearton, S. J.; Abernathy, C. R.; Norton, D. P.; Hebard, A. F.; Park, Y. D.; Boatner, L. A.; Budai, J. D., Advances in Wide Bandgap Materials for Semiconductor Spintronics. *Materials Science & Engineering R-Reports* 2003, 40, 137.

7. Pearton, S. J.; Ren, F.; Wang, Y. L.; Chu, B. H.; Chen, K. H.; Chang, C. Y.; Lim, W.; Lin, J. S.; Norton, D. P., Recent Advances in Wide Bandgap Semiconductor Biological and Gas Sensors. *Progress in Materials Science* 2010, 55, 1.

8. Janotti, A.; Van de Walle, C. G., Fundamentals of Zinc Oxide as A Semiconductor. *Reports on Progress in Physics* 2009, 72 (12).

9. Ohno, H., Making nonmagnetic semiconductors ferromagnetic. *Science (Washington, D. C.)* 1998, 281, 951.

10. Ohno, H., Properties of Ferromagnetic III-V Semiconductors. *Journal of Magnetism and Magnetic Materials* 1999, 200, 110.

11. Dietl, T.; Ohno, H.; Matsukura, F.; Cibert, J.; Ferrand, D., Zener Model Description of Ferromagnetism in Zinc-blende Magnetic Semiconductors. *Science (Washington, D. C.)* 2000, 287, 1019.

12. Sato, K.; Katayama-Yoshida, H., Material Design for Transparent Ferromagnets With ZnO-based Magnetic Semiconductors. *Japanese Journal of Applied Physics, Part 2: Letters* 2000, 39, L555.

13. Pearton, S. J.; Heo, W. H.; Ivill, M.; Norton, D. P.; Steiner, T., Dilute Magnetic Semiconducting Oxides. *Semiconductor Science and Technology* 2004, 19, R59.

14. Reynolds, D. C.; Look, D. C.; Jogai, B.; Litton, C. W.; Cantwell, G.; Harsch, W. C., Valence-band Ordering in ZnO. *Physical Review B* 1999, 60, 2340.

15. Phillips, J., Bonds and Bands in Semiconductors: New insight into Covalent Bonding in Crystals Has Followed from Studies of Energy-band Spectroscopy. *Science (New York, NY)* 1970, 169, 1035.

16. Lide, D., CRC Handbook of Chemistry and Physics, 73rd. *CRC Press Inc., Boca Raton, Florida* 1992, 1993, 9.

17. Harrison, D. E., Lamellar Glass-crystal Structures in the System ZnO-B_2O_3. *Journal of Crystal Growth* 1968, 3-4, 674.

18. Makarov, V.; Fotiev, A.; Serebryakova, L., Phase Composition and Equilibrium Diagram of the V_2O_5 ZnO System. *Journal of . Inoranic. Chemistry* 1971, 16.

19. Burdese, A., Systems of Vanadic Anhydride and Sesquioxides of Chromium, Iron, and Aluminum. *Annali di Chimica* 1957, 47, 797.

20. Wanklyn, B. M., The growth of ZnO Crystals from Phosphate and Vanadate Fluxes *Journal of Crystal Growth* 1970, 7, 107.

21. Harrison, D. E.; Hummel, F. A., Phase Equilibria and Fluorescence in the System Zinc Oxide-Boric Oxide. *Journal of Electrochemical Society* 1956, 103, 491.

22. Leonov, Y. S., The Reaction Between Zinc Oxide and Boric Anhydride by the Observation of Luminescence. *Zhurnal Neorganicheskoi Khimii* 1958, 3, 1245.

23. Oka, K.; Shibata, H.; Kashiwaya, S., Crystal growth of ZnO. *Journal of Crystal Growth* 2002, 237, 509.

24. Nielsen, J. W.; Dearborn, E. F., The Growth of Large Single Crystals of Zinc Oxide. *Journal of Physical Chemistry* 1960, 64, 1762.

25. Wanklyn, B. M., Growth of Zinc Oxide Crystals From Phosphate and Vanadate Fluxes. *Journal of Crystal Growth* 1970, 7, 107.

26. Ushio, M.; Sumiyoshi, Y., Synthesis of Zinc Oxide Single Crystals by the Flux Method. *Journal of Materials Science* 1993, 28, 218.

27. Kashyap, S. C., Growth of ZnO Needles from Molten Hydrous KOH Solutions. *Journal of Applied Physics* 1973, 44, 4381.

28. Hashimoto, H.; Hayashi, F.; Uematsu, T.; Moriyoshi, Y., Microstructure in Zno Thin Plates from Molten Mixed Alkali Solutions. *Journal of Materials Science Letters* 1982, 1, 4.

29. Yurkinskii, V. P.; Firsova, E. G.; Proskura, S. A., Thermal Dissociation of Sodium Hydroxide Upon Evacuation. *Russian Journal of Applied Chemistry* 2005, 78, 360.

30. http://en.wikipedia.org/wiki/Manganese(II)_carbonate (accessed April 14).

31. Zaki, M. I.; Hasan, M. A.; Pasupulety, L.; Kumari, K., Thermochemistry of Manganese Oxides in Reactive Gas Atmospheres: Probing Redox Compositions in the Decomposition Course MnO_2 --> MnO. *Thermochimica Acta* 1997, 303, 171.

32. Tauchi, S., Diffusion of Impurities in the Semiconductor Melt. *Journal of the Physical Society of Japan* 1962, 17, 220.

33. Blasco, J.; Bartolome, F.; Garcia, L. M.; Garcia, J., Extrinsic Origin of Ferromagnetism in Doped ZnO. *Journal of Materials Chemistry* 2006, 16, 2282.

34. Garcia, M. A.; Ruiz-Gonzalez, M. L.; Quesada, A.; Costa-Kramer, J. L.; Fernandez, J. F.; Khatib, S. J.; Wennberg, A.; Caballero, A. C.; Martin-Gonzalez, M. S.; Villegas, M.; Briones, F.; Gonzalez-Calbet, J. M.; Hernando, A., Interface Double-exchange Ferromagnetism in the Mn-Zn-O System: New Class of Biphase Magnetism. *Physical Review Letters* 2005, 94, 217206.

35. Kundaliya, D. C.; Ogale, S. B.; Lofland, S. E.; Dhar, S.; Metting, C. J.; Shinde, S. R.; Ma, Z.; Varughese, B.; Ramanujachary, K. V.; Salamanca-Riba, L.; Venkatesan, T., On the Origin of High-temperature Ferromagnetism in the Low-temperature-processed Mn-Zn-O System. *Nature Materials* 2004, 3, 709.

36. Rao, C. N. R.; Deepak, F. L., Absence of Ferromagnetism in Mn- and Co-doped ZnO. *Journal of Materials Chemistry* 2005, 15, 573.

37. Lawes, G.; Risbud, A. S.; Ramirez, A. P.; Seshadri, R., Absence of Ferromagnetism in Co and Mn Substituted Polycrystalline ZnO. *Physical Review B* 2005, 71, 045201.

38. Kolesnik, S.; Dabrowski, B., Absence of Room Temperature Ferromagnetism in Bulk Mn-doped ZnO. *Journal of A pplied Physics* 2004, 96, 5379.

39. WANG, T.; LIU, S.-w.; WEI, H.-m.; XUE, C.-j., Resent Situations and Trend of Studies on the Hydrothermal Sedimentary Deposit. *Journal of Earth Sciences and Environment* 2004, 26, 6.

40. Palache, C., The minerals of Franklin and Sterling Hill, Sussex County, New Jersey *USGS Professional Paper* 1935, 180, 2.

41. Tarr, W. A., The origin of the zinc deposits at Franklin and Sterling Hill, New Jersey. *American Mineralogist* 1929, 14, 207.

42. McSween, H. Y., Jr., Manganese-rich Ore Assemblages from Franklin, New Jersey. *Economic Geology and the Bulletin of the Society of Economic Geologists* 1976, 71, 814.

43. Hou, D.-L.; Ye, X.-J.; Meng, H.-J.; Zhou, H.-J.; Li, X.-L.; Zhen, C.-M.; Tang, G.-D., Magnetic Properties of Mn-doped ZnO Powder and Thin Films. *Materials Science&Engineering, B: Solid-State Materials for Advanced Technology* 2007, 138, 184.

44. Chen, W.; Zhao, L. F.; Wang, Y. Q.; Miao, J. H.; Liu, S.; Xia, Z. C.; Yuan, S. L., Magnetism in Mn-doped ZnO Bulk Samples. *Solid State Communications* 2005, 134, 827.

45. Jung, S.; An, S.; Yi, G.; Jung, C.; Lee, S.; Cho, S., Ferromagnetic Properties of ZnMnO Epitaxial Thin Films. *Applied Physics Letters* 2002, 80, 4561.

46. Norton, D.; Pearton, S.; Hebard, A.; Theodoropoulou, N.; Boatner, L.; Wilson, R., Ferromagnetism in Mn-implanted ZnO: Sn Single Crystals. *Applied Physics Letters* 2003, 82, 239.

47. Ueda, K.; Tabata, H.; Kawai, T., Magnetic and Electric Properties of Transition-metal-doped ZnO Films. *Applied Physics Letters* 2001, 79, 988.

48. Fukumura, T.; Jin, Z. W.; Ohtomo, A.; Koinuma, H.; Kawasaki, M., An Oxide-diluted Magnetic Semiconductor: Mn-doped ZnO. *Applied Physics Letters* 1999, 75, 3366.

49. Fukumura, T.; Jin, Z.; Kawasaki, M.; Shono, T.; Hasegawa, T.; Koshihara, S.; Koinuma, H., Magnetic Properties of Mn-doped ZnO. *Applied Physics Letters* 2001, 78, 958.

50. Jin, Z.; Fukumura, T.; Kawasaki, M.; Ando, K.; Saito, H.; Sekiguchi, T.; Yoo, Y.; Murakami, M.; Matsumoto, Y.; Hasegawa, T., High Throughput Fabrication of Transition-metal-doped Epitaxial ZnO Thin Films: A Series of Oxide-diluted Magnetic Semiconductors and Their Properties. *Applied Physics Letters* 2001, 78, 3824.

51. Tiwari, A.; Jin, C.; Kvit, A.; Kumar, D.; Muth, J.; Narayan, J., Structural, Optical and Magnetic Properties of Diluted Magnetic Semiconducting $Zn_{1-x}Mn_xO$ Films. *Solid State Communications* 2002, 121, 371.

52. Pearton, S.; Norton, D.; Ip, K.; Heo, Y.; Steiner, T., Recent Advances in Processing of ZnO. *Journal of Vacuum Science & Technology B: Microelectronics and Nanometer Structures* 2004, 22, 932.

53. Cheng, X.; Chien, C., Magnetic Properties of Epitaxial Mn-doped ZnO Thin Films. *Journal of Applied Physics* 2003, 93, 7876.

54. Ivill, M.; Pearton, S.; Norton, D.; Kelly, J.; Hebard, A., Magnetization Dependence on Electron Density in Epitaxial ZnO Thin Films Codoped With Mn and Sn. *Journal of Applied Physics* 2005, 97, 053904.

55. Lim, S.-W.; Jeong, M.-C.; Ham, M.-H.; Myoung, J.-M., Hole-Mediated Ferromagnetic Properties in $Zn_{1-x}Mn_xO$ Thin Films. *Japanese Journal of Applied Physics* 2004, 43, L280.

56. Guo, L.; Peng, D.; Makino, H.; Inaba, K.; Ko, H.; Sumiyama, K.; Yao, T., Structural and Magnetic Properties of Mn_3O_4 Films Grown on MgO (001) Substrates by Plasma-assisted MBE. *Journal of Magnetism and Magnetic Materials* 2000, 213, 321.

57. Chartier, A.; DArco, P.; Dovesi, R.; Saunders, V., Ab initio Hartree-Fock Investigation of the Structural, Electronic, and Magnetic Properties of Mn_3O_4. *Physical Review B* 1999, 60, 14042.

58. Han, S.; Jang, T.; Kim, Y.; Park, B.; Park, J.; Jeong, Y., Magnetism in Mn-doped ZnO Bulk Samples Prepared by Solid State Reaction. *Applied Physical Letters* 2003, 83, 920.

59. Liu, C.; Yun, F.; Xiao, B.; Cho, S.; Moon, Y.; H, M.; Abouzaid, M.; Ruterana, R.; Yu, K.; Walukiewicz, W., Structural Analysis of Ferromagnetic Mn-doped ZnO Thin Films Deposited by Radio Frequency Magnetron Sputtering. *Journal of Applied Physics* 2005, 97, 126107.

Chapter 4 Origin of Ferromagnetism in Mn substituted II-IV-V_2 Ternary Phosphide Semiconductors

4.1 Metal Phosphides

Almost all metallic elements will react with phosphorus to form phosphides. Numerous reports of metal phosphides have been published in previous literatures, and the identity of these compounds was confirmed by X-ray diffraction methods. Table 4.1 lists unit cell and space group data. The various phosphides differ greatly in their physical and chemical properties. These differences can be associated with the differences of crystal structure and bond type. Several review papers have discussed in detail of the properties and structures of binary transition metal phosphides.[1-5]

Transition metal phosphides are the largest and most studied group of phosphides due to their interesting chemical and physical properties. Base on the stoichiometry, metal phosphides can be classified into three types: metal-rich phosphides, monophosphides, and phosphorus-rich phosphides. The metal-rich varieties are often formed by the transition metal borides, silicides, nitrides, and carbides. These materials have similar properties, such as hardness, high melting point, high thermal and electrical conductivity and the resistance of chemical attack. The bonding is usually regarded as metallic, but the metal-metal bond distances are greater than those found in corresponding pure metals due to the presence of P, Si, B, N, or C.

Another group of phosphides are those that contain partial ionic bonding. These phosphides, which seem to be confined to group I and group II metals, have a much lower

melting point than transition metal phosphides. Also, these alkali (group I) and alkaline earth (group II) phosphides have no metallic luster, and decompose in water to form phosphine.[4, 6, 7] The Li_3P and Na_3P have been reported to have Na_3As type (hexagonal) structure.[8] In these compounds, phosphorus (P) atoms are surrounded by five mental atoms. These metal phosphides have dsp^3 covalent bonding. The arrangement of Na in the structure resembles metallic packing. The average distance of Na-Na bond is 3.24 Å with a radius of 1.62 Å, which is smaller than the metallic radius of 1.91 Å. This is suggests considerable ionic or covalent character in these structures. Zinc and cadmium phosphides, Zn_3P_2 and Cd_3P_2, have a tetragonal structure in which the metal atoms are coordinated by P atoms; the P atoms are surrounded by six metal atoms.[9]

Tabel 4.1 Unit cell and space group data for phosphides.[5, 8-18]

Phosphide	Structure type	Space group	*a*	*b*	*c*	z
Li_3P	Na_3As	*C6/mmc*	4.264		7.579	2
Na_3P		*C6/mmc*	4.98		8.797	2
Mg_3P_2	Mn_2O_3	*Ia3*	12.01			16
Zn_3P_2	Zn_3As_2	$P4_2/nmc$	8.09		11.45	8
Cd_3P_2		$P4_2/nmc$	8.74		12.28	8
InP	ZnS	*F-43m*	4.538			4
$ZnSiP_2$	Chalcopyrite	*I-42d*	5.398		10.440	4
$ZnGeP_2$		*I-42d*	5.46		10.76	4
$CdGeP_2$		*I-42d*	5.738		10.776	4
Mn_3P	Fe_3P	*I-4*	9.181		4.568	8
MnP	MnP	*Pnma*	5.258	3.172	5.918	4
Mn_2P	Fe_2P	*P-62m*	6.059		3.440	3
ZnP_2	Monoclinic	$P2_1/c$	9.28	7.68	8.03	4
CdP_2	Tetragonal	$P4_{13}22$	5.28		19.70	8

4.2 Semiconducting Metal Phosphides and Mn-Substituted Compounds

Semiconducting phosphides play an important role in many electronics-based applications. For instance, InP is a popular semiconductor in telecommunications and optical computing.[19] There are many isomorphous, cubic phosphides which have zinc-blend structure: GaAs, GaP, InAs, InP, and AlP. In these phosphides, each P atom is tetragonally coordinated. Each tetrahedron shares a corner with the next tetrahedral unit; this stacks up in a three-dimensional direction, forming a crystal structure. The isomorphs, $ZnGeP_2$, $ZnSiP_2$, and $CdGeP_2$ have tetragonal chalcopyrite type structure in which each P atom is in a tetrahedral coordination with other atoms, forming a zinc blende-type structure. These compounds form an ordered structure with tetrahedrally bonded atoms that are arranged as two stacked unit cells of the zinc blende structure (Figure 4.1) with stoichiometric ratio of 1Cd:1Si:2P ($CdSiP_2$). The chalcopyrite-structured (Figure 4.2) semiconductors consist of the elements found in group II (Be, Mg, Zn, Cd), group IV (C, Si, Ge, Sn), and group V (N, P, As, Sb).[20] These three groups compose the II-IV-V_2 system.

Semiconductors and magnetic materials are important constituents in modern industry. Most semiconductor devices use electron-hole pairs to manipulate information, while magnetic materials use electron spin to transmit information. Although the applications of semiconductor and magnetic devices have developed independently, in spintronic logic devices, it appears to coalesce both properties in order to increase functionality.[21, 22]

Among the possible adamantine ternary compounds, the II-IV-V_2 compounds with a wide energy gap, including phosphorus as a constituent, are of interest because of their possible application as new optical materials.[23] The development of wide band gap semiconductors has procured attention because it attains a high Curie temperature (T_c).[24]

The desired ternary chalcopyrites, such as $ZnSiP_2$ and $CdSiP_2$ with band gaps of 2.2 and 2.1 eV, respectively, are not able to exhibit intrinsic ferromagnetism without substitution of magnetic ions. A recent approach to practical ferromagnetic semiconductors was the dilute magnetic semiconductor (DMS), where transition metal ions substitute the cations of the host semiconductor. The zinc blende or sphalerite type semiconducting materials have been considered as most promising host lattices.[25, 26] Furthermore, long range ferromagnetic behavior in Mn-substituted InAs and GaAs has been investigated due to their wide application in industry.[27, 28] The existing III-V semiconductors, including Mn-substituted GaAs having sphalerite type structure, have been well studied for ferromagnetism in dilute magnetic semiconductor (DMS) materials.[29] Ferromagnetism, with $T_c \sim 110$ K, has been observed for Mn-substituted GaAs. Similar to zinc blende structure, the chalcopyrite group has drawn lots of attention since the discovery of III-V based ferromagnetic semiconductors.

Crystallizing in the tetragonal chalcopyrite structure is derived directly from the cubic zinc blende lattice by arranging the cations.[23, 30, 31] In this chapter, the detailed results of preparation and crystal growth of Mn substitution in $CdSiP_2$ and $ZnSiP_2$ chalcopyrites are explained.

In such lattices, Mn can easily substitute group II elements without creating structural defects; therefore, high Mn concentrations can be obtained in equilibrium conditions.[32] This offers a novel design principle for obtaining both high Mn solubility and intrinsic defect-induced high T_c ferromagnetic semiconducting systems.[33]

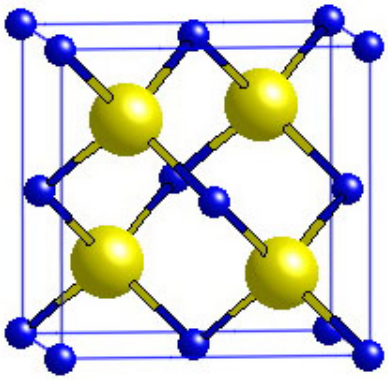

Figure 4.1 Zinc blende Structure (Unit Cell).

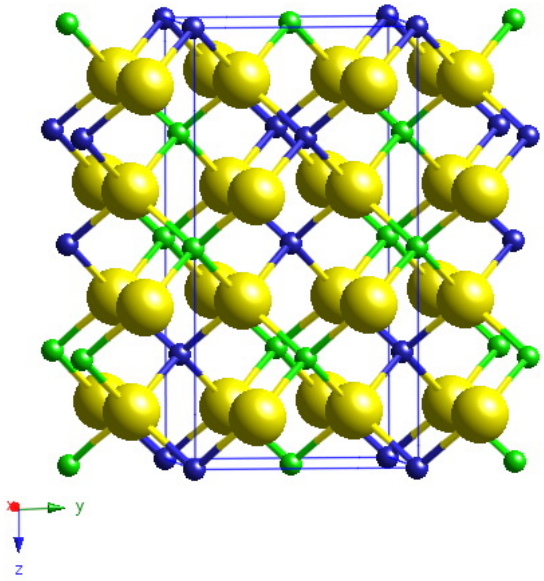

Figure 4.2 Chalcopyrite structure.

4.3 Experimental Methods

Elemental reactants, Zn powder (3 N), Si powder (5 N), P lump (6 N), Cd powder (99.5%), and Mn powder (99.95%) (all purchased from Alfa Aesar) were used for polycrystalline and single crystal preparations.

4.3.1 Single Phase Powder from Constituent Elements

Well homogenized starting materials were pressed into pellets with a stainless steel die plunger with a diameter 0.75 inch and sealed in fused silica ampoules under vacuum. In order to increase the fraction of desired phases, and to avoid excess P vapor pressure, stepwise heat treatment was adopted. An optimized, two-stage heating procedure (Figure 4.3) was used to retrieve a single phase of the desired product. During the first heat treatment, the samples dwelled at temperatures of 450 ˚C for 24 hours, 900 ˚C for 24 hours, and 1000 ˚C for 24 hours. After the first heat treatment, both $ZnSiP_2$ and $CdSiP_2$ samples showed three layers in the quartz tubes. In the second heat treatment, the samples dwelled at 1130 ˚C for 72 hours and then at 500 ˚C for 24 hours. For the transition metal-substituted polycrystalline sample, similar heat treatments were applied, and the concentration of Mn varied from 2 at.% to 30 at.%. MnP was prepared by heating mixtures of Mn powder and red P in an evacuated fused quartz ampoule at 1130 ˚C.

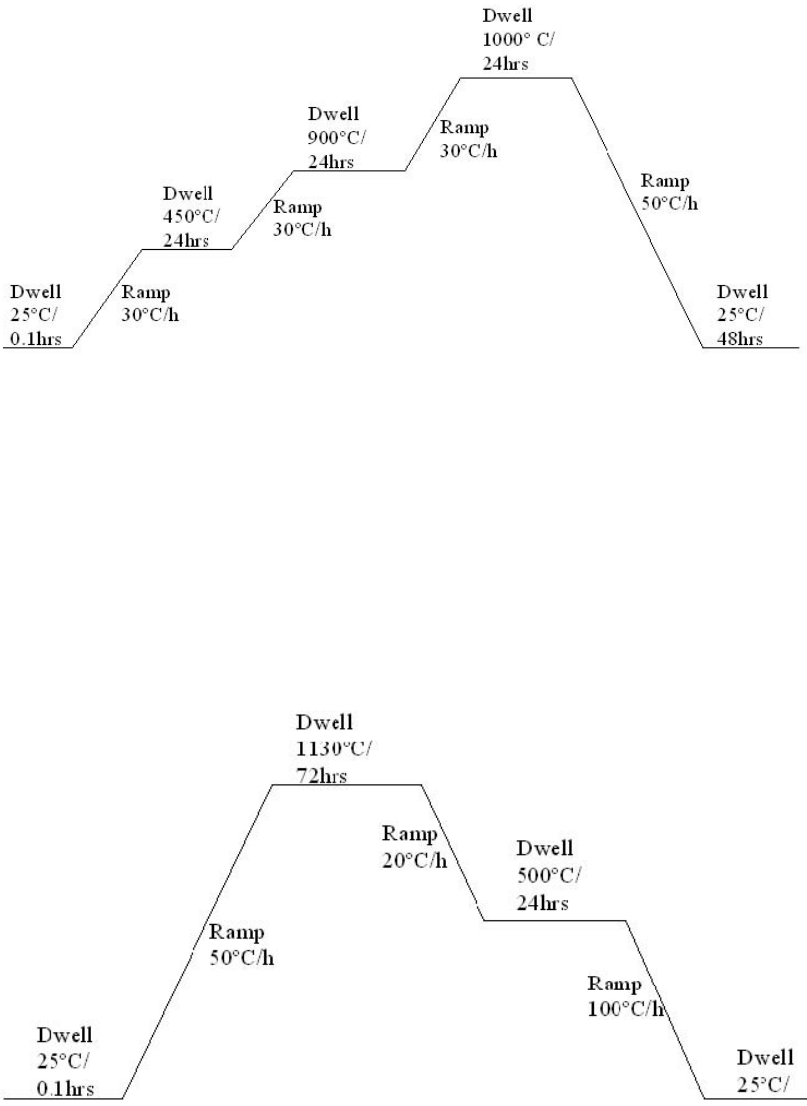

Figure 4.3 Reaction heating profile for two different heat treatments.

4.3.2 Crystal Growth from Metal Flux

Crystal growth experiments of $ZnSiP_2$ and $CdSiP_2$ were also carried out using sodium flux techniques. Mixtures of constituent elements were placed in stainless steel tubes. Different proportions of Na metal were added to the tubes and sealed under argon atmosphere in an arc melting furnace. Subsequently, the tubes were placed inside quartz tubes and sealed under vacuum. Experiments of crystal growth were carried out by heating the tubes at 900°C, 1000 ˚C and 1130 ˚C.

In a similar manner, crystal growth of $ZnSiP_2$ was carried out in Sn flux. However, this time, the graphite crucibles were used. Appropriate amounts of elements, along with Sn granules, were placed in graphite crucibles, quartz tubes, and sealed under vacuum. These tubes were heated up to 1150 ˚C for 12 hours, and then cooled down to 400 ˚C. The crystals were washed with mercury between 100 ˚C and 150 ˚C to remove excess tin flux. According to the Hg-Sn binary phase diagram, 60 wt.% of Sn was removed.

4.3.3 Characterization Methods

To identify phases of polycrystalline samples, X-ray powder diffraction (XRD) data were collected with a PANalytical X-ray diffractometer (PW3830) with Cu Kα radiation (λ=1.54178 Å). Unit cell parameters were determined by profile refinement of the X-ray diffraction data using Fullprof-2000 software package with Winplotr interface. Si was used as internal standard for the determination of accurate unit cell parameters. Crystal images and elemental analysis were obtained through digital scanning electron microscopy (Zeiss DSM-940) and energy dispersive spectroscopy (EDS) (Princeton Gamma Tech). Samples for XRD and SEM were prepared in an argon filled glove box. The powder X-ray sample used an agate mortar pestle to homogeneously mix the sample with Si powder. The ground powder sample was mixed with grease and placed on a microscopic slide. A piece of kapton was used to cover it in order to avoid sample decomposition. Sintered powder was spread out on a SEM specimen mounted with carbon tape. A zip-lock bag was used to prevent air exposure.

4.4 Results and Discussions

4.4.1 The Synthesis of $ZnSiP_2$ and $CdSiP_2$

$ZnSiP_2$ and $CdSiP_2$ crystals were synthesized in both solid state synthesis and flux techniques. Solid state reaction to form $ZnSiP_2$ and $CdSiP_2$ was demonstrated in both quartz and stainless tubes. To reduce the vapor pressure effects, the system dwelled at a relatively lower temperature, viz. 450 ˚C. During this step, Zn or Cd reacted with phosphorus to produce binary zinc or cadmium phosphides.[30] This can be presented by the Zn-P and Zn-Si binary phase equilibrium phase diagrams. Both phase diagrams show the eutectic points at the temperature close to the Zn rich side (> 99 at.%) (Figure 4.4 and 4.5).[34, 35] The mutual solubility of Zn and Si is extremely low. Therefore the reaction of Zn and P is prevailing at the first dwelling temperature, 450 ˚C. The further reaction occurred when the temperature increased. According to the Zn-P binary phase diagram, the possible binary phosphides of zinc are Zn_3P_2 and ZnP_2; both have been discovered. The importance of two different heat treatments to achieve the reaction in the II-IV-V_2 family and crystal growth is discussed. The analysis of the products at different stages reveals the course of reaction. Different phases in various heat treated samples were analyzed by powder XRD patterns and Rietveld refinements.

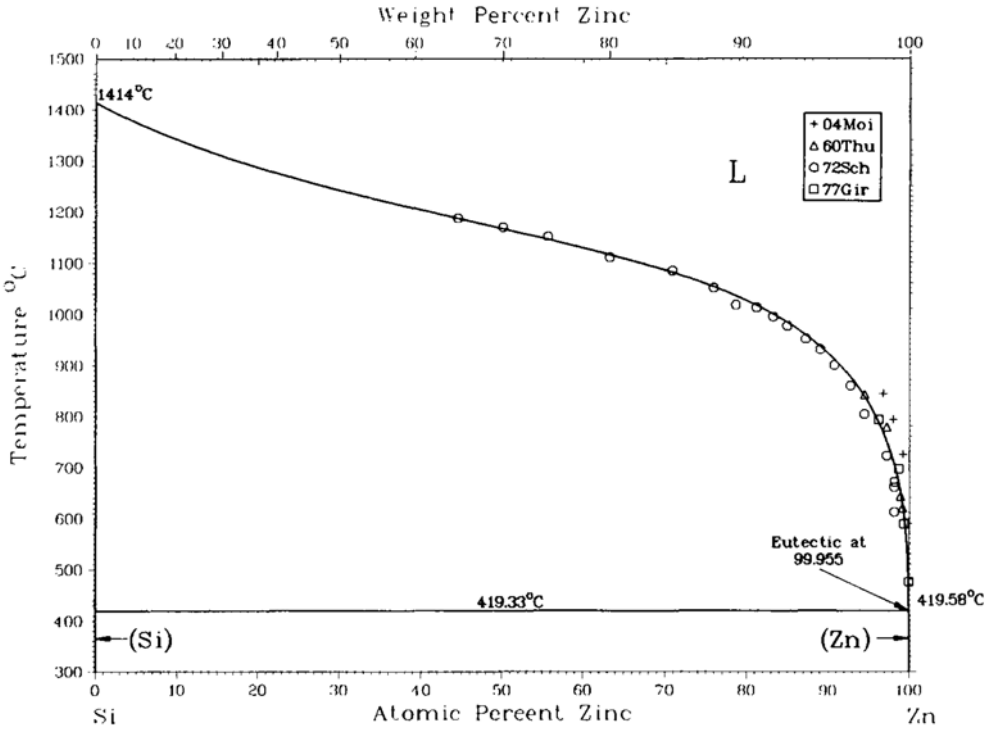

Figure 4.4 Phase equilibrium diagram of Zinc-Silicon system.

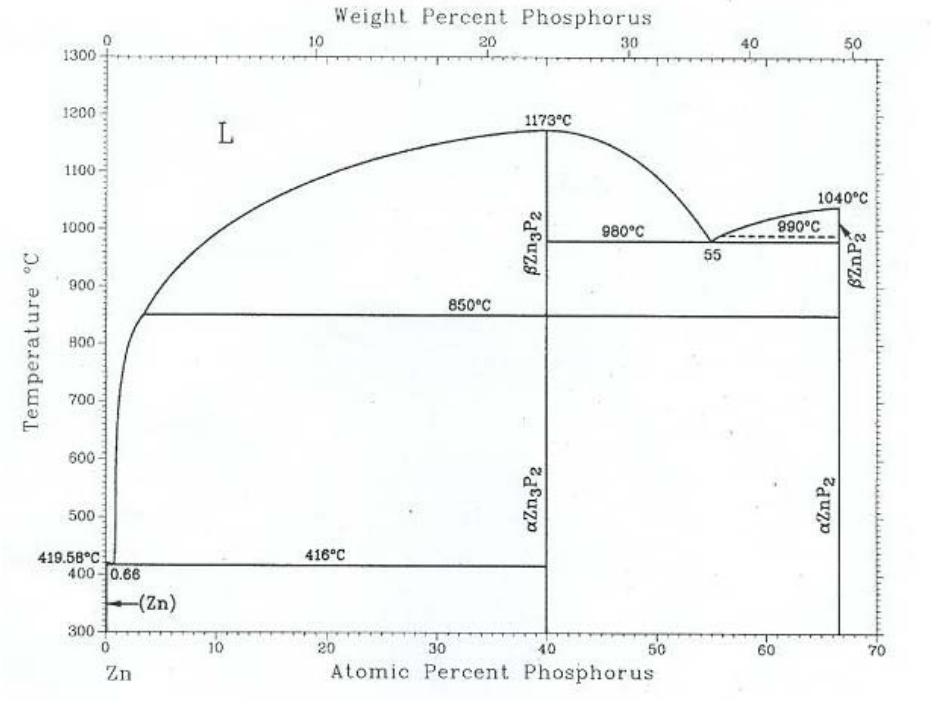

Figure 4.5 Phase equilibrium diagram of Zinc-Phosphorous system.

After the first heat treatment (maximum temperature 1000˚C), phases in distinct three layers were observed. The XRD patterns of the powdered product after this heat treatment showed different phases: ZnP_2, Zn_3P_2 and Si along with $ZnSiP_2$. They were found at the bottom as bright, silver luster crystals. The fraction of the $ZnSiP_2$, estimated from the powder XRD data (Figure 4.6), is about 65 wt.%. However, after the second heat treatment, the fraction of desired $ZnSiP_2$ phase was scaled up to 97 wt.%. In the first heat treatment, three different phases, $CdSiP_2$, CdP_2, and Si secondary phases were observed in the following quantities: 53.3 wt.%, 38.7 wt.%, and 8 wt.%, respectively. Pure $CdSiP_2$ was formed at the end of second heat treatment. (Figure 4.7) The details of the phase formation after the first heat treatment are given in Table 4.2.

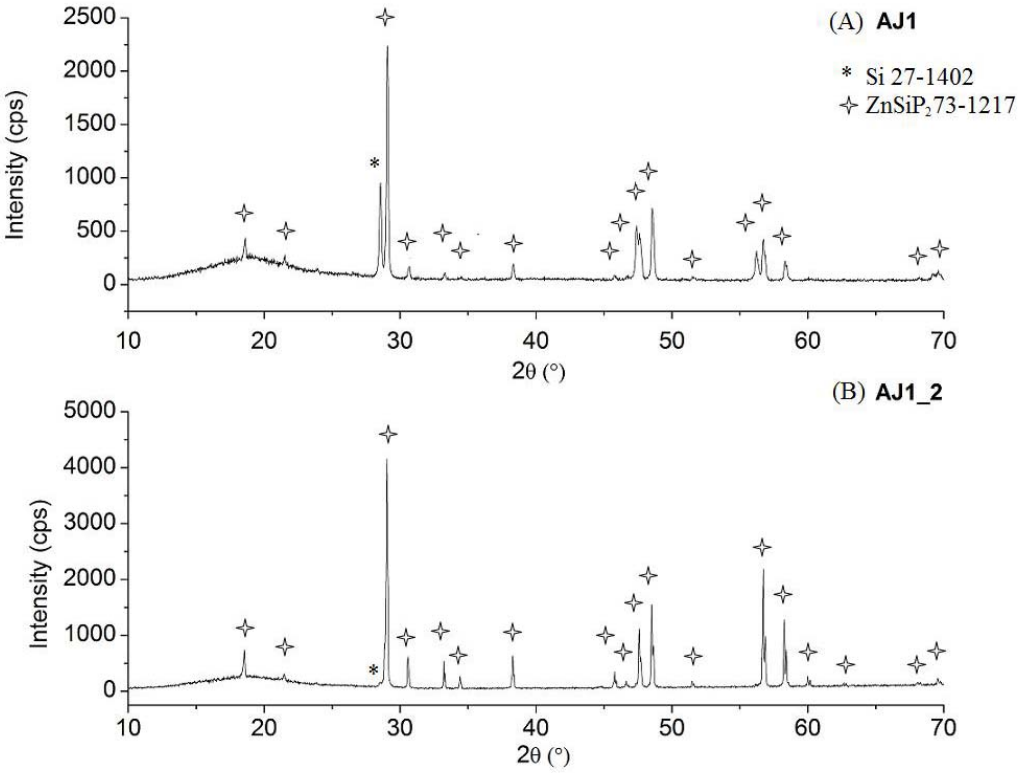

Figure 4.6 The powder XRD powder pattern of $ZnSiP_2$ after (A) first heat treatment (AJ1) and (B) second heat treatment (AJ1_2).

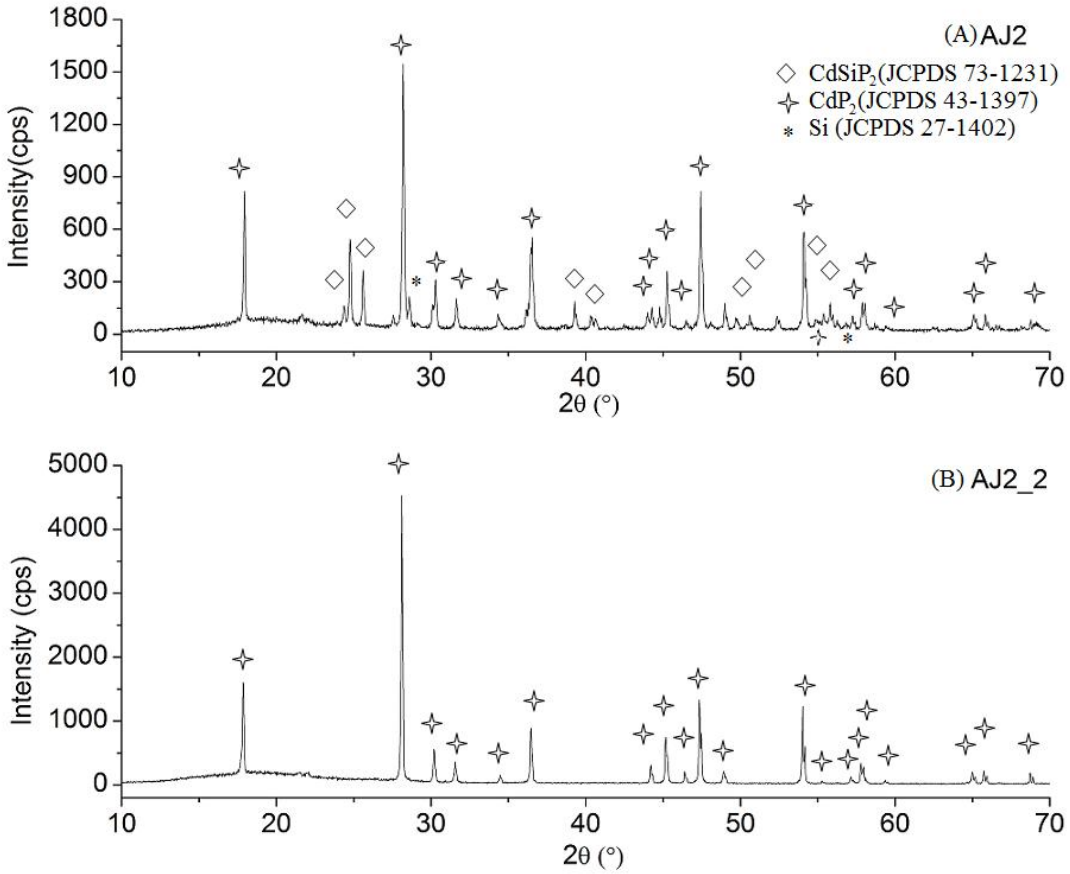

Figure 4. 7 The powder XRD powder pattern of $CdSiP_2$ after (A) first heat treatment (AJ2) and (B) second heat treatment (AJ2_2).

Tabel 4.2 Details of phase analysis of various studied compositions after the first heat treatment. (Tetragonal unit cell parameters of the chalcopyrite type phase are given.)

Reaction Name	a (Å)	c (Å)	Volume $(Å)^3$	Phases
$Zn_{0.98}Mn_{0.02}SiP_2$ (AJMn2)	5.3991(11)	10.4398(40)	304.3(1)	Si, $ZnSiP_2$, Zn_3P_2,
$Zn_{0.95}Mn_{0.05}SiP_2$ (AJMn4)	5.4068(1)	10.4454(5)	305.35(2)	$ZnSiP_2$, Si, Zn_3P_2
$Zn_{0.90}Mn_{0.10}SiP_2$ (AJMn4)	5.4059(2)	10.4447(6)	305.22(2)	$ZnSiP_2$, Zn_3P_2, Si
$Zn_{0.80}Mn_{0.20}SiP_2$ (AJMn5)	5.4048(2)	10.4377(7)	304.91(2)	$ZnSiP_2$, Zn_3P_2, Si
$Cd_{0.98}Mn_{0.02}SiP_2$ (AJMn7)	5.6849(4)	10.4317(10)	337.13(4)	$CdSiP_2$, Cd_7P_{10}, MnP, Si
$Cd_{0.95}Mn_{0.05}SiP_2$ (AJMn8)	5.6814(4)	10.4325(11)	336.74(5)	$CdSiP_2$, Cd_7P_{10}
$Cd_{0.92}Mn_{0.08}SiP_2$ (AJMn9)	5.6792(3)	10.4207(7)	336.11(3)	$CdSiP_2$, Cd_7P_{10}
$Cd_{0.90}Mn_{0.10}SiP_2$ (AJMn10)	5.6795(2)	10.4237(7)	336.23(3)	$CdSiP_2$, Si, MnP, Cd_7P_{10}
$Cd_{0.80}Mn_{0.20}SiP_2$ (AJMn11)	5.6741(2)	10.4127(5)	335.24(2)	$CdSiP_2$, Si, MnP
$Cd_{0.70}Mn_{0.30}SiP_2$ (AJMn12)	5.6727(3)	10.4106(7)	335.01(3)	$CdSiP_2$, Si

4.4.2 Crystal Growth of $ZnSiP_2$ from Metal Flux

Comparison of the product formed in the crystal growth experiments with Na or Sn flux showed that Sn is a better flux to synthesize phosphide crystals under relative low temperatures. The desired chalcopyrite phase crystals and their Mn substituted analogue, DMS material grown from Sn flux, were also displayed. Two different phases, $ZnSiP_2$ and Zn_3P_2, were identified in the powder XRD pattern. EDS data showed only small amounts of Mn appearing in the original 5 at.% Mn-substituted $ZnSiP_2$. Tin-rich matrix crystals commonly use hydrochloric acid to eliminate extra tin flux; however, the acid attack was notorious for these particular examples.[36] In search of an alternative to remove flux from crystals, Hg was selected. According to the tin-mercury (Sn-Hg) binary phase diagram (Figure 4.8), the solubility of tin in mercury is 60 wt.% at 150 °C.[37] It is interesting to note the crystal shows no obvious solvent attack after Hg washing as seen in SEM images (Figure 4.9). Conclusively, mercury is a feasible candidate to clean tin flux without solvent attack of $ZnSiP_2$.

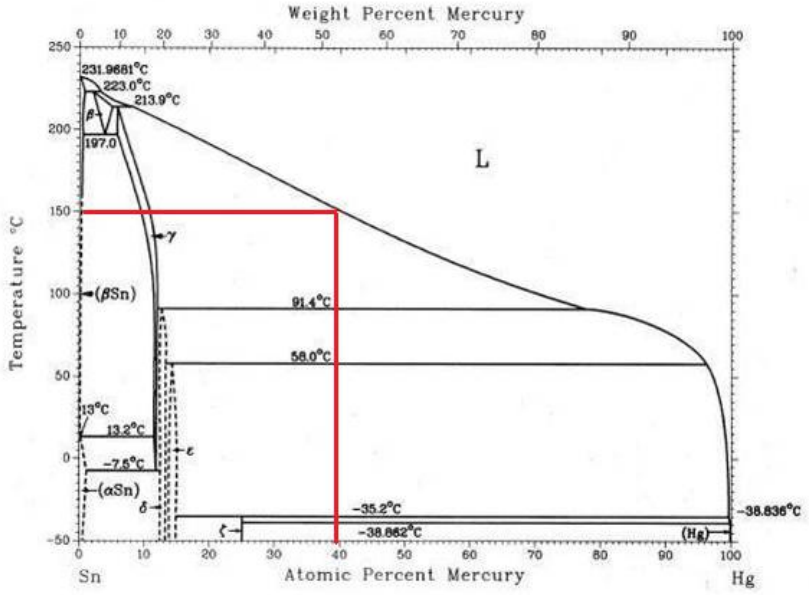

Figure 4.8 Sn-Hg binary alloy phase diagram.

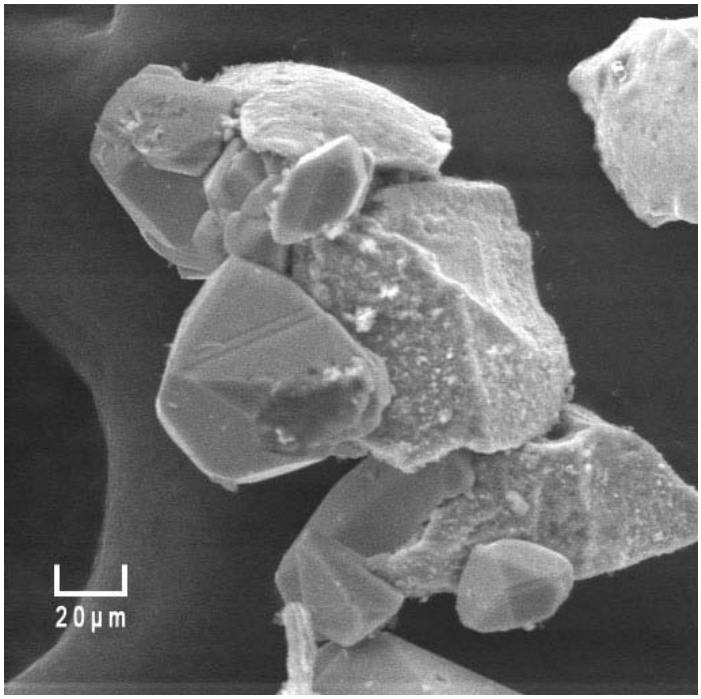

Figure 4.9 SEM image of pure $ZnSiP_2$ with an extra Sn flux coating. After Hg washing, there is no obvious solvent attack (Bas-3).

The characterizations, XRD and SEM/EDS analyses, for the products obtained from crystal growth experiments in molten Na flux at 900˚C and 1000 ˚C indicate no signature of chalcopyrite type $ZnSiP_2$ or $CdSiP_2$ phases. All compounds decomposed in these heat treatments. The products show a dominant phase of sodium phosphide (Na_3P). In $CdSiP_2$, only polycrystalline powders of Si, sodium phosphide (Na_3P), and binary cadmium phosphide (CdP_2, Cd_3P_2, and Cd_7P_{10}) appeared.

4.4.3 Lattice constants of Mn-Substituted Chalcopyrites

The lattice parameters of pure materials and Mn-substituted compounds are listed in the Table 4.2 and Table 4.3 list the compounds from previous reports and our experimental values. The variation of unit cell parameters with Mn concentration in $ZnSiP_2$ and $CdSiP_2$ are depicted in Figure 4.10 and Figure 4.11, respectively. The unit cell volume of Mn-substituted $ZnSiP_2$ was increased from 304.241 $Å^3$ (for 0 at.% Mn) to 305.35 $Å^3$ (for 5 at.% Mn), after which no significant variation is seen. However, the unit cell volume of Mn-substituted $CdSiP_2$ decreased from 336.506 $Å^3$ (for 0 at.% Mn) to 335.01 $Å^3$ (for 30 at.% Mn) when the Mn concentration increased. The increase in $ZnSiP_2$ and decrease in $CdSiP_2$ are expected as per the ionic radii of Mn. The unit cell parameters of $CdGeP_2$ with Mn replacing group II site coincided with our results. Although the substitution is possible on either group II or group IV, based on these results, substitution of group II elements is a major possibility. The quantitative analysis from EDS analysis were also summarized in the Table 4.4.

Tabel 4.3 Unit cell parameters for $ZnSiP_2$ and $CdSiP_2$.[38, 39]

Compounds	a (Å)	c (Å)	α (˚)	β (˚)	γ (˚)	Space Group	Volume (Å^3)
$ZnSiP_2$	5.399	10.43	90	90	90	$I\bar{4}2d$	304.17
$CdSiP_2$	5.680	10.43	90	90	90	$I\bar{4}2d$	336.26

Tabel 4.4 EDS data for $ZnSiP_2$ and$CdSiP_2$ crystals with various starting Mn concentration.

Reaction name	Zn (at.%)	Si(at.%)	P(at.%)	Mn (at.%)
$Zn_{0.98}Mn_{0.02}SiP_2$ (AJMn2)	20.47	25.59	53.59	0.35
$Zn_{0.95}Mn_{0.05}SiP_2$ (AJMn4)	18.40	27.05	54.55	
$Zn_{0.80}Mn_{0.20}SiP_2$ (AJMn5)	29.34	23.75	46.69	0.21
Reaction name	Cd (at.%)	Si(at.%)	P(at.%)	Mn (at.%)
$Cd_{0.98}Mn_{0.02}SiP_2$ (AJMn7)	28.08	19.55	51.81	0.56
$Cd_{0.95}Mn_{0.05}SiP_2$ (AJMn8)	26.27	19.87	52.50	1.35
$Cd_{0.92}Mn_{0.08}SiP_2$ (AJMn9)	23.79	19.89	53.70	2.62
$Cd_{0.90}Mn_{0.10}SiP_2$ (AJMn10)	26.85	19.27	50.70	3.19
$Cd_{0.80}Mn_{0.20}SiP_2$ (AJMn11)	23.41	20.19	53.01	3.39
$Cd_{0.70}Mn_{0.30}SiP_2$ (AJMn12)	25.03	19.32	51.10	4.55

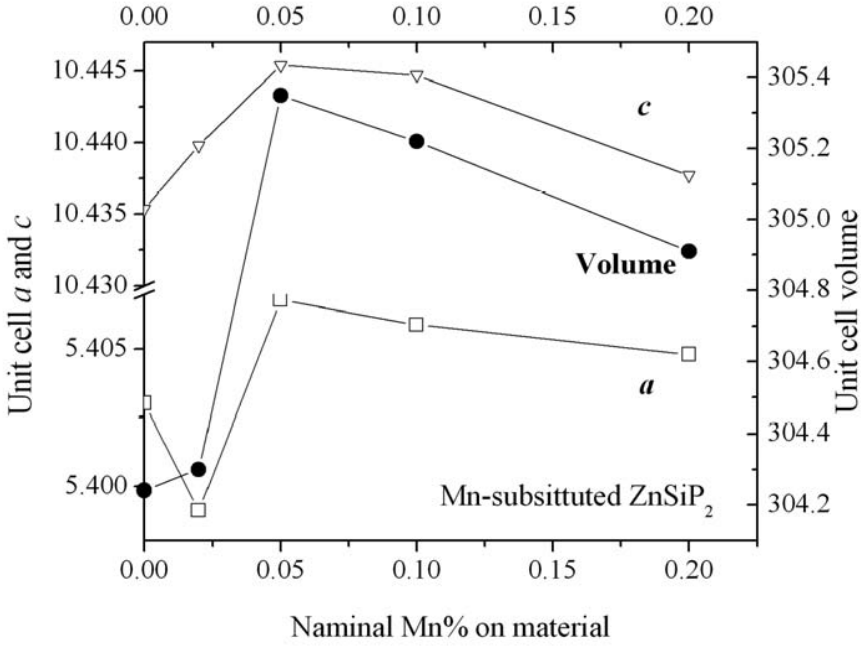

Figure 4.10 Unit cell parameters and volumes (□, a ▽, c ●, volume) of Mn-substituted $ZnSiP_2$ with various nominal manganese compositions.

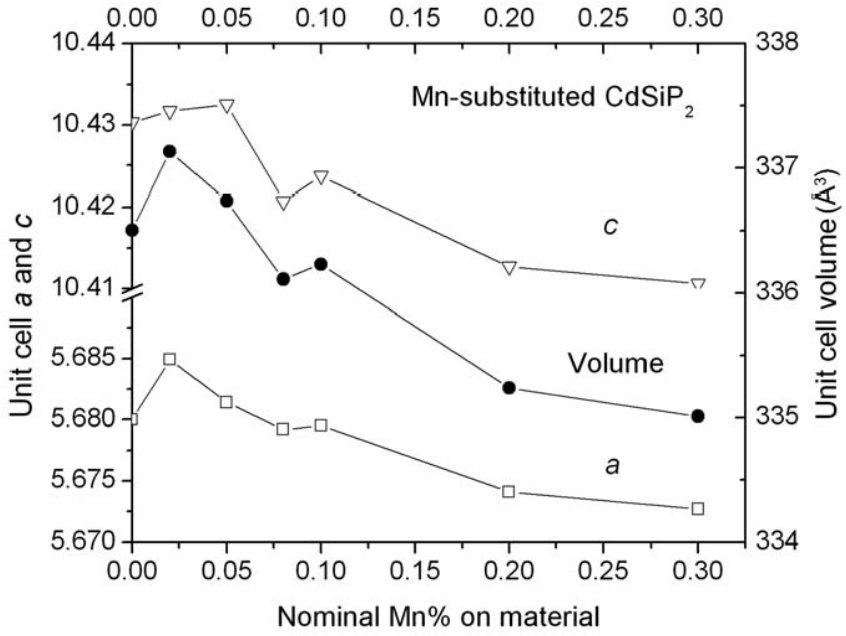

Figure 4.11 Unit cell parameters and volumes (□, a ▽, c ●, volume) of Mn-substituted $CdSiP_2$ with various nominal manganese compositions.

4.4.4 Magnetic properties of Mn-substituted II-IV-V_2 phosphides

The temperature dependent susceptibility curves of $Cd_{0.80}Mn_{0.20}SiP_2$ and $Zn_{0.95}Mn_{0.05}SiP_2$ have been studied by the SQUID magnetometer from 5 K to 370 K with an external applied field of 1000 Oe. The temperature dependent magnetization of various samples shows a sharp increase in magnetization at 317 K, indicating a ferromagnetic transition. Magnetization decreases around 50 K in all the samples, indicating the onset of an antiferromagnetic interaction. Typical traces of temperature dependent susceptibilities of $Cd_{0.80}Mn_{0.20}SiP_2$, $Zn_{0.95}Mn_{0.05}SiP_2$ and MnP are shown in Figure 4.12. The ferromagnetic behavior is further confirmed from the hysteresis loop (Figure 4.13). No coercivity and remanence were observed at 350 ˚C, indicating typical paramagnetic behavior. The sufficient carriers in the Mn 3d band stabilize the ferromagnetism. This is because the magnetic state is mainly determined by the competition between double-exchange and super-exchange interactions. In the present case, the substitution of Mn in group II site does not lead to any extra carriers in the unit cell. Thus, the magnetic interaction should originate from the interaction of the intrinsic carrier of the host lattice with Mn.

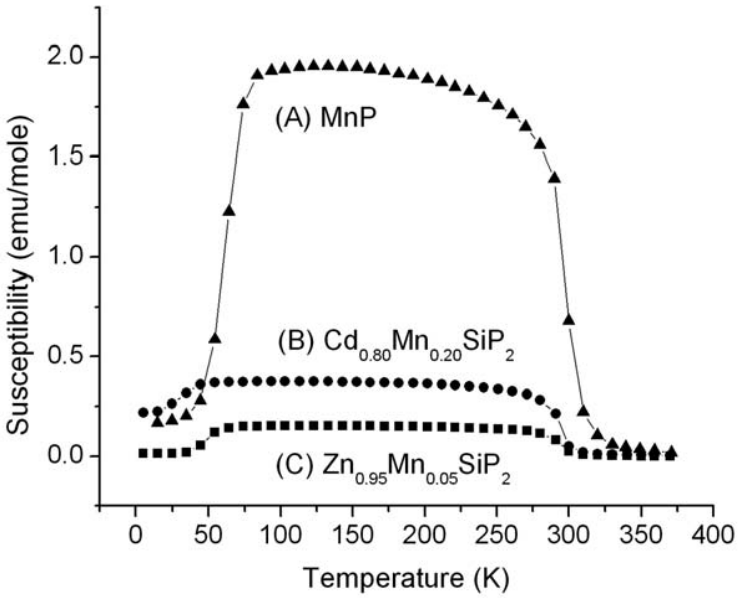

Figure 4.12 Temperature dependence magnetic susceptibility of (A) MnP (B) $Cd_{0.80}Mn_{0.20}SiP_2$ (AJMn11) and (C) $Zn_{0.95}Mn_{0.05}SiP_2$ (AJMn4).

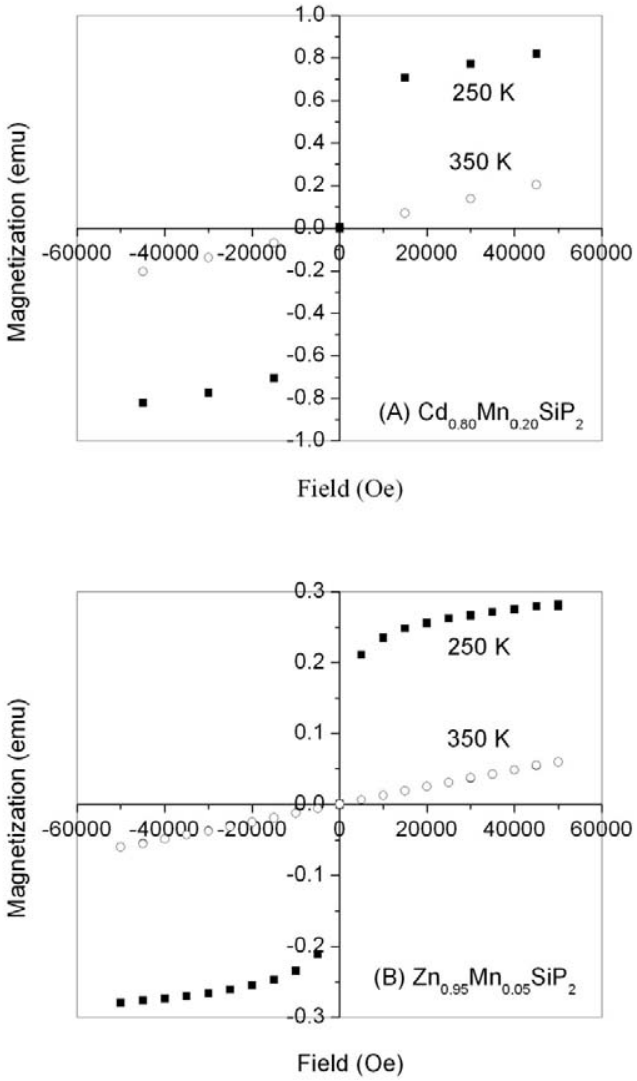

Figure 4.13 Field dependent magnetization of (A) $Cd_{0.80}Mn_{0.20}SiP_2$ (AJMn11) and (B) $Zn_{0.95}Mn_{0.05}SiP_2$ (AJMn4).

The magnetic behavior of studies of Mn substituted II-IV-V_2 phosphides are quite similar to that of MnP in both ferromagnetic and antiferromagnetic states. In the case of MnP, the ferromagnetic Curie point is ~ 300 K and the Néel temperature is ~ 50 K. This is in agreement with earlier reported values. The susceptibility of MnP, along the *c* direction from previous research, coincided with this observation, which processes ferromagnetism at high temperature and antiferromagnetic interaction at low temperature.[40, 41]

The typical remanence of 0.004 emu is observed even in such heavily substituted samples. A comparison of ferromagnetic saturation magnetization of $Cd_{0.80}Mn_{0.20}P_2$ with that of MnP indicates almost all the Mn remains as MnP phase. Usually, the MnP does not scatter X-ray significantly in comparison to $CdSiP_2$ or $ZnGeP_2$. Thus, they remain as hidden phases in the XRD background. The variation of the unit cell parameter may be attributed to either intermixing of Zn or Cd with Si in the chalcopyrite structure or Si substitution in Zn/Cd sites. MnP appeared in the samples due to phase segregation, which is a major obstacle in DMS materials. These results are in agreement with the earlier reported secondary phase, MnP and in other Mn-substituted II-IV-V_2 chalcopyrites.[41, 42]

In the case of Mn-substituted $ZnGeP_2$, ferromagnetic behavior is observed up to room temperature. This observation of the magnetic curves is similar to our product and the MnP precipitates predominates magnetic properties in these chalcopyrites.

4.5 Conclusions

The II-IV-V_2 chalcopyrites, $CdSiP_2$, $ZnSiP_2$, and their DMS materials with Mn substition, grown in both single crystal layers and polycrystalline bulks, were demonstrated in flux synthesis and solid state reactions. Tin flux was utilized for the synthesis of $ZnSiP_2$. The tin flux was washed out by Hg at 150 ˚C. The $ZnSiP_2$ single samples demonstrate typical crystallographic behavior as those in previous reports, and there was no solvent attack observed on the sample surface.

Solid state reactions and two different heat treatments were brought in our powder samples synthesis. Large peaks corresponding to binary phosphides were observed in the XRD powder patterns. Nearly single phase $ZnSiP_2$ and $CdSiP_2$ were obtained after the second heat treatment. Both $ZnSiP_2$ and $CdSiP_2$ polycrystalline samples with various concentration of Mn, 2 at.% to 30 at. %, were synthesized. Unit cell volumes of Mn-substituted $CdSiP_2$ samples were decreased from 336.506 $Å^3$ to 335.01 $Å^3$. For the Mn-substituted $ZnSiP_2$ powder samples, unit cell volumes increased below 5 at.% Mn incorporation, and then saturated at around 305.35 $Å^3$. The SQUID magnetometer data revealed that the temperature dependence susceptibility curves of both $Zn_{0.95}Mn_{0.05}SiP_2$ and $Cd_{0.80}Mn_{0.20}SiP_2$ showed MnP like behavior. The field dependence magnetization curves of $Zn_{0.95}Mn_{0.05}SiP_2$ and $Cd_{0.80}Mn_{0.20}SiP_2$ displayed well defined ferromagnetic hysteresis with a saturation behavior in the magnetization curve above room temperature.

4.6 Chapter 4 References

1. Hansen, M.; Anderko, K., *Constitution of binary alloys*. McGraw-Hill New York: 1958.

2. Pearson, W., *Latice Spacings and Structure of Mal Aloys*. Pergamon: New York, 1958.

3. Samsonov, G.; Vereikina, L., Phosphides. *AN USSR, Kiev* 1961.

4. Van Wazer, J., *Phosphorus and Its Compounds: Technology, Biological Functions, and Applications*. Interscience Publishers: 1958.

5. Rundqvist, S., Binary Transition Metal Phosphides (and Crystal-Chemical Relations Between Them and Transition Metal Compounds With Other Nonmetals of Small Atomic Radius). *Arkiv Kemi* 1962, 20, 67.

6. Pleskov, V.; Monoszon, A., Activity of Ammonium Ions in Liquid Ammonia Solutions. *Acta Physica et Chimica. URSS* 1935, 1, 725.

7. Zintl, E.; Woltersdorf, G., Gitterstruktur von LiAl. *Zeitschrift fur Elektrochemie* 1935, 41, 877.

8. Brauer, G.; Zintl, E., Metals and Alloys. XXIII. Phosphides, Arsenides, Antimonides, and Bismuthides of Li, Na, and K. *Zeitschrift fur Physikalische Chemie, B* 1937, 37, 323.

9. Von Stackelberg, M.; Paulus, R., Phosphides and Arsenides of Zinc and Cadmium. The Zn_3P_2 Lattice. *Zeitschrift fur Physikalische Chemie* 1935, 28, 427

10. Iandelli, A., Modifications of Sesquioxides of the Rare Earths. *Gazzetta Chimica Italiana* 1948, 71, 58.

11. Folberth, O.; Pfister, H., Die Kristallstruktur von $ZnSnAs_2$. *Acta Crystallographica*

1960, 13, 199.

12. Folberth, O. G.; Pfister, H., New Ternary Semiconducting Compounds Having Chalcopyrite Structure. *Semiconductors and Phosphors, Proc. Intern. Colloqs., Garmisch-Partenkirchen* 1958, 474.

13. Goodman, C., A New Group of Compounds with Diamond type (Chalcopyrite) Structure. *Nature* 1957, 179, 828.

14. Arstsd, O.; Nowotny, H., X-ray Investigation of The System Manganese-phosphorus. *Zeitschrift fur Physikalische Chemie B* 1937, 38, 356.

15. Rundqvist, S., X-ray Investigations of Mn_3P, Mn_2P, and Ni_2P. *Acta Chemica Scandinavica* 1962, 16, 1.

16. Rundqvist, S., X-ray Investigations of the Ternary System Fe-BP. *Acta Chemica Scandinavica* 1962, 16, 287.

17. Rundqvist, S.; Hassler, E.; Lundvik, L., Refinement of the Ni_3P Structure. *Acta Chemica Scandinavica* 1962, 16, 212.

18. Rundqvist, S.; Jellinek, F., The Structures of Ni_6Si_2B, Fe_2P and Some Related Phases. *Acta Chemica Scandinavica* 1959, 13, 3.

19. Streit, D.; Oki, A.; Gutierrez-Aitken, A.; Grossman, P.; Block, T.; Chin, P.; Lai, R.; Chen, Y.; Grundbacher, R., Indium Phosphide Microelectronics Revolutionary Technology for Advanced Telecommunications. *Technology Review* 2000, 1.

20. Erwin, S., Tailoring Ferromagnetic Chalcopyrites. *Nature Materials* 2004, 3, 410.

21. Wolf, S. A.; Awschalom, D. D.; Buhrman, R. A.; Daughton, J. M.; von Molnar, S.; Roukes, M. L.; Chtchelkanova, A. Y.; Treger, D. M., Spintronics: A Spin-Based Electronics Vision for The Future. *Science* 2001, 294, 1488.

22. Prinz, G. A., Hybrid Ferromagnetic-Semiconductor Structures. *Science* 1990, 250, 1092.

23. Cho, S.; Choi, S.; Cha, G. B.; Hong, S. C.; Kim, Y.; Zhao, Y. J.; Freeman, A. J.; Ketterson, J. B.; Kim, B. J.; Kim, Y. C., Room-Temperature Ferromagnetism in (Zn_{1-x} Mn_x) GeP_2 Semiconductors. *Physical Review Letters* 2002, 88, 257203.

24. Dietl, T.; Ohno, H.; Matsukura, F.; Cibert, J.; Ferrand, D., Zener Model Description of Ferromagnetism in Zinc-Blende Magnetic Semiconductors. *Science* 2000, 287, 1019.

25. Dietl, T.; Ohno, H.; Matsukura, F.; Cibert, J.; Ferrand, D., Zener Model Description of Ferromagnetism in Zinc-blende Magnetic Semiconductors. *Science (Washington, D. C.)* 2000, 287, 1019.

26. Dietl, T.; Ohno, H.; Matsukura, F., Hole-mediated Ferromagnetism in Tetrahedrally Coordinated Semiconductors. *Physical Review B* 2001, 63, 195205.

27. Ohno, H.; Munekata, H.; Penney, T.; Vonmolnar, S.; Chang, L. L., Magnetotransport Properties of *p*-type (In,Mn)AS Diluted Magnetic III-V Semiconductors. *Physical Review Letters* 1992, 68, 2664.

28. Ohno, H.; Shen, A.; Matsukura, F.; Oiwa, A.; Endo, A.; Katsumoto, S.; Iye, Y., (Ga,Mn)As: A New Diluted Magnetic Semiconductor Based on GaAs. *Applied Physics Letters* 1996, 69, 363.

29. Kamatani, T.; Akai, H., The Magnetic Properties in Transition Metal-doped Chalcopyrite Semiconductors. *Materials Science in Semiconductor Processing* 2003, 6, 389.

30. Mughal, S. A.; Payne, A. J.; Ray, B., Preparation and Phase Studies of The Ternary Semiconducting Compounds $ZnSnP_2$, $ZnGeP_2$, $ZnSiP_2$, $CdGeP_2$, and $CdSiP_2$. *Journal of*

Materials Science 1969, 4, 895.

31. Krivosheeva, A. V.; Shaposhnikov, V. L.; Lyskouski, V. V.; Borisenko, V. E.; d'Avitaya, F. A.; Lazzari, J. L., Prospects on Mn-doped $ZnGeP_2$ for Spintronics. *Microelectronics and Reliability* 2006, 46, 1747.

32. Mahadevan, P.; Zunger, A., Room-Temperature Ferromagnetism in Mn-Doped Semiconducting $CdGeP_2$. *Physical Review Letters* 2002, 88, 47205.

33. Kanatzidis, M. G.; Pottgen, R.; Jeitschko, W., The Metal Flux: A Preparative Tool for The Exploration of Intermetallic Compounds. *Angewandte Chemie International Edition* 2005, 44, 6996.

34. Olesinski, R. W.; Abbaschian, G. J., The Si-Zn (Silicon-Zinc) System. *Journal of Phase Equilibria* 1985, 6, 545.

35. Dutkiewlcz, J., The P-Zn (Phosphorus-Zinc) System *Journal of Phase Equilibria* 1991, 12, 435.

36. Massalski, T. B., *Binary Alloy Phase Diagrams*. 2 ed.; The Materials Internation Society: Vol. 3, p 2168.

37. Huber Jr, E. E.; Ridgley, D. H., Magnetic Properties of a Single Crystal of Manganese Phosphide *Physical Review* 1964, 135, A1033.

38. Abrahams, S. C.; Bernstein, J. L., Crystal Structure of Luminescent Silicon Zinc Phosphide. *Journal of Chemical Physics* 1970, 52, 5607.

39. Abrahams, S. C.; Bernstein, J. L., Luminescent Piezoelectric Cadmium Silicon Phosphide. Normal Probability Plot Analysis, Crystal Structure and Generalized Structure of the AIIBIVC2V Family. *Journal of Chemical Physics* 1971, 55, 796.

40. Paduan-Filho, A.; Becerra, C. C., Critical Fluctuations in MnP Near the Curie

Temperature. *Journal of Magnetism and Magnetic Materials* 2003, 261, 161.

41. Aitken, J. A.; Tsoi, G. M.; Wenger, L. E.; Brock, S. L., Phase Segregation of MnP in Chalcopyrite Dilute Magnetic Semiconductors: A Cautionary Tale. *Chemistry of Materials* 2007, 19, 5272.

42. Hwang, T.; Shim, J. H.; Lee, S., Observation of MnP Magnetic Clusters in Room-temperature Ferromagnetic Semiconductor $Zn_{1-x}Mn_xGeP_2$ Using Nuclear Magnetic Resonance. *Applied Physics Letters* 2003, 83, 1809.

Chapter 5 Pure and Mn substituted $KGaS_2$ and $KGaSe_2$ Synthesis and Characterization

5.1 Introduction

Pure semiconductors with a large bandgap energies have intrinsic properties that include high electrical resistivity, thus making the material an insulator.[1] Computer devices, spintronics, optoelectronics, and photovoltaic devices are areas that exploit the application of semiconductors. Dilute magnetic semiconductor (DMS) have the magnetic character that is regulated by the transition metal substituent in quantities of five to six percent.[2] Substitution can permit the control of ferromagnetism in the material. Gallium arsenide (GaAs) is currently a semiconductor that has been substituted with Mn. It performs at the highest known Curie temperature of 150 K. However, this high temperature ferromagnetism is not retained above room temperature (298 K). The solubility limits of transition metals in III-V semiconductors is relative low, generally ~ 10^{17} cm^{-3}.[3] Due to solubility restrictions, phase segregation will often occur.

Ternary I-III-IV_2 chalcopyrites, a large group of semiconductors, possess various structural, electrical and optical properties[4, 5]. Examples of group I include Li, Na, K, Cs, Cu, Au and Ag; group II: Al and Ga; and group IV: O, S, Se and Te.

Potassium gallium sulfide ($KGaS_2$) and potassium gallium selenide ($KGaSe_2$), I-III-VI_2 group semiconductors, are examples for host materials for DMS applications. The title compounds are similar in structure of tetrahedral coordination

stacking in unit cells with GaAs. The single crystal structures of ternary chalcogenides, $KAlTe_2$ and $KGaTe_2$, have been reported in Hugbanks's paper.[6] Similarly, the isostructural compound, $KGaS_2$, has adamantine-like supertetrahedra, Ga_4S_{10}, which consists of four GaS_4 tetrahedrons. (Figure 5.1) Each Ga_4Se_{10} forms two-dimensional $GaSe_2$ layers by sharing corner chalcogen atoms with neighboring Ga_4Se_{10}. The unit cell parameters for both $KGaSe_2$ and $KGaS_2$ are listed in Table 5.1.[6, 7]

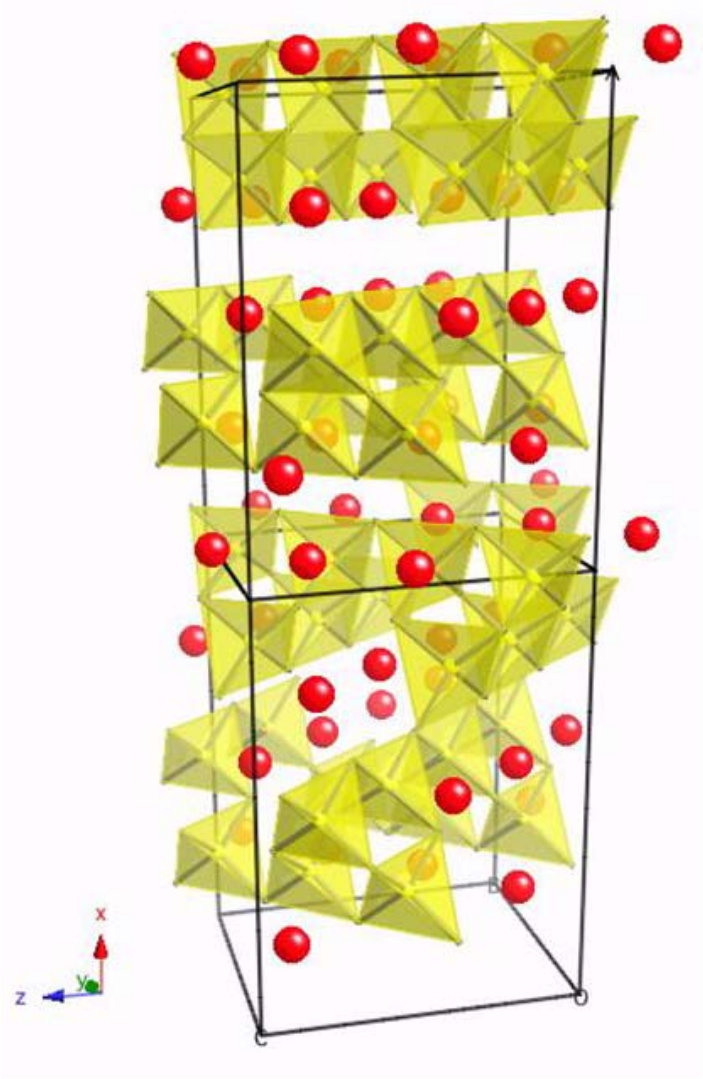

Fighre 5.1 Monoclinic structure of $KGaS_2$ with Ga_4S_{10} layer structure.

Our motivation in this project is to produce high quality host lattices and high T_c ferromagnetic materials. The synthesis of binary polychalcogenides, $KGaS_2$ and $KGaSe_2$ was described bellow.

Table 5.1 Structure and fractional atomic positions for both $KGaS_2$ and $KGaSe_2$.

Atom	**x**	**y**	**z**	**Wyck**
Ga 1	1	1	0.1876	4a
Ga 2	0.5011	0.7482	0.0649	4a
Ga 3	-0.1735	0.4578	-0.0627	4a
Ga 4	0.3258	0.7039	0.3099	4a
K 1	0.7743	0.8190	0.0688	4a
K 2	0.0517	0.6387	0.3152	4a
K 3	-0.2299	0.5672	0.3094	4a
K 4	0.0537	0.3889	0.0556	4a
S 1	0.4111	0.6062	0.4395	4a
S 2	0.5903	0.9051	-0.0593	4a
S 3	0.5966	0.6458	0.1854	4a
S 4	0.9141	0.6067	0.0700	4a
S 5	0.2318	0.8134	0.4353	4a
S 6	0.4186	0.8601	0.1915	4a
S 7	0.2331	0.5552	0.1898	4a
S 8	-0.0817	0.8496	0.3117	4a
$KGaS_2$: a =14.791(5) Å, b =10.425(3) Å, c =10.424(2) Å $\alpha = 90^{\circ}$, $\beta = 90^{\circ}$, $\gamma = 100.16(2)^{\circ}$ Space group: *Aa* (9)				
Atom	**x**	**y**	**z**	**Wyck**
Ga 1	0.6029	0.6860	0.1608	8f
Ga 2	0.1470	0.4400	0.3380	8f
K 1	0.4670	0.3132	0.1135	8f
K 2	0.2860	0.0610	0.3876	8f
Se 1	0	0.5710	0.2500	4e
Se 2	0	0.0540	0.2500	4e
Se 3	0.2037	0.0624	0.0635	8f
S 4	0.2600	0.3124	0.2480	8f
S 5	0.0468	0.3125	0.4356	8f
$KGaSe_2$:a =10.945(4) Å, b =10.947(3) Å, c =15.314(6) Å $\alpha = 90^{\circ}$, $\beta = 90^{\circ}$, $\gamma = 100.22(5)^{\circ}$ Space group: *C2c* (15)				

5.2 Alkali Metal Polychalcogenides

Alkali metal polychalcogenides, such as K_2S_x, have been studied in previous literature.[8-10] Phase diagram investigations have demonstrated the existence of six different compounds (x=1, 2….6) and five eutectics shown in Figure 5.2.[11] For the potassium sulfides, K_2S_x, (x=2, 3 4, and 5) are well defined. However when the sulfur composition is over 75 at.%, a two liquid region had been reported.[8, 10] The monosulfide has a melting point of 948 ˚C, and the tetrasulfide shows the lowest melting point of 120 ˚C. Generally alkali metal polychalcogenides have a low melting point. Melting points of some known alkali metal polychalcogenides are listed in Table 5.2.[10, 12-16]

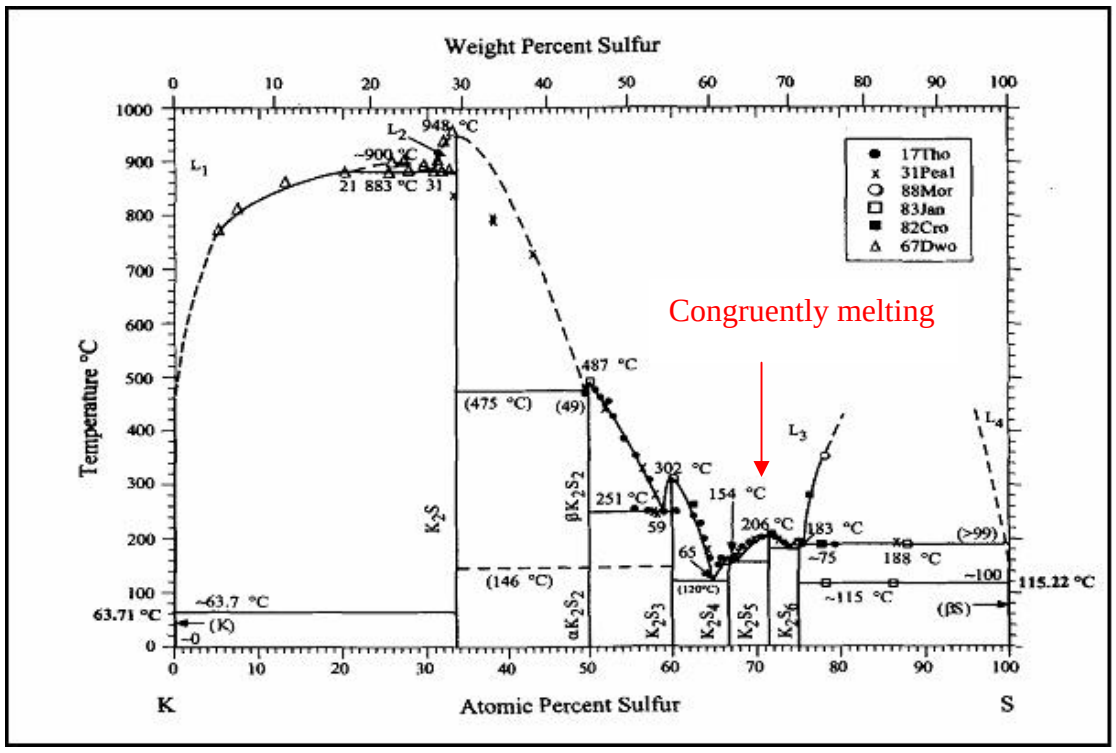

Figure 5.2 K-S binary phase diagram.

Table 5.2 Melting Points (˚C) for alkali metal polychalcogenides. (A_2B_x where A= alkali metal and B is chalcogenide atom)

X=1	X=2	X=3	X=4	X=5	X=6
Li_2S (1372)	Li_2S_2 (369.5)				
Na_2S (1200)	Na_2S2 (490)	Na_2S_3 (261)	Na_2S_4 (300)	Na_2S_5 (252)	
Na_2Se (>875)	Na_2Se_2 (495)	Na_2Se_3 (313)	Na_2Se_4 (290)		Na_2Se_6 (221)
Na_2Te (953)	Na_2Te_2 (348)				Na_2Te_6 (436)
K_2S (948)	K_2S_2 (487)	K_2S_3 (302)	K_2S_4 (120)	K_2S_5 (206)	K_2S_6 (183)
K_2Se (800)	K_2Se_2 (460)	K_2Se_3 (375)	K_2Se_4 (205)	K_2Se_5 (195)	
K_2Te (920)	K_2Te_2	K_2Te_3 (432)			
Rb_2S (530)	Rb_2S_2 (420)	Rb_2S_3 (213)	Rb_2S_4 (160)	Rb_2S_5 (225)	Rb_2S_6 (201)
Cs_2S	Cs_2S_2 (460)	Cs_2S_3 (217)	Cs_2S_4 (160)	Cs_2S_5 (210)	Cs_2S_6 (186)
Cs_2Se (770)		Cs_2Se_3 (338)		Cs_2Se_5 (242)	

5.3 Experimental Methods

The synthesis of ternary alkali metal polychalcogenides was carried out in a lower alkali metal chalcogeide melt. An appropriate amount of high purity gallium was added in binary chalcogenides; the gallium reacted the chalcogenide at high temperature to form a ternary compound.

High purity elemental starting materials, germanium (7N), potassium (99.95% Alfa), and selenium (Aldrich), was used for preparation of $KGaS_2$ and $KGaSe_2$. Phase identification was characterized by the PANalytical powder X-ray diffractometer (PW 60/40 and PW 3830). A Field Emission Scanning Electron Microscopy (Zeiss DSM 940) and an Energy Dispersive Spectroscope detector (EDS, Apollo 40) were utilized for crystal examination and elemental composition, respectively. All preparation for the starting materials was carried out in an argon filled glove box. Table 5.3 lists the starting materials and reaction conditions.

Table 5.3 The list of reaction conditions.

Solid state Reaction	KSe_2 (g)	Ga (g)	Mn (g)	Tmax (ºC)	t_{dwell} (h)
SA 5	0.960	0.689	0.020	600	24
SA 6	1.051	0.704	0.061	600	24
SA 7	0.966	1.291	0.072	600	24
SA 8	0.997	0.824	0.169	600	24
Flux Growth	K_2S_5 (g)	Ga (g)	Mn (g)	Tmax (ºC)	t_{dwell} (h)
QN 3	1.20	0.005	0.0005	600	48
QN 4	0.635	0.003	0.0007	600	48
QN 5	0.555	0.002	0.0004	600	48

5.3.1 Synthesis of the Potassium Selenides (KSe_2), Potassium Gallium Selenides ($KGaSe_2$) and its Mn-substituted Compounds

The synthesis of KSe_2 (SA2): The reaction of potassium selenium (KSe_2) took place in a quartz crucible and an argon filled glove box. Potassium (K) was placed in a quartz crucible and was heated to its melting point, 63.38 ˚C. Selenium (Se) powder was then added into the K melt. To avoid an exoethermic event that leads to an explosion, 0.502 g Se powder was added slowly into preheated 2.065 g K melt. Dark brown colored KSe_2 crystals were in the quartz crucible after the end of the reaction.

The synthesis of pure and Mn-substituted $KGaSe_2$ (SA3, SA4, SA5, SA6, SA7, SA8): $KGaSe_2$ polycrystalline samples were synthesized from the stoichiometric melt, KSe_2. The starting materials, KSe_2 and Ga with molar ratio of 1:1, were placed in a quartz reaction ampoule. However, the difficulty in weighting liquid Ga precisely needed to be taken into account. Layer packing was brought out to vary the mass of KSe_2 as Ga concentration. First, 1 g of KSe_2 powder was added in the tube and then 0.778 g Ga was added into the reaction tube. In order to mainatin the stoichiometric ratio, the mass of KSe_2 powder was regulated as the mass of Ga. The quartz ampoule was sealed under vacuum. After sealing, the ampoule was placed in a muffle furnace. The maximum reaction temperature was 600 ˚C, and the system dwelled at the maximum temperature for 24 hours. The quartz ampoules slowly cooled down to 300 ˚C by 5 ˚C/hr.

$KGaSe_2$ DMS materials with Mn substitution were also synthesized.

Mn-substituted $KGaSe_2$ were prepared by solid state reactions with a stoichiometric ratio. Various concentrations of Mn, from 4 at.% to 20 at.%, were added to the mixture of KSe_2 and Ga to grow Mn-substituted $KGaSe_2$ crystals. The mixtures were then placed in quartz reaction tubes, and the samples were heated to 600 ˚C in 6 hours and then held for 24 hours. The system temperature was lowered to 300 ˚C in 60 hours, and then it was drastically decreased to room temperature

5.3.2 The Synthesis for Potassium Selenides (K_2S_5), Potassium Gallium Selenides ($KGaS_2$) and its Mn-substituted DMS materials

The synthesis of K_2S_5 (QN1): The precursor, K_2S_5 was synthesized in the mixture of K and S. Similarly due to the large enthalpy release, the S powder was added slowly into the molten metal K. A proper amount of 4.637 g (0.1446 mole) sulfur was sprinkled gently into the system with 2.827 g (0.0723 mole) potassium. When S powder was added into the quartz crucible, a violent reaction came with a flame, without oxygen surrounding. The brownish K_2S_5 powder sample was sitting in the crucible when the reaction finished.

The synthesis of pure $KGaS_2$ (QN2): The $KGaS_2$ single crystals were synthesized in self-flux crystal growth. Starting materials, a mixture of K_2S_5 1.222 g and Ga 0.505 g , were placed in a quartz ampoule. The reaction occurred in a vacuum sealed quartz ampoule at 600 ˚C. The same heating profile as $KGaSe_2$ crystal growth was used to synthesize $KGaS_2$. When room temperature was reached, crystals were observed in the reaction tube.

The synthesis of Mn-substituted $KGaS_2$ (QN4, QN5): Manganese substituted

Potassium gallium selenide ($KGa_{1-x}Mn_xSe$) single crystal were grown from the K_2S_5 self-flux technique. For the single crystal synthesis of Mn-substituted $KGaS_2$ with 15 at.% and 20 at.% Mn, K_2S_5, Ga, and metal Mn were packed in the quartz tubes and were sealed under vacuum. The same muffle furnace and heating profile were used for the synthesis. Mn-substituted $KGaS_2$ single crystals were synthesized when room temperature was reached.

5.3.3 Purification of as Grown Crystals

Non-hygroscopic $KGaS_2$ and $KGaSe_2$ crystals were cleaned using suction filtration (Figure 5.3). As grown crystals were cleaned by suction filtration technique with a Büchner funnel using filter paper and DW (deionized water).

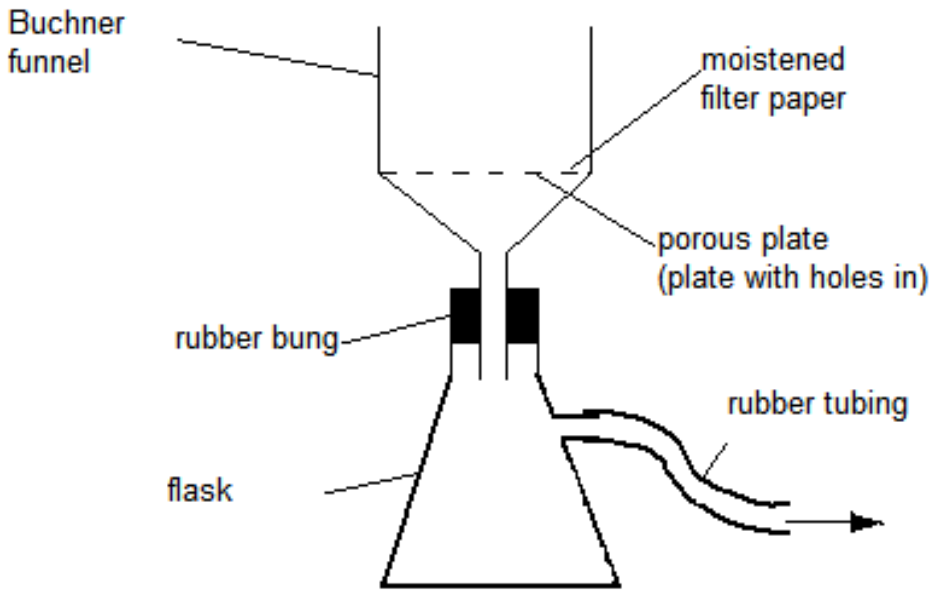

Figure 5.3 Suction filtration set up.

5.4 Results and Discussions

5.4.1 The Crystal Growth of Pure $KGaSe_2$ and Mn-substituted $KGaSe_2$

Synthesis of pure $KGaSe_2$ (SA3): In order to synthesis KSe_2, selenium was added wisely into the K melt. Two steps were used to achieve KSe_2 crystals to reduce the risk avoiding an explotion. One mole of Se powder was added in liquid K to make K_2Se first.

The mechanism for the K_2Se synthesis is shown in below:

$$2K + Se \rightarrow K_2Se \quad (5.1)$$

Comparing to the XRD powder pattern of K_2Se sample to the JCPDS database, the XRD powder pattern reveals K_2Se (JCPDS 47-1703)(Figure 5.4). Afterwards the rest of Se powder was mixed with K_2Se to form KSe_2.

$$K_2Se + 3Se \rightarrow 2KSe_2 \quad (5.2)$$

This highly exothermic reaction came with the presence of anoxycausis when the reaction took place.

The heat released from this reaction brought K and Se together and formed potassium selenide products. Then the high purity metal Ga was added in KSe_2 within a 1:1 stoichiometric ratio to grow $KGaSe_2$ crystal.

$$KSe_2 + Ga \rightarrow KGaSe_2 \quad (5.3)$$

When room temperature was reached, the non-air sensitive sample was identified from the XRD powder pattern. (Figure 5.4)

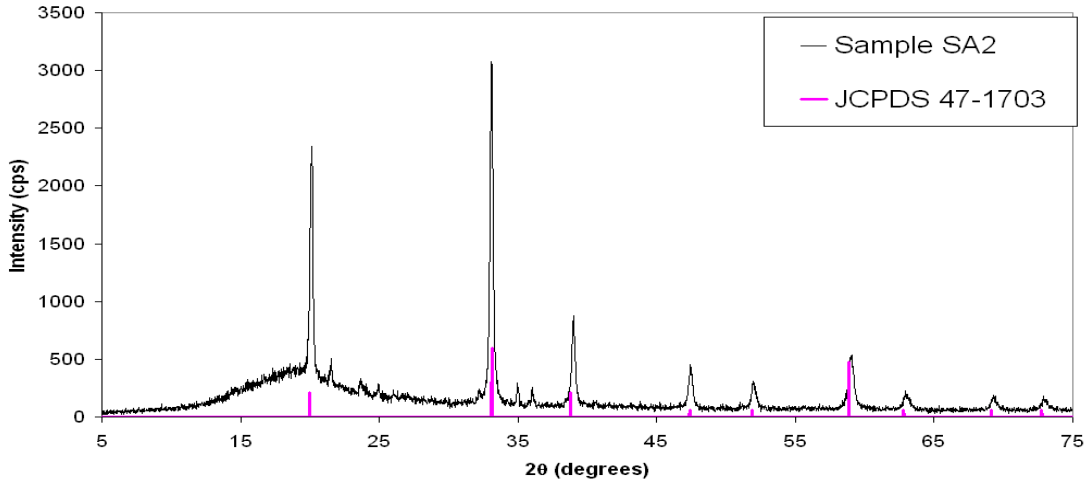

Figure 5.4 Powder XRD pattern of K_2Se from reaction SA2.

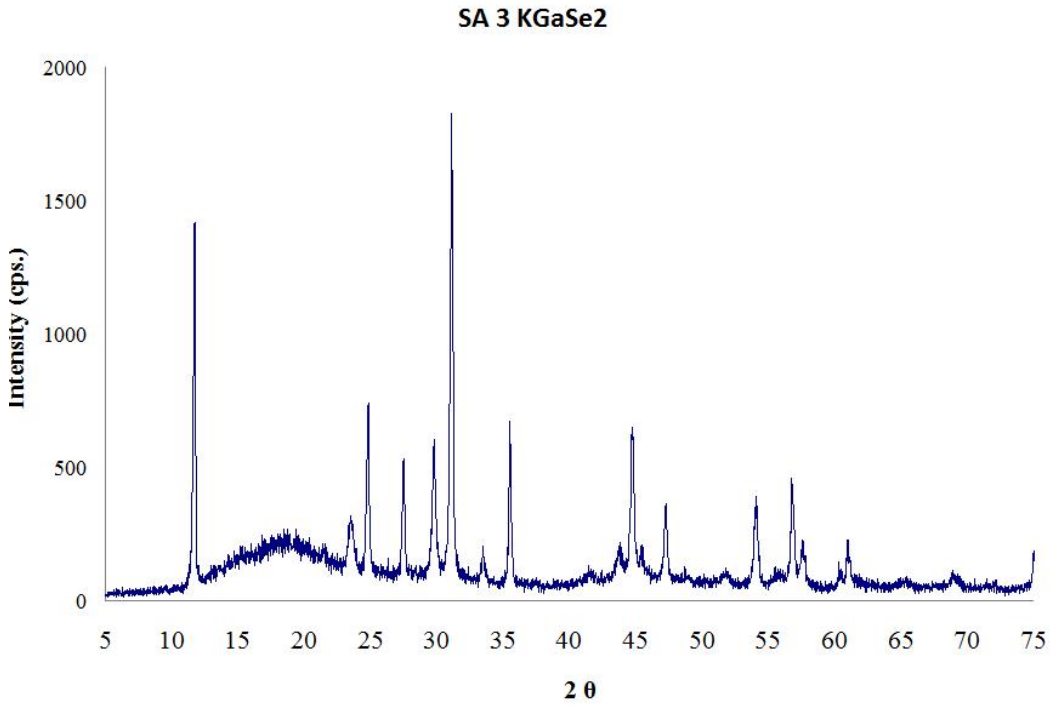

Figure 5.5 Powder X-ray pattern for the pure $KGaSe_2$ from the reaction SA3.

Synthesis of Mn-substituted $KGaSe_2$ (SA4, SA5, SA6, SA7, SA8): For Mn-substituted polyatomic selenide crystals, traditional solid state reactions were

used. Various Mn concentration from 4 at.% to 20 at.% was added to the $KGaSe_2$ reaction. The $KGa_{0.90}Mn_{0.10}Se_2$ single crystal, 230 μm x 340 μm is shown in the SEM image. (Figure 5.6)

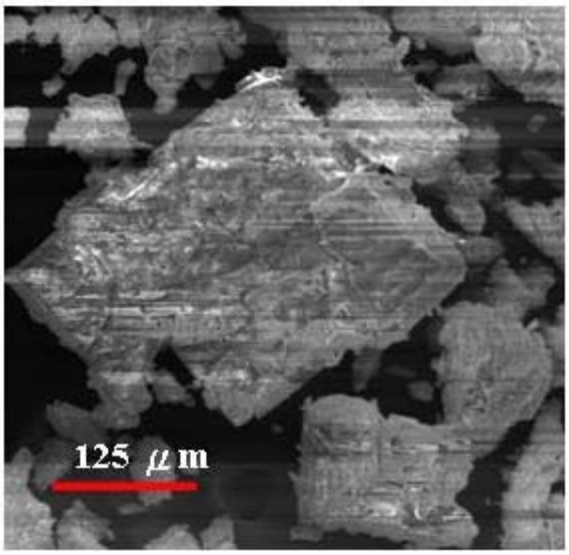

Figure 5.6 The SEM image of $KGa_{0.90}Mn_{0.10}Se_2$ (SA7).

The $KGaSe_2$ crystals with Mn substituents were identified via XRD. The major peaks in the powder pattern correspond to $KGaSe_2$ (compared to the Hugbank report). (Figure 5.7) The secondary phase is identified as MnSe (JCPDS 73-1741) The peak shift toward lower angles,as Mn concentration increased, was observed. (Figure 5.8) In order to further study the Mn-substituted $KGaSe_2$, an EDS quantitative analysis was utilized. The EDS data of Mn concentration in various samples with original concentrations of 4 at.% to 20 at.% are listed in Table 5.4. For all the Mn-substituted compounds, less than 1 at.% of Mn concentration was detected in the EDS quantitative analysis data.

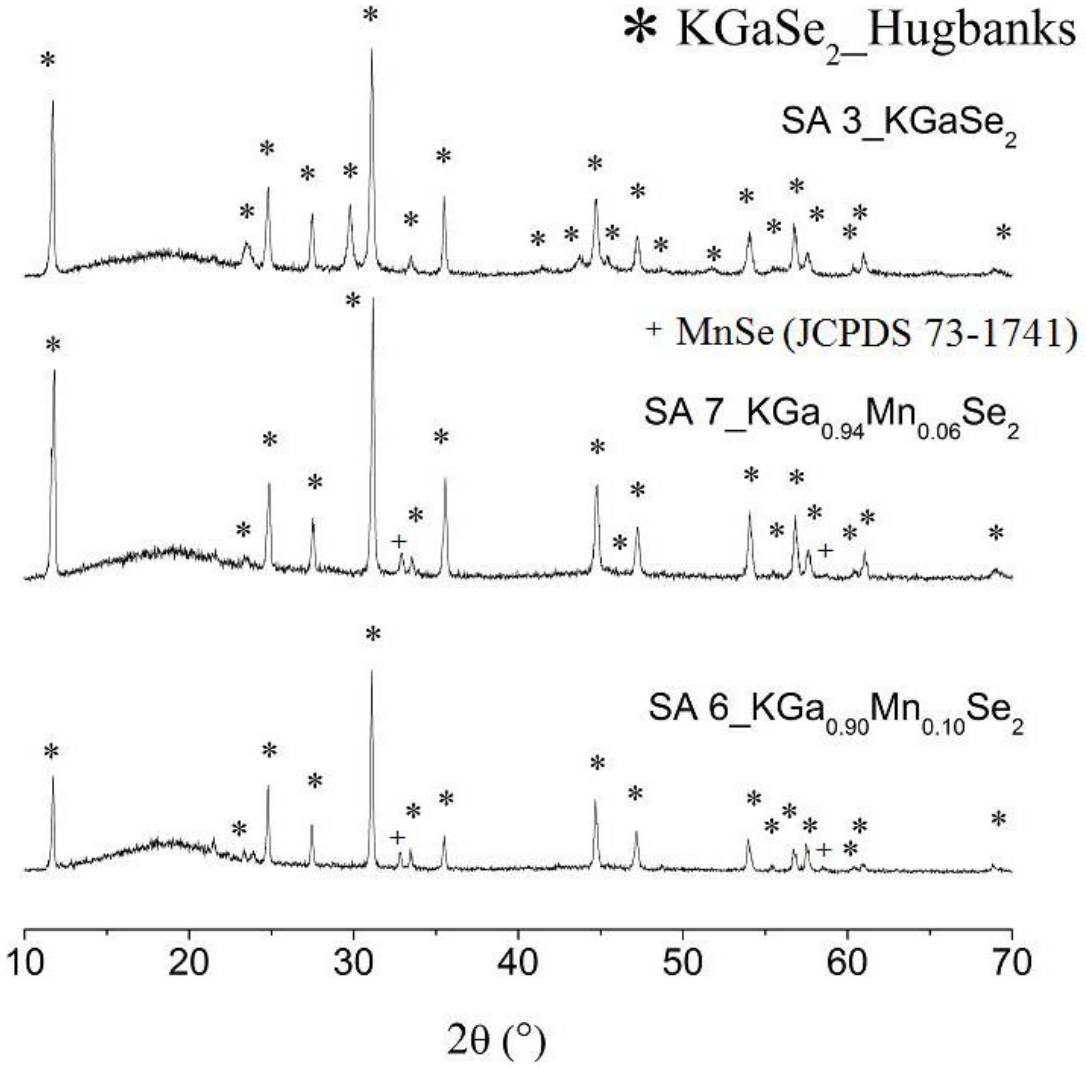

Figure 5.7 X-ray powder diffraction patterns of $KGaSe_2$ (SA3),, $KGa_{0.90}Mn_{0.10}Se_2$, $KGa_{0.94}Mn_{0.06}Se_2$(SA6), and $KGa_{0.90}Mn_{0.10}Se_2$ (SA7). The peaks are labeled with (*), which correspond to K $GaSe_2$ and those peaks labeled with (+) are from MnSe (JCPDS 73-1741).

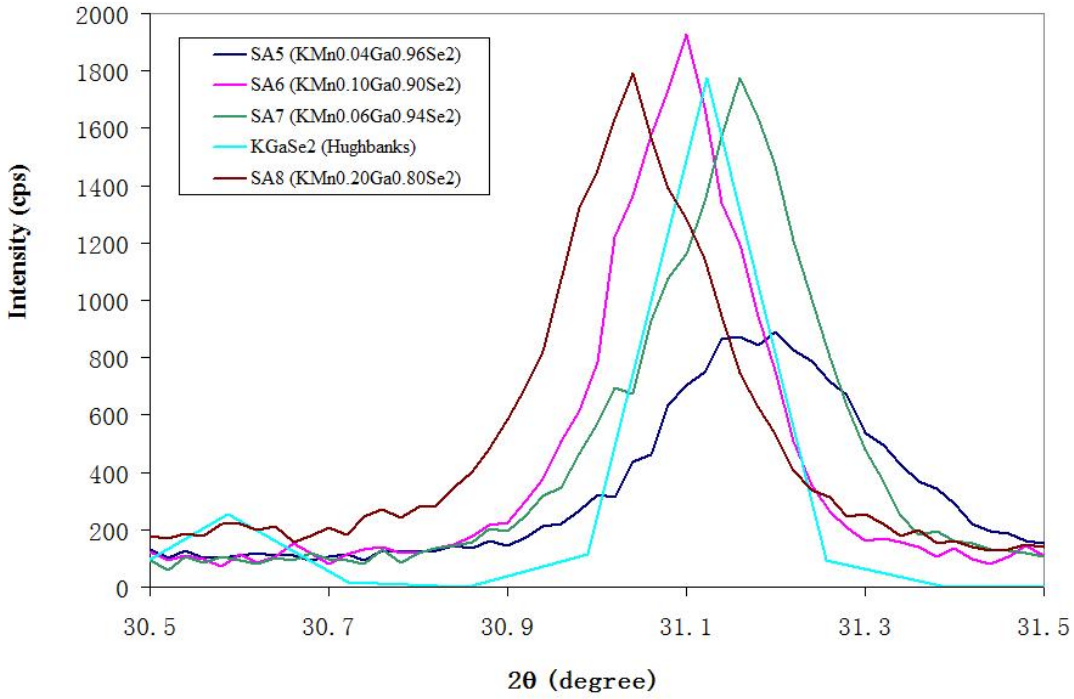

Figure 5.8 The peak shift of X-ray powder diffraction patterns for Mn-substituted $KGaSe_2$ are observed. (SA5, SA6, SA7, SA8)

Table 5.4 The EDS observation Mn compositions and the original Mn fractions.

Reactions	Original Mn (at.%)	Observed Mn (at.%)
SA5-$KGa_{0.96}Mn_{0.04}Se_2$	4	0.01
SA6-$KGa_{0.94}Mn_{0.06}Se_2$	6	0.61
SA7-$KGa_{0.90}Mn_{0.10}Se_2$	10	0.59
SA8-$KGa_{0.80}Mn_{0.20}Se_2$	20	0.39

5.4.2 The Crystal Growth of Pure $KGaS_2$ and Mn-substituted $KGaS_2$

Synthesis of pure $KGaS_2$ (QN2): The yellow $KGaS_2$ single crystals were prepared by the self-flux technique. (Figure 5.12) The flux, K_2S_5, was grown previously in the dry box. Dark purple K_2S_5 crystals were synthesized by adding S powder in the liquid K. Due to the same aforementioned reason, a two-step synthesis was proposed.

There are some other preparations of K_2S_5, including the reaction in aqua solution, organic solvent and dry chemical synthesis routes. In addition, K_2S_5 polycalcogenide compound can be prepared by the reaction of K_2S with S in ethanol (solvent); the desulfurization of K_2S_6 in water.[17] The reaction of K and S may also be carried out under boiling toluene or in liquid ammonia to obtain K_2S_5.[18, 19] There are other dry chemical reactions of S with binary potassium sulfide, K_2S_3 and K_2S_4.[8, 17, 20]

K_2S_5, a congruent melting compound, is a promising candidate for this sulfide crystal growth because of its low congruent melting point of 206 ºC, which has been reported in the previous investigation of the K-S equilibrium system (Figure 5.2).[17, 21, 22]

Yellowish $KGaS_2$ crystals were obtained from K_2S_5 self-flux synthesis. (Figure 5.9) The $KGaS_2$ was a predominant phase in XRD powder pattern. (Figure 5.10)

Synthesis of Mn-substituted $KGaS_2$ (QN4, QN5): Single crystal, Mn-substituted $KGaS_2$ was synthesized with K_2S_5 polysulfide flux in a quartz tube. Phase identification was performed via XRD. (Figure 5.11) The powder X-ray

pattern confirmed the presence of $KGaS_2$ (JCPDS 04-010-1520) as major component. Beside $KGaS_2$ peaks, MnS (JCPDS 72-1534) peaks in both $KGa_{0.8}Mn_{0.2}S_2$ (QN4) and $KGa_{0.85}Mn_{0.15}S_2$ (QN5) samples were observed.

Figure 5.9 The optical image for the yellow $KGaS_2$ polycrystalline sample. (QN2)

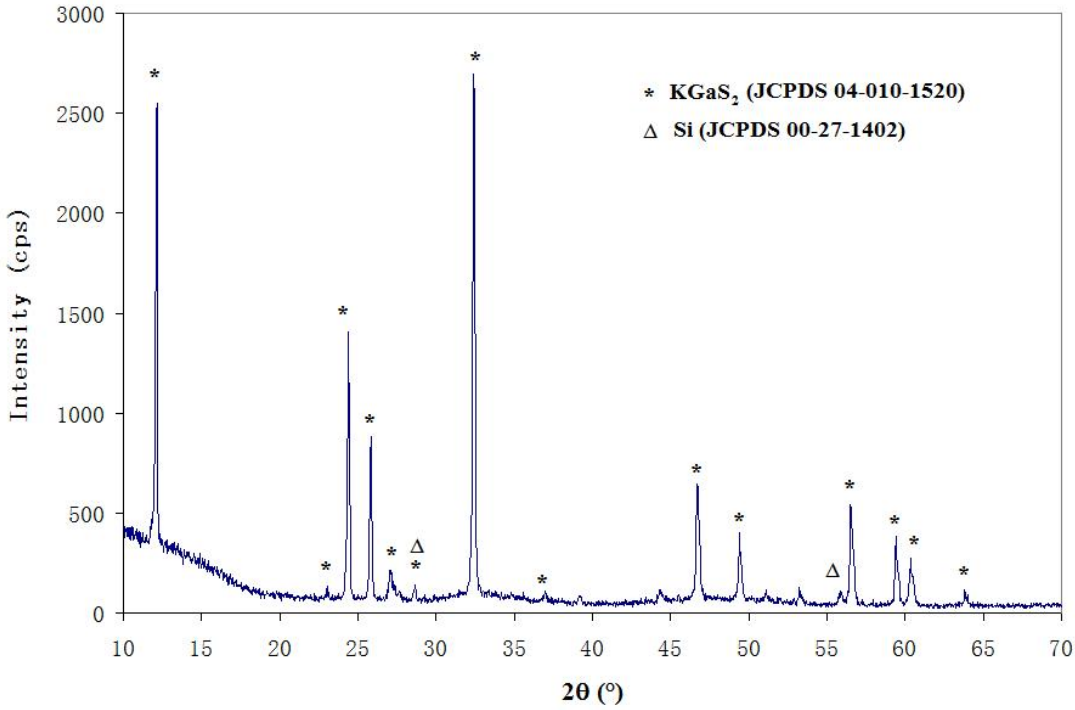

Figure 5.10 The XRD powder pattern of pure $KGaS_2$ (QN2) crystals with internal standard Si. The major phase is pure $KGaS_2$.

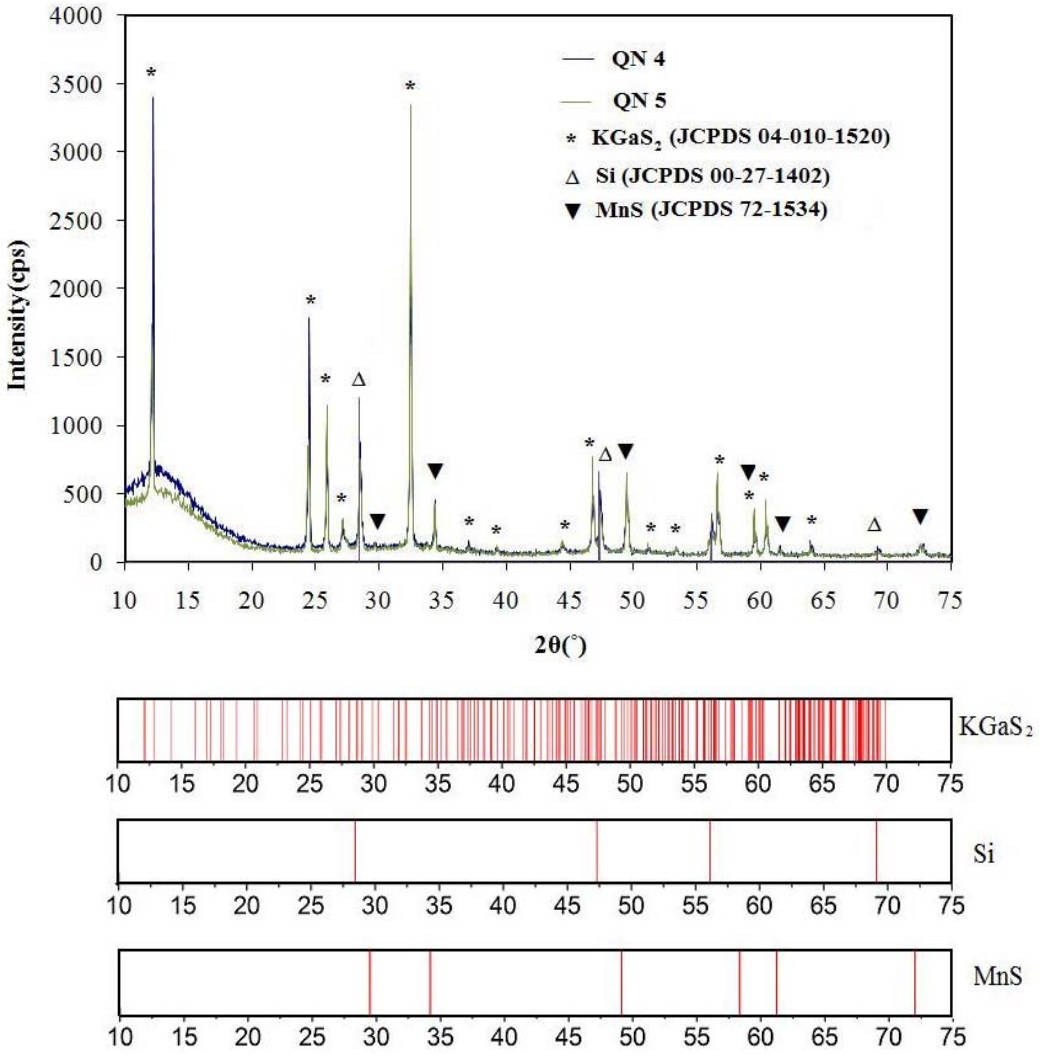

Figure 5.11 Powder X-ray diffraction patterns of Mn-substituted $KGaS_2$ samples (QN4, QN5) show the peaks of $KGaS_2$ (JCPDS 04-010-1520), Si (JCPDS 27-1402), and MnS (JCPDS 72-1534). The Si phase is the internal standard. The secondary phase, MnS, was observed in both $KGa_{0.8}Mn_{0.2}S_2$ and $KGa_{0.85}Mn_{0.15}S_2$ samples.

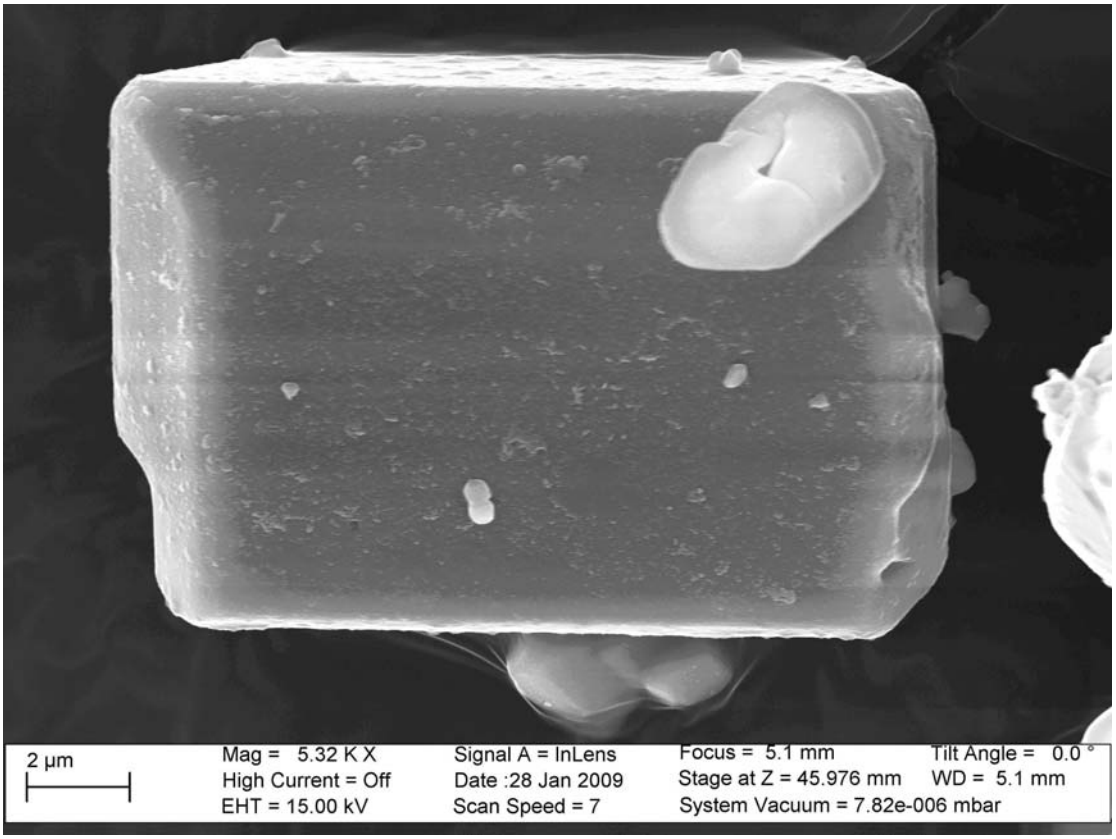

Figure 5.12 SEM image of $KGaS_2$ single crystal (QN2). Single $KGaS_2$ crystal surface information and morphology was determined by a field emission scanning microscope.

5.5 Conclusions

Polychalcogenide crystals have been prepared from exothermic reactions, and the products were characterized by powder XRD analysis. An interesting phenomenon, anoxycausis, was observed when the K and Se or S bonded together. These ionic interactions were formed along with the enthalpy release.

The layered compounds, $KGaS_2$ and $KGaSe_2$, have been synthesized from the reactions of binary polychalcogenides and Ga. These desired ternary chalcogenide semiconductors were indentified by powder XRD.

Crystal growth of Mn-substituted $KGaSe_2$ was demonstrated from solid state synthesis with seal quartz ampoules. In the X-rays pattern, peaks shift as Mn concentration was observed. Several samples with Mn, 4 at.% to 20 at.%, exhibited less than 1 at.% Mn signals in the EDS investigation.

Mn-substituted $KGaS_2$ crystals were grown from the K_2S_5 flux technique. In the XRD investigation, the peaks matching MnS (JCPDS 04-003-1892) as a secondary phase in the Mn-substituted $KGaS_2$ were identified. The water washed crystals exhibited less than 1 at.% Mn incorporation in the host lattices.

.

5.6 Chapter 5 References

1. Sze, S. M., *Semiconductor Devices: Physics and Technology, 2nd Edition*. 2001; p 568 pp.

2. Agrawal, M., Magnetic Properties of Materials, Dilute Magnetic Semiconductors, Magnetic Resonances (NMR and ESR) and Spintronics. Dec: 2003.

3. Umehara, Y.; Koda, S., Structure and Phase-boundary Energies of the Directionally Solidified Indium Antimonide-manganese Antimonide, Indium antimonide-nickel Antimonide, Indium Antimonide-iron Antimonide, and Indium Antimonide-chromium Antimonide Eutectic Alloys. *Metallography* 1974, 7, 313.

4. Birkmire, R. W.; Eser, E., Polycrystalline Thin Film Solar Cells: Present Status and Future Potential. *Annual Review of Materials Science.* 1997, 27, 625.

5. Gabor, A. M.; Tuttle, J. R.; Albin, D. S.; Tennant, A. L.; Contreras, M. A.; Noufi, R., High Efficiency Polycrystalline Cu(In,Ga)Se_2-based solar cells. *AIP Conference. Proceeding.* 1994, 306, 59.

6. Hughbanks, J. K. a. T., Synthesis of Structures of Ternary Chalcogenides of Alumnium and Gallium with Stacking Faults: KMQ_2 (M = Al, Ga; Q = Se, Te). *Journal of Solid State Chemistry* 1999, 149, 242.

7. Lemoine, P.; Carre, D.; Guittard, M., The Structure of Gallium and Potasium Sulfide, $KGaS_2$ *Acta Crystallographica Section C-Crystal Structure Communications* 1984, 40, 910.

8. Janz, G. J.; Rogers, D. J., Melting and Premelting Properties for a Series of

Potassim Polysulfides *Journal of Chemical and Engineering Data* 1983, 28, 331.

9. Janz, G. J.; Rogers, D. J., Thermal-behavior of the Potassium-sulfur Electrolte in Advanced Battery Concepts. *Journal of the Electrochemical Society* 1983, 130, C128.

10. Kanatzidis, M., Molten Alkali-metal Polychalcogenides as Reagents and Solvents for the Synthesis of New Chalcogenide Materials. *Chemistry of Materials* 1990, 2, 353.

11. Sangster, J., The K-S (Potassium-sulfur) System. *Journal of Phase Equilibria and Diffusion* 1997, 18, 82.

12. *Okamoto, H.,* The Li-S (lithium-sulfur) System. *Journal of Phase Equilibria and Diffusion* 1995, 16, 94.

13. Sangster, J.; Pelton, A. D., The Na-S (sodium-sulfur) System. *Journal of Phase Equilibria and Diffusion,*1997, 18, 89.

14. Sangster, J.; Pelton, A. D., The Na-Se (sodium-selenium) System. *Journal of Phase Equilibria and Diffusion* 1997, 18, 185.

15. Pelton, A. D.; Petric, A., The Na-Te (Sodium-Tellurium) System *Journal of Phase Equilibria and Diffusion,* 1990, 11, 447.

16. Okamoto, H., K-Te (Potassium-Tellurium) *Journal of Phase Equilibria and Diffusion* 1999, 20, 541.

17. Pearson, T. G.; Robinson, P. L., The polysulphides of the Alkali Metals Part III Potassium. *Journal of the Chemical Society* 1931, 1304.

18. Draves, C. Z.; Tartat, H. V., The Polysulfides of Sodium and Potassium. *Journal*

of the American Chemical Society 1926, 48, 1527.

19. Hugot, C., Action of Sodammonium and Potassammonium on Selenium. *Compt. rend.* 1899, 129, 299.

20. Cleaver, B.; Davies, A. J.; Hames, M. D., Properties of Fused Polysulfides.1. Electtrical Conductivity of Fused Sodium and Potasium Polysulfides. *Electrochimica Acta* 1973, 18, 719.

21. Thomas, J. S.; Rule, A., The Polysulphides of the Alkali Metals. Part III. The Solidifying Points of the Systems, Sodium Monosulphide-sulphur, and Potassium Monosulphide-sulphur. *Journal of the Chemical Society* 1917, 111, 1063.

22. Bousquet, J.; Letoffe, J. M.; Diot, M., Thermal-behavior of Potassium Polysulfides. *Journal De Chimie Physique Et De Physico-Chimie Biologique* 1974, 71, 1180.

Appendix A : ZnO Crystal Growth Reaction List

Reaction Name	Reaction System	T_{max} (ºC)	Cooling Rate (ºC/hour)	Dwelling Time (hr)	ZnO (g)	ZnO (mole)	V_2O_5 (g)	V_2O_5 (mole)	Crucible
CMF 1	ZnO-V_2O_5	1300	1.2	40	24.42	0.3000	10.14	0.0558	Al_2O_3
CMF 2	ZnO-V_2O_5	1300	1.2	40	16.84	0.2069	7.7	0.0423	Al_2O_3
CMF 3	ZnO-V_2O_5	1300	1.2	40	5.5	0.0676	4.1	0.0225	Al_2O_3
CMF 4	ZnO-V_2O_5	1300	1.2	40	16.95	0.2082	7.19	0.0395	Al_2O_3
CMF 10	ZnO-V_2O_5	1300	500	0	5.5	0.0676	4.1	0.0225	
Reaction Name	**Reaction System**	**T_{max} (ºC)**	**Cooling Rate (ºC/hour)**	**Dwelling Time (hr)**	**ZnO (g)**	**ZnO (mole)**	**B_2O_3 (g)**	**B_2O_3 (mole)**	**Crucible**
CMF 7	ZnO-B_2O_3	1300	100	0	71.34	0.8763	13.4	0.1925	Pt
CMF 8	ZnO-B_2O_3	1300	3.2	2	230.2	2.8277	43.19	0.6204	Pt
CMF 9	ZnO-B_2O_3	1300	100	0		0.0000		0.0000	
CMF 11	ZnO-B_2O_3	1300	800	0	8	0.0983	1.5	0.0215	Al_2O_3
CMF 18	ZnO-B_2O_3	1300	250	10	4.72	0.0580	0.21	0.0030	Pt foil

Reaction Name	Reaction System	T_{max} (ºC)	Cooling Rate (ºC/hour)	Dwelling Time (hr)	ZnO (g)	ZnO (mole)	WO_3 (g)	WO_3 (mole)	Crucible
CMF12A	ZnO- WO_3	1350	800	0	5.11	0.0628	6.31	0.0003	Al_2O_3
CMF12B	ZnO- WO_3	1350	800	0	3.1	0.0381	3.83	0.0002	Al_2O_3
CMF 13	ZnO- WO_3	1350	800	2	3.11	0.0382	3.83	0.0002	Quartz
Reaction Name	**Reaction System**	**T_{max} (ºC)**	**Cooling Rate (ºC/hour)**	**Dwelling Time (hr)**	**ZnO (g)**	**ZnO (mole)**	**Na_3AlF_6 (g)**	**Na_3AlF_6 (mole)**	**Crucible**
CMF 14	ZnO-Na_3AlF_6	1350	500	0	5.1	0.0626	3.29	0.0157	Pt foil
CMF 15	ZnO-Na_3AlF_6	1450	500	0	5.1	0.0626	3.29	0.0157	Pt foil
CMF19A	ZnO- Na_3AlF_6	950	250	10	1.88	0.0231	0.15	0.0007	Pt foil
CMF19B	ZnO-Na_3AlF_6	950	250	10	1.5	0.0184	0.43	0.0020	Pt foil
Reaction Name	**Reaction System**	**T_{max} (ºC)**	**Cooling Rate (ºC/hour)**	**Dwelling Time (hr)**	**ZnO (g)**	**ZnO (mole)**	**Na_3AlF_6 (g)**	**Na_3AlF_6 (mole)**	**Crucible**
CMF19C	ZnO-Na_3AlF_6	950	250	10	1.2	0.0147	3.09	0.0147	Pt foil
CMF19D	ZnO-Na_3AlF_6	950	250	10	0	0.0000	0.62	0.0030	Pt foil
CMF20A	ZnO-Na3AlF_6	950	250	10	0.46	0.0057	0.04	0.0002	Pt foil
CMF20B	ZnO-Na_3AlF_6	950	250	10	0.39	0.0048	0.11	0.0005	Pt foil
CMF20C	ZnO-Na_3AlF_6	950	250	10	0.14	0.0017	0.36	0.0017	Pt foil
CMF20D	ZnO-Na_3AlF_6	950	250	10	0	0.0000	0.5	0.0024	Pt foil
CMF20E	ZnO-Na_3AlF_6	950	250	10	0.5	0.0061	0	0.0000	Pt foil

Reaction Name	**Reaction System**	**T_{max} (ºC)**	**Cooling Rate (ºC/hour)**	**Dwelling Time (hr)**	**ZnO (g)**	**ZnO (mole)**	**MoO3 (g)**	**MoO_3 (mole)**	**Crucible**
CMF 16	ZnO-MoO_3	1300	100	1	6.11	0.0751	5.82	0.0404	Al_2O_3
CMF 17	ZnO-MoO_3	1300	1	2	4.24	0.0521	0.76	0.0053	Al_2O_3
Reaction Name	**Reaction System**	**T_{max} (ºC)**	**Cooling Rate (ºC/hour)**	**Dwelling Time (hr)**	**ZnO (g)**	**ZnO (mole)**	**KPF_6 (g)**	**KPF_6 (mole)**	**Crucible**
CMF 21 A	ZnO-KPF_6	500	250	15	1.43	0.0176	0.1	0.0005	Pt foil
CMF 21 B	ZnO-KPF_6	500	250	15	1.23	0.0151	0.31	0.0017	Pt foil
CMF 21 C	ZnO-KPF_6	500	250	15	0.52	0.0064	1.18	0.0064	Pt foil
CMF 21 D	ZnO-KPF_6	500	250	15	0	0.0000	0.52	0.0028	Pt foil
CMF 22A	ZnO-KPF_6	1000	250	10	0.46	0.0057	0.04	0.0002	Pt foil

Reaction Name	Reaction System	T_{max} (ºC)	Cooling Rate (ºC/hour)	Dwelling Time (hr)	ZnO (g)	ZnO (mole)	KPF_6 (g)	KPF_6 (mole)	Crucible
CMF22B	ZnO-KPF_6	1000	250	10	0.4	0.0049	0.1	0.0005	Pt foil
CMF22C	ZnO-KPF_6 pellet	1000	250	10	0.15	0.0018	0.35	0.0019	Pt foil
CMF22D	ZnO-KPF_6	1000	250	10	0.36	0.0044	0.14	0.0008	Pt foil
CMF22E	Pure ZnO pellet	1000	250	10	0.5	0.0061	0	0.0000	Pt foil
Reaction Name	**Reaction System**	**T_{max} (ºC)**	**Cooling Rate (ºC/hour)**	**Dwelling Time (hr)**	**ZnO (g)**	**ZnO (mole)**	**NaF (g)**	**NaF (mole)**	**Crucible**
CMF23A	ZnO-NaF	900	250	7	0.49	0.0060	0.01	0.0001	Pt foil
CMF23B	ZnO-NaF	900	250	7	0.47	0.0058	0.03	0.0002	Pt foil
CMF23C	ZnO-NaF	900	250	7	0.33	0.0041	0.17	0.0009	Pt foil
CMF23D	Pure NaF	900	250	7	0	0.0000	0.5	0.0027	Pt foil
Reaction Name	**Reaction System**	**T_{max} (ºC)**	**Cooling Rate (ºC/hour)**	**Dwelling Time (hr)**	**ZnO (g)**	**ZnO (mole)**	**Mn_2O_3 (g)**	**Mn_2O_3 (mole)**	**Crucible**
CMF24A	ZnO-Mn_2O_3	1300	250	10	2.8	0.0344	0.05	0.0003	Pt foil
CMF24B	ZnO-Mn_2O_3	1300	250	10	1.65	0.0203	0.09	0.0005	Pt foil
CMF24C	ZnO-Mn_2O_3	1300	250	10	1.53	0.0188	0.3	0.0016	Pt foil
CMF24D	ZnO-Mn_2O_3	1300	250	10	1.51	0.0185	0.67	0.0036	Pt foil
CMF26D	ZnO-Mn2O3	750	1.1	10	4.48	0.0550	0.08	0.0005	Al_2O_3

Reaction Name	Reaction System	T_{max} (ºC)	Cooling Rate (ºC/hour)	Dwelling Time (hr)	ZnO (g)	ZnO (mole)	NaCl (g)	NaCl (mole)	Crucible
CMF28A	ZnO-NaCl	500	2	48	0.37	0.0045	13.29	0.2274	Al_2O_3
CMF28B	ZnO-NaCl	500	2	48	0.84	0.0103	12.06	0.2064	Al_2O_3
CMF28C	ZnO-NaCl	500	2	48	2.81	0.0345	10.09	0.1726	Al_2O_3
Reaction Name	**Reaction System**	**T_{max} (ºC)**	**Cooling Rate (ºC/hour)**	**Dwelling Time (hr)**	**ZnO (g)**	**ZnO (mole)**	**KOH (g)**	**KOH (mole)**	**Crucible**
CMF27C	ZnO-KOH	750	1.1	10	1.27	0.0156	43.95	0.7833	Al_2O_3
CMF27D	ZnO-KOH	750	1.1	10	1.27	0.0156	8.8	0.1568	Al_2O_3
CMF29A	ZnO-KOH	500	2	48	12.5	0.1535	25.89	0.4615	Al_2O_3
CMF29B	ZnO-KOH	500	2	48	5.08	0.0624	35.09	0.6254	Al_2O_3
CMF29C	ZnO-KOH	500	2	48	2.46	0.0302	34.01	0.6062	Al_2O_3
Reaction Name	**Reaction System**	**T_{max} (ºC)**	**Cooling Rate (ºC/hour)**	**Dwelling Time (hr)**	**ZnO (g)**	**ZnO (mole)**	**NaOH (g)**	**NaOH (mole)**	**Crucible**
CMF25A	ZnO-NaOH	750	5	1	4.1	0.0504	2	0.0500	Al_2O_3
CMF25B	ZnO-NaOH	750	5	1	1	0.0123	2.4	0.0600	Al_2O_3
CMF26A	ZnO-NaOH	750	1.1	10	4.12	0.0506	2.02	0.0505	Al_2O_3
CMF26B	ZnO-NaOH	750	1.1	10	1.71	0.0210	4.2	0.1050	Al_2O_3
CMF26C	ZnO-NaOH	750	1.1	10	1.01	0.0124	4.88	0.1220	Al_2O_3
CMF27A	ZnO-NaOH	750	1.1	10	5.25	0.0645	25.38	0.6345	Al_2O_3

Reaction Name	Reaction System	Tmax (ºC)	Cooling Rate (ºC/hour)	Dwelling Time (hr)	ZnO (g)	ZnO (mole)	NaOH (g)	NaOH (mole)	Crucible
CMF 27B	ZnO-NaOH	750	1.1	10	2	0.0246	48	1.2001	Al_2O_3
CMF 27E	ZnO-NaOH	750	1.1	10	1	0.0123	12	0.3000	Al_2O_3
CMF 31A	ZnO-NaOH	750	1.1	10	13.55	0.1664	66.67	1.6669	Al_2O_3
CMF 31B	ZnO-NaOH	750	1.1	10	2.99	0.0367	14.64	0.3660	Al_2O_3
CMF 31C	ZnO-NaOH	750	1.1	10	1.81	0.0222	8.89	0.2223	Al_2O_3
CMF 31D	ZnO-NaOH	750	1.1	10	1.01	0.0124	4.88	0.1220	Al_2O_3
CMF 31E	ZnO-NaOH	750	1.1	10		0.0000	3.48	0.0870	Al_2O_3

Reaction Name	Reaction System	Tmax (ºC)	Dwelling Time (hr)	ZnO (g)	ZnO (mole)	NaOH (g)	NaOH (mole)	KPF_6 (g)	KPF_6 (mole)	Crucible
CMF30A	ZnO-NaOH-KPF_6	650	5	9	0.1106	4.44	0.1110	20.45	0.1111	Al_2O_3
CMF30B	ZnO-NaOH-KPF_6	650	5	4.07	0.0500	20	0.5000	9.26	0.0503	Al_2O_3
Reaction Name	**Reaction System**	**Tmax (ºC)**	**Dwelling Time (hr)**	**ZnO (g)**	**ZnO (mole)**	**NaOH (g)**	**NaOH (mole)**	**Mn_2O_3 (g)**	**Mn_2O_3 (mole)**	**Crucible**
CMF32A	ZnO-NaOH-Mn_2O_3	500	48	13.5616	0.1666	66.6519	1.6664	0.1918	0.0012	Al_2O_3
CMF32B	ZnO-NaOH-Mn_2O_3	500	48	13.5617	0.1666	66.6597	1.6666	0.096	0.0006	Al_2O_3
CMF32C	ZnO-NaOH-Mn_2O_3	500	48	5.498	0.0675	27.052	0.6763	0.0238	0.0002	Al_2O_3
CMF32D	ZnO-NaOH-Mn_2O_3	500	48	2.7123	0.0333	13.4542	0.3364	0.0767	0.0005	Al_2O_3
CMF32E	ZnO-NaOH-Mn_2O_3	500	48	2.7128	0.0333	13.4001	0.3350	0.01912	0.0001	Al_2O_3
CMF94	ZnO-NaOH-Mn_2O_3	500	60	3.016		5.504	0.1376			silver tube

Reaction Name	Reaction System	T_{max} (ºC)	Dwelling Time (hr)	ZnO (g)	ZnO (mole)	NaOH (g)	NaOH (mole)	$MnCO_3$ (g)	$MnCO_3$ (mole)	Crucible
CMF33A	ZnO-NaOH-$MnCO_3$	500	48	5.4238	0.0666	26.6	0.6650	0.7665	0.00667	Al_2O_3
CMF33B	ZnO-NaOH-$MnCO_3$	500	48	5.4245	0.0666	26.63	0.6658	1.1491	0.01	Al_2O_3
CMF33C	ZnO-NaOH-$MnCO_3$	500	48	5.4247	0.0666	26.68	0.6670	1.5324	0.01333	Al_2O_3
CMF33D	ZnO-NaOH-$MnCO_3$	500	48	5.4246	0.0666	26.71	0.6678	0.7661	0.00666	Al_2O_3
CMF34A	ZnO-NaOH-$MnCO_3$	500	48	5.0858	0.0625	25	0.6250	5.7477	0.05	Al_2O_3
CMF34B	ZnO-NaOH-$MnCO_3$	500	48	5.086	0.0625	25.02	0.6255	3.593	0.03126	Al_2O_3
CMF34_2	ZnO-NaOH-$MnCO_3$	500	48	1.13	0.0139	5.48	0.1370	1.27	0.01105	Pt
CMF34_3	ZnO-NaOH-$MnCO_3$	500	48	1.13	0.0139	5.48	0.1370	0.78	0.00679	Al_2O_3
CMF34E	ZnO-NaOH-$MnCO_3$	500	48	1.13	0.0139	5.48	0.1370	1.27	0.01105	Al_2O_3
CMF34F	ZnO-NaOH-$MnCO_3$	500	48	1.13	0.0139	5.48	0.1370	0.78	0.00679	Al_2O_3
CM 35A	ZnO-NaOH-$MnCO_3$	500	48	10.1728	0.1250	50.03	1.2508	11.4967	0.10002	Al_2O_3
CMF 35B	ZnO-NaOH-$MnCO_3$	500	48	1.1297	0.0139	5.58	0.1395	1.5975	0.0139	Al_2O_3

Appendix B: $ZnSiP_2$ and $CdSiP_2$ Crystal Growth Reaction List

Reaction Name	Reaction System	Cd (g)	Cd (mole)	Ge (g)	Ge (mole)	P (g)	P mole)	T_{max} (ºC)	Reaction Container
AJ3	Cd-Ge-P	1.1241	0.0100	0.7261	0.0100	0.6119	0.0198	1000	Sealed Quartz Tubes
AJ3-2	Cd-Ge-P	Second heat treatment						1130	
Reaction Name	**Reaction System**	**Mn (g)**	**Mn (mole)**	**Si (g)**	**Si (mole)**	**P (g)**	**P (mole)**	**T_{max} (ºC)**	
AJ4	Mn-Si-P	0.5494	0.0100	0.2809	0.0100	0.6195	0.0200	1000	
AJ4-2	Mn-Si-P	Regrind pellet from first heat treatment						1130	
AJ5	Mn-Si-P	0.5494	0.0100	0.2808	0.0100	0.6195	0.0200	1000	
AJ5-2	Mn-Si-P	Grind pellet from first heat treatment						1130	
Reaction Name	**Reactin System**	**Mn (g)**	**Mn (mole)**	**Ge (g)**	**Ge (mole)**	**P (g)**	**P (mole)**	**T_{max} (ºC)**	
AJ6	Mn-Ge-P	0.5494	0.0100	0.7261	0.0100	0.6195	0.0200	1000	
AJ6-2	Mn-Ge-P	Regrind pellet from first heat treatment						1130	

Reaction Name	Reactin System	Zn (g)	Zn (mole)	Mn (g)	Mn (mole)	Si (g)	Si (mole)	P (g)	P (mole)	T_{max} (°C)
AJ-1-u_0	Zn-Si-P	1.3081	0.0200			0.5618	0.0200	1.2416	0.0401	1000
AJ-1-2		Regrind pellet from AJ-1-u_0								1130
AJ-Mn-1h		0.6408	0.0098	0.0151	0.0003	0.2809	0.0100	0.6194	0.0200	1130
AJ-Mn-2h		0.6212	0.0095	0.0378	0.0007	0.2809	0.0100	0.6194	0.0200	1130
AJ-Mn-3h										
AJ-Mn-4h		0.5885	0.0090	0.0756	0.0014	0.2809	0.0100	0.6194	0.0200	1130
AJ-Mn-5h		0.5231	0.0080	0.1512	0.0028	0.2809	0.0100	0.6194	0.0200	1130
AJ-Mn-6h										
CMF 63		2.6172	0.0400	0.0000	0.0000	1.1232	0.0400	2.4832	0.0802	1130
CMF 65		2.6161	0.0400	0.0000	0.0000	1.1240	0.0400	2.4832	0.0802	1130
CMf 67		2.6165	0.0400	0.0000	0.0000	1.1239	0.0400	2.4841	0.0802	1130
CMF 69		2.6161	0.0400	0.0000	0.0000	1.1235	0.0400	2.4832	0.0802	1130
CMF 71		0.4220	0.0065			0.1812	0.0065	0.4005	0.0129	1000

Reaction Name	Reaction System	Cd (g)	Cd (mole)	Mn (g)	Mn (mole)	Si (g)	Si (mole)	P (g)	P (mole)	T_{max} (ºC)	Reaction Container
AJ-2	Cd-Si-P	1.1241	0.0100			0.2809	0.0100	0.6210	0.0200	1000	Quartz Tube
AJ-2-2		Regrind pellet from first heat treatment								1130	
AJ-Mn-7h		1.1016	0.0098	0.0151	0.0003	0.2809	0.0100	0.6194	0.0200	1130	Quartz Tube
AJ-Mn-8h		1.0679	0.0095	0.0378	0.0007	0.2809	0.0100	0.6194	0.0200	1130	Quartz Tube
AJ-Mn-9h		1.0342	0.0092	0.0604	0.0011	0.2809	0.0100	0.6194	0.0200	1130	Quartz Tube
AJ-Mn-10h		1.0117	0.0090	0.0756	0.0014	0.2809	0.0100	0.6194	0.0200	1130	Quartz Tube
AJ-Mn-11h		0.8999	0.0080	0.1512	0.0028	0.2809	0.0100	0.6194	0.0200	1130	Quartz Tube
AJ-Mn-12h		0.7869	0.0070	0.2267	0.0041	0.2809	0.0100	0.6194	0.0200	1130	Quartz Tube
CMF 64		4.4970	0.0400	0.0000	0.0000	1.1240	0.0400	2.4843	0.0802	1130	Quartz Tube
CMF 66		4.9673	0.0442	0.0000	0.0000	1.1242	0.0400	2.4843	0.0802	1130	Quartz Tube
CMF 68		4.4968	0.0400	0.0000	0.0000	1.1243	0.0400	2.4827	0.0802	1130	Quartz Tube
CMF 70		4.4964	0.0400	0.0000	0.0000	1.1241	0.0400	2.4844	0.0802	1130	Quartz tube Graphite
CMF 72		0.5551	0.0049	0.0000	0.0000	0.1387	0.0049	0.3670	0.0118	1000	Quartz tube Graphite

Reaction Name	Reaction System	Zn (g)	Zn (mole)	Mn (g)	Mn (mole)	Si (g)	Si (mole)	P (g)	P (mole)	T_{max} (ºC)	Reaction Container
AJ-1-u_0	Zn-Si-P	1.3081	0.0200			0.5618	0.0200	1.2416	0.0401	1000	Quartz Tube
AJ-1-2		Regrind pellet from AJ-1-u_0								1130	
AJ-Mn-1h		0.6408	0.0098	0.0151	0.0003	0.2809	0.0100	0.6194	0.0200	1130	Quartz Tube
AJ-Mn-2h		0.6212	0.0095	0.0378	0.0007	0.2809	0.0100	0.6194	0.0200	1130	Quartz Tube
AJ-Mn-4h		0.5885	0.0090	0.0756	0.0014	0.2809	0.0100	0.6194	0.0200	1130	Quartz Tube
AJ-Mn-5h		0.5231	0.0080	0.1512	0.0028	0.2809	0.0100	0.6194	0.0200	1130	Quartz Tube
CMF 63		2.6172	0.0400	0.0000	0.0000	1.1232	0.0400	2.4832	0.0802	1130	Quartz Tube
CMF 65		2.6161	0.0400	0.0000	0.0000	1.1240	0.0400	2.4832	0.0802	1130	Quartz Tube
CMf 67		2.6165	0.0400	0.0000	0.0000	1.1239	0.0400	2.4841	0.0802	1130	Quartz Tube
CMF 69		2.6161	0.0400	0.0000	0.0000	1.1235	0.0400	2.4832	0.0802	1130	Quartz tube Graphite
CMF 71		0.4220	0.0065			0.1812	0.0065	0.4005	0.0129	1000	Quartz tube Graphite

Reaction Name	Reaction System	Cd (g)	Cd (mole)	Si (g)	Si (mole)	P (g)	P (mole)	Na (g)	Na (mole)	T_{max} (ºC)	Reaction Container
DM 5	Cd-Si-P	0.3380	0.0030	0.0849	0.0030	0.1866	0.0060	0.6890	0.0300	900	Stainless tube + quartz tube
DM 6	Cd-Si-P	0.3370	0.0030	0.0847	0.0030	0.2787	0.0090	0.6899	0.0300	900	Stainless tube + quartz tube
DM 7	Cd-Si-P	0.3377	0.0030	0.0851	0.0030	0.3722	0.0120	0.6892	0.0300	900	Stainless tube + quartz tube
DM 8	Cd-Si-P	0.1127	0.0010	0.0286	0.0010	0.1246	0.0040	0.4598	0.0200	900	Stainless tube + quartz tube
DM 9	Cd-Si-P	0.1111	0.0010	0.0304	0.0011	0.0611	0.0020	0.2290	0.0100	1000	Stainless tube + quartz tube
DM 10	Cd-Si-P	0.1096	0.0010	0.0345	0.0012	0.0901	0.0029	0.2242	0.0098	1000	Stainless tube + quartz tube
DM 12	Cd-Si-P	0.4335	0.0039	0.1166	0.0042	0.2408	0.0078	0	0	1000	Stainless tube + quartz tube
DM 13	Cd-Si-P	0.4330	0.0039	0.1090	0.0039	0.4043	0.0131	0	0	1000	Stainless tube + quartz tube
DM 14	Cd-Si-P	0.4332	0.0039	0.1022	0.0036	0.5290	0.0171	0	0	1000	Stainless tube + quartz tube
DM 15	Cd-Si-P	0.4335	0.0039	0.1082	0.0039	0.2389	0.0077	0	0	1000	Stainless tube
DM 20	Cd-Si-P	1.1235	0.0100	0.2822	0.0100	0.6203	0.0200	0	0	1000	Stainless tube
DM 21	Cd-Si-P	1.1244	0.0100	0.2804	0.0100	0.7735	0.0250	0	0	1000	Stainless tube + quartz tube
DM 22	Cd-Si-P	1.1251	0.0100	0.2812	0.0100	0.9291	0.0300	0	0	1130	Stainless tube + quartz tube
DM 23	Cd-Si-P	1.1235	0.0100	0.2822	0.0100	0.6203	0.0200	0	0	1000	Stainless tube
DM 24	Cd-Si-P	1.1244	0.0100	0.2804	0.0100	0.7735	0.0250	0	0	1000	Stainless tube + quartz tube
DM 25	Cd-Si-P	1.1251	0.0100	0.2812	0.0100	0.9291	0.0300	0	0	1000	Stainless tube + quartz tube
DM 26	Cd-Si-P	1.1235	0.0100	0.2822	0.0100	0.6203	0.0200	0	0	1000	Stainless tube
DM 27	Cd-Si-P	1.1244	0.0100	0.2804	0.0100	0.7735	0.0250	0	0	1130	Stainless tube + quartz tube
DM 28	Cd-Si-P	1.1251	0.0100	0.2812	0.0100	0.9291	0.0300	0	0	1130	Stainless tube + quartz tube

Reaction Name	Reaction System	Zn (g)	Zn (mole)	Si (g)	Si (mole)	P (g)	P (mole)	Na (g)	Na (mole)	T_{max} (ºC)	Reaction Container
DM 1	Zn-Si-P	0.0660	0.0010	0.2840	0.0101	0.0631	0.0020	0.1155	0.0050	900	Stainless tube + quartz tube
DM 2	Zn-Si-P	0.0655	0.0010	0.2820	0.0100	0.6300	0.0203	0.2303	0.0100	900	Stainless tube + quartz tube
DM 3	Zn-Si-P	0.0667	0.0010	0.2910	0.0104	0.0924	0.0030	0.1153	0.0050	900	Stainless tube + quartz tube
DM 4	Zn-Si-P	0.0656	0.0010	0.2770	0.0099	0.1240	0.0040	0.1156	0.0050	900	Stainless tube + quartz tube
DM 11	Zn-Si-P	0.2618	0.0040	0.1123	0.0040	0.2480	0.0080	0.4653	0.0202	1000	Stainless tube + quartz tube

Appendix C: $KGaSe_2$ and $KGaS_2$ Crystal Growth Reaction List

Reaction Name	Reaction System	KSe_2 (g)	KSe_2 (mole)	Ga (g)	Ga (mole)	Mn (g)	Mn mole)	Mn fraction	T_{max} (ºC)	
SA 5	K-Ga-Se	0.9600	0.0049	0.6890	0.0099	0.0200	0.0004	0.0355	600	
SA 6	K-Ga-Se	1.0510	0.0053	0.7040	0.0101	0.0610	0.0011	0.0991	600	
SA 7	K-Ga-Se	0.9660	0.0049	1.2910	0.0185	0.0720	0.0013	0.0661	600	
SA 8	K-Ga-Se	0.9970	0.0051	0.8240	0.0118	0.1690	0.0031	0.2065	600	
SA 9	K-Ga-Se	5.0970	0.0259	2.4700	0.0354				600	
Reaction Name	**Reaction System**	**KSe_2 (g)**	**KSe_2 (mole)**	**Ga (g)**	**Ga (mole)**	**Mn (g)**	**Mn (mole)**	**Zn (g)**	**Zn (mole)**	**T_{max} (ºC)**
SA 10	K-Ga-Se-Zn	3.0730	0.0156	1.0010	0.0144	0.0470	0.0009	0.0099	0.0002	600
SA 11	K-Ga-Se-Zn	3.2680	0.0166	1.0510	0.0151	0.0670	0.0012	0.0110	0.0002	600
SA 12	K-Ga-Se-Zn	3.0420	0.0154	0.9480	0.0136	0.0840	0.0015	0.0110	0.0002	600
SA 13	K-Ga-Se-Zn	3.6700	0.0186	1.0130	0.0145	0.2260	0.0041	0.0110	0.0002	600

Reaction Name	Reaction System	K (g)	K mole)	Se (g)	Se (mole)	Products
SA 1	K-Se	0.6300	0.0161	0.6077	0.0077	K_2Se
SA 2	K-Se	0.8550	0.0219	0.7896	0.0100	K_2Se

Reaction Name	Reaction System	k_2Se_5 (g)	K_2Se_5 (mole)	Ga (g)	Ga (mole)	T_{max} (ºC)	Dwelling time (hour)
SA 3	K-Ga-Se	4.3000	0.0091	1.1000	0.0158	600	24

Reaction Name	Reaction System	kSe_2 (g)	KSe_2 (mole)	Ga (g)	Ga (mole)	T_{max} (ºC)	Dwelling time (hour)	Reaction Container
SA 4	K-Ga-Se	2.4190	0.0123	0.7780	0.0112	600	24	Quartz Tube

Reaction Name	Reaction System	K_2S_5 (g)	K_2S_5 mole)	Ga (g)	Ga (mole)	Mn (g)	Mn (mole)	T_{max} (ºC)	Dwelling time (hour)
QN 2	K-S								
QN 3	K-Ga-S	1.2000	0.0050	0.0050	0.3507	0.0006	0.0304	600	48
QN 4	K-Ga-S	0.6350	0.0027	0.0027	0.1856	0.0007	0.0366	600	48
QN 5	K-Ga-S	0.5550	0.0023	0.0023	0.1622	0.0004	0.0225	600	48

Appendix D: Na_3AlP_2 related compound reaction list

Reaction Name	Reaction System	Na (g)	Na (mole)	P (g)	P (mole)	T_{max} (°C)	Dwelling time (hour)	Products
TC 1	Na-P	0.6889	0.0300	0.3108	0.0100	800	48	Na_3P
TC 5		0.6889	0.0300	0.3097	0.01	800	48	Na_3P

Reaction Name	Reaction System	Na (g)	Na (mole)	P (g)	P (mole)	Ga (g)	Ga (mole)	Mn (g)	Mn (mole)	T_{max} (°C)	Dwelling time (hour)
TC 2	Na-Ga-P	0.6897	0.0300	0.6195	0.0200	0.6972	0.0100	0	0	800	48
TC 6		0.3458	0.0150	0.3100	0.0100	0.3500	0.0050	0	0	800	48
TC9		0.3453	0.0150	0.3097	0.0100	0.3385	0.0049	0.0083	0.0002	800	48
TC10		0.3449	0.0150	0.3096	0.0100	0.3339	0.0048	0.0136	0.0002	800	48
TC11		0.3448	0.0150	0.3097	0.0100	0.3139	0.0045	0.0276	0.0005	800	48
TC12		0.3455	0.0150	0.3098	0.0100	0.2796	0.0040	0.0546	0.0010	800	48
TC13		0.3459	0.0150	0.3106	0.0100	0.2456	0.0035	0.0824	0.0015	800	48

All the reaction were took place in a sealed stainless tube and quartz tube

Reaction Name	Reaction System	Na (g)	Na mole)	P (g)	P (mole)	Al (g)	Al (mole)	Mn (g)	Mn (mole)	Tmax (ºC)	Reaction Container
TC 3	Na-Al-P	0.6897	0.0300	0.6195	0.0200	0.2698	0.0100			800	Stainless tube + quartz tube
TC 7		0.3449	0.0150	0.3090	0.0100	0.1347	0.0050			800	Stainless tube + quartz tube
TC 14		0.3453	0.0150	0.3098	0.0100	0.3443	0.0128	0.0083	0.0002	800	Stainless tube + quartz tube
RB		0.3425	0.0149	0.2924	0.0094	0.1285	0.0048	0.0129	0.0002	800	Stainless tube
RB 1		0.3331	0.0145	0.3107	0.0100	0.1353	0.0050	0.0000	0.0000	800	Stainless tube
RB 2		0.3343	0.0145	0.2950	0.0095	0.1020	0.0038	0.0543	0.0010	800	Stainless tube
RB 3		0.3403	0.0148	0.2974	0.0096	0.1203	0.0045	0.0283	0.0005	800	Stainless tube
RB 13		0.3426	0.0149	0.3053	0.0099	0.1304	0.0048	0.0000	0.0000	1000	Stainless tube
RB 14		0.3449	0.0150	0.2972	0.0096	0.1281	0.0047	0.0130	0.0002	1000	Stainless tube
RB 15		0.3396	0.0148	0.3006	0.0097	0.1223	0.0045	0.0262	0.0005	1000	Stainless tube
RB 16		0.3378	0.0147	0.3082	0.0100	0.1065	0.0039	0.0546	0.0010	1000	Stainless tube
Reaction Name	**Reaction System**	**Na (g)**	**Na mole)**	**P (g)**	**P (mole)**	**Al (g)**	**Al (mole)**	**Cr (g)**	**Cr (mole)**	**Tmax (ºC)**	**Reaction Container**
RB 4	Na-Al-P	0.3449	0.0150	0.3097	0.0100	0.1322	0.0049	0.0051	0.0001	800	Stainless tube
RB 5		0.3413	0.0148	0.3002	0.0097	0.1270	0.0047	0.0120	0.0002	800	Stainless tube
RB 6		0.3431	0.0149	0.3042	0.0098	0.1202	0.0045	0.0274	0.0005	800	Stainless tube
RB 7		0.3396	0.0148	0.3003	0.0097	0.1074	0.0040	0.0498	0.0009	800	Stainless tube
RB 17		0.3437	0.0149	0.3010	0.0097	0.1231	0.0046	0.0122	0.0002	1000	Stainless tube
RB 18		0.3420	0.0149	0.3094	0.0100	0.1214	0.0045	0.0277	0.0005	1000	Stainless tube
RB 19		0.3403	0.0148	0.3100	0.0100	0.1101	0.0041	0.0616	0.0011	1000	Stainless tube
The reaction dwelling time are 48 hours											

Appendix E: NbNiP Reaction List

Reaction Name	Reaction System	Nb (g)	Nb (mole)	Ni (g)	Ni (mole)	P (g)	P (mole)	Na (g)	Na (mole)	Crucible
CMF 39A	Nb-Ni-P-Na	0.082	0.000883	0.0521	0.0009	0.02789	0.0009	0.3068	0.0133	Stainless Steel tube
CMF 39B	Nb-Ni-P-Na	0.083	0.000893	0.0525	0.0009	0.0273	0.000881	0.2052	0.0089	
CMF 42	Nb-Ni-P	0.648	0.006975	0.4111	0.0070	0.217	0.007006	0.0000	0.0000	
CMF 43	Nb-Ni-P-Na	0.1612	0.001735	0.1015	0.0017	0.0539	0.00174	0.8111	0.0353	
CMF 44	Nb-Ni-P	1.062	0.011431	0.0840	0.0014	0.0454	0.001466	0.0000	0.0000	
CMF 45	Nb-Ni-P-Na	0.4383	0.004718	0.0357	0.0006	0.0191	0.000617	0.6797	0.0296	
CMF 46	Nb-Ni-P-Na	0.6194	0.006667	0.0497	0.0008	1.0774	0.034784	0.4045	0.0176	
CMF 47	Nb-Ni-P	0.3087	0.003323	0.7057	0.0120	0.1247	0.004026	0.0000	0.0000	
CMF 48	Nb-Ni-P-Na	0.0719	0.000774	0.1357	0.0023	0.0289	0.000933	0.8850	0.0385	
CMF 49	Nb-Ni-P	0.311	0.003347	0.1960	0.0033	0.8271	0.026703	0.0000	0.0000	
CMF 50	Nb-Ni-P-Na	0.0663	0.000714	0.0426	0.0007	0.1779	0.005744	0.8230	0.0358	

Reaction Name	Reaction System	Nb (g)	Nb (mole)	Ni (g)	Ni (mole)	P (g)	P (mole)	Na_3P (g)	Na_3P (mole)	Crucible
VC-1	Nb-Ni-P	0.619373	0.006667	0.3913	0.0067	0.6194	0.019998	0.0000	0.0000	Stainless Steel tube
VC-2	Nb-Ni-P	1.083903	0.011667	0.2250	0.0038	0.552298	0.017831	0.0000	0.0000	
VC-3	Nb-Ni-P	1.083903	0.011667	0.4695	0.0080	0.423257	0.013665	0.0000	0.0000	
VC-4	Nb-Ni-P	0.154843	0.001667	0.2935	0.0050	0.825867	0.026663	0.0000	0.0000	
VC-5	Nb-Ni-P	0.603889	0.0065	0.1076	0.0018	0.77425	0.024997	0.0000	0.0000	
VC-6	Nb-Ni-P	0.294202	0.003167	0.5967	0.0102	0.6194	0.019998	0.0000	0.0000	
VC-7	Nb-Ni-P	0.309687	0.003333	0.4891	0.0083	0.671017	0.021664	0.0000	0.0000	
VC-8	Nb-Ni-P	0.619373	0.006667	0.5869	0.0100	0.516167	0.016665	0.0000	0.0000	
VC-9	Nb-Ni-P	0.46453	0.005	0.2935	0.0050	0.722633	0.023331	0.0000	0.0000	
VC-10	Nb-Ni-P	0.851638	0.009167	0.1956	0.0033	0.645208	0.020831	0.0000	0.0000	
VC-11	Nb-Ni-P	0.294202	0.003167	0.5967	0.0102	0.6194	0.019998	1.8597	0.0186	
VC-12	Nb-Ni-P	0.309687	0.003333	0.4891	0.0083	0.671017	0.021664	1.8597	0.0186	
VC-13	Nb-Ni-P	0.619373	0.006667	0.5869	0.0100	0.516167	0.016665	1.8597	0.0186	
VC-14	Nb-Ni-P	0.46453	0.005	0.2935	0.0050	0.722633	0.023331	1.8597	0.0186	
VC-15	Nb-Ni-P	0.851638	0.009167	0.1956	0.0033	0.645208	0.020831	1.8597	0.0186	

Reaction Name	Reaction System	Ni (g)	Ni (mole)	Nb (g)	Nb (mole)	P (g)	P (mole)	Na (g)	Na (mole)	Crucible
CMF 40-7	Ni-Nb-P	0.1176	0.0020	0.1853	0.0020	0.0621	0.0020	0.9193	0.0400	Nb tube
CMF 40-8	Ni-Nb-P	0.1189	0.0020	0.3711	0.0040	0.0624	0.0020	0.9197	0.0400	ss tube
CMF 40-9	Ni-Nb-P	0.2345	0.0040	0.1845	0.0020	0.0629	0.0020	0.9196	0.0400	ss tube
CMF 40-10	Ni-Nb-P	0.2525	0.0043	0.2658	0.0029	0.0437	0.0014	0.6571	0.0286	ss tube
CMF 40-11	Ni-Nb-P	0.0843	0.0014	0.3992	0.0043	0.0435	0.0014	0.6574	0.0286	ss tube
Reaction Name	**Reaction System**	**Ni (g)**	**Ni (mole)**	**Nb (g)**	**Nb (mole)**	**P (g)**	**P (mole)**	**Na (g)**	**Na (mole)**	**Crucible**
CMF 41-7	Ni-Nb-P	0.0451	0.0008	0.0715	0.0008	0.1191	0.0038	0.8842	0.0385	Nb tube
CMF 41-8	Ni-Nb-P	0.0391	0.0007	0.1239	0.0013	0.1032	0.0033	0.7663	0.0333	ss tube
CMF 41-9	Ni-Nb-P	0.0783	0.0013	0.0619	0.0007	0.1033	0.0033	0.7663	0.0333	ss tube
CMF 41-10	Ni-Nb-P	0.0978	0.0017	0.1032	0.0011	0.0860	0.0028	0.7663	0.0333	ss tube
CMF 41-11	Ni-Nb-P	0.0931	0.0016	0.1858	0.0020	0.1032	0.0033	0.7663	0.0333	ss tube

Appendix F: NiGeNbP Reaction List

Reaction Name	Reaction System	Ni (g)	Ni (mole)	Ge (g)	Ge (mole)	Nb (g)	Nb (mole)	P (g)	P (mole)	Na (g)	Na (mole)	Crucible
CMF 51	Ni-Ge-Nb-P	0.3521	0.0060	0.0073	0.0001	0.6503	0.0070	0.1858	0.0060	0	0	ss tube
CMF 52	Ni-Ge-Nb-P	0.1956	0.0033	0.2423	0.0033	0.6194	0.0067	0.1032	0.0033	0	0	ss tube
CMF 53	Ni-Ge-Nb-P	0.4633	0.0079	0.3826	0.0053	0.2445	0.0026	0.0815	0.0026	0	0	ss tube
CMF 54	Ni-Ge-Nb-P	0.1012	0.0017	0.6266	0.0086	0.3204	0.0034	0.1068	0.0034	0	0	ss tube
CMF 55	Ni-Ge-Nb-P	0.2445	0.0042	0.1512	0.0021	0.3871	0.0042	0.3226	0.0104	0	0	ss tube
CMF 56	Ni-Ge-Nb-P	0.1761	0.0030	0.0363	0.0005	0.3252	0.0035	0.0929	0.0030	0.5750	0.0250	ss tube
CMF 57	Ni-Ge-Nb-P	0.0451	0.0008	0.0559	0.0008	0.1429	0.0015	0.0238	0.0008	0.8846	0.0385	ss tube
CMF 58	Ni-Ge-Nb-P	0.1174	0.0020	0.0969	0.0013	0.0619	0.0007	0.0206	0.0007	0.7666	0.0333	ss tube
CMF 59	Ni-Ge-Nb-P	0.0326	0.0006	0.2019	0.0028	0.1032	0.0011	0.0344	0.0011	0.6389	0.0278	ss tube

Reaction Name	Reaction System	Ni (g)	Ni (mole)	Ge (g)	Ge (mole)	Nb (g)	Nb (mole)	P (g)	P (mole)	Na (g)	Na (mole)	Crucible
CMF 40-1	Ni-Ge-Nb-P	0.2351	0.0040	0.0965	0.0013	0.2447	0.0026	0.1234	0.0040	0.7679	0.0334	ss tube
CMF 40-2	Ni-Ge-Nb-P	0.1953	0.0033	0.0968	0.0013	0.3091	0.0033	0.1241	0.0040	0.7677	0.0334	ss tube
CMF 40-3	Ni-Ge-Nb-P	0.1473	0.0025	0.0603	0.0008	0.3714	0.0040	0.0775	0.0025	0.9589	0.0417	Nb tube
CMF 40-4	Ni-Ge-Nb-P	0.1953	0.0033	0.0490	0.0007	0.3725	0.0040	0.1243	0.0040	0.7655	0.0333	ss tube
CMF 40-5	Ni-Ge-Nb-P	0.1565	0.0027	0.0973	0.0013	0.3094	0.0033	0.1245	0.0040	0.7673	0.0334	ss tube
CMF 40-6	Ni-Ge-Nb-P	0.2356	0.0040	0.0486	0.0007	0.1500	0.0016	0.1240	0.0040	0.7665	0.0333	ss tube
CMF 41-1	Ni-Ge-Nb-P	0.1467	0.0025	0.0605	0.0008	0.1548	0.0017	0.3872	0.0125	0.4709	0.0205	ss tube
CMF 41-2	Ni-Ge-Nb-P	0.1174	0.0020	0.0581	0.0008	0.1858	0.0020	0.3717	0.0120	0.4598	0.0200	ss tube
CMF 41-3	Ni-Ge-Nb-P	0.1174	0.0020	0.0290	0.0004	0.2230	0.0024	0.3717	0.0120	0.4598	0.0200	Nb tube
CMF 41-4	Ni-Ge-Nb-P	0.1409	0.0024	0.0290	0.0004	0.1858	0.0020	0.3717	0.0120	0.4598	0.0200	ss tube
CMF 41-5	Ni-Ge-Nb-P	0.0978	0.0017	0.0608	0.0008	0.2320	0.0025	0.3872	0.0125	0.4790	0.0208	ss tube
CMF 41-6	Ni-Ge-Nb-P	0.1174	0.0020	0.0290	0.0004	0.1858	0.0020	0.3717	0.0120	0.4598	0.0200	ss tube

Appendix G: MnNaP Reaction List

Reaction Name	Reaction System	Mn (g)	Mn (mole)	P (g)	P (mole)	Na (g)	Na (mole)	Crucible
CMF 40-12	Mn-P-Na	0.0546	0.0010	0.0007	2E-05	0.3600	0.0157	Nb tube
CMF 40-13	Mn-P-Na	0.1097	0.0020	0.0013	4E-05	0.5000	0.0217	ss tube
CMF 41-12	Mn-P-Na	0.0458	0.00083	0.1291	0.0042	0.9579	0.0417	Nb tube
CMF 41-13	Mn-P-Na	0.0845	0.00154	0.1191	0.0038	0.8842	0.0385	ss tube
CMF 41-14	Mn-P-Na	0.5494	0.01	0.3097	0.01	0.2299	0.0100	ss tube
CMF 41-15	Mn-P-Na	0.2747	0.005	0.7744	0.025	0.2295	0.0100	ss tube

Appendix H : Detail Reaction List

Reaction Name	Reaction System	T_{max} (ºC)	Cooling Rate (ºC/hour)	Dwelling Time (hr)	ZnO (g)	ZnO (mole)	V_2O_5 (g)	V_2O_5 (mole)	Crucible	XRD	SEM /EDS	SQUID	Photos	Page	Date
CMF 1	ZnO-V_2O_5	1300	1.2	40	24.42	0.3000	10.14	0.0558	Al_2O_3 crucible					73 (CMF B1)	2005/3/7
CMF 2	ZnO-V_2O_5	1300	1.2	40	16.84	0.2069	7.7	0.0423	Al_2O_3 crucible				CMF 2	73 (CMF B1)	2005/3/7
CMF 3	ZnO-V_2O_5	1300	1.2	40	5.5	0.0676	4.1	0.0225	Al_2O_3 crucible					73 (CMF B1)	2005/3/7
CMF 4	ZnO-V_2O_5	1300	1.2	40	16.95	0.2082	7.19	0.0395	Al_2O_3 crucible					73 (CMF B1)	2005/3/7
CMF 10	ZnO-V_2O_5	1300	500	0	5.5	0.0676	4.1	0.0225						97 (CMF B1)	2005/4/12
Reaction Name	**Reaction System**	**T_{max} (ºC)**	**Cooling Rate (ºC/hour)**	**Dwelling Time (hr)**	**ZnO (g)**	**ZnO (mole)**	**B_2O_3 (g)**	**B_2O_3 (mole)**	**Crucible**					**Page**	**Date**
CMF 7	ZnO-B_2O_3	1300	100	0	71.34	0.8763	13.4	0.1925	Pt crucible	CMF 7			CMF 7	79 (CMF B1)	2005/3/25
CMF 8	ZnO-B_2O_3	1300	3.2	2	230.2	2.8277	43.19	0.6204	Pt crucible	CMF 8			CMF 8	79 (CMF B1)	2005/3/25
CMF 9	ZnO-B_2O_3	1300	100	0		0.0000		0.0000						96 (CMF B1)	2005/4/9
CMF 11	ZnO-B_2O_3	1300	800	0	8	0.0983	1.5	0.0215	Al_2O_3 crucible	CMF 11				108 (CMF B1)	2005/4/15
CMF 18	ZnO-B_2O_3	1300	250	10	4.72	0.0580	0.21	0.0030	Pellet placed on Pt foil					26 (CMF B2)	2005/6/14
Reaction Name	**Reaction System**	**T_{max} (ºC)**	**Cooling Rate (ºC/hour)**	**Dwelling Time (hr)**	**ZnO (g)**	**ZnO (mole)**	**WO_3 (g)**	**WO_3 (mole)**	**Crucible**					**Page**	**Date**

CMF 12A	$ZnO-WO_3$	1350	800	0	5.11	0.0628	6.31	0.0003	Al_2O_3 crucible	CMF 12				110 (CMF B1)	2005/4/20
CMF 12B	$ZnO-WO_3$	1350	800	0	3.1	0.0381	3.83	0.0002	Al_2O_3 crucible	CMF 12				111 (CMF B1)	2005/4/23
CMF 13	$ZnO-WO_3$	1350	800	2	3.11	0.0382	3.83	0.0002	Quartz crucible	CMF 13				116 (CMF B1)	2005/4/29
Reaction Name	**Reaction System**	**T_{max} (ºC)**	**Cooling Rate (ºC/hour)**	**Dwelling Time (hr)**	**ZnO (g)**	**ZnO (mole)**	**Na_3AlF_6 (g)**	**Na_3AlF_6 (mole)**	**Crucible**					**Page**	**Date**
CMF 14	$ZnO-Na_3AlF_6$	1350	500	0	5.1	0.0626	3.29	0.0157	Pellet placed on Pt foil					118 (CMF B1)	2005/5/2
CMF 15	$ZnO-Na_3AlF_6$	1450	500	0	5.1	0.0626	3.29	0.0157	Pellet placed on Pt foil	CMF 15				120 (CMF B1)	2005/5/13
CMF 19 A	$ZnO-Na_3AlF_6$ pellet	950	250	10	1.88	0.0231	0.15	0.0007	Pellet placed on Pt foil					34 (CMF B2)	2005/6/16
CMF 19 B	$ZnO-Na_3AlF_6$ pellet	950	250	10	1.5	0.0184	0.43	0.0020	Pellet placed on Pt foil					34 (CMF B2)	2005/6/16
CMF 19 C	$ZnO-Na_3AlF_6$ pellet	950	250	10	1.2	0.0147	3.09	0.0147	Pellet placed on Pt foil					34 (CMF B2)	2005/6/16
CMF 19 D	$ZnO-Na_3AlF_6$ pellet	950	250	10	0	0.0000	0.62	0.0030	Pellet placed on Pt foil					34 (CMF B2)	2005/6/16
CMF 20 A	$ZnO-Na_3AlF_6$ pellet	950	250	10	0.46	0.0057	0.04	0.0002	Pellet placed on Pt foil					38 (CMF B2)	2005/6/17
CMF 20 B	$ZnO-Na_3AlF_6$ pellet	950	250	10	0.39	0.0048	0.11	0.0005	Pellet placed on Pt foil					38 (CMF B2)	2005/6/17
CMF 20 C	$ZnO-Na_3AlF_6$ pellet	950	250	10	0.14	0.0017	0.36	0.0017	Pellet placed on Pt foil					38 (CMF B2)	2005/6/17
CMF 20 D	$ZnO-Na_3AlF_6$ pellet	950	250	10	0	0.0000	0.5	0.0024	Pellet placed on Pt foil					38 (CMF B2)	2005/6/17
CMF 20 E	$ZnO-Na_3AlF_6$ pellet	950	250	10	0.5	0.0061	0	0.0000	Pellet placed on Pt foil					38 (CMF B2)	2005/6/17
Reaction Name	**Reaction System**	**T_{max} (ºC)**	**Cooling Rate**	**Dwelling Time (hr)**	**ZnO (g)**	**ZnO (mole)**	**MoO_3 (g)**	**MoO_3 (mole)**	**Crucible**					**Page**	**Date**

			(ºC/hour)												
CMF 16	ZnO-MoO_3	1300	100	1	6.11	0.0751	5.82	0.0404	Al_2O_3 crucible					1 (CMF B2)	2005/5/6
CMF 17	ZnO-MoO_3	1300	1	2	4.24	0.0521	0.76	0.0053	Al_2O_3 crucible				CMF 17	4 (CMF B2)	2005/5/8
Reaction Name	**Reaction System**	**T_{max} (ºC)**	**Cooling Rate (ºC/hour)**	**Dwelling Time (hr)**	**ZnO (g)**	**ZnO (mole)**	**KPF_6 (g)**	**KPF_6 (mole)**	**Crucible**	**XRD**	**SEM /EDS**	**SQUID**	**Photos**	**Page**	**Date**
CMF 21 A	ZnO-KPF_6 pellet	500	250	15	1.43	0.0176	0.1	0.0005	Pellet placed on Pt foil					42 (CMF B2)	2005/6/18
CMF 21 B	ZnO-KPF_6 pellet	500	250	15	1.23	0.0151	0.31	0.0017	Pellet placed on Pt foil					42 (CMF B2)	2005/6/18
CMF 21 C	ZnO-KPF_6 pellet	500	250	15	0.52	0.0064	1.18	0.0064	Pellet placed on Pt foil					42 (CMF B2)	2005/6/18
CMF 21 D	ZnO-KPF_6 pellet	500	250	15	0	0.0000	0.52	0.0028	Pellet placed on Pt foil					42 (CMF B2)	2005/6/18
CMF 22A	ZnO-KPF_6 pellet	1000	250	10	0.46	0.0057	0.04	0.0002	Pellet placed on Pt foil					46 (CMF B2)	2005/6/19
CMF 22B	ZnO-KPF_6 pellet	1000	250	10	0.4	0.0049	0.1	0.0005	Pellet placed on Pt foil					46 (CMF B2)	2005/6/19
CMF 22C	ZnO-KPF_6 pellet	1000	250	10	0.15	0.0018	0.35	0.0019	Pellet placed on Pt foil					46 (CMF B2)	2005/6/19
CMF 22D	ZnO-KPF_6 pellet	1000	250	10	0.36	0.0044	0.14	0.0008	Pellet placed on Pt foil					46 (CMF B2)	2005/6/19
CMF 22E	Pure ZnO pellet	1000	250	10	0.5	0.0061	0	0.0000	Pellet placed on Pt foil					46 (CMF B2)	2005/6/19
Reaction Name	**Reaction System**	**T_{max}(ºC)**	**Cooling Rate (ºC/hour)**	**Dwelling Time (hr)**	**ZnO (g)**	**ZnO (mole)**	**NaF (g)**	**NaF (mole)**	**Crucible**	**XRD**	**SEM /EDS**	**SQUID**	**Photos**	**Page**	**Date**
CMF 23A	ZnO-NaF pellet	900	250	7	0.49	0.0060	0.01	0.0001	Pellet placed on Pt foil					50 (CMF B2)	2005/6/20

CMF 23B	ZnO-NaF pellet	900	250	7	0.47	0.0058	0.03	0.0002	Pellet placed on Pt foil					50 (CMF B2)	2005/6/20
CMF 23C	ZnO-NaF pellet	900	250	7	0.33	0.0041	0.17	0.0009	Pellet placed on Pt foil					50 (CMF B2)	2005/6/20
CMF 23D	Pure NaF pellet	900	250	7	0	0.0000	0.5	0.0027	Pellet placed on Pt foil					50 (CMF B2)	2005/6/20
Reaction Name	**Reaction System**	**T_{max}(ºC)**	**Cooling Rate (ºC/hour)**	**Dwelling Time (hr)**	**ZnO (g)**	**ZnO (mole)**	**Mn_2O_3 (g)**	**Mn_2O_3 (mole)**	**Crucible**	**XRD**	**SEM /EDS**	**SQUID**	**Photos**	**Page**	**Date**
CMF 24A	ZnO-Mn_2O_3 pellet	1300	250	10	2.8	0.0344	0.05	0.0003	Pellet placed on Pt foil	CMF 24		CMF 24		56 (CMF B2)	2005/6/21
CMF 24B	ZnO-Mn_2O_3 pellet	1300	250	10	1.65	0.0203	0.09	0.0005	Pellet placed on Pt foil	CMF 24		CMF 24		56 (CMF B2)	2005/6/21
CMF 24C	ZnO-Mn_2O_3 pellet	1300	250	10	1.53	0.0188	0.3	0.0016	Pellet placed on Pt foil	CMF 24				56 (CMF B2)	2005/6/21
CMF 24 D	ZnO-Mn_2O_3 pellet	1300	250	10	1.51	0.0185	0.67	0.0036	Pellet placed on Pt foil	CMF 24				56 (CMF B2)	2005/6/21
CMF 26D	ZnO-Mn_2O_3	750	1.1	10	4.48	0.0550	0.08	0.0005	Al_2O_3 crucible					67 (CMF B2)	2005/6/24
Reaction Name	**Reaction System**	**T_{max}(ºC)**	**Cooling Rate (ºC/hour)**	**Dwelling Time (hr)**	**ZnO (g)**	**ZnO (mole)**	**NaCl (g)**	**NaCl (mole)**	**Crucible**	**XRD**	**SEM /EDS**	**SQUID**	**Photos**	**Page**	**Date**
CMF 28A	ZnO-NaCl	500	2	48	0.37	0.0045	13.29	0.2274	Al_2O_3 crucible				CMF 28	100 (CMF B2)	2005/7/11
CMF 28B	ZnO-NaCl	500	2	48	0.84	0.0103	12.06	0.2064	Al_2O_3 crucible				CMF 28	100 (CMF B2)	2005/7/11
CMF 28C	ZnO-NaCl	500	2	48	2.81	0.0345	10.09	0.1726	Al_2O_3 crucible				CMF 28	100 (CMF B2)	2005/7/11
Reaction Name	**Reaction System**	**T_{max}(ºC)**	**Cooling Rate (ºC/hour)**	**Dwelling Time (hr)**	**ZnO (g)**	**ZnO (mole)**	**KOH (g)**	**KOH (mole)**	**Crucible**	**XRD**	**SEM /EDS**	**SQUID**	**Photos**	**Page**	**Date**

CMF 27C	ZnO-KOH	750	1.1	10	1.27	0.0156	43.95	0.7833	Al_2O_3 crucible					88 (CMF B2)	2005/7/1
CMF 27D	ZnO-KOH	750	1.1	10	1.27	0.0156	8.8	0.1568	Al_2O_3 crucible	CMF 27				88 (CMF B2)	2005/7/1
CMF 29A	ZnO-KOH	500	2	48	12.5	0.1535	25.89	0.4615	Al_2O_3 crucible					9 (CMF B3)	2005/7/16
CMF 29B	ZnO-KOH	500	2	48	5.08	0.0624	35.09	0.6254	Al_2O_3 crucible	CMF 29	CMF 29			9 (CMF B3)	2005/7/16
CMF 29C	ZnO-KOH	500	2	48	2.46	0.0302	34.01	0.6062	Al_2O_3 crucible	CMF 29				9 (CMF B3)	2005/7/16
Reaction Name	**Reaction System**	**T_{max}(ºC)**	**Cooling Rate (ºC/hour)**	**Dwelling Time (hr)**	**ZnO (g)**	**ZnO (mole)**	**NaOH (g)**	**NaOH (mole)**	**Crucible**	**XRD**	**SEM /EDS**	**SQUID**	**Photos**	**Page**	**Date**
CMF 25A	ZnO-NaOH	750	5	1	4.1	0.0504	2	0.0500	Al_2O_3 crucible				CMF 25	59 (CMF B2)	2005/6/22
CMF 25B	ZnO-NaOH	750	5	1	1	0.0123	2.4	0.0600	Al_2O_3 crucible		CMF 25		CMF 25	59 (CMF B2)	2005/6/22
CMF 26A	ZnO-NaOH	750	1.1	10	4.12	0.0506	2.02	0.0505	Al_2O_3 crucible					67 (CMF B2)	2005/6/24
CMF 26B	ZnO-NaOH	750	1.1	10	1.71	0.0210	4.2	0.1050	Al_2O_3 crucible					67 (CMF B2)	2005/6/24
CMF 26C	ZnO-NaOH	750	1.1	10	1.01	0.0124	4.88	0.1220	Al_2O_3 crucible	CMF 26	CMF 26		CMF 26	67 (CMF B2)	2005/6/24
CMF 27A	ZnO-NaOH	750	1.1	10	5.25	0.0645	25.38	0.6345	Al_2O_3 crucible				CMF 27	88 (CMF B2)	2005/7/1
CMF 27B	ZnO-NaOH	750	1.1	10	2	0.0246	48	1.2001	Al_2O_3 crucible				CMF 27	88 (CMF B2)	2005/7/1
CMF 27E	ZnO-NaOH	750	1.1	10	1	0.0123	12	0.3000	Al_2O_3 crucible				CMF 27	88 (CMF B2)	2005/7/1
CMF 31A	ZnO-NaOH	750	1.1	10	13.55	0.1664	66.67	1.6669	Al_2O_3 crucible					43 (CMF B3)	2005/8/22
CMF 31B	ZnO-NaOH	750	1.1	10	2.99	0.0367	14.64	0.3660	Al_2O_3 crucible					43 (CMF B3)	2005/8/22

CMF31C	ZnO-NaOH	750	1.1	10	1.81	0.0222	8.89	0.2223	Al_2O_3 crucible					43 (CMF B3)	2005/8/22
CMF 31D	ZnO-NaOH	750	1.1	10	1.01	0.0124	4.88	0.1220	Al_2O_3 crucible					43 (CMF B3)	2005/8/22
CMF 31E	ZnO-NaOH	750	1.1	10		0.0000	3.48	0.0870	silver tube					43 (CMF B3)	2005/8/22
Reaction Name	**Reaction System**	**T_{max}(ºC)**	**Cooling Rate (ºC/hour)**	**Dwelling Time (hr)**	**ZnO (g)**	**ZnO (mole)**	**NaOH (g)**	**NaOH (mole)**	**KPF_6 (g)**	**KPF_6 (mole)**	**XRD**	**SEM/EDS**	**SQUID**	**Photos**	**Page**
CMF 30A	ZnO-NaOH-KPF_6	650	35	5	9	0.1106	4.44	0.1110	20.45	0.1111					31 (CMF B3)
CMF 30B	ZnO-NaOH-KPF_6	650	35	5	4.07	0.0500	20	0.5000	9.26	0.0503					31 (CMF B3)
Reaction Name	**Reaction System**	**T_{max}(ºC)**	**Cooling Rate (ºC/hour)**	**Dwelling Time (hr)**	**ZnO (g)**	**ZnO (mole)**	**NaOH (g)**	**NaOH (mole)**	**Mn_2O_3 (g)**	**Mn_2O_3 (mole)**					
CMF 32A	ZnO-NaOH-Mn_2O_3	500	2	48	13.5616	0.1666	66.6519	1.6664	0.1918	0.0012		CMF 32		CMF 32	52 (CMF B3)
CMF 32B	ZnO-NaOH-Mn_2O_3	500	2	48	13.5617	0.1666	66.6597	1.6666	0.096	0.0006		CMF 32		CMF 32	52 (CMF B3)
CMF 32C	ZnO-NaOH-Mn_2O_3	500	2	48	5.498	0.0675	27.052	0.6763	0.0238	0.0002		CMF 32		CMF 32	52 (CMF B3)
CMF 32D	ZnO-NaOH-Mn_2O_3	500	2	48	2.7123	0.0333	13.4542	0.3364	0.0767	0.0005		CMF 32		CMF 32	52 (CMF B3)
CMF 32E	ZnO-NaOH-Mn_2O_3	500	2	48	2.7128	0.0333	13.4001	0.3350	0.01912	0.0001		CMF 32		CMF 32	52 (CMF B3)
CMF 94	ZnO-NaOH-Mn_2O_3	500	8	60	3.016 (ZnO+Mn_2O_3)		5.504	0.1376							74 (CMF B8)
Reaction Name	**Reaction System**	**T_{max}(ºC)**	**Cooling Rate (ºC/hour)**	**Dwelling Time (hr)**	**ZnO (g)**	**ZnO (mole)**	**NaOH (g)**	**NaOH (mole)**	**$MnCO_3$ (g)**	**$MnCO_3$ (mole)**	**XRD**	**SEM/EDS**	**SQUID**	**Photos**	**Page**

CMF 33A	ZnO-NaOH-$MnCO_3$	500	2	48	5.4238	0.0666	26.6	0.6650	0.7665	0.0067	CMF 33			CMF 33	53 (CMF B3)
CMF 33B	ZnO-NaOH-$MnCO_3$	500	2	48	5.4245	0.0666	26.63	0.6658	1.1491	0.0100				CMF 33	53 (CMF B3)
CMF 33C	ZnO-NaOH-$MnCO_3$	500	2	48	5.4247	0.0666	26.68	0.6670	1.5324	0.0133	CMF 33			CMF 33	53 (CMF B3)
CMF 33D	ZnO-NaOH-$MnCO_3$	500	2	48	5.4246	0.0666	26.71	0.6678	0.7661	0.0067				CMF 33	53 (CMF B3)
CMF 34A	ZnO-NaOH-$MnCO_3$	500	2	48	5.0858	0.0625	25	0.6250	5.7477	0.0500				CMF 34	54 (CMF B3)
CMF 34B	ZnO-NaOH-$MnCO_3$	500	2	48	5.086	0.0625	25.02	0.6255	3.593	0.0313				CMF 34	54 (CMF B3)
CMF 34_2	ZnO-NaOH-$MnCO_3$	500	2	48	1.13	0.0139	5.48	0.1370	1.27	0.0110		CMF 34		CMF 34	54 (CMF B3)
CMF 34_3	ZnO-NaOH-$MnCO_3$	500	2	48	1.13	0.0139	5.48	0.1370	0.78	0.0068				CMF 34	54 (CMF B3)
CMF 34E	ZnO-NaOH-$MnCO_3$	500	2	48	1.13	0.0139	5.48	0.1370	1.27	0.0110				CMF 34	54 (CMF B3)
CMF34F	ZnO-NaOH-$MnCO_3$	500	2	48	1.13	0.0139	5.48	0.1370	0.78	0.0068				CMF 34	54 (CMF B3)
CMF 35A	ZnO-NaOH-$MnCO_3$	500	2	48	10.1728	0.1250	50.03	1.2508	11.4967	0.1000				CMF 35	67 (CMF B3)
CMF 35B	ZnO-NaOH-$MnCO_3$	500	2	48	1.1297	0.0139	5.58	0.1395	1.5975	0.0139				CMF 35	67 (CMF B3)
Reaction Name	**Reaction System**	**T_{max}(ºC)**	**Cooling Rate (ºC/hour)**	**Dwelling Time (hr)**	**ZnO (g)**	**ZnO (mole)**	**K_2CO_3 (g)**	**K_2CO_3 (mole)**	**$MnCO_3$ (g)**	**$MnCO_3$ (mole)**	**XRD**	**SEM/EDS**	**SQUID**	**Photos**	**Page**
CMF 36A	ZnO-K_2CO_3-MnCO3	1050	5	12	0.7397	0.0091	12.5697	0.3143	0	0					68 (CMF B3)
CMF 36B	ZnO-K_2CO_3-MnCO3	1050	5	12	0.6786	0.0083	11.5172	0.2880	0.9584	0.0083					68 (CMF B3)
Reaction Name	**Reaction System**	**T_{max}(ºC)**	**Cooling Rate**	**Dwelling Time (hr)**	**ZnO (g)**	**ZnO (mole)**	**KOH (g)**	**KOH (mole)**	**K_2CO_3 (g)**	**K_2CO_3**	**XRD**	**SEM/EDS**	**SQUID**	**Photos**	**Page**

			(ºC/hour)							(mole)					
CMF 37A	ZnO-KOH-K_2CO_3-$MnCO_3$	500	2	48	0.8136	0.0100	5.6238	0.1002	6.9106	0.0500	CMF 37				78 (CMF B3)
CMF 37B	ZnO-KOH-K_2CO_3-$MnCO_3$	500	2	48	0.7395	0.0091	6.2816	0.1120	6.2816	0.0455	CMF 37	CMF 37			78 (CMF B3)
Reaction Name	**Reaction System**	**T_{max}(ºC)**	**Cooling Rate (ºC/hour)**	**Dwelling Time (hr)**	**ZnO (g)**	**ZnO (mole)**	**KOH (g)**	**KOH (mole)**	**K_2CO_3 (g)**	**K_2CO_3 (mole)**	**XRD**	**SEM/EDS**	**SQUID**	**Photos**	**Page**
CMF 38A	ZnO-KOH-K_2CO_3	500	2	48	0.49	0.0060	3.33	0.0594	4.1	0.0297	CMF 38			CMF 38	80 (CMF B3)
CMF 38B	ZnO-KOH-K_2CO_3	500	2	48	4.89	0.0601	33.02	0.5885	41.66	0.3014	CMF 38	CMF 38		CMF 38	80 (CMF B3)
Reaction Name	**Reaction System**	**T_{max}(ºC)**	**Cooling Rate (ºC/hour)**	**Dwelling Time (hr)**	**$Zn_{0.95}Mn_{0.05}O$ (g)**	**$Zn_{0.95}Mn_{0.05}O$ (mole)**	**NaOH (g)**	**NaOH (mole)**	**H_2O (g)**	**H_2O (mole)**	**XRD**	**SEM/EDS**	**SQUID**	**Photos**	**Page**
AF4	$Zn_{0.95}Mn_{0.05}O$-NaOH-H_2O	500	8	60	3		4.932	0.1233	0.5408	0.0300	AF 4	AF 4		AF 4	
CMF 90	$Zn_{0.95}Mn_{0.05}O$-NaOH-H_2O	500	2	48	1.179		1.936	0.0484	0.215	0.0119					46 (CMF B8)
AF5	$Zn_{0.95}Mn_{0.05}O$-NaOH	500	8	60	3		5.48	0.1370			AF 5	AF 5		AF 5	
CMF 91	$Zn_{0.95}Mn_{0.05}O$-NaOH-H_2O	500	2	48	1.119		2.046	0.0512			CMF 91				46 (CMF B8)
CMF 93	$Zn_{0.95}Mn_{0.05}O$-NaOH	500	8	60	2.919		5.502	0.1376			CMF 93				74 (CMF B8)

Reaction Name	Reactin System	Cd:Ge:P	Cd (g)	Cd (mole)	Ge (g)	Ge (mole)	P (g)	P (mole)	T_{max} (ºC)	Reaction Container	Pellet	XRD	SEM/EDS	Page	Date
AJ3	Cd-Ge-P		1.1241	0.01	0.7261	0.01	0.6119	0.0198	1000	sealed fused silica ampoules	Yes	AJ3		39 (AJ B1)	2005/9/6
AJ3-2	Cd-Ge-P		Second heat treatment						1130	sealed fused silica ampoules	Yes	AJ3-2			
Reaction Name	**Reactin System**	**(Zn or Cd):Mn:Si:P**	**Mn (g)**	**Mn (mole)**	**Si (g)**	**Si (mole)**	**P (g)**	**P (mole)**	**T_{max} (ºC)**	**Reaction Container**	**Pellet**	**XRD**	**SEM/EDS**		
AJ4	Mn-Si-P		0.5494	0.01	0.2809	0.01	0.6195	0.02	1000	sealed fused silica ampoules	Yes	AJ4		39 (AJ B1)	2005/9/6
AJ4-2	Mn-Si-P		Regrind pellet from first heat treatment						1130	sealed fused silica ampoules	Yes	AJ4-2			
AJ5	Mn-Si-P		0.5494	0.01	0.2808	0.01	0.6195	0.02	1000	sealed fused silica ampoules	Yes	AJ5		39 (AJ B1)	2005/9/6
AJ5-2	Mn-Si-P		Grind pellet from first heat treatment						1130	sealed fused silica ampoules	Yes	AJ5-1			
Reaction Name	**Reactin System**	**(Zn or Cd):Mn:Si:P**	**Mn (g)**	**Mn (mole)**	**Ge (g)**	**Ge (mole)**	**P (g)**	**P (mole)**	**T_{max} (ºC)**	**Reaction Container**	**Pellet**	**XRD**	**SEM/EDS**		
AJ6	Mn-Ge-P		0.5494	0.01	0.7261	0.01	0.6195	0.02	1000	sealed fused silica ampoules	Yes	AJ6		39 (AJ B1)	2005/9/6
AJ6-2	Mn-Ge-P		Regrind pellet from first heat treatment						1130	sealed fused silica ampoules	Yes	AJ6-2	AJ6-2		

Reaction Name	Reaction System	Zn:Si:P:Mn	Zn (g)	Zn (mole)	Mn (g)	Mn (mole)	Si (g)	Si (mole)	P (g)	P (mole)	T_{max} (°C)	Reaction Container	Pellet	Products (Ratios)	*a*	*c*	V	XRD	SEM/EDS	SQUID	Photo	Page	Date
AJ-1-u_0	Zn-Si-P	1:0:1:2	1.3081	0.02			0.5618	0.02	1.2416	0.0401	1000	sealed fused silica ampoules	Yes	ZnSiP2:Si (65%:35%)				AJ 1				39 (AJ B1)	2005/9/6
AJ-1-2	Zn-Si-P		Regrind pellet from AJ-1-u_0								1130 second heat treatment		Yes	ZnSiP2:Si (97%:3%)				AJ 2				39 (AJ B1)	2005/9/6
AJ-Mn-1h	Zn-Si-P	0.98:0.02:1:2	0.6408	0.0098	0.0151	0.0003	0.2809	0.01	0.6194	0.02	1130	sealed fused silica ampoules	Yes	ZnSiP2/Zn3P2/Si	5.3991(11)	10.4398(40)	304.3(1)	AJMn1	AJMn1			81 (AJ B1)	2005/11/20
AJ-Mn-2h	Zn-Si-P	0.95:0.05:1:2	0.6212	0.0095	0.0378	0.0007	0.2809	0.01	0.6194	0.02	1130	sealed fused silica ampoules	Yes	ZnSiP2/Zn3P2/Si	5.4068(1)	10.4454(5)	305.35(2)	AJMn2	AJMn2	AJMn2		81 (AJ B1)	2005/11/20
AJ-Mn-3h	Zn-Si-P													ZnSiP2/Zn3P2/Si								81 (AJ B1)	2005/11/20
AJ-Mn-4h	Zn-Si-P	0.90:0.10:1:2	0.5885	0.01	0.0756	0.0014	0.2809	0.01	0.6194	0.02	1130	sealed fused silica ampoules	Yes	ZnSiP2/Zn3P2/Si	5.4059(2)	10.4447(6)	305.22(2)	AJMn4	AJMn4			81 (AJ B1)	2005/11/20
AJ-Mn-5h	Zn-Si-P	0.80:0.20:1:2	0.5231	0.01	0.1512	0.0028	0.2809	0.01	0.6194	0.02	1130	sealed fused silica ampoules	Yes	ZnSiP2/Zn3P2/Si	5.4048(2)	10.4377(7)	304.91(2)	AJMn5	AJMn5			81 (AJ B1)	2005/11/20
AJ-Mn-6h	Zn-Si-P																					81 (AJ B1)	2005/11/20
CMF 63	Zn-Si-P	1:0:1:2	2.6172	0.04	0	0	1.1232	0.04	2.4832	0.0802	1130	sealed fused silica ampoules	Yes					CMF 63			CMF 63	67 (CMF B5)	2008/5/12
CMF 65	Zn-Si-P	1:0:1:2	2.6161	0.04	0	0	1.124	0.04	2.4832	0.0802	1130	sealed fused silica ampoules	Yes								CMF 65	104 (CMF B5)	2008/6/3
CMf 67	Zn-Si-P	1:0:1:2	2.6165	0.04	0	0	1.1239	0.04	2.4841	0.0802	1130	sealed fused silica ampoules	Yes	exploded								107 (CMF B5)	2008/6/9
CMF 69	Zn-Si-P	1:0:1:2	2.6161	0.04	0	0	1.1235	0.04	2.4832	0.0802	1130	Quartz tube + Graphite	Yes	exploded							CMF 69	2 (CMF B6)	2008/7/1
CMF 71	Zn-Si-P	1:0:1:2	0.422	0.0065			0.1812	0.0065	0.4005	0.0129	1000	Quartz tube + Graphite	Yes								CMF 71	37 (CMF B6)	2008/8/25

Reaction Name	Reaction System	(Zn or Cd):Mn:Si:P	Cd (g)	Cd (mole)	Mn (g)	Mn (mole)	Si (g)	Si (mole)	P (g)	P (mole)	T_{max} (ºC)	Reaction Container	Pellet	Products (Ratios)	*a*	*c*	V	XRD	SEM/EDS	SQUID	Photo	Page	Date
AJ-2	Cd-Si-P	1:0:1:2	1.1241	0.01			0.2809	0.01	0.621	0.02	1000	sealed fused silica ampoules	Yes	$CdSiP_2/CdP_2/Si$ (53.3%/38.7%/8%)								39 (AJB1)	2005/9/6
AJ-2-2	Cd-Si-P		Regrind pellet from first heat treatment								1130 second heat treatment		Yes	$CdSiP_2$ (100%)								39 (AJB1)	2005/9/6
AJ-Mn-7h	Cd-Si-P	0.98:0.02:1:2	1.1016	0.0098	0.0151	0.0003	0.2809	0.01	0.6194	0.02	1130	sealed fused silica ampoules	Yes	$CdSiP_2/Si/MnP/Cd_7P_{10}$	5.6849(4)	10.4317(10)	337.13(4)	AJMn7	AJMn7			101 (AJB1)	2006/12/19
AJ-Mn-8h	Cd-Si-P	0.95:0.05:1:2	1.0679	0.0095	0.0378	0.0007	0.2809	0.01	0.6194	0.02	1130	sealed fused silica ampoules	Yes	$CdSiP_2/Cd_7P_{10}$	5.6814(4)	10.4325(11)	336.74(5)	AJMn8				101 (AJB1)	2006/12/19
AJ-Mn-9h	Cd-Si-P	0.92:0.08:1:2	1.0342	0.0092	0.0604	0.0011	0.2809	0.01	0.6194	0.02	1130	sealed fused silica ampoules	Yes	$CdSiP_2/Cd_7P_{11}$	5.6792(3)	10.4207(7)	336.11(3)	AJMn9				101 (AJB1)	2006/12/19
AJ-Mn-10h	Cd-Si-P	0.90:0.10:1:2	1.0117	0.0090	0.0756	0.0014	0.2809	0.01	0.6194	0.02	1130	sealed fused silica ampoules	Yes	$CdSiP_2/Si/MnP/Cd_7P_{10}$	5.6795(2)	10.4237(7)	336.23(3)	AJMn10				101 (AJB1)	2006/12/19
AJ-Mn-11h	Cd-Si-P	0.80:0.20:1:2	0.8999	0.0080	0.1512	0.0028	0.2809	0.01	0.6194	0.02	1130	sealed fused silica ampoules	Yes	$CdSiP_2/Si/MnP$	5.6741(2)	10.4127(5)	335.24(2)	AJMn11		AJMn11		101 (AJB1)	2006/12/19
AJ-Mn-12h	Cd-Si-P	0.70:0.30:1:2	0.7869	0.0070	0.2267	0.0041	0.2809	0.01	0.6194	0.02	1130	sealed fused silica ampoules	Yes	$CdSiP_2/Si$	5.6727(3)	10.4106(7)	335.01(3)	AJMn12		AJMn12		101 (AJB1)	2006/12/19
CMF 64	Cd-Si-P	1:0:1:2	4.497	0.0400	0	0	1.124	0.04	2.4843	0.0802	1130	sealed fused silica ampoules	Yes					CMF 64			CMF 64	67 (CMF B5)	2008/5/12
CMF 66	Cd-Si-P	1:0:1:2	4.9673	0.0442	0	0	1.1242	0.04	2.4843	0.0802	1130	sealed fused silica ampoules	Yes								CMF 66	105 (CMF B5)	2008/6/3
CMF 68	Cd-Si-P	1:0:1:2	4.4968	0.0400	0	0	1.1243	0.04	2.4827	0.0802	1130	sealed fused silica ampoules	Yes	exploded								107 (CMF B5)	2008/6/9
CMF 70	Cd-Si-P	1:0:1:2	4.4964	0.0400	0	0	1.1241	0.04	2.4844	0.0802	1130	Quartz tube + Graphite	Yes	exploded							CMF 70	2 (CMF B6)	2008/7/1

CMF 72	Cd-Si-P	1:0:1:2	0.5551	0.00499	0	0	0.1387	0.0049	0.367	0.0118	1000	Quartz tube + Graphite									CMF 72	37 (CMF B6)	2008/8/25

Reaction Name	Reaction System	K (g)	K (mole)	Se (g)	Se (mole)	Reaction Container	Products	XRD	SEM/EDS	Photo	Page	Date
SA 1	K-Se	0.63	0.0161	0.6077	0.0077	Quartz Crucible	K_2Se					
SA 2	K-Se	0.855	0.0219	0.7896	0.01	Quartz Crucible	K_2Se	SA 2				

Reaction Name	Reaction System	K_2Se_5 (g)	K_2Se_5 (mole)	Ga (g)	Ga (mole)	T_{max} (°C)	Dwelling time (hour)	Reaction Container	XRD	SEM/EDS	Photo	Page	Date
SA 3	K-Ga-Se	4.3	0.0091	1.1	0.0158	600	24.0000	sealed fused silica ampoules	SA 3			3 (SA B2)	2008/2/5

Reaction Name	Reaction System	KSe_2 (g)	KSe_2 (mole)	Ga (g)	Ga (mole)	T_{max} (°C)	Dwelling time (hour)	Reaction Container	XRD	SEM/EDS	Photo	Page	Date
SA 4	K-Ga-Se	2.419	0.0123	0.7780	0.0112	600	24	sealed fused silica ampoules	SA 4			11 (SA B2)	2008/3/2

Reaction Name	Reaction System	KSe_2 (g)	KSe_2 (mole)	Ga (g)	Ga (mole)	Mn (g)	Mn (mole)	Mn fraction	T_{max} (°C)	Dwelling time (hour)	Reaction Container	XRD	SEM/EDS	Photo	Page	Date
SA 5	K-Ga-Se	0.96	0.0049	0.689	0.0099	0.0200	0.0004	0.0355	600	24	sealed fused silica ampoules	SA 5	SA 5		27 (SA B2)	2008/3/23
SA 6	K-Ga-Se	1.051	0.0053	0.704	0.0101	0.0610	0.0011	0.0991	600	24	sealed fused silica ampoules	SA 6	SA 6		27 (SA B2)	2008/3/23
SA 7	K-Ga-Se	0.966	0.0049	1.291	0.0185	0.0720	0.0013	0.0661	600	24	sealed fused silica ampoules	SA 7	SA 7		27 (SA B2)	2008/3/23

SA 8	K-Ga-Se	0.997	0.0051	0.824	0.0118	0.1690	0.0031	0.2065	600	24	sealed fused silica ampoules	SA 8	SA 8					43 (SAB2)	2008/7/23
SA 9	K-Ga-Se	5.097	0.0259	2.47	0.0354				600	24	sealed fused silica ampoules	SA 9						43 (SAB2)	2008/7/23

Reaction Name	**Reaction System**	**KSe_2 (g)**	**KSe_2 (mole)**	**Ga (g)**	**Ga (mole)**	**Mn (g)**	**Mn (mole)**	**Zn (g)**	**Zn (mole)**	**Pellet**	**T_{max} (°C)**	**Dwelling time (hour)**	**Reaction Container**	**Products**	**XRD**	**SEM/EDS**	**Photo**	**Page**	**Date**
SA 10	K-Ga-Se-Zn	3.0730	0.0156	1.001	0.0144	0.0470	0.0009	0.0099	0.0002	Yes	600	24	sealed fused silica ampoules		SA 10		SA 10	43 (SAB2)	2008/7/23
SA 11	K-Ga-Se-Zn	3.2680	0.0166	1.051	0.0151	0.0670	0.0012	0.0110	0.0002	Yes	600	24	sealed fused silica ampoules		SA 11		SA 11	43 (SAB2)	2008/7/23
SA 12	K-Ga-Se-Zn	3.0420	0.0154	0.948	0.0136	0.0840	0.0015	0.0110	0.0002	Yes	600	24	sealed fused silica ampoules				SA 12	43 (SAB2)	2008/7/23
SA 13	K-Ga-Se-Zn	3.6700	0.0186	1.013	0.0145	0.2260	0.0041	0.0110	0.0002	Yes	600	24	sealed fused silica ampoules				SA 13	43 (SAB2)	2008/7/23

Reaction Name	**Reaction System**	**K_2S_5 (g)**	**K_2S_5 (mole)**	**Ga (g)**	**Ga (mole)**	**Mn (g)**	**Mn (mole)**	**T_{max} (°C)**	**Dwelling time (hour)**	**Reaction Container**	**XRD**	**SEM/EDS**	**Photo**	**Page**	**Date**
QN 2	K-Ga-S	1.48	0.0062	0.431	30.0493	0	0	600	48	Quartz Crucible	QN 2		QN2	24 (QNB1)	2008/10/9
QN 3	K-Ga-S-Mn	1.20	0.0050	0.005	0.3507	0.00055	0.0304	600	48	sealed fused silica ampoules				32 (QNB1)	2008/10/23
QN 4	K-Ga-S-Mn	0.635	0.0027	0.0027	0.1856	0.00067	0.03656	600	48	sealed fused silica ampoules	QN 4	QN 4		33 (QNB1)	2008/10/23
QN 5	K-Ga-S-Mn	0.555	0.0023	0.0023	0.1622	0.00041	0.022496	600	48	sealed fused silica ampoules	QN 5	QN 5		33 (QNB1)	2008/10/23

Reaction Name	Reactin System	Na (g)	Na (mole)	P (g)	P (mole)	T_{max} (ºC)	Dwelling time (hour)	Reaction Container	Products	XRD		Page	Date
TC 1	Na-P	0.689	0.03	0.311	0.01	800	48	Stainless tube + quartz tube	Na_3P			10 (TC B1)	2006/11/16
TC 5	Na-P	0.689	0.03	0.31	0.01	800	48	Stainless tube + quartz tube	Na_3P	TC 5		16 (TC B1)	2006/11/28

Reaction Name	Reactin System	Na (g)	Na (mole)	P (g)	P (mole)	Ga (g)	Ga (mole)	Mn (g)	Mn (mole)	T_{max} (ºC)	Dwelling time (hour)	Reaction Container	XRD		Page	Date
TC 2	Na-Ga-P	0.69	0.03	0.619	0.02	0.697	0.01	0	0	800	48	Stainless tube + quartz tube	TC 2		10 (TC B1)	2006/11/16
TC 6	Na-Ga-P	0.346	0.015	0.31	0.01	0.35	0.0050	0	0	800	48	Stainless tube + quartz tube	TC 6		16 (TC B1)	2006/11/28
TC9	Na-Ga-P-Mn	0.345	0.015	0.31	0.01	0.339	0.0049	0.008	0.0002	800	48	Stainless tube + quartz tube			18 (TC B1)	2006/12/7
TC10	Na-Ga-P-Mn	0.345	0.015	0.31	0.01	0.334	0.0048	0.014	0.0002	800	48	Stainless tube + quartz tube			18 (TC B1)	2006/12/7
TC11	Na-Ga-P-Mn	0.345	0.015	0.31	0.01	0.314	0.0045	0.028	0.0005	800	48	Stainless tube + quartz tube			18 (TC B1)	2006/12/7
TC12	Na-Ga-P-Mn	0.346	0.015	0.31	0.01	0.28	0.0040	0.055	0.0010	800	48	Stainless tube + quartz tube			18 (TC B1)	2006/12/7
TC13	Na-Ga-P-Mn	0.346	0.015	0.311	0.01	0.246	0.0035	0.082	0.0015	800	48	Stainless tube + quartz tube	TC 13		18 (TC B1)	2006/12/7

Reaction Name	Reactin System	Na (g)	Na (mole)	P (g)	P (mole)	Al (g)	Al (mole)	Mn (g)	Mn (mole)	T_{max} (ºC)	Dwelling time (hour)	Reaction Container	XRD	SEM_EDS	Page	Date
TC 3	Na-Al-P	0.69	0.03	0.619	0.02	0.27	0.0100			800	48	Stainless tube + quartz tube			10 (TC B1)	2006/11/16
TC 7	Na-Al-P	0.345	0.015	0.309	0.01	0.135	0.0050			800	48	Stainless tube + quartz tube	TC 7		16 (TC B1)	2006/11/28

TC 14	Na-Al-P-Mn	0.345	0.015	0.31	0.01	0.344	0.0128	0.0083	0.0002	800	48	Stainless tube + quartz tube			19 (TC B1)	2006/12/8
RB	Na-Al-P-Mn	0.343	0.015	0.292	0.009	0.129	0.0048	0.0129	0.0002	800	48	Stainless tube			53 (RB B1)	2008/3/31
RB 1	Na-Al-P-Mn	0.333	0.014	0.311	0.01	0.135	0.0050	0	0	800	48	Stainless tube	RB1		53 (RB B1)	2008/3/31
RB 2	Na-Al-P-Mn	0.334	0.015	0.295	0.01	0.102	0.0038	0.0543	0.0010	800	48	Stainless tube	RB2	RB 2	53 (RB B1)	2008/3/31
RB 3	Na-Al-P-Mn	0.34	0.015	0.297	0.01	0.12	0.0045	0.0283	0.0005	800	48	Stainless tube	RB 3		53 (RB B1)	2008/3/31
RB 13	Na-Al-P-Mn	0.343	0.015	0.305	0.01	0.13	0.0048	0	0	1000	48	Stainless tube	RB 13		79 (RB B1)	2008/9/9
RB 14	Na-Al-P-Mn	0.345	0.015	0.297	0.01	0.128	0.0047	0.013	0.0002	1000	48	Stainless tube	RB 14		79 (RB B1)	2008/9/9
RB 15	Na-Al-P-Mn	0.34	0.015	0.301	0.01	0.122	0.0045	0.026	0.0005	1000	48	Stainless tube	RB 15		79 (RB B1)	2008/9/9
RB 16	Na-Al-P-Mn	0.338	0.015	0.308	0.01	0.107	0.0039	0.055	0.0010	1000	48	Stainless tube	RB 16		79 (RB B1)	2008/9/9

Reaction Name	**Reacting System**	**Na (g)**	**Na (mole)**	**P (g)**	**P (mole)**	**Ti (g)**	**Ti (mole)**	**T_{max} (ºC)**	**Dwelling time (hour)**	**Reaction Container**	**Products**	**XRD**	**Page**	**Date**
TC 4	Na-Ti-P	0.46	0.02	0.695	0.022	0.479	0.0100	800	48	Stainless tube + quartz tube			13 (TC B1)	2006/11/17
TC 8	Na-Ti-P	0.465	0.02	0.36	0.012	0.345	0.0072	800	48	Stainless tube + quartz tube		TC 8	16 (TC B1)	2006/11/28

Reaction Name	**Reacting System**	**Na (g)**	**Na (mole)**	**P (g)**	**P (mole)**	**Al (g)**	**Al (mole)**	**Cr (g)**	**Cr (mole)**	**T_{max} (ºC)**	**Dwelling time (hour)**	**Reaction Container**	**XRD**	**Page**	**Date**
RB 4	Na-Al-P-Cr	0.345	0.015	0.31	0.01	0.132	0.0049	0.005	0.0001	800	48	Stainless tube	RB 4	53 (RB B1)	2008/3/31
RB 5	Na-Al-P-Cr	0.341	0.015	0.3	0.01	0.127	0.0047	0.012	0.0002	800	48	Stainless tube	RB 5	53 (RB B1)	2008/3/31
RB 6	Na-Al-P-Cr	0.343	0.015	0.304	0.01	0.12	0.0045	0.027	0.0005	800	48	Stainless tube	RB 6	53 (RB B1)	2008/3/31

RB 7	Na-Al-P-Cr	0.34	0.015	0.3	0.01	0.107	0.0040	0.05	0.0009	800	48	Stainless tube	RB 7	53 (RB B1)	2008/3/31
RB 17	Na-Al-P-Cr	0.344	0.015	0.301	0.01	0.123	0.0046	0.012	0.0002	1000	48	Stainless tube	RB 17	79 (RB B1)	2008/9/9
RB 18	Na-Al-P-Cr	0.342	0.015	0.309	0.01	0.121	0.0045	0.028	0.0005	1000	48	Stainless tube	RB 18	79 (RB B1)	2008/9/9
RB 19	Na-Al-P-Cr	0.34	0.015	0.31	0.01	0.11	0.0041	0.062	0.0011	1000	48	Stainless tube	RB 19	79 (RB B1)	2008/9/9

Reaction Name	Reaction System	T_{max} (ºC)	Cooling Rate (ºC/hour)	Dwelling Time (hr)	Nb (g)	Nb (mole)	Ni (g)	Ni (mole)	P (g)	P (mole)	Na (g)	Na (mole)	Crucible	XRD	SEM/EDS	Photos	Page	Date
CMF 39A	Nb-Ni-P-Na	900	4.1	72	0.082	0.0009	0.0521	0.0009	0.028	0.0009	0.3068	0.0133	Stainless tube	CMF 39			89 (CMF B3)	2006/5/18
CMF 39B	Nb-Ni-P-Na	900	4.1	72	0.083	0.0009	0.0525	0.0009	0.027	0.0009	0.2052	0.0089	Stainless tube				89 (CMF B3)	2006/5/18
CMF 42	Nb-Ni-P	900	4.1	72	0.648	0.0070	0.4111	0.0070	0.217	0.0070	0.0000	0.0000	Stainless tube	CMF 42			83 (CMF B3)	2007/6/21
CMF 43	Nb-Ni-P-Na	900	4.1	72	0.1612	0.0017	0.1015	0.0017	0.054	0.0017	0.8111	0.0353	Stainless tube	CMF 43			83 (CMF B3)	2007/6/21
CMF 44	Nb-Ni-P	900	4.1	72	1.062	0.0114	0.0840	0.0014	0.045	0.0015	0.0000	0.0000	Stainless tube	CMF 44			83 (CMF B3)	2007/6/21
CMF 45	Nb-Ni-P-Na	900	4.1	72	0.4383	0.0047	0.0357	0.0006	0.019	0.0006	0.6797	0.0296	Stainless tube	CMF 45			83 (CMF B3)	2007/6/21
CMF 46	Nb-Ni-P-Na	900	4.1	72	0.6194	0.0067	0.0497	0.0008	1.077	0.0348	0.4045	0.0176	Stainless tube	CMF 46			83 (CMF B3)	2007/6/21
CMF 47	Nb-Ni-P	900	4.1	72	0.3087	0.0033	0.7057	0.0120	0.125	0.0040	0.0000	0.0000	Stainless tube	CMF 47			84 (CMF B3)	2007/7/4
CMF 48	Nb-Ni-P-Na	900	4.1	72	0.0719	0.0008	0.1357	0.0023	0.029	0.0009	0.8850	0.0385	Stainless tube	CMF 48			84 (CMF B3)	2007/7/4
CMF 49	Nb-Ni-P	900	4.1	72	0.311	0.0033	0.1960	0.0033	0.827	0.0267	0.0000	0.0000	Stainless tube	CMF 49			84 (CMF B3)	2007/7/4
CMF 50	Nb-Ni-P-Na	900	4.1	72	0.0663	0.0007	0.0426	0.0007	0.178	0.0057	0.8230	0.0358	Stainless tube	CMF 50			84 (CMF B3)	2007/7/4

Reaction Name	Reaction System	T_{max} (ºC)	Cooling Rate (ºC/hour)	Dwelling Time (hr)	Nb (g)	Nb (mole)	Ni (g)	Ni (mole)	P (g)	P (mole)	Na_3P (g)	Na_3P (mole)	Crucible	XRD	SEM/EDS	Photos	Page	Date
VC-1	Nb-Ni-P	900	4.1	72	0.6194	0.0067	0.3913	0.0067	0.619	0.02	0	0	Stainless tube	VC-1			49 (VC B1)	2009/1/2
VC-2	Nb-Ni-P	900	4.1	72	1.0839	0.0117	0.2250	0.0038	0.552	0.01783	0	0	Stainless tube	VC-2			49 (VC B1)	2009/1/2
VC-3	Nb-Ni-P	900	4.1	72	1.0839	0.0117	0.4695	0.0080	0.423	0.01367	0	0	Stainless tube	VC-3			49 (VC B1)	2009/1/2
VC-4	Nb-Ni-P	900	4.1	72	0.1548	0.0017	0.2935	0.0050	0.826	0.02666	0	0	Stainless tube	VC-4			49 (VC B1)	2009/1/2
VC-5	Nb-Ni-P	900	4.1	72	0.6039	0.0065	0.1076	0.0018	0.774	0.025	0	0	Stainless tube	VC-5			49 (VC B1)	2009/1/2
VC-6	Nb-Ni-P	900	4.1	72	0.2942	0.0032	0.5967	0.0102	0.619	0.02	0	0	Stainless tube	VC-6			49 (VC B1)	2009/1/2
VC-7	Nb-Ni-P	900	4.1	72	0.3097	0.0033	0.4891	0.0083	0.671	0.02166	0	0	Stainless tube	VC-7			49 (VC B1)	2009/1/2
VC-8	Nb-Ni-P	900	4.1	72	0.6194	0.0067	0.5869	0.0100	0.516	0.01666	0	0	Stainless tube	VC-8			49 (VC B1)	2009/1/2
VC-9	Nb-Ni-P	900	4.1	72	0.4645	0.0050	0.2935	0.0050	0.723	0.02333	0	0	Stainless tube	VC-9			49 (VC B1)	2009/1/2
VC-10	Nb-Ni-P	900	4.1	72	0.8516	0.0092	0.1956	0.0033	0.645	0.02083	0	0	Stainless tube	VC-10			49 (VC B1)	2009/1/2
VC-11	Nb-Ni-P-Na_3P	900	4.1	72	0.2942	0.0032	0.5967	0.0102	0.619	0.02	1.8597	0.0186	Stainless tube	VC-11			49 (VC B1)	2009/1/2
VC-12	Nb-Ni-P-Na_3P	900	4.1	72	0.3097	0.0033	0.4891	0.0083	0.671	0.0216	1.8597	0.0186	Stainless tube	VC-12			49 (VC B1)	2009/1/2

										6							
VC-13	Nb-Ni-P-Na_3P	900	4.1	72	0.6194	0.0067	0.5869	0.0100	0.516	0.01666	1.8597	0.0186	Stainless tube	VC-13		49 (VC B1)	2009/1/2
VC-14	Nb-Ni-P-Na_3P	900	4.1	72	0.4645	0.0050	0.2935	0.0050	0.723	0.02333	1.8597	0.0186	Stainless tube	VC-14		49 (VC B1)	2009/1/2
VC-15	Nb-Ni-P-Na_3P	900	4.1	72	0.8516	0.0092	0.1956	0.0033	0.645	0.02083	1.8597	0.0186	Stainless tube	VC-15		49 (VC B1)	2009/1/2

Reaction Name	**Reaction System**	**T_{max} (°C)**	**Cooling Rate (°C/hour)**	**Dwelling Time (hr)**	**Ni (g)**	**Ni (mole)**	**Ge (g)**	**Ge (mole)**	**Nb (g)**	**Nb (mole)**	**P (g)**	**P (mole)**	**Na (g)**	**Na (mole)**	**Crucible**	**XRD**	**SEM/EDS**	**Photos**	**Page**	**Data**
CMF 51	Ni-Ge-Nb-P	900	4.1	72	0.3521	0.006	0.0073	0.0001	0.65	0.007	0.1858	0.006	0	0	Stainless tube				84 (CMF B4)	2007/7/4
CMF 52	Ni-Ge-Nb-P	900	4.1	72	0.1956	0.0033	0.2423	0.0033	0.619	0.0067	0.1032	0.00333	0	0	Stainless tube				84 (CMF B4)	2007/7/4
CMF 53	Ni-Ge-Nb-P	900	4.1	72	0.4633	0.0079	0.3826	0.0053	0.245	0.0026	0.0815	0.00263	0	0	Stainless tube				84 (CMF B4)	2007/7/4
CMF 54	Ni-Ge-Nb-P	900	4.1	72	0.1012	0.0017	0.6266	0.0086	0.32	0.0034	0.1068	0.00345	0	0	Stainless tube				84 (CMF B4)	2007/7/4
CMF 55	Ni-Ge-Nb-P	900	4.1	72	0.2445	0.0042	0.1512	0.0021	0.387	0.0042	0.3226	0.01042	0	0	Stainless tube				84 (CMF B4)	2007/7/4
CMF 56	Ni-Ge-Nb-P-Na	900	4.1	72	0.1761	0.003	0.0363	0.0005	0.325	0.0035	0.0929	0.003	0.5750	0.0250	Stainless tube				85 (CMF B4)	2007/7/5
CMF 57	Ni-Ge-Nb-P-Na	900	4.1	72	0.0451	0.0008	0.0559	0.0008	0.143	0.0015	0.0238	0.00077	0.8846	0.0385	Stainless tube				85 (CMF B4)	2007/7/5
CMF 58	Ni-Ge-Nb-P-Na	900	4.1	72	0.1174	0.0020	0.0969	0.0013	0.062	0.0007	0.0206	0.00067	0.7666	0.0333	Stainless tube				85 (CMF B4)	2007/7/5
CMF 59	Ni-Ge-Nb-P-Na	900	4.1	72	0.0326	0.0006	0.2019	0.0028	0.103	0.0011	0.0344	0.00111	0.6389	0.0278	Stainless tube				85 (CMF B4)	2007/7/5
Reaction Name	**Reaction System**	**T_{max} (°C)**	**Cooling Rate (°C/hour)**	**Dwelling Time (hr)**	**Ni (g)**	**Ni (mole)**	**Ge (g)**	**Ge (mole)**	**Nb (g)**	**Nb (mole)**	**P (g)**	**P (mole)**	**Na (g)**	**Na (mole)**	**Crucible**	**XRD**	**SEM/EDS**	**Photos**		
CMF 40-1	Ni-Ge-Nb-P-Na	900	4.1	72	0.2351	0.004	0.0965	0.0013	0.245	0.0026	0.1234	0.00398	0.7679	0.0334	Stainless tube	CMF 40-1	CMF 40-1		96 (CMF B3)	2006/7/6

CMF 40-2	Ni-Ge-Nb-P-Na	900	4.1	72	0.1953	0.0033	0.0968	0.0013	0.309	0.0033	0.1241	0.00401	0.7677	0.0334	Stainless tube	CMF 40-2	CMF 40-2		96 (CMF B3)	2006/7/6
CMF 40-3	Ni-Ge-Nb-P-Na	900	4.1	72	0.1473	0.0025	0.0603	0.0008	0.371	0.0040	0.0775	0.0025	0.9589	0.0417	Nb tube				96 (CMF B3)	2006/7/6
CMF 40-4	Ni-Ge-Nb-P-Na	900	4.1	72	0.1953	0.0033	0.0490	0.0007	0.373	0.0040	0.1243	0.00401	0.7655	0.0333	Stainless tube	CMF 40-4	CMF 40-4		96 (CMF B3)	2006/7/6
CMF 40-5	Ni-Ge-Nb-P-Na	900	4.1	72	0.1565	0.0027	0.0973	0.0013	0.309	0.0033	0.1245	0.00402	0.7673	0.0334	Stainless tube	CMF 40-5	CMF 40-5		96 (CMF B3)	2006/7/6
CMF 40-6	Ni-Ge-Nb-P-Na	900	4.1	72	0.2356	0.004	0.0486	0.0007	0.15	0.0016	0.124	0.004	0.7665	0.0333	Stainless tube	CMF 40-6	CMF 40-6		96 (CMF B3)	2006/7/6
Reaction Name	**Reaction System**	**T_{max} (°C)**	**Cooling Rate (°C/hour)**	**Dwelling Time (hr)**	**Ni (g)**	**Ni (mole)**	**Nb (g)**	**Nb (mole)**	**P (g)**	**P (mole)**	**Na (g)**	**Na (mole)**			**Crucible**	**XRD**	**SEM/EDS**	**Photos**		
CMF 40-7	Ni-Nb-P-Na	900	4.1	72	0.1176	0.002	0.1853	0.002	0.062	0.002	0.9193	0.04			Nb tube	CMF 40-7			97 (CMF B3)	2006/7/7
CMF 40-8	Ni-Nb-P-Na	900	4.1	72	0.1189	0.002	0.3711	0.004	0.062	0.0020	0.9197	0.04			Stainless tube	CMF 40-8			97 (CMF B3)	2006/7/7
CMF 40-9	Ni-Nb-P-Na	900	4.1	72	0.2345	0.004	0.1845	0.002	0.063	0.0020	0.9196	0.04			Stainless tube	CMF 40-9			97 (CMF B3)	2006/7/7
CMF 40-10	Ni-Nb-P-Na	900	4.1	72	0.2525	0.0043	0.2658	0.0029	0.044	0.0014	0.6571	0.0286			Stainless tube	CMF 40-10			97 (CMF B3)	2006/7/7
CMF 40-11	Ni-Nb-P-Na	900	4.1	72	0.0843	0.0014	0.3992	0.0043	0.044	0.0014	0.6574	0.0286			Stainless tube	CMF 40-11	CMF 40-11		97 (CMF B3)	2006/7/7
Reaction Name	**Reaction System**	**T_{max} (°C)**	**Cooling Rate (°C/hour)**	**Dwelling Time (hr)**	**Mn (g)**	**Mn (mole)**	**P (g)**	**P (mole)**	**Na (g)**	**Na (mole)**					**Crucible**	**XRD**	**SEM/EDS**	**Photos**		
CMF 40-12	Mn-P-Na	900	4.1	72	0.0546	0.00	0.0007	2E-05	0.36	0.0157					Nb tube	CMF 40-12	CMF 40-12		97 (CMF B3)	2006/7/7
CMF 40-13	Mn-P-Na	900	4.1	72	0.1097	0.00	0.0013	4E-05	0.5	0.0217					Stainless tube		CMF 40-13		97 (CMF B3)	2006/7/7
Reaction Name	**Reaction System**	**T_{max} (°C)**	**Cooling Rate (°C/hour)**	**Dwelling Time (hr)**	**Ni (g)**	**Ni (mole)**	**Ge (g)**	**Ge (mole)**	**Nb (g)**	**Nb (mole)**	**P (g)**	**P (mole)**	**Na (g)**	**Na (mole)**	**Crucible**	**XRD**	**SEM/EDS**	**Photos**		

CMF 41-1	Ni-Ge-Nb-P-Na	900	4.1	72	0.1467	0.0025	0.0605	0.0008	0.155	0.0017	0.3872	0.0125	0.4709	0.0205	Stainless tube	CMF 41-1			15 (CMF B4)	2006/9/16
CMF 41-2	Ni-Ge-Nb-P-Na	900	4.1	72	0.1174	0.0020	0.0581	0.0008	0.186	0.002	0.3717	0.012	0.4598	0.0200	Stainless tube	CMF 41-2			15 (CMF B4)	2006/9/16
CMF 41-3	Ni-Ge-Nb-P-Na	900	4.1	72	0.1174	0.0020	0.0290	0.0004	0.223	0.0024	0.3717	0.012	0.4598	0.0200	Nb tube				15 (CMF B4)	2006/9/16
CMF 41-4	Ni-Ge-Nb-P-Na	900	4.1	72	0.1409	0.0024	0.0290	0.0004	0.186	0.002	0.3717	0.012	0.4598	0.0200	Stainless tube	CMF 41-4			15 (CMF B4)	2006/9/16
CMF 41-5	Ni-Ge-Nb-P-Na	900	4.1	72	0.0978	0.0017	0.0608	0.0008	0.232	0.0025	0.3872	0.0125	0.4790	0.0208	Stainless tube	CMF 41-5			15 (CMF B4)	2006/9/16
CMF 41-6	Ni-Ge-Nb-P-Na				0.1174	0.0020	0.0290	0.0004	0.186	0.002	0.3717	0.012	0.4598	0.0200	Stainless tube	CMF 41-6			15 (CMF B4)	2006/9/16
Reaction Name	**Reaction System**	**T_{max} (°C)**	**Cooling Rate (°C/hour)**	**Dwelling Time (hr)**	**Ni (g)**	**Ni (mole)**	**Nb (g)**	**Nb (mole)**	**P (g)**	**P (mole)**	**Na (g)**	**Na (mole)**			**Crucible**	**XRD**	**SEM/EDS**	**Photos**		
CMF 41-7	Ni-Nb-P-Na	900	4.1	72	0.0451	0.0008	0.0715	0.0008	0.119	0.0038	0.8842	0.0385			Nb tube				16 (CMF B4)	2006/9/6
CMF 41-8	Ni-Nb-P-Na	900	4.1	72	0.0391	0.0007	0.1239	0.0013	0.103	0.0033	0.7663	0.0333			Stainless tube				16 (CMF B4)	2006/9/6
CMF 41-9	Ni-Nb-P-Na	900	4.1	72	0.0783	0.0013	0.0619	0.0007	0.103	0.0033	0.7663	0.0333			Stainless tube		CMF 41-9		16 (CMF B4)	2006/9/6
CMF 41-10	Ni-Nb-P-Na	900	4.1	72	0.0978	0.0017	0.1032	0.0011	0.086	0.0028	0.7663	0.0333			Stainless tube		CMF 41-10		16 (CMF B4)	2006/9/6
CMF 41-11	Ni-Nb-P-Na	900	4.1	72	0.0931	0.0016	0.1858	0.002	0.103	0.0033	0.7663	0.0333			Stainless tube				16 (CMF B4)	2006/9/6
Reaction Name	**Reaction System**	**T_{max} (°C)**	**Cooling Rate (°C/hour)**	**Dwelling Time (hr)**	**Mn (g)**	**Mn (mole)**	**P (g)**	**P (mole)**	**Na (g)**	**Na (mole)**					**Crucible**	**XRD**	**SEM/EDS**	**Photos**		
CMF 41-12	Mn-P-Na	900	4.1	72	0.0458	0.0008	0.1291	0.0042	0.958	0.0417					Nb tube				16 (CMF B4)	2006/9/6
CMF 41-13	Mn-P-Na	900	4.1	72	0.0845	0.0015	0.1191	0.0038	0.884	0.0385					Stainless tube				16 (CMF B4)	2006/9/6

CMF 41-14	Mn-P-Na	900	4.1	72	0.5494	0.0100	0.3097	0.01	0.23	0.0100					Stainless tube				16 (CMF B4)	2006/9/6
CMF 41-15	Mn-P-Na	900	4.1	72	0.2747	0.0050	0.7744	0.025	0.23	0.0100					Stainless tube				16 (CMF B4)	2006/9/6

Reaction Name	**Reactin System**	**Mg (g)**	**Mg (mole)**	**Si (g)**	**Si (mole)**	**P (g)**	**P (mole)**	**Reaction Name**	**Sn (g)**	**Sn (mole)**	**Maximum Growing Temperature (ºC)**	**Dwelling time (hour)**	**Reaction Container**	**XRD**	**SEM/EDS**	**Photo**
Bas-SS	Mg-Si-P-Sn							Bas-SS			1150	20	Stainless Steel + Quartz tube			Bas-ss
Reaction Name	**Reactin System**	**Mg (g)**	**Mg (mole)**	**Si (g)**	**Si (mole)**	**P (g)**	**P (mole)**	**Reaction Name**	**Sn (g)**	**Sn (mole)**	**Maximum Growing Temperature (ºC)**	**Dwelling time (hour)**	**Reaction Container**	**XRD**	**SEM/EDS**	**Photo**
Bas-Nb	Mg-Si-P							Bas-Nb			1150	20	Niobium + Quartz tube			Bas-Nb
Reaction Name	**Reactin System**	**Mg (g)**	**Mg (mole)**	**Si (g)**	**Si (mole)**	**P (g)**	**P (mole)**	**Reaction Name**	**Sn (g)**	**Sn (mole)**	**Maximum Growing Temperature (ºC)**	**Dwelling time (hour)**	**Reaction Container**	**XRD**	**SEM/EDS**	**Photo**
Bas-Al	Mg-Si-P							Bas-Al			1150	20	Al2O3 crucible + Quartz tube	Bas-Al		Bas-Al
Reaction Name	**Reactin System**	**Mg (g)**	**Mg (mole)**	**Si (g)**	**Si (mole)**	**P (g)**	**P (mole)**	**Reaction Name**	**Sn (g)**	**Sn (mole)**	**Maximum Growing Temperature (ºC)**	**Dwelling time (hour)**	**Reaction Container**	**XRD**	**SEM/EDS**	**Photo**
Bas-1	Mg-Si-P	0.045	0.002	0.053	0.002	0.116	0.004	Bas-1	2.000	0.017	1150	20	Graphite + Quartz tube	Bas-1		Bas-1
Reaction Name	**Reactin System**	**Mg (g)**	**Mg (mole)**	**Ge (g)**	**Ge (mole)**	**P (g)**	**P (mole)**	**Reaction Name**	**Sn (g)**	**Sn (mole)**	**Maximum Growing Temperature (ºC)**	**Dwelling time (hour)**	**Reaction Container**	**XRD**	**SEM/EDS**	**Photo**
Bas-2	Mg-Ge-P	0.046	0.002	0.136	0.002	0.116	0.004	Bas-2	2.004	0.017	1150	20	Graphite + Quartz tube	Bas-2		Bas-2
Reaction Name	**Reactin System**	**Zn (g)**	**Zn (mole)**	**Si (g)**	**Si (mole)**	**P (g)**	**P (mole)**	**Reaction Name**	**Sn (g)**	**Sn (mole)**	**Maximum Growing Temperature (ºC)**	**Dwelling time (hour)**	**Reaction Container**	**XRD**	**SEM/EDS**	**Photo**
Bas-3	Zn-Si-P	0.092	0.001407	0.039	0.001	0.087	0.003	Bas-3	1.498	0.013	1150	20	Graphite + Quartz tube	Bas-3		Bas-3

Reaction Name	Reactin System	Zn (g)	Zn (mole)	Ge (g)	Ge (mole)	P (g)	P (mole)	Reaction Name	Sn (g)	Sn (mole)	Maximum Growing Temperature (ºC)	Dwelling time (hour)	Reaction Container	XRD	SEM/EDS	Photo
Bas-4	Zn-Ge-P	0.092	0.001407	0.201	0.003	0.087	0.003	Bas-4	1.501	0.013	1150	20	Graphite + Quartz tube	Bas-4		Bas-4
Reaction Name	**Reactin System**	**Mg (g)**	**Mg (mole)**	**Si (g)**	**Si (mole)**	**As (g)**	**As (mole)**	**Reaction Name**	**Sn (g)**	**Sn (mole)**	**Maximum Growing Temperature (ºC)**	**Dwelling time (hour)**	**Reaction Container**	**XRD**	**SEM/EDS**	**Photo**
Bas-5	Mg-Si-As	0.034	0.001	0.039	0.001	0.210	0.003	Bas-5	1.500	0.013	1150	20	Graphite + Quartz tube			Bas-5
Reaction Name	**Reactin System**	**Mg (g)**	**Mg (mole)**	**Ge (g)**	**Ge (mole)**	**As (g)**	**As (mole)**	**Reaction Name**	**Sn (g)**	**Sn (mole)**	**Maximum Growing Temperature (ºC)**	**Dwelling time (hour)**	**Reaction Container**	**XRD**	**SEM/EDS**	**Photo**
Bas-6	Mg-Ge-As	0.034	0.001	0.102	0.001	0.211	0.003	Bas-6	1.502	0.013	1150	20	Graphite + Quartz tube	Bas-6		Bas-6
Reaction Name	**Reactin System**	**Mg (g)**	**Mg (mole)**	**Si (g)**	**Si (mole)**	**As (g)**	**As (mole)**	**Reaction Name**	**Sn (g)**	**Sn (mole)**	**Maximum Growing Temperature (ºC)**	**Dwelling time (hour)**	**Reaction Container**	**XRD**	**SEM/EDS**	**Photo**
Bas-7	Mg-Si-As	0.034		0.039	0.001	0.210	0.003	Bas-7	1.500	0.013	1150	20	Nb tube + Quartz tube			Bas-7
Reaction Name	**Reactin System**	**Mg (g)**	**Mg (mole)**	**Ge (g)**	**Ge (mole)**	**As (g)**	**As (mole)**	**Reaction Name**	**Sn (g)**	**Sn (mole)**	**Maximum Growing Temperature (ºC)**	**Dwelling time (hour)**	**Reaction Container**	**XRD**	**SEM/EDS**	**Photo**
Bas-8	Mg-Ge-As	0.034	0.001	0.102	0.001	0.211	0.003	Bas-8	1.502	0.013	1150	20	Nb tube + Quartz tube			Bas-8

Reaction Name	Reactin System	Mg (g)	Mg (mole)	Si (g)	Si (mole)	P (g)	P (mole)	Reaction Name	Mn (g)	Mn (mole)	Sn (g)	Sn (mole)	Maximum Growing Temperature (ºC)	Dwelling time (hour)	Reaction Container	XRD	SEM/EDS	Photo
Bas-3-1	Mg-Si-P	0.032	0.001	0.040	0.001	0.087	0.003	Bas-3-1	0.0039	0.00007	1.503	0.013	1150	20	Graphite + Quartz tube	Bas-3-1		Bas-3-1
Reaction Name	**Reactin System**	**Zn (g)**	**Zn (mole)**	**Si (g)**	**Si (mole)**	**P (g)**	**P (mole)**	**Reaction Name**	**Mn (g)**	**Mn (mole)**	**Sn (g)**	**Sn (mole)**	**Maximum Growing Temperature (ºC)**	**Dwelling time (hour)**	**Reaction Container**	**XRD**	**SEM/EDS**	**Photo**
Bas-3-2	Zn-Si-P	0.087	0.00133	0.04	0.001	0.087	0.003	Bas-3-2	0.0039	0.00007	1.503	0.013	1150	20	Graphite + Quartz tube	**Bas-3-2**		**Bas-3-2**
Reaction Name	**Reactin System**	**Zn (g)**	**Zn (mole)**	**Ge (g)**	**Ge (mole)**	**P (g)**	**P (mole)**	**Reaction Name**	**Mn (g)**	**Mn (mole)**	**Sn (g)**	**Sn (mole)**	**Maximum Growing Temperature (ºC)**	**Dwelling time (hour)**	**Reaction Container**	**XRD**	**SEM/EDS**	**Photo**

Bas-3-3	Zn-Ge-P	0.087	0.00133	0.102	0.001	0.087	0.003	Bas-3-3	0.0039	0.00007	1.5	0.013	1150	20	Graphite + Quartz tube			**Bas-3-3**
Reaction Name	**Reactin System**	**Mg (g)**	**Mg (mole)**	**Si (g)**	**Si (mole)**	**As (g)**	**As (mole)**	**Reaction Name**	**Mn (g)**	**Mn (mole)**	**Sn (g)**	**Sn (mole)**	**Maximum Growing Temperature (ºC)**	**Dwelling time (hour)**	**Reaction Container**	**XRD**	**SEM/EDS**	**Photo**
Bas-3-4	Mg-Si-As	0.032	0.001	0.039	0.001	0.21	0.003	Bas-3-4	0.0039	0.00007	1.5	0.013	1150	20	Graphite + Quartz tube	**Bas-3-4**		**Bas-3-4**
Reaction Name	**Reactin System**	**Mg (g)**	**Mg (mole)**	**Ge (g)**	**Ge (mole)**	**As (g)**	**As (mole)**	**Reaction Name**	**Mn (g)**	**Mn (mole)**	**Sn (g)**	**Sn (mole)**	**Maximum Growing Temperature (ºC)**	**Dwelling time (hour)**	**Reaction Container**	**XRD**	**SEM/EDS**	**Photo**
3-5	Mg-Ge-As	0.032	0.001	0.102	0.001	0.211	0.003	3-5	0.0039	0.00007	1.502	0.013	1150	20	Graphite + Quartz tube	Bas-3-5		Bas-3-5

CuF2 (g)	**CuF2 (mole)**	**ZrF4 (g)**	**ZrF4 (mole)**	**Maximum Growing Temperature (ºC)**	**Cooling Rate (ºC/hour)**	**Dwelling Time (hr)**	**Reaction Container**	**XRD**	**SEM/EDS**	**Photo**	Page	Date
3.0451	101.543	1.6734	0.010008	700	2.2	4	Pt tube	CMF 60			3 (CMF B5)	2008/2/26
3.0457	101.543	1.6685	0.009978	650	10	4	Au sealed Pt tube	CMF 61			4 (CMF B5)	2008/2/26
3.0464	101.543	1.673	0.010005	700	10	10	Au sealed Pt tube + Quartz tube	CMF 62			6 (CMF B5)	2008/2/28

Reaction Name	Reactin System	Zn:Si:P: Na	Zn (g)	Zn (mole)	Si (g)	Si (mole)	P (g)	P (mole)	Na (g)	Na (mole)	Maximum Growing Temperature (°C)	Reaction Container	Pellet	XRD	SEM/ EDS	Photo
DM 1	Zn-Si-P-Na	1:1:2:5	0.066	0.001	0.284	0.01	0.063	0.002	0.116	0.005	900	Stainless tube + quartz tube	No			
DM 2	Zn-Si-P-Na	1:1:2:10	0.066	0.001	0.282	0.01	0.63	0.02	0.23	0.01	900	Stainless tube + quartz tube	No			
DM 3	Zn-Si-P-Na	1:1:3:5	0.067	0.001	0.291	0.01	0.092	0.003	0.115	0.005	900	Stainless tube + quartz tube	No			
DM 4	Zn-Si-P-Na	1:1:4:5	0.066	0.001	0.277	0.01	0.124	0.004	0.116	0.005	900	Stainless tube + quartz tube	No			
DM 11	Zn-Si-P-Na	1:1:2:5	0.262	0.004	0.112	0.004	0.248	0.008	0.465	0.02	1000	Stainless tube + quartz tube	No			
Reaction Name	**Reactin System**	**Cd:Si:P: Na**	**Cd (g)**	**Cd (mole)**	**Si (g)**	**Si (mole)**	**P (g)**	**P (mole)**	**Na (g)**	**Na (mole)**	**Maximum Growing Temperature (°C)**	**Reaction Container**	**Pellet**	**XRD**	**SEM/ EDS**	**Photo**
DM 5	Cd-Si-P-Na	1:1:2:10	0.338	0.003	0.085	0.003	0.187	0.006	0.689	0.03	900	Stainless tube + quartz tube	No			
DM 6	Cd-Si-P-Na	1:1:3:10	0.337	0.003	0.085	0.003	0.279	0.009	0.69	0.03	900	Stainless tube + quartz tube	No			
DM 7	Cd-Si-P-Na	1:1:4:10	0.338	0.003	0.085	0.003	0.372	0.012	0.689	0.03	900	Stainless tube + quartz tube	No			
DM 8	Cd-Si-P-Na	1:1:4:20	0.113	0.001	0.029	0.001	0.125	0.004	0.46	0.02	900	Stainless tube + quartz tube	No			
DM 9	Cd-Si-P-Na	1:1:2:10	0.111	1E-03	0.03	0.001	0.061	0.002	0.229	0.01	1000	Stainless tube + quartz tube	No			
DM 10	Cd-Si-P-Na	1:1:3:10	0.11	1E-03	0.035	0.001	0.09	0.003	0.224	0.01	1000	Stainless tube + quartz tube	No			
DM 12	Cd-Si-P-Na	1:1:2:0	0.434	0.004	0.117	0.004	0.241	0.008	0	0	1000	Stainless tube + quartz tube	No			
DM 13	Cd-Si-P-Na	1:1:3:0	0.433	0.004	0.109	0.004	0.404	0.013	0	0	1000	Stainless tube + quartz tube	No			
DM 14	Cd-Si-P-Na	1:1:4:0	0.433	0.004	0.102	0.004	0.529	0.017	0	0	1000	Stainless tube + quartz tube	No			
DM 15	Cd-Si-P-Na	1:1:2:0	0.434	0.004	0.108	0.004	0.239	0.008	0	0	1000	Stainless tube	No			

DM 18	Cd-P	Cd:2P									1000	Stainless tube	No			
DM 19	DC 18-Si	DM 18:Si									1000	Stainless tube	No			
DM 20	Cd-Si-P	1:1:2:0	1.124	0.01	0.282	0.01	0.62	0.02	0	0	1000	Stainless tube	No			
DM 21	Cd-Si-P	1:1:2.5:0	1.124	0.01	0.28	0.01	0.774	0.025	0	0	1000	Stainless tube + quartz tube	No			
DM 22	Cd-Si-P	1:1:3:0	1.125	0.01	0.281	0.01	0.929	0.03	0	0	1130	Stainless tube + quartz tube	No			
DM 23	Cd-Si-P	1:1:2:0	1.124	0.01	0.282	0.01	0.62	0.02	0	0	1000	Stainless tube	No			
DM 24	Cd-Si-P	1:1:2.5:0	1.124	0.01	0.28	0.01	0.774	0.025	0	0	1000	Stainless tube + quartz tube	No			
DM 25	Cd-Si-P	1:1:3:0	1.125	0.01	0.281	0.01	0.929	0.03	0	0	1000	Stainless tube + quartz tube	No			
DM 26	Cd-Si-P	1:1:2:0	1.124	0.01	0.282	0.01	0.62	0.02	0	0	1000	Stainless tube	No			
DM 27	Cd-Si-P	1:1:2.5:0	1.124	0.01	0.28	0.01	0.774	0.025	0	0	1130	Stainless tube + quartz tube	No			
DM 28	Cd-Si-P	1:1:3:0	1.125	0.01	0.281	0.01	0.929	0.03	0	0	1130	Stainless tube + quartz tube	No			
Reaction Name	**Reactin System**	**Cd:Si:P: Mn**	**Zn (g)**	**Zn (mole)**	**Mn (g)**	**Mn (mole)**	**Si (g)**	**Si (mole)**	**P (g)**	**P (mole)**	**Maximum Growing Temperature (ºC)**	**Reaction Container**	**Pellet**	**XRD**	**SEM/ EDS**	**Photo**
DM 16	Cd-Si-P-Mn	0.98:1:2:0 .02									1000	Stainless tube	No			
DM 17	Cd-Si-P-Mn	0.95:1:2:0 .05									1000	Stainless tube	No			

Reaction Name	Reaction system	Co_3O_4 (g)	Co_3O_4 (mole)	$CaCO_3$ (g)	$CaCO_3$ (mole)	$CaCl_2$ (g)	$CaCl_2$ (mole)	T_{max} (ºC)	Cooling Rate (ºC/hour)	Dwelling Time (hr)	crucible	XRD	SEM_EDS	SQUID	Photo	Page	Date
CMF 73	Co_3O_4-$CaCo_3$-$CaCl_2$	2.021	0.008	6.369	0.0636			850	quench in air	24	Al_2O_3	CMF 73				4 (CMF B7)	2008/12/10
CMF 74	Co_3O_4-$CaCo_3$-$CaCl_2$	2.021	0.008	6.369	0.0636			850	quench in air	24	Al_2O_3	CMF 74				5 (CMF B7)	2008/12/12
CMF 75	Co_3O_4-$CaCo_3$-$CaCl_2$	2.021	0.008	6.369	0.0636			900	quench in air	24	Al_2O_3					7 (CMF B7)	2008/12/12
CMF 76	Co_3O_4-$CaCo_3$-$CaCl_2$	16.378	0.068	15.615	0.1560	3.201		900	quench in air	24	Al_2O_3	CMF 76	CMF 76			26 (CMF B7)	2008/12/16
CMF 77	Co_3O_4-$CaCo_3$-$CaCl_2$	5.856	0.024	6.143	0.0614	23.993		900	quench in air	24	Al_2O_3	CMF 77	CMF 77			27 (CMF B7)	2008/12/16
CMF 78	Co_3O_4-$CaCo_3$-$CaCl_2$	3.071	0.013	2.931	0.0293	6.000		900	quench in air	24	Pt	CMF 78	CMF 78			28 (CMF B7)	2008/12/16
CMF 79	Co_3O_4-$CaCo_3$-$CaCl_2$	4.095	0.017	3.903	0.039	3.999		900	quench in air	24	Al2O3	CMF 79	CMF 79			27 (CMF B7)	2008/12/16
Reaction Name	**Reaction system**	**Co_3O_4 (g)**	**Co_3O_4 (mole)**	**$CaCO_3$ (g)**	**$CaCO_3$ (mole)**	**crucible**		**T_{max} (ºC)**	**Cooling Rate (ºC/hour)**	**Dwelling Time (hr)**	**XRD**	**SEM_EDS**	**SQUID**	**Photo**		**Page**	**Date**
CMF 80	Co_3O_4-$CaCo_3$ pellet	4.096	0.017	3.905	0.039	Pt foil		900	quench in air	24						30 (CMF B7)	2008/12/19
CMF 81	Co_3O_4-$CaCo_3$ pellet	4.905	0.02	3.903	0.039	Pt foil		900	quench in air	24	CMF 81					30 (CMF B7)	2008/12/19
CMF 82	Co_3O_4-$CaCo_3$ pellet					Pt foil		900	quench in air	24	CMF 82					34 (CMF B7)	2008/12/22
CMF 83	Co_3O_4-$CaCo_3$ pellet					Pt foil		900	quench in air	24	CMF 83					34 (CMF B7)	2008/12/22
CMF 84	Co_3O_4-$CaCo_3$ pellet					Pt foil		900	quench in air	24	CMF 84					41 (CMF B7)	2009/1/1

CMF 85	Co_3O_4-$CaCo_3$ pellet					Pt foil		900	quench in air	24	CMF 85	CMF 85	CMF 85			41 (CMF B7)	2009/1/1
Reaction Name	**Reaction system**	**Co_3O_4 (g)**	**Co_3O_4 (mole)**	**$CaCO_3$ (g)**	**$CaCO_3$ (mole)**	**$SrCl_2$ (g)**	**$SrCl_2$ (mole)**	**Maximum Growing Temperature (ºC)**	**Cooling Rate (ºC/hour)**	**Dwelling Time (hr)**	**crucible**	**XRD**	**SEM_EDS**	**SQUID**	**Photo**	**Page**	**Date**
CMF 86	Co_3O_4-$CaCo_3$-$SrCl_2$	16.38	0.068	15.618	0.1561	16	0.101	900	quench in air	24	Al_2O_3	CMF 86	CMF 86			89 (CMF B7)	2009/2/12
CMF 87	Co_3O_4-$CaCo_3$-$SrCl_2$	6.143	0.026	5.856	0.0585	24	0.151	900	quench in air	24	Al_2O_3	CMF 87	CMF 87			89 (CMF B7)	2009/2/12
CMF 88	Co_3O_4-$CaCo_3$-$SrCl_2$	3.071	0.013	2.937	0.0293	6.001	0.038	900	quench in air	24	Pt	CMF 88	CMF 88			89 (CMF B7)	2009/2/12
CMF 89	Co_3O_4-$CaCo_3$-$SrCl_2$	2.731	0.011	2.602	0.026	10.67	0.067	900	quench in air	24	Al_2O_3	CMF 89	CMF 89	CMF 89		90 (CMF B7)	2009/2/12

BIBLIOGRAPHY

CAPTER 1 REFERENCES

1. Heck, C., *Magnetic Materials and Their Applications*. Butterworths: 1974.

2. Grant, P., High-Temperature Superconductivity: Four Years Science Bednorz end Mueller. *Advanced Materials* 1990, 2, 232.

3. Lines, E. M.; Glass, M. A., *Principles and Applications of Ferroelectrics and Related Materials*. Clarendon Press 1977.

4. Nye, F. J., *Physical Properties of Crystals: their Representation by Tensors and Matrices*. Oxford University Press: 1985.

5. Nassau, K., Reconstructed or Geneva ruby. *Journal of Crystal Growth* 1969,*5*, 338.

6. Verneuil, A., Production Artificielle du Rubis par Fusion. *Paris Acad. ScL, Comptes Rendus* 1902, 135,791.

7. Bohm, J., The Historical Development of Crystal Growing - a bibliography. *Crystal Research and Technology* 1981, 16, 275.

8. Hulliger, J., Chemistry and Crystal Growth. *Angewandte Chemie International Edition in English* 1994, 33, 143.

9. Scheel, H., Historical Aspects of Crystal Growth Technology. *Journal of Crystal Growth* 2000, 211, 1.

10. Scheel, J. H., Historical Introduction in *Handbook of Crystal Growth*. Hurle, T. J. D., Ed. North-Holland: 1993; Vol. Volume 1, Part 1.

11. Buckley, E. H., *Crystal Growth*. John Wiley and Sons Inc.: 1951.

12. Laudise, R. A., *Growth of Single Crystal*. Prentice Hall Inc. Englewood Cliffs,

New Jersey 1970.

13. Lawson, W. D.; Nielsen, S., *Preparation of Single Crystal*. 1st edition ed.; Academic Press: 1958.

14. Pamplin, B. R., *Crystal Growth*. The Science of Solid State. Pergamon Press: 1975; Vol. 6.

15. Rosenberger, F., *Fundamental of Crystal Growth*. Spinger Verlag, Gemany: 1979.

16. Dirksen, J.; Ring, T., Fundamentals of Crystallization: Kinetic Effects on Particle Size Distributions and Morphology. *Chemical Engineering Science* 1991, 46, 2389.

17. Larson, M.; Garside, J., Solute clustering and interfacial tension. *Journal of Crystal Growth* 1986, 76, 88.

18. Söhnel, J., Solute clustering and nucleation. *Journal of Crystal Growth* 1988, 89, 202.

19. Larson, M.; Garside, J., Solute Clusering in Supersaturated Solutions. *Chemical Engineering Science* 1986, 41, 1285.

20. Na, H.; Arnold, S.; Myerson, A., Cluster Formation in Highly Supersaturated Solution Droplets. *Journal of Crystal Growth* 1994, 139, 104.

21. Azároff, V. L., *Introduction to Solids*. McGraw-Hill: 1960.

22. Hartman, P.; Perdok, W., On the Relations Between Structure and Morphology of Crystals. III. *Acta Crystallographica* 1955, 8, 525.

23. Boek, E.; Feil, D.; Briels, P., From Wave Function to Crystal Morphology: Application to Urea and Alpha-glycine. *Journal of Crystal Growth* 1991, 114, 389.

24. Hartmai, P.; Perdok, W., On the Relations Between Structure and Morphology of

Crystals. II. *Acta Cryst* 1955, 8, 521.

25. Hartman, P.; Perdok, G. W., On the Relations Between Structure and Morphology of Crystals. I. *Acta Crystallographica* 1955, 8, 49.

26. Burda, C.; Chen, X.; Narayanan, R.; El-Sayed, M., Chemistry and Properties of Nanocrystals of Different Shapes. *Chemical Reviews* 2005, *105* (4), 1025.

27. Cullen, W. G.; Wang, C.-C.; Ban, S. V., *Heteroepitaxial Semiconductors for Electronic Devices*. Springer-Verlag 1978.

28. Arthur, J., Molecular Beam Epitaxy. *Frontiers in Surface and Interface Science* 2002, 500, 189.

29. Czochralski, J., Measuring the Velocity of Crystallization of Metals. *Zeitschrift fur Physikalische Chemie* 1918, 92, 219.

30. Czochralski, J.; Garlicka, W., Crystallization Rate of Sodium and the Relations Between Atomic Heat of Solidification and Crystallization Rate. *Wiadomoœci Instytut Metalurgii i Metaloznawstwo* 1936, 3, 39.

31. Sonnenberg, K.; Kuessel, E., Developments in Vertical Bridgman Growth of Large Diameter GaAs. *III-Vs Review* 1997, 10, 30.

32. Laudise, A. R., Hydrothermal Synthesis of Crystals. *Chemical And Engineering News* 1987, 65, 30.

33. Johnson, G.; Foise, J., Quartz. *Encyclopedia of Applied Physics* 1996, *15*, 365.

34. Byrappa, K.; Haber, M., *Handbook of Hydrothermal Technology* William Andrew Publishing: 2001.

35. Caporaso, J. A.; Kolb, D. E.; Laudise, A. R. *Hydrothermal Crystal Growth*

Processes. United States Patent 4579622, 1986.

36. Bardsley, W., *Hydrothermal Growth in Crystal Growth: An Introduction*. North Holland Publishing Co. Amsterdam: 1973.

37. Bordui, P., Growth of Large Single Crystals from Aqueous Solution: A Review. *Journal of Crystal Growth* 1987, 85, 199.

38. Elwell, D.; Scheel, J. H., *Crystal Growth from High Temperature Solutions*. Academic Press, London: 1975.

39. Laudise, A. R.; Carruthers, R. J.; Jackson, A. K., Crystal Growth. *Annual Review of Materials Science* 1971, 1, 253.

40. Scheel, J. H.; Fukuda, T., *Crystal Growth Technology*. John Wiley, Chichester: 2004.

41. Wanklyn, B., The Present Status of Flux Growth. *Journal of Crystal Growth* 1983, 65, 533.

42. Kanatzidis, M.; Pottgen, R.; Jeitschko, W., The Metal Flux: A Preparative Tool Tor the Exploration of Intermetallic Compounds. *Angewandte Chemie International Edition in English* 2005, 44, 6996.

CAPTER 2 REFERENCES

1. Hodgkin, D., The X-ray Analysis of Complicated Molecules. *Science* 1965, 150, 979.

2. Filler, A., The History, Development and Impact of Computed Imaging in Neurological Diagnosis and Neurosurgery: CT, MRI, and DTI. 2009.

3. Laue, M., Die Interferenzerscheinungen an Rötgenstrahlen, Hervorgerufen Durch das Raumgitter der Kristalle. *Jahrb. Radioakt. Elektron* 1914, 11, 308.

4. Bragg, W., X-rays and Crystals. *Nature* 1912, 90, 219.

5. West, A., *Solid state Cemistry and its Applications*. Wiley-India: 2009.

6. Compton, A., A Quantum Theory of the Scattering of X-rays by Light Elements. *Physical Review* 1923**,** 21, 483.

7. Hartree, D., The Atomic Structure Factor in the Intensity of Reflexion of X-rays by Crystals. *Philosophical Magazine,* 1925**,** 50, 289.

8. James, R., The Optical Principles of the Diffraction of X-rays, p. 622. *London: Bell* 1954.

9. Cromer, D.; Waber, J., Scattering Factors Computed from Relativistic Dirac-Slater Wave Functions. *Acta Crystallographica* 1965, 18, 104.

10. James, R.; Brindley, G., Some Numerical Calculation of Atomic Scattering Facetors. *Philosophical Magazine* 1932, 12, 81.

11. Stewart, R.; Davidson, E.; Simpson, W., Coherent X-ray scattering for the Hydrogen Atom in the Hydrogen Molecule. *The Journal of Chemical Physics* 1965, 42, 3175.

12. Viervoll, H.; Ögrim, O., An Extended Table of Atomic Scattering Factors. *Acta Crystallographica* 1949, 2, 277.

13. KSAnalytical KS Analytical Systems.

14. Knoll, M., Charging Potential and Secondary Emission of Bodies Under Electron Irradiation. *Zeitschrift fur Technische Physik*, 1935, 16, 467.

15. Von Ardenne, M., Das Elektronen-Rastermikroskop. *Zeitschrift fur Physik A Hadrons and Nuclei* 1938, 109, 553.

16. Zworykin, V.; Hillier, J.; Snyder, R., A Scanning Electron Microscope, ASTM. *Bulletin No* 1942, 117, 15.

17. Oatley, C.; Everhart, T., The Examination of pn Junctions with the Scanning Electron Microscope. *Journal of Electronics* 1957, 2, 568.

18. Smith, K.; Oatley, C., The Scanning Electron Microscope and its Fields of Application. *British Journal of Applied Physics* 1955**,** 6, 391-399.

19. Pease, R.; Nixon, W., High Resolution Scanning Electron Microscopy. *Journal of Scientific Instruments* 1965**,** 42, 81.

20. Danilatos, G., Review and Outline of Environmental SEM at Present. *J. Microsc* 1991**,** 162, 391.

21. Danilatos, G., Introduction to the ESEM Instrument. *Microscopy Research and Technique* 1993**,** 25, 354.

22. Hiller, J. Electron Probe Analysis Employing chi-ray Spectrography 1947.

23. Castaing, R. Application of Electron Beams to a Method of Local Chemical and Crystallographic Analysis. Ph. D. thesis, University of Paris, 1951.

24. Duncumb, P.; Reed, S., In Quantitative Electron Probe Microanalysis (KFJ HEINRICH, ed.), NBS Spec. *Publ* 1968**,** 298, 133.

25. Philibert, J., Proceedings of the 3rd International Conference on X-ray Optics and Microanalysis. 1963.

26. Reed, S., Characteristic Fluorescence Corrections in Electron-probe Microanalysis. *British Journal of Applied Physics* 1965**,** 16, 913.

CAPTER 3 REFERENCES

1. Ohno, H.; Shen, A.; Matsukura, F.; Oiwa, A.; Endo, A.; Katsumoto, S.; Iye, Y., (Ga,Mn)As: A New Diluted Magnetic Semiconductor Based on GaAs. *Applied Physics Letters* 1996, 69, 363.

2. Prellier, W.; Fouchet, A.; Mercey, B., Oxide Diluted Magnetic Semiconductors: A Review of the Experimental Status. *Journal of Physics: Condensed Matter* 2003, 15,

R1583.

3. Sharma, P.; Gupta, A.; Rao, K. V.; Owens, F. J.; Sharma, R.; Ahuja, R.; Guillen, J. M. O.; Johansson, B.; Gehring, G. A., Ferromagnetism Above Room Temperature in Bulk and Transparent Thin Films of Mn-doped ZnO. *Nature Materials* 2003, 2, 673.

4. Reed, M. L.; El-Masry, N. A.; Stadelmaier, H. H.; Ritums, M. K.; Reed, M. J.; Parker, C. A.; Roberts, J. C.; Bedair, S. M., Room Temperature Ferromagnetic Properties of (Ga,Mn)N. *Appiedl Physics Letters* 2001, 79, 3473.

5. Frazier, R. M.; Stapleton, J.; Thaler, G. T.; Abernathy, C. R.; Pearton, S. J.; Rairigh, R.; Kelly, J.; Hebard, A. F.; Nakarmi, M. L.; Nam, K. B.; Lin, J. Y.; Jiang, H. X.; Zavada, J. M.; Wilson, R. G., Properties of Co-, Cr-, or Mn-implanted AlN. *Journal of Applied Physics* 2003, 94, 1592.

6. Pearton, S. J.; Abernathy, C. R.; Norton, D. P.; Hebard, A. F.; Park, Y. D.; Boatner, L. A.; Budai, J. D., Advances in Wide Bandgap Materials for Semiconductor Spintronics. *Materials Science & Engineering R-Reports* 2003, 40, 137.

7. Pearton, S. J.; Ren, F.; Wang, Y. L.; Chu, B. H.; Chen, K. H.; Chang, C. Y.; Lim, W.; Lin, J. S.; Norton, D. P., Recent Advances in Wide Bandgap Semiconductor Biological and Gas Sensors. *Progress in Materials Science* 2010, 55, 1.

8. Janotti, A.; Van de Walle, C. G., Fundamentals of Zinc Oxide as A Semiconductor. *Reports on Progress in Physics* 2009, 72 (12).

9. Ohno, H., Making nonmagnetic semiconductors ferromagnetic. *Science (Washington, D. C.)* 1998, 281, 951.

10. Ohno, H., Properties of Ferromagnetic III-V Semiconductors. *Journal of*

Magnetism and Magnetic Materials 1999, 200, 110.

11. Dietl, T.; Ohno, H.; Matsukura, F.; Cibert, J.; Ferrand, D., Zener Model Description of Ferromagnetism in Zinc-blende Magnetic Semiconductors. *Science (Washington, D. C.)* 2000, 287, 1019.

12. Sato, K.; Katayama-Yoshida, H., Material Design for Transparent Ferromagnets With ZnO-based Magnetic Semiconductors. *Japanese Journal of Applied Physics, Part 2: Letters* 2000, 39, L555.

13. Pearton, S. J.; Heo, W. H.; Ivill, M.; Norton, D. P.; Steiner, T., Dilute Magnetic Semiconducting Oxides. *Semiconductor Science and Technology* 2004, 19, R59.

14. Reynolds, D. C.; Look, D. C.; Jogai, B.; Litton, C. W.; Cantwell, G.; Harsch, W. C., Valence-band Ordering in ZnO. *Physical Review B* 1999, 60, 2340.

15. Phillips, J., Bonds and Bands in Semiconductors: New insight into Covalent Bonding in Crystals Has Followed from Studies of Energy-band Spectroscopy. *Science (New York, NY)* 1970, 169, 1035.

16. Lide, D., CRC Handbook of Chemistry and Physics, 73rd. *CRC Press Inc., Boca Raton, Florida* 1992, 1993, 9.

17. Harrison, D. E., Lamellar Glass-crystal Structures in the System ZnO-B_2O_3. *Journal of Crystal Growth* 1968, 3-4, 674.

18. Makarov, V.; Fotiev, A.; Serebryakova, L., Phase Composition and Equilibrium Diagram of the V_2O_5 ZnO System. *Journal of . Inoranic. Chemistry* 1971, 16.

19. Burdese, A., Systems of Vanadic Anhydride and Sesquioxides of Chromium, Iron, and Aluminum. *Annali di Chimica* 1957, 47, 797.

20. Wanklyn, B. M., The growth of ZnO Crystals from Phosphate and Vanadate Fluxes *Journal of Crystal Growth* 1970, 7, 107.

21. Harrison, D. E.; Hummel, F. A., Phase Equilibria and Fluorescence in the System Zinc Oxide-Boric Oxide. *Journal of Electrochemical Society* 1956, 103, 491.

22. Leonov, Y. S., The Reaction Between Zinc Oxide and Boric Anhydride by the Observation of Luminescence. *Zhurnal Neorganicheskoi Khimii* 1958, 3, 1245.

23. Oka, K.; Shibata, H.; Kashiwaya, S., Crystal growth of ZnO. *Journal of Crystal Growth* 2002, 237, 509.

24. Nielsen, J. W.; Dearborn, E. F., The Growth of Large Single Crystals of Zinc Oxide. *Journal of Physical Chemistry* 1960, 64, 1762.

25. Wanklyn, B. M., Growth of Zinc Oxide Crystals From Phosphate and Vanadate Fluxes. *Journal of Crystal Growth* 1970, 7, 107.

26. Ushio, M.; Sumiyoshi, Y., Synthesis of Zinc Oxide Single Crystals by the Flux Method. *Journal of Materials Science* 1993, 28, 218.

27. Kashyap, S. C., Growth of ZnO Needles from Molten Hydrous KOH Solutions. *Journal of Applied Physics* 1973, 44, 4381.

28. Hashimoto, H.; Hayashi, F.; Uematsu, T.; Moriyoshi, Y., Microstructure in Zno Thin Plates from Molten Mixed Alkali Solutions. *Journal of Materials Science Letters* 1982, 1, 4.

29. Yurkinskii, V. P.; Firsova, E. G.; Proskura, S. A., Thermal Dissociation of Sodium Hydroxide Upon Evacuation. *Russian Journal of Applied Chemistry* 2005, 78, 360.

30. http://en.wikipedia.org/wiki/Manganese(II)_carbonate (accessed April 14).

31. Zaki, M. I.; Hasan, M. A.; Pasupulety, L.; Kumari, K., Thermochemistry of Manganese Oxides in Reactive Gas Atmospheres: Probing Redox Compositions in the Decomposition Course MnO_2 --> MnO. *Thermochimica Acta* 1997, 303, 171.

32. Tauchi, S., Diffusion of Impurities in the Semiconductor Melt. *Journal of the Physical Society of Japan* 1962, 17, 220.

33. Blasco, J.; Bartolome, F.; Garcia, L. M.; Garcia, J., Extrinsic Origin of Ferromagnetism in Doped ZnO. *Journal of Materials Chemistry* 2006, 16, 2282.

34. Garcia, M. A.; Ruiz-Gonzalez, M. L.; Quesada, A.; Costa-Kramer, J. L.; Fernandez, J. F.; Khatib, S. J.; Wennberg, A.; Caballero, A. C.; Martin-Gonzalez, M. S.; Villegas, M.; Briones, F.; Gonzalez-Calbet, J. M.; Hernando, A., Interface Double-exchange Ferromagnetism in the Mn-Zn-O System: New Class of Biphase Magnetism. *Physical Review Letters* 2005, 94, 217206.

35. Kundaliya, D. C.; Ogale, S. B.; Lofland, S. E.; Dhar, S.; Metting, C. J.; Shinde, S. R.; Ma, Z.; Varughese, B.; Ramanujachary, K. V.; Salamanca-Riba, L.; Venkatesan, T., On the Origin of High-temperature Ferromagnetism in the Low-temperature-processed Mn-Zn-O System. *Nature Materials* 2004, 3, 709.

36. Rao, C. N. R.; Deepak, F. L., Absence of Ferromagnetism in Mn- and Co-doped ZnO. *Journal of Materials Chemistry* 2005, 15, 573.

37. Lawes, G.; Risbud, A. S.; Ramirez, A. P.; Seshadri, R., Absence of Ferromagnetism in Co and Mn Substituted Polycrystalline ZnO. *Physical Review B* 2005, 71, 045201.

38. Kolesnik, S.; Dabrowski, B., Absence of Room Temperature Ferromagnetism in

Bulk Mn-doped ZnO. *Journal of A pplied Physics* 2004, 96, 5379.

39. WANG, T.; LIU, S.-w.; WEI, H.-m.; XUE, C.-j., Resent Situations and Trend of Studies on the Hydrothermal Sedimentary Deposit. *Journal of Earth Sciences and Environment* 2004, 26, 6.

40. Palache, C., The minerals of Franklin and Sterling Hill, Sussex County, New Jersey *USGS Professional Paper* 1935, 180, 2.

41. Tarr, W. A., The origin of the zinc deposits at Franklin and Sterling Hill, New Jersey. *American Mineralogist* 1929, 14, 207.

42. McSween, H. Y., Jr., Manganese-rich Ore Assemblages from Franklin, New Jersey. *Economic Geology and the Bulletin of the Society of Economic Geologists* 1976, 71, 814.

43. Hou, D.-L.; Ye, X.-J.; Meng, H.-J.; Zhou, H.-J.; Li, X.-L.; Zhen, C.-M.; Tang, G.-D., Magnetic Properties of Mn-doped ZnO Powder and Thin Films. *Materials Science&Engineering, B: Solid-State Materials for Advanced Technology* 2007, 138, 184.

44. Chen, W.; Zhao, L. F.; Wang, Y. Q.; Miao, J. H.; Liu, S.; Xia, Z. C.; Yuan, S. L., Magnetism in Mn-doped ZnO Bulk Samples. *Solid State Communications* 2005, 134, 827.

45. Jung, S.; An, S.; Yi, G.; Jung, C.; Lee, S.; Cho, S., Ferromagnetic Properties of ZnMnO Epitaxial Thin Films. *Applied Physics Letters* 2002, 80, 4561.

46. Norton, D.; Pearton, S.; Hebard, A.; Theodoropoulou, N.; Boatner, L.; Wilson, R., Ferromagnetism in Mn-implanted ZnO: Sn Single Crystals. *Applied Physics Letters*

2003, 82, 239.

47. Ueda, K.; Tabata, H.; Kawai, T., Magnetic and Electric Properties of Transition-metal-doped ZnO Films. *Applied Physics Letters* 2001, 79, 988.

48. Fukumura, T.; Jin, Z. W.; Ohtomo, A.; Koinuma, H.; Kawasaki, M., An Oxide-diluted Magnetic Semiconductor: Mn-doped ZnO. *Applied Physics Letters* 1999, 75, 3366.

49. Fukumura, T.; Jin, Z.; Kawasaki, M.; Shono, T.; Hasegawa, T.; Koshihara, S.; Koinuma, H., Magnetic Properties of Mn-doped ZnO. *Applied Physics Letters* 2001, 78, 958.

50. Jin, Z.; Fukumura, T.; Kawasaki, M.; Ando, K.; Saito, H.; Sekiguchi, T.; Yoo, Y.; Murakami, M.; Matsumoto, Y.; Hasegawa, T., High Throughput Fabrication of Transition-metal-doped Epitaxial ZnO Thin Films: A Series of Oxide-diluted Magnetic Semiconductors and Their Properties. *Applied Physics Letters* 2001, 78, 3824.

51. Tiwari, A.; Jin, C.; Kvit, A.; Kumar, D.; Muth, J.; Narayan, J., Structural, Optical and Magnetic Properties of Diluted Magnetic Semiconducting $Zn_{1-x}Mn_xO$ Films. *Solid State Communications* 2002, 121, 371.

52. Pearton, S.; Norton, D.; Ip, K.; Heo, Y.; Steiner, T., Recent Advances in Processing of ZnO. *Journal of Vacuum Science & Technology B: Microelectronics and Nanometer Structures* 2004, 22, 932.

53. Cheng, X.; Chien, C., Magnetic Properties of Epitaxial Mn-doped ZnO Thin Films. *Journal of Applied Physics* 2003, 93, 7876.

54. Ivill, M.; Pearton, S.; Norton, D.; Kelly, J.; Hebard, A., Magnetization Dependence on Electron Density in Epitaxial ZnO Thin Films Codoped With Mn and Sn. *Journal of Applied Physics* 2005, 97, 053904.

55. Lim, S.-W.; Jeong, M.-C.; Ham, M.-H.; Myoung, J.-M., Hole-Mediated Ferromagnetic Properties in $Zn_{1-x}Mn_xO$ Thin Films. *Japanese Journal of Applied Physics* 2004, 43, L280.

56. Guo, L.; Peng, D.; Makino, H.; Inaba, K.; Ko, H.; Sumiyama, K.; Yao, T., Structural and Magnetic Properties of Mn_3O_4 Films Grown on MgO (001) Substrates by Plasma-assisted MBE. *Journal of Magnetism and Magnetic Materials* 2000, 213, 321.

57. Chartier, A.; DArco, P.; Dovesi, R.; Saunders, V., Ab initio Hartree-Fock Investigation of the Structural, Electronic, and Magnetic Properties of Mn_3O_4. *Physical Review B* 1999, 60, 14042.

58. Han, S.; Jang, T.; Kim, Y.; Park, B.; Park, J.; Jeong, Y., Magnetism in Mn-doped ZnO Bulk Samples Prepared by Solid State Reaction. *Appiedl Physical Letters* 2003, 83, 920.

59. Liu, C.; Yun, F.; Xiao, B.; Cho, S.; Moon, Y.; H, M.; Abouzaid, M.; Ruterana, R.; Yu, K.; Walukiewicz, W., Structural Analysis of Ferromagnetic Mn-doped ZnO Thin Films Deposited by Radio Frequency Magnetron Sputtering. *Journal of Applied Physics* 2005, 97, 126107.

CHAPTER 4 REFERENCES

1. Hansen, M.; Anderko, K., *Constitution of binary alloys*. McGraw-Hill New York: 1958.

2. Pearson, W., *Latice Spacings and Structure of Mal Aloys*. Pergamon: New York, 1958.

3. Samsonov, G.; Vereikina, L., Phosphides. *AN USSR, Kiev* 1961.

4. Van Wazer, J., *Phosphorus and Its Compounds: Technology, Biological Functions, and Applications*. Interscience Publishers: 1958.

5. Rundqvist, S., Binary Transition Metal Phosphides (and Crystal-Chemical Relations Between Them and Transition Metal Compounds With Other Nonmetals of Small Atomic Radius). *Arkiv Kemi* 1962, 20, 67.

6. Pleskov, V.; Monoszon, A., Activity of Ammonium Ions in Liquid Ammonia Solutions. *Acta Physica et Chimica. URSS* 1935, 1, 725.

7. Zintl, E.; Woltersdorf, G., Gitterstruktur von LiAl. *Zeitschrift fur Elektrochemie* 1935, 41, 877.

8. Brauer, G.; Zintl, E., Metals and Alloys. XXIII. Phosphides, Arsenides, Antimonides, and Bismuthides of Li, Na, and K. *Zeitschrift fur Physikalische Chemie, B* 1937, 37, 323.

9. Von Stackelberg, M.; Paulus, R., Phosphides and Arsenides of Zinc and Cadmium. The Zn_3P_2 Lattice. *Zeitschrift fur Physikalische Chemie* 1935, 28, 427

10. Iandelli, A., Modifications of Sesquioxides of the Rare Earths. *Gazzetta Chimica Italiana* 1948, 71, 58.

11. Folberth, O.; Pfister, H., Die Kristallstruktur von $ZnSnAs_2$. *Acta*

Crystallographica 1960, 13, 199.

12. Folberth, O. G.; Pfister, H., New Ternary Semiconducting Compounds Having Chalcopyrite Structure. *Semiconductors and Phosphors, Proc. Intern. Colloqs., Garmisch-Partenkirchen* 1958, 474.

13. Goodman, C., A New Group of Compounds with Diamond type (Chalcopyrite) Structure. *Nature* 1957, 179, 828.

14. Arstsd, O.; Nowotny, H., X-ray Investigation of The System Manganese-phosphorus. *Zeitschrift fur Physikalische Chemie B* 1937, 38, 356.

15. Rundqvist, S., X-ray Investigations of Mn_3P, Mn_2P, and Ni_2P. *Acta Chemica Scandinavica* 1962, 16, 1.

16. Rundqvist, S., X-ray Investigations of the Ternary System Fe-BP. *Acta Chemica Scandinavica* 1962, 16, 287.

17. Rundqvist, S.; Hassler, E.; Lundvik, L., Refinement of the Ni_3P Structure. *Acta Chemica Scandinavica* 1962, 16, 212.

18. Rundqvist, S.; Jellinek, F., The Structures of Ni_6Si_2B, Fe_2P and Some Related Phases. *Acta Chemica Scandinavica* 1959, 13, 3.

19. Streit, D.; Oki, A.; Gutierrez-Aitken, A.; Grossman, P.; Block, T.; Chin, P.; Lai, R.; Chen, Y.; Grundbacher, R., Indium Phosphide Microelectronics Revolutionary Technology for Advanced Telecommunications. *Technology Review* 2000, 1.

20. Erwin, S., Tailoring Ferromagnetic Chalcopyrites. *Nature Materials* 2004, 3, 410.

21. Wolf, S. A.; Awschalom, D. D.; Buhrman, R. A.; Daughton, J. M.; von Molnar, S.; Roukes, M. L.; Chtchelkanova, A. Y.; Treger, D. M., Spintronics: A Spin-Based

Electronics Vision for The Future. *Science* 2001, 294, 1488.

22. Prinz, G. A., Hybrid Ferromagnetic-Semiconductor Structures. *Science* 1990, 250, 1092.

23. Cho, S.; Choi, S.; Cha, G. B.; Hong, S. C.; Kim, Y.; Zhao, Y. J.; Freeman, A. J.; Ketterson, J. B.; Kim, B. J.; Kim, Y. C., Room-Temperature Ferromagnetism in (Zn_{1-x} Mn_x) GeP_2 Semiconductors. *Physical Review Letters* 2002, 88, 257203.

24. Dietl, T.; Ohno, H.; Matsukura, F.; Cibert, J.; Ferrand, D., Zener Model Description of Ferromagnetism in Zinc-Blende Magnetic Semiconductors. *Science* 2000, 287, 1019.

25. Dietl, T.; Ohno, H.; Matsukura, F.; Cibert, J.; Ferrand, D., Zener Model Description of Ferromagnetism in Zinc-blende Magnetic Semiconductors. *Science (Washington, D. C.)* 2000, 287, 1019.

26. Dietl, T.; Ohno, H.; Matsukura, F., Hole-mediated Ferromagnetism in Tetrahedrally Coordinated Semiconductors. *Physical Review B* 2001, 63, 195205.

27. Ohno, H.; Munekata, H.; Penney, T.; Vonmolnar, S.; Chang, L. L., Magnetotransport Properties of *p*-type (In,Mn)AS Diluted Magnetic III-V Semiconductors. *Physical Review Letters* 1992, 68, 2664.

28. Ohno, H.; Shen, A.; Matsukura, F.; Oiwa, A.; Endo, A.; Katsumoto, S.; Iye, Y., (Ga,Mn)As: A New Diluted Magnetic Semiconductor Based on GaAs. *Applied Physics Letters* 1996, 69, 363.

29. Kamatani, T.; Akai, H., The Magnetic Properties in Transition Metal-doped Chalcopyrite Semiconductors. *Materials Science in Semiconductor Processing* 2003,

6, 389.

30. Mughal, S. A.; Payne, A. J.; Ray, B., Preparation and Phase Studies of The Ternary Semiconducting Compounds $ZnSnP_2$, $ZnGeP_2$, $ZnSiP_2$, $CdGeP_2$, and $CdSiP_2$. *Journal of Materials Science* 1969, 4, 895.

31. Krivosheeva, A. V.; Shaposhnikov, V. L.; Lyskouski, V. V.; Borisenko, V. E.; d'Avitaya, F. A.; Lazzari, J. L., Prospects on Mn-doped $ZnGeP_2$ for Spintronics. *Microelectronics and Reliability* 2006, 46, 1747.

32. Mahadevan, P.; Zunger, A., Room-Temperature Ferromagnetism in Mn-Doped Semiconducting $CdGeP_2$. *Physical Review Letters* 2002, 88, 47205.

33. Kanatzidis, M. G.; Pottgen, R.; Jeitschko, W., The Metal Flux: A Preparative Tool for The Exploration of Intermetallic Compounds. *Angewandte Chemie International Edition* 2005, 44, 6996.

34. Olesinski, R. W.; Abbaschian, G. J., The Si-Zn (Silicon-Zinc) System. *Journal of Phase Equilibria* 1985, 6, 545.

35. Dutkiewlcz, J., The P-Zn (Phosphorus-Zinc) System *Journal of Phase Equilibria* 1991, 12, 435.

36. Massalski, T. B., *Binary Alloy Phase Diagrams*. 2 ed.; The Materials Internation Society: Vol. 3, p 2168.

37. Huber Jr, E. E.; Ridgley, D. H., Magnetic Properties of a Single Crystal of Manganese Phosphide *Physical Review* 1964, 135, A1033.

38. Abrahams, S. C.; Bernstein, J. L., Crystal Structure of Luminescent Silicon Zinc Phosphide. *Journal of Chemical Physics* 1970, 52, 5607.

39. Abrahams, S. C.; Bernstein, J. L., Luminescent Piezoelectric Cadmium Silicon Phosphide. Normal Probability Plot Analysis, Crystal Structure and Generalized Structure of the AIIBIVC2V Family. *Journal of Chemical Physics* 1971, 55, 796.

40. Paduan-Filho, A.; Becerra, C. C., Critical Fluctuations in MnP Near the Curie Temperature. *Journal of Magnetism and Magnetic Materials* 2003, 261, 161.

41. Aitken, J. A.; Tsoi, G. M.; Wenger, L. E.; Brock, S. L., Phase Segregation of MnP in Chalcopyrite Dilute Magnetic Semiconductors: A Cautionary Tale. *Chemistry of Materials* 2007, 19, 5272.

42. Hwang, T.; Shim, J. H.; Lee, S., Observation of MnP Magnetic Clusters in Room-temperature Ferromagnetic Semiconductor $Zn_{1-x}Mn_xGeP_2$ Using Nuclear Magnetic Resonance. *Applied Physics Letters* 2003, 83, 1809.

CHAPTER 5 REFERENCES

1. Sze, S. M., *Semiconductor Devices: Physics and Technology, 2nd Edition*. 2001; p 568 pp.

2. Agrawal, M., Magnetic Properties of Materials, Dilute Magnetic Semiconductors, Magnetic Resonances (NMR and ESR) and Spintronics. Dec: 2003.

3. Umehara, Y.; Koda, S., Structure and Phase-boundary Energies of the Directionally Solidified Indium Antimonide-manganese Antimonide, Indium antimonide-nickel Antimonide, Indium Antimonide-iron Antimonide, and Indium Antimonide-chromium Antimonide Eutectic Alloys. *Metallography* 1974, 7, 313.

4. Birkmire, R. W.; Eser, E., Polycrystalline Thin Film Solar Cells: Present Status and

Future Potential. *Annual Review of Materials Science.* 1997, 27, 625.

5. Gabor, A. M.; Tuttle, J. R.; Albin, D. S.; Tennant, A. L.; Contreras, M. A.; Noufi, R., High Efficiency Polycrystalline Cu(In,Ga)Se_2-based solar cells. *AIP Conference. Proceeding.* 1994, 306, 59.

6. Hughbanks, J. K. a. T., Synthesis of Structures of Ternary Chalcogenides of Alumnium and Gallium with Stacking Faults: KMQ_2 (M = Al, Ga; Q = Se, Te). *Journal of Solid State Chemistry* 1999, 149, 242.

7. Lemoine, P.; Carre, D.; Guittard, M., The Structure of Gallium and Potasium Sulfide, $KGaS_2$ *Acta Crystallographica Section C-Crystal Structure Communications* 1984, 40, 910.

8. Janz, G. J.; Rogers, D. J., Melting and Premelting Properties for a Series of Potassim Polysulfides *Journal of Chemical and Engineering Data* 1983, 28, 331.

9. Janz, G. J.; Rogers, D. J., Thermal-behavior of the Potassium-sulfur Electrolte in Advanced Battery Concepts. *Journal of the Electrochemical Society* 1983, 130, C128.

10. Kanatzidis, M., Molten Alkali-metal Polychalcogenides as Reagents and Solvents for the Synthesis of New Chalcogenide Materials. *Chemistry of Materials* 1990, 2, 353.

11. Sangster, J., The K-S (Potassium-sulfur) System. *Journal of Phase Equilibria and Diffusion* 1997, 18, 82.

12. *Okamoto, H.*, The Li-S (lithium-sulfur) System. *Journal of Phase Equilibria and Diffusion* 1995, 16, 94.

13. Sangster, J.; Pelton, A. D., The Na-S (sodium-sulfur) System. *Journal of Phase*

*Equilibria and Diffusion,*1997, 18, 89.

14. Sangster, J.; Pelton, A. D., The Na-Se (sodium-selenium) System. *Journal of Phase Equilibria and Diffusion* 1997, 18, 185.

15. Pelton, A. D.; Petric, A., The Na-Te (Sodium-Tellurium) System *Journal of Phase Equilibria and Diffusion,* 1990, 11, 447.

16. Okamoto, H., K-Te (Potassium-Tellurium) *Journal of Phase Equilibria and Diffusion* 1999, 20, 541.

17. Pearson, T. G.; Robinson, P. L., The polysulphides of the Alkali Metals Part III Potassium. *Journal of the Chemical Society* 1931, 1304.

18. Draves, C. Z.; Tartat, H. V., The Polysulfides of Sodium and Potassium. *Journal of the American Chemical Society* 1926, 48, 1527.

19. Hugot, C., Action of Sodammonium and Potassammonium on Selenium. *Compt. rend.* 1899, 129, 299.

20. Cleaver, B.; Davies, A. J.; Hames, M. D., Properties of Fused Polysulfides.1. Electtrical Conductivity of Fused Sodium and Potasium Polysulfides. *Electrochimica Acta* 1973, 18, 719.

21. Thomas, J. S.; Rule, A., The Polysulphides of the Alkali Metals. Part III. The Solidifying Points of the Systems, Sodium Monosulphide-sulphur, and Potassium Monosulphide-sulphur. *Journal of the Chemical Society* 1917, 111, 1063.

22. Bousquet, J.; Letoffe, J. M.; Diot, M., Thermal-behavior of Potassium Polysulfides. *Journal De Chimie Physique Et De Physico-Chimie Biologique* 1974, 71, 1180.